UCLouvain

Institute of Condensed Matter and Nanosciences

Transaminase-membrane reactor for intensified chiral amines production

Thesis presented in partial fulfilments of the requirements for the degree of Doctor of Philosophy in Agricultural Sciences and Biological Engineering by

Hippolyte Meersseman Arango
PhD candidate (UCLouvain/IMCN)

Supervisors

Prof. Damien Debecker (UCLouvain/IMCN)
Prof. Tom Leyssens (UCLouvain/IMCN)

Committee members

Prof. Patricia Luis Alconero (UCLouvain/IMMC)
Prof. Francesca Paradisi (University of Bern, Switzerland)
Prof. Jan von Langermann (University of Magdeburg, Germany)
Prof. Arnaud Delcorte (UCLouvain/BSMA) – Head of Jury

Louvain-la-Neuve
September 2024

IMCN

Acknowledgments

Tout d'abord je tiens à remercier mon promoteur, le Professeur Damien Debecker, pour son encadrement et sa motivation contagieuse tout au long de cette thèse. De par ses idées, sa décontraction et la confiance qu'il m'a accordé au quotidien, il a été le catalyseur de cette thèse, et a su m'offrir des conditions idéales de travail pour que je puisse exploiter mon plein potentiel durant ces quatre ans. Merci pour tout, Damien !

Mes remerciements vont aussi aux membres de mon jury de thèse. Je remercie le Professeur Arnaud Delcorte d'avoir accepté de présider ce jury. Je remercie également les Professeurs Tom Leyssens et Patricia Luis pour les discussions scientifiques, leurs conseils pertinents lors de nos réunions ARC, et leur implication dans les révisions du manuscrit de thèse. I also wish to thank Professor Francesca Paradisi for being part of my committee and of my PhD thesis jury. Without a doubt, the meetings we had were immensely helpful in improving my understanding of biocatalysis and in the production of this PhD thesis manuscript. Many thanks also to Professor von Langermann for the valuable discussions we had at Biocat 2022 in Hamburg and during my private defense!

Ensuite, je tiens à remercier mes collègues du C3 et du C2, sans qui ce doctorat aurait probablement été très différent. Tout particulièrement, je souhaite remercier François pour sa bonne humeur et sa présence indispensable au laboratoire. Nul doute que les pauses café, nos sorties aux bars et nos discussions sportives (entre autres) ont grandement contribué à la réussite de ma thèse ! Merci à Nathalie et à Jean-Charles pour leur implication et leur présence au labo et à la cafétéria. Merci aussi à mes collègues doctorants (ou maintenant docteurs, pour certain(e)s !) les plus anciens - Denis, Margot, Marty et Fanny – pour les journées au labo, les midis en

cafétéria, les conférences et les sorties mémorables. Merci à Giovanni et Michele d'avoir amené une touche d'*Italian style* au laboratoire. Merci à Cédric pour les entrainements de course, les sorties à vélo et pour sa bonne humeur quotidienne. Enfin, merci aussi à Juliette, Arnaud, Corentin, Aurélien, Noé, Guillaume, Alexis, Benjamin, Mehdi, Sophie et Maximiliano avec qui j'ai pu partager de très bons moments au C2, au C3 ou en conférence. Muchas gracias tambien a Sebastian y Evelin por los buenos momentos que pasamos juntos !

En dehors du laboratoire, je voudrais remercier Nico (Tchouk), Clément, Aurore et Auriane pour leur précieuse présence. Un tout grand merci également à ma famille, en particulier à mes parents, pour leur soutien inconditionnel et plus globalement pour toute l'attention qu'ils m'ont toujours portée.

Enfin, je tiens à exprimer une immense gratitude à Isaure pour son excellente compagnie, son énergie au quotidien et son soutien sans faille. Toujours attentionnée et à l'écoute, elle m'a été d'une aide précieuse dans la finalisation de ce travail. Merci pour tout !

List of scientific communications

Articles:

- "Continuous flow-mode synthesis of (chiral) amines with transaminase: a strategic biocatalytic approach to essential building blocks". **H. M. Arango**, L. van den Biggelaar, P. Soumillion, P. Luis, T. Leyssens, F. Paradisi and D. P. Debecker, *React. Chem. Eng.*, 2023, **8**, 1505–1544.
- "Hybrid chemoenzymatic heterogeneous catalysts". D. P. Debecker, V. Smeets, M. Van der Verren, **H. M. Arango**, M. Kinnaer, F. Devred, *Curr. Opin. Green Sustain. Chem*., 2021, **28**, 100437.
- "Membrane-immobilized transaminases for the synthesis of enantiopure amines". **H. M. Arango**, X. D. L. Nguyen, P. Luis, T. Leyssens, D. Roura Padrosa, F. Paradisi and D. P. Debecker, *RSC Sustain.*, **2**, 3139-3152.
- "Enzyme-membrane-reactors: recent trends and applications for the production of fine chemicals and pharmaceuticals". **H. M. Arango**, P. Luis, T. Leyssens and D. P. Debecker. Submitted upon invitation in *Comptes-Rendus Chimie*

Oral communications:

- **H. M. Arango**, T. Leyssens, P. Luis Alconero, F. Paradisi, D. P. Debecker, *Membrane-immobilized transaminase for intensified chiral amine production,* 29e colloque du Club Biocatalyse en Synthèse Organique (CBSO), Paris (France), 2022
- **H. M. Arango**, T. Leyssens, P. Luis Alconero, F. Paradisi, D. P. Debecker, *Membrane-immobilized transaminase for integrated processes,* 10th International Congress on Biocatalysis, Hamburg (Germany), 2022
- **H. M. Arango**, T. Leyssens, P. Luis Alconero, F. Paradisi, D. P. Debecker, *Transaminase membrane-immobilization for intensified chiral amines production*, PREPA13-13th International Symposium

on" Scientific Bases for the Preparation of Heterogeneous Catalysts", Louvain-La-Neuve (Belgium), 2023

- **H. M. Arango**, T. Leyssens, P. Luis Alconero, F. Paradisi, D. P. Debecker, *Transaminase-membrane reactor for intensified chiral amines synthesis*, EuropaCat2023, Prague (Czech Republic), 2023
- **H. M. Arango**, T. Leyssens, P. Luis Alconero, F. Paradisi, D. P. Debecker, *Crystallization-assisted enantiopure amine synthesis using membrane immobilized transaminases*, 10th International Congress on Catalysis (ICC), Lyon (France), 2024

Poster presentations:

- **H. M. Arango**, T. Leyssens, P. Luis Alconero, F. Paradisi, D. P. Debecker, *Membrane-immobilized transaminase for integrated processes*, Next Generation Biocatalysis – An International Young Investigator Symposium 2022 NextGenBiocat", Delft (Netherlands), 2022
- **H. M. Arango**, T. Leyssens, P. Luis Alconero, F. Paradisi, D. P. Debecker, *Membrane-immobilized transaminase for intensified processes*, Chemical Research in Flanders - Chemistry Conference for Young Scientists (CRF-ChemCYS), Blankerberg (Belgium), 2022

Awards

- Best oral presentation at CBSO (2022)
- 3rd best poster presentation at CRF-ChemCYS (2022)

Summary of the Thesis

To produce active pharmaceutical ingredients in a greener way, developing more sustainable methods for enantiopure amines synthesis is crucial. Enzymes are attractive for this purpose given their ability to operate in mild conditions and to shorten synthesis pathways. Transaminases (TAs) offer promising routes for producing chiral amines with excellent enantioselectivity. Yet, challenges like unfavorable thermodynamics and poor soluble enzyme stability remain. Enhancing TAs robustness and shifting the transamination equilibrium towards high product yields, are thus essential. In this context, immobilizing TAs on membranes appears particularly appealing, as it enables simultaneous biocatalysis and product separation in one-pot. Along this line, the main objectives of this thesis are: (i) immobilizing TAs on membranes to develop biocatalytic membranes, (ii) displacing the chemical equilibrium towards the amines asymmetric synthesis and (iii) producing chiral amines in flow mode.

First, TAs immobilization on polymeric membranes is investigated. Among the studied strategies, the covalent immobilization on functionalized polypropylene proved particularly effective, resulting in enantioselective biocatalytic membranes yielding high activity and reusability without leaching. These biocatalytic membranes are then applied to an industrially relevant reaction. Their ability to catalyze such asymmetric synthesis is demonstrated: enhanced activity and stability with respect to soluble TAs and to benchmark heterogeneous TAs, were obtained. To improve process productivity, product crystallization is employed. This approach allowed shifting the reaction equilibrium and reaching high yields of product crystals.

Finally, the immobilized TAs are implemented in a flow reactor, intensifying the biocatalytic process. The benefits of such transfer to flow mode are highlighted: the TA immobilization yield and transamination space-time yield were boosted with respect to the batch operations.

List of abbreviations

API – active pharmaceutical ingredient
APTES - (3-aminopropyl)triethoxylsilane
ATA – amine transaminase
BAP – 4'-bromoacetophenone
BMBA - 4-bromo-α-methylbenzylamine
DCM - dichloromethane
DMSO - dimethylsulfoxide
DPPA – 3,3-diphenylpropionic acid
ee – enantiomeric excess
EMR – enzyme-membrane-reactor
EtOH - ethanol
GA - glutaraldehyde
GDE – glycerol diglycidyl ether
GDH - glucose dehydrogenase
FAP – 2'-fluoroacetophenone
FMBA – 2'-fluoromethylbenzylamine
HEPES - *N*-2-Hydroxyethylpiperazine-*N*'-2-ethane sulphonic acid
HeWT – transaminase from *Halomonas elongata*
ISO – isopropylamine
IPA – isopropanol
LDH – lactate dehydrogenase
MBA - methylbenzylamine
MES - 2-(*N*-Morpholino)-ethane sulphonic acid
PAN - polyacrylonitrile
PBR – packed-bed reactor
PDA - polydopamine
PEI - polyethyleneimine
PLP – pyridoxal-5'-phospate
PP - polypropylene
STY – space-time yield
TA - transaminase
TsRTA – transaminase from *Thermomyces stellatus*

Table of contents

Context of the thesis, objectives and strategy

ABSTRACT

This part outlines the context in which this research has been carried out. It provides a literature survey on the studied target molecules (chiral amines), biocatalytic reaction (transamination), and about the types of biocatalytic systems employed in this work (enzyme-membrane reactors). The existing limitations, challenges and opportunities related to this topic are exposed in relation with our own objectives. Finally, our strategy established in order to address these issues is presented.

1 Context of the thesis

1.1 Introduction

The synthesis of active pharmaceutical ingredients (APIs) is of utmost importance since APIs are the essential compounds in medications, responsible for their therapeutic effects. Overall, producing APIs is essential for maintaining public health, supporting medical advances, and ensuring the safety and availability of essential medications [1].

Chemo-catalytic synthesis processes used for the production of APIs have been identified as problematic from an environmental point of view [2–4]. The molecular complexity of APIs requires multistep synthesis that consumes large amounts of reagents and solvents. Moreover, while highly (enantio)pure products are generally needed for the targeted applications, chemo-catalytic reactions are rarely 100% (enantio)selective. Because of this, laborious, costly, and waste-generating downstream purifications steps have to be applied [5]. The pharmaceutical industry is known to generate significant waste per unit mass of product produced (e-factor often above 250). It is estimated that the pharmaceutical industry is responsible for the formation of about 10 billion kg of waste per year for active pharmaceutical ingredients production, which implies a disposal cost of more than $20 billion per year [6].

The specific case of the synthesis of chiral amines is telling. Chiral amines are essential building blocks used to manufacture a plethora of APIs. It is estimated that about half of the current APIs contain chiral amines in their structure [7,8]. Pharmaceutical industries have been relying on chemocatalytic processes to produce chiral amines for decades [9], usually *via* indirect reductive amination (of an imine precursor)[10] using chiral organometallic homogeneous catalysts [11]. The latter operate at relatively high temperature, require pressurized hydrogen, are difficult to recover, and are often based on toxic and

depleted heavy metals [11,12]. The incentives and opportunities to the make such processes greener are evident.

In this context, the development of alternative synthesis methods of chiral amines following more closely the principles of green chemistry and the good practice of sustainability in catalysis science [13,14], is of particular importance. Green chemistry is more than preventing waste and minimizing energy consumption; it is also about operating in a more sustainable way, increasing efficiency and reducing hazards for operators, for consumers, and for the environment. In addition to focusing on the reduction of waste quantity and cost, managing inputs (*e.g.* solvents, reagents, catalysts) is an important driver. Life cycle analyses of API production processes indeed demonstrated that the synthesis of material inputs account for at least 80% of the overall life cycle impact [15].

The last two decades saw the emergence of biocatalysis as a potential greener approach for pharmaceutical processes. Biocatalysis represents a vibrant field of research since enzymes tend to be highly enantioselective, non-toxic and usually work in mild conditions (*e.g.* aqueous media, low temperature) [16]. Interestingly, amine transaminases (ATAs) enable the direct synthesis of chiral amines from pro-chiral ketones using cheap and readily available amino donors (*e.g.* isopropylamine, amino-acids) through transamination. As highlighted by the ACS Green Chemistry Institute Pharmaceutical Roundtable, such transamination may present major advantages in terms of overall efficiency and atom economy with respect to conventional indirect reductive amination of imines (which involve multistep production and isolation of imine precursors) [4]. As a result, ATAs are catching the eye and getting increasingly studied [17]. For instance, the greener production of Sitagliptin (Figure i-1) taking advantage of a genetically engineered transaminase has been implemented at the pilot scale by Merck [18,19]. Also, the production of Pseudoephedrine by transaminases was recently demonstrated [20].

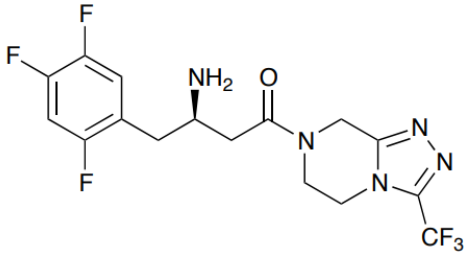

Figure i-1. R-Sitagliptin is an anti-diabetic drug. An engineered transaminase is able to catalyze the synthesis of this compound at large scale from the corresponding ketone.

Nevertheless, despite notable examples of kg and pilot-scale batch processes employing ATAs (see section 1.4.1), industrial applications remain currently scarce as they suffer from several limitations, mainly linked with substrate and product inhibition and with the unfavourable thermodynamic equilibrium for the targeted reactions [21]. Additionally, the enzymes are often employed in the "free" form, i.e. as homogenous biocatalysts, that are hardly reusable, remain restricted to batch reactors, and feature limited stability. To overcome these limitations, strategies aiming at enhancing chiral amine production by transaminases have been intensively investigated. Of particular interest: (i) the development of equilibrium shifting strategies, as well as (ii) the design of more versatile and reusable heterogenized biocatalysts amenable to continuous flow-mode processes.

In this review, we first summarize the state of the art on the production of chiral amines and we highlight the key – emerging – role of biocatalysis. The focus is then put on transaminase enzymes themselves, for which we describe the main properties and the catalytic mechanism. After highlighting the main issues that currently preclude a general deployment of chiral amine synthesis using transaminases at the industrial level, we discuss and exemplify a number of strategies that have been proposed to round these corners. This includes methods to expand the substrate scope and robustness, to shift the thermodynamic equilibrium, to enhance recoverability and reusability (mainly by immobilization). Importantly, the coupling of transaminases with

membrane technology in enzyme-membrane-reactors (EMR) is highlighted as a promising strategic route capable of intensifying transamination processes in an efficient way.

1.2 Chiral amines

1.2.1 Importance of chiral amines

Chiral compounds represented 56 % of active pharmaceutical ingredients (API) available on the drug market in 2005 [22]. In 2020, more than 95 % of the commercialized API are chiral [23]. This is not surprising, given that all living organisms are built on chiral biomolecules, and drug targets such as proteins, that are built from L-amino acids, will interact differently with R- and S-enantiomers of a given compound. In biology, proteins are built exclusively from L-amino acids (plus glycine which does not bear any chiral centre) [24]. For chiral drugs, the enantiomer that exhibits the desired physiologic properties is called the eutomer, while the other enantiomer is called the distomer [25]. The latter may exhibit weak positive properties (sometimes different from the eutomer properties), or can be totally inactive. For example, the R-enantiomer of methamphetamine is a powerful decongestant, while S-methamphetamine is a recreational drug [26]. In the worst cases, however, the distomer is highly toxic. S-Penicillamine (Figure i-2) is a chiral amine drug prescribed for the treatment of polyarthritis, while R-Penicillamine is highly toxic [27].

Nevertheless, 88 % of current chiral drugs are sold as racemic mixture [22].In such case, it is obviously crucial to know the properties of each enantiomer. Since 1992, the U.S. Federal Food and Drug Administration (FDA) demands that the drug manufacturers either clinically test both enantiomers when selling a racemic mixture, or commercialize only the pure eutomer [28,29].

Getting enantiomerically pure drugs is still a complicated task; it requires to either produce only the eutomer (need for enantioselective chemical methods) or to produce a racemic mixture and resolve or deracemize it [30] (which is often expensive and generates waste).

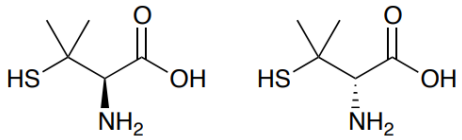

(S)-Penicillamine *Polyarthritis treatment* **(R)-Penicillamine** *Toxic*

Figure i-2. Penicillamine enantiomers. The enantiomers of Penicillamine have different properties: the S-eutomer is a drug used in polyarthritis treatment; the R-distomer is toxic.

Chiral amines can be defined as compounds bearing a nitrogen atom adjacent, or α, to a stereogenic carbon [5]. 45% of the current drugs contain a chiral amine in their structure[7,8]. Therefore, most of the largest pharmaceutical industries are actively looking into chiral amine synthesis: Pseudoephedrine (Sinutab®, Johnson & Johnson), Sertraline (Zoloft®, Pfizer), Oseltamivir (Tamiflu®, Roche), Rivastigmine (Exelon®, Novartis), Clopidogrel (Plavix®, Sanofi), Sitagliptine (Januvia®, Merck), Lisdexamfetamine (Vyvanse®, Shire), Linagliptine (Tradjenta®, Boehringer-Ingelheim Pharmaceuticals), etc. are all chiral amine drugs. Those highly consumed medicines act as decongestants, anti-depressants, antiviral drugs, treatments for neurological disorders, diabetes, etc. For instance, Clopidogrel – antiplatelet agent – is prescribed to more than 100 million people worldwide [31], Sertraline – a treatment against neurological disorder – was prescribed to more than 37 million people in the USA in 2011 [32]. As for all chiral drugs, the development of enantioselective synthesis methods (i.e. to obtain directly enantiomerically pure chiral amines) is of crucial importance[33].

1.2.2 Chiral amines synthesis

There are two conventional ways to produce chiral amines using a chemical approach: asymmetric synthesis and chiral resolution [5]. These are presented here briefly as benchmark case (section 1.2.2.1.), before putting the focus of the review on biocatalytic routes (section 1.2.2.2.) which arguably represent a promising alternative.

1.2.2.1 Chemical routes

In the first approach (asymmetric synthesis), only one enantiomer is produced, leading to a maximal theoretical yield of 100 %, starting from a non-chiral substrate, or optically pure chiral substrate. There are three main kinds of asymmetric synthesis [22]. First, an enantioselective catalyst – typically a chiral homogeneous organometallic catalysts [34] – can be used for the production of a chiral compound with a high enantiomeric excess. As subsequent purification of the desired enantiomer is usually needed, as well as removal of the catalyst from the final product, further purification steps are imposed [35,36]. In a second type of asymmetric synthesis, a chiral auxiliary is temporarily added to a compound to guide the reaction towards the production of the desired enantiomer, after which the auxiliary is removed. In a third approach, the enantioselective compound is built starting from a chiral precursor (for example, an amino-acid) [37].

Asymmetric synthesis is ubiquitous in the pharmaceutical sector. Hereafter, we briefly present three examples for chiral amines.

S-Clopidogrel (Figure i-3) is the second world most sold medicine [31]. Its current production involves the reduction of a carbonyl centre into a chiral alcohol.

This step is catalyzed by a ruthenium-based organometallic catalyst, [Ru(*p*-cymene)Cl_2]$_2$, using a chiral ligand to bring enantioselectivity to the process.

The reaction is run at 0 °C, requiring extra energy for cooling. The final product exhibits an enantiomeric excess of 92 % [38,39].

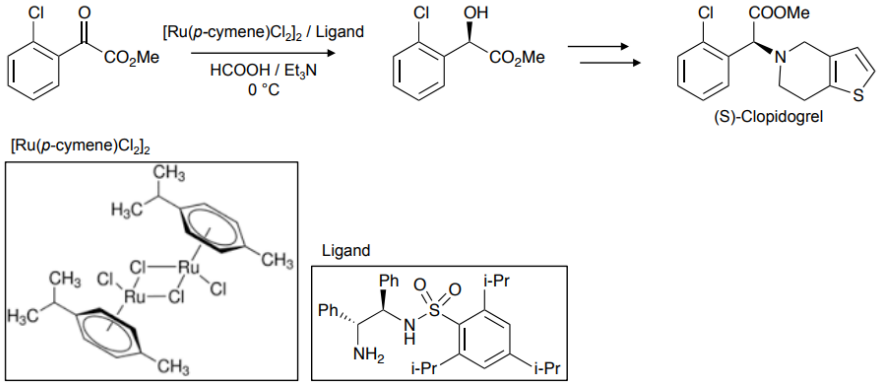

Figure i-3. S-Clopidogrel synthesis, adapted from Li *et al.* [38].

R-Sitagliptin (Figure i-4), produced by Merck, is used in the treatment of type II diabetes. Its chemocatalytic synthesis, implemented for decades, involves the use of a Ru- or Rh-based organometallic enantioselective catalyst with a chiral ligand featuring phosphine groups (such as $[Rh(COD)Cl]_2$-^{t}Bu-JOSIPHOS) [40]. After the imination of a ketone group, the imine group is reduced under high-pressure hydrogen (17 bars) with the enantioselective catalyst. The final enantiomeric excess reaches 95 % [41]. Further purification of the R-enantiomer, as well as a final step to obtain the sitagliptin phosphate salt (the active form), are required. Recently, a greener biocatalytic pathway (vide infra) has been implemented by Merck.

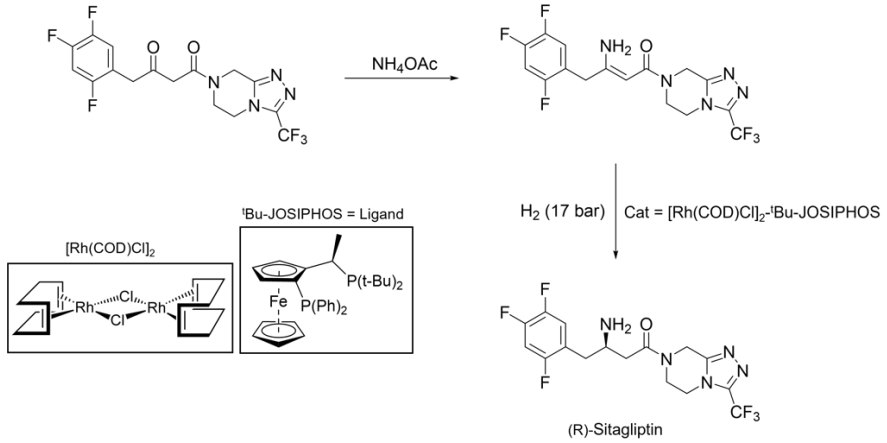

Figure i-4. R-Sitagliptin synthesis, adapted from Hansen *et al.* [40].

S-Rivastigmine (Figure i-5) is a chiral amine used in the treatment of Alzheimer disease. The synthesis pathway typically involved the enantioselective transformation of a ketone into a chiral alcohol. This step is catalyzed by an iridium-based enantioselective catalyst, under gaseous hydrogen (10 atm). A relatively toxic solvent (tetrahydrofuran) is used [42]. Recently, a biocatalytic pathway has been implemented (see vide infra).

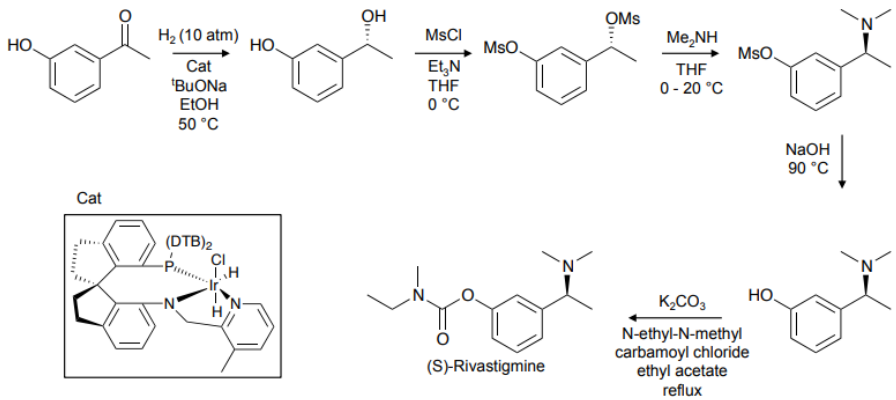

Figure i-5. S-Rivastigmine synthesis, adapted from Che *et al.* [42].

In the second approach (chiral resolution), a racemic mixture is first produced. Then, the enantiomers are separated and the distomer is eliminated (removed, consumed, or recycled in the most favourable cases). Thus, the maximal theoretical yield of the chiral resolution is only 50 %. Such a method is applied in industry when no suitable enantioselective catalyst can be found to perform an asymmetric synthesis [43]. Preparative chiral High Performance Liquid Chromatography (HPLC) – based on the use of chiral stationary phase – can in some cases be used to separate enantiomers [44]. However, most methods for enantiomer separation are based on the formation of diastereoisomers (enantiomers that are combined with optically pure chiral compounds) [22]. Diastereoisomers can then be separated according to their physico-chemical properties. For example, when a mixture of diastereoisomers is cooled, one compound crystallizes first and can therefore be removed from the medium while the other compound remains in solution. A liquid mixture of diastereoisomers can also be separated by preparative HPLC on a non-chiral phase. These methods, however, often score poorly in terms of sustainability metrics (large amounts of solvents, low atom economy, etc.).

To illustrate the chiral resolution approach for the synthesis of a chiral amine, Figure i-6 shows the synthesis of (S,S)-Sertraline. A S-imine precursor is produced first, starting from the ketone and using methylamine as a reagent in hot toluene. Then, the non-enantioselective reduction of the imine is carried out under pressurized hydrogen with a palladium reduction catalyst. The intermediate product is a diastereoisomeric mixture of (S,R) and (S,S) compounds. The last step consists in the separation of the diastereoisomers, using R-mandelic acid: (S,S)-Sertraline forms an insoluble salt with R-mandelic acid, which crystallizes and is easy to recover. The other salt (S,R)-Sertraline-mandelate remains soluble [45]. The maximal yield is only 50 % [46,47].

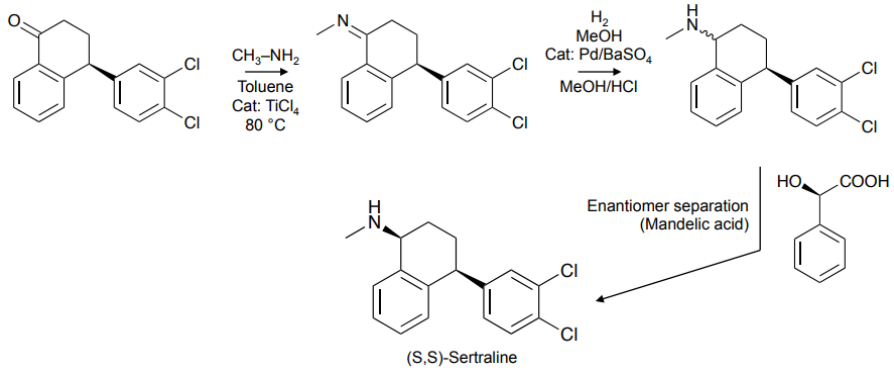

Figure i-6. (S,S)-Sertraline synthesis, adapted from Khamar and Modi [47].

A sub-case of chiral resolution is kinetic resolution: starting from a racemic mixture, an enantioselective catalyst aims at the consumption of the distomer, while the eutomer stays unreacted. This method of resolution, that needs an efficient enantioselective catalyst, is of particular interest when the direct asymmetric synthesis of the eutomer is not thermodynamically favoured. Thus, for such reactions, starting from a racemic mixture, the distomer is removed from the reaction medium as it is converted into the product, keeping the eutomer unreacted.

As already mentioned, the above-shown chemocatalytic methods, often score poorly in terms of sustainability. To better align the routes to chiral amines with the principles of green chemistry, it is essential to develop alternative synthesis strategies.

1.2.2.2 Enzymatic routes to chiral amines

Enzymes are Nature's catalysts, designed along the timespan of evolution to catalyze the chemical transformations in living organisms. They usually exhibit high activity: most of them show turnover rates between 10 and 10000 catalytic cycles per second. Most enzymes are also highly enantioselective (i.e. 100% enantioselective for their natural reactions), and they usually work

in mild conditions: aqueous media, mild pH, and low temperature. Cherry on the cake: they are biodegradable and non-toxic (traces of enzymes in the final product would not represent an important issue in many cases) [16].

Various characterized enzymes are currently available in large libraries, ready for industrial use [48]. Moreover, thanks to the great advances in genetic technologies of the last decades, and especially with the advent of directed evolution technologies, recently recognized by a Nobel Price [49], it is now possible to engineer enzymes towards mutated variants endowed with desired properties, *e.g.* higher resistance to organic solvent, higher temperature or pressure resistance, tuned (enantio-)selectivity, broader substrate specificity or even as catalysts of non-natural chemistries [18,50]. Thus, enzymes seem to be the ideal catalysts to process chemical reactions of industrial interest in a greener way. Enzymes can be used to replace some steps in a given chemical process, and can easily be combined with non-enzymatic steps [51,52].

Several enzymes are able to catalyze reactions leading to the production of chiral amines [53]. A selection of these is presented in Figure i-7. Lipases have been used by BASF to resolve chiral amines, by catalysing enantioselective amidation, leading to optically pure chiral amines and amides, with excellent enantioselectivity (Figure i-7a) [54]. L-selective amidases have been implemented by DSM to produce non-proteinogenic amino acids (*i.e.* that are not naturally found in living organisms): a racemic mixture of 2-aminoamides was converted into optically pure L-amino acids and D-amino amides (Figure i-7b) [54]. Similarly, hydrolases catalyze the enantioselective hydrolysis of amides into chiral amines starting form a racemic mixture of amides (Figure i-7c) [5].

Ammonia-lyases (AL) are a class of enantioselective enzymes that are able to add ammonia on a carbon-carbon double bound, leading to chiral amines. Among them, aspartic acid ammonia-lyase (AAAL) has been used by Holland Sweetener Company: the addition of ammonia on fumaric acid led to L-aspartic acid, precursor of the famous sweetener Aspartame (Figure i-7d) [54].

Tyrosine Ammonia-lyase (TAL) catalyzes the enantioselective addition of ammonia on coumaric acid, providing L-tyrosine amino acid (Figure i-7e) [55].

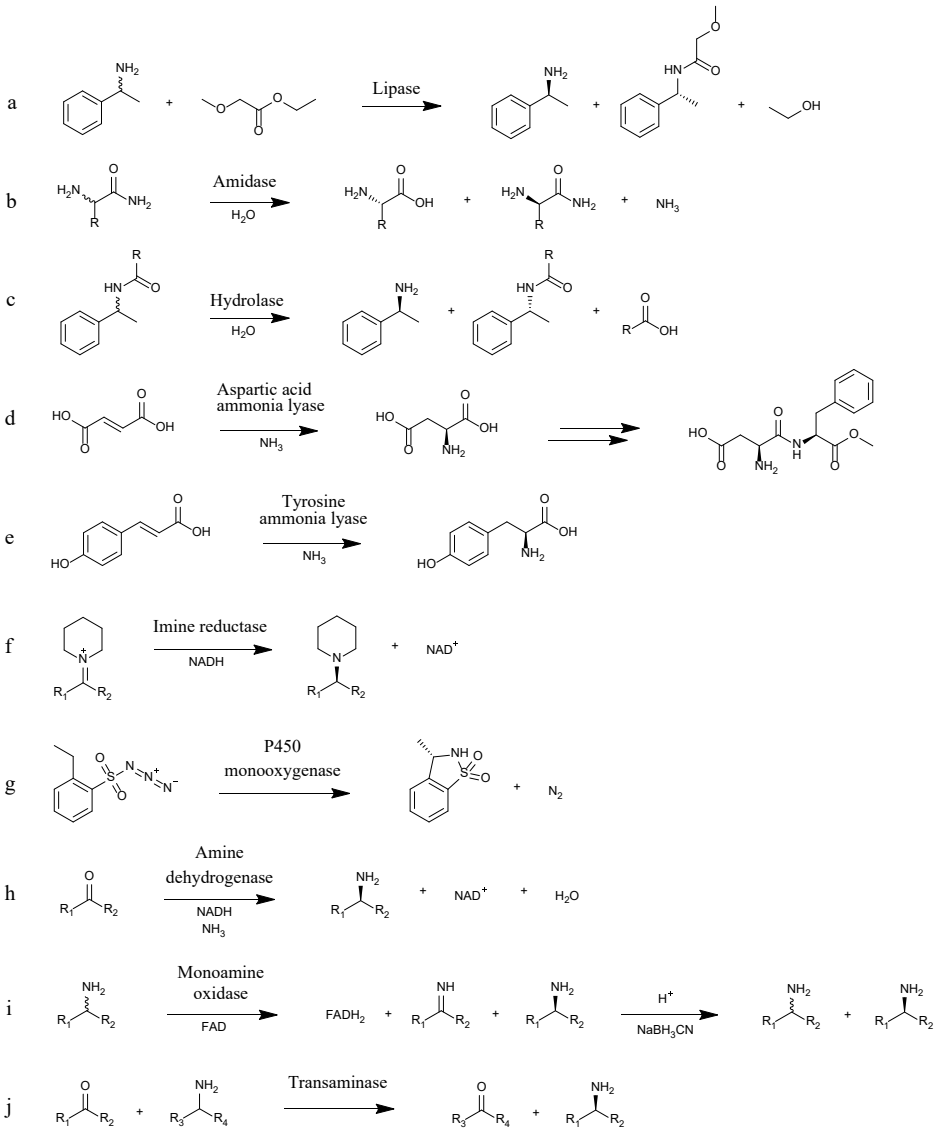

Figure i-7. Selection of enzymes catalysing chiral amines production. (a) lipase, (b) amidase, (c) hydrolase, (d) aspartic acid ammonia-lyase and (e) tyrosine ammonia-lyase, (f) imine reductases, (g) P450 monooxygenase, (h) amine dehydrogenase, (i) monoamine oxidase; and (j) transaminase. NADH stands for Nicotinamide Adenine Dinucleotide reduced form, and is a reductant. FAD stands for Flavine Adenine Dinucleotide oxidized form.

Chiral amines can also be produced by the reduction of an imine using imine reductases (Figure i-7f). Importantly, such enzyme enables the asymmetric synthesis of chiral secondary amines (*via* reductive amination of ketones). For years, this technology was limited to a narrow scope of substrates that are accepted by the enzyme (mostly cyclic secondary imines) [5,53,56], and required important molar equivalents of amino substrate. However, recent discoveries reported IREDs activity towards acyclic imines, even at low amine:ketone (c.a. 1:1) ratios [57]. Such reports led to the creation of a sub-class of IREDs called the reductive aminases (RedAms). Since its discovery [58], this technology has developed very rapidly in both academic and industrial sectors (*e.g.* Pfizer), leading to multi-kilograms scale chiral amine syntheses [59].

P450 monooxygenase (Figure i-7g) is an enzyme that catalyzes chiral intra-molecular C-H amidation, leading to cyclic chiral amines [60]. Amine dehydrogenases and amino-acid dehydrogenases (Figure i-7h) catalyze the reductive amination of carbonyl centres into chiral amines. Such enzymes catalyze the addition of ammonia on a carbonyl centre, using NADH as a cofactor [56,61].

Monoamine oxidases (MAO) catalyze the enantioselective oxidation of the distomer amine into a non-chiral imine, using FAD as cofactor (flavine adenine dinucleotide; Figure i-7i), leaving the eutomer untouched. The imine is then reduced back to the racemic amine with a non-chiral chemical reagent and can be re-oxidised by MAO. Multiple chemo-enzymatic cycles of oxidation and reduction affords full deracemization of the starting amine [62]. Variants with broader specificities have been engineered to accommodate a wide variety of amine substrates.

Finally, transaminases (TA), also called amino-transferases, are enzymes that catalyze the reversible enantioselective transfer of an amino group from an amino donor (*e.g.* an amine) to an amino-acceptor (*e.g.* a ketone; Figure i-7j) [5]. Transaminases currently represent a vibrant field of research for the greener and more concise synthesis of chiral primary amines as they allow

shortening their synthesis methods (*e.g.* by avoiding protecting steps) and hence, reducing chemical waste compared to their chemical counterparts [63–65]. Moreover, they show relatively broad substrate scope [63,66], and their cofactor, pyridoxal 5'-phosphate (PLP) is not consumed during the reaction. These aspects make them particularly appealing from an industrial point of view.

1.3 Transaminases

1.3.1 Classification

For the transamination catalytic act, transaminases need a cofactor, namely pyridoxal 5'-phosphate (PLP, Figure i-8) [67]. This molecule is biosynthesized from vitamin B6. Around 240 different reactions are catalyzed by PLP-dependent enzymes that are divided into seven classes (based on the enzyme structure): (I) aspartate transaminase, (II) tryptophan synthase, (III) alanine racemase, (IV) D-alanine transaminase, (V) glycogen phosphorylase, (VI) D-lysine-5,6-aminomutase and (VII) lysine-2,3-aminomutase. PLP-dependent enzymes catalyze racemization, transamination, decarboxylation, elimination, retro-aldol cleavage or Claisen condensation reactions. Many of these enzymes are involved into the metabolism of amino-compounds (amino acids, amino-sugars, polyamines, etc.) [19,67].

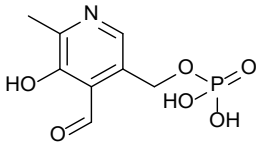

Figure i-8. Pyridoxal 5'-phosphate (PLP), the cofactor of PLP-dependent enzymes.

Transaminases are PLP-dependent enzymes of types I and IV (depending on the folding). In living organisms, TAs are involved in the synthesis and the degradation of amino acids, and in the synthesis of some secondary metabolites [21,68,69].

There are two sub-classes of transaminases. α-TA catalyze the transfer of an amino function between alpha-amino acids and alpha-keto acids (the acceptor-carbonyl functions is directly bound to a carboxylic function). ω-TA catalyze the amino transfer on a non-alpha carbon (in addition to the acceptor-carbonyl function, the acceptor molecule may contain a carboxylic function, but is not located on the α-carbon). Among ω-TA, amine-transaminases (ATA), are enzymes that accept amino-acceptors even if they do not bear a carboxylic function next to the carbonyl-acceptor function. Thus, ATA enzymes can convert ketones and aldehydes [19,70,71].

The R-selective ATA transaminase from the soil microorganism *Arthrobacter sp*. KNK 168 has been intensively studied and characterized in the last decade [72,73]. A homologue of this enzyme (99.7% identity) has been commercialized by Codexis, as ATA-117, and the 3D structure has been recently published [74]. It has been the starting point for the production of an engineered enzyme, ATA-117-11Rd, that was developed for the biocatalytic production of R-Sitagliptin [18], and Suvorevant [75,76]. We use this enzyme as the starting point for a more detailed description of the structure, active site, specificity and reaction mechanism; then we discuss the limitations of ATA and the corresponding mitigation strategies.

1.3.2 Structure, specificity and mechanism

ATA transaminases are homo-dimeric enzymes. Two half-active sites are located on each monomer. The two monomers must be assembled for the active sites to be catalytically active [77] (Figure i-9, left).

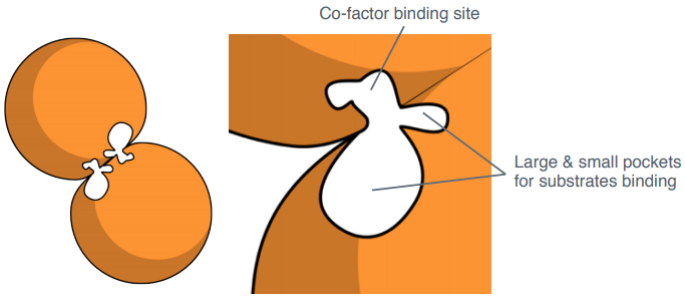

Figure i-9. Schematic representation of ATA enzymes. (Left) Scheme of ATA homo-dimers. Subunits must be assembled to form two sites that are catalytically active. The two active sites are located at the interface between subunits. (Right) Schematic representation of an active site.

The active site is made of three pockets: one is dedicated to the PLP binding (Figure i-9, right), the two others are assigned to the substrate binding. The PLP-binding pocket exhibits an essential lysine residue for the reversible covalent fixation of the cofactor in its imine derivative (see mechanism, Figure i-10). The small substrate pocket only accepts small organic functions (*e.g.* methyl groups). The large pocket is more versatile and accepts larger organic groups (alkyls chains, carboxylic acids, ethers functions, aromatics, etc.) [50]. Thus, ATA-117 is able to catalyze the formation/consumption of amines that contain a methyl group on one side, and larger organic functions on the other side of the amine.

Transaminases act through a "ping-pong bi-bi" mechanism [19,78,79] (Figure i-10), catalysing two successive bi-molecular reactions (hence "bi-bi"), the second one following the exact reversed sequence of the forward one. The enzyme reaches an intermediate state after the first half-reaction, and "bounces back" into its initial state after the end of the second half-reaction (hence "ping-pong").

The first step (Figure i-10a) consists in the formation of internal aldimine: the cofactor is covalently, but reversibly, bound to the lysine residue located in the PLP-binding pocket.

Then, the amino donor (here, represented as an amino acid, *e.g.* D-alanine) enters into the active site and is placed in its binding pocket (Figure i-10b). The active site only accommodate one enantiomer of a given chiral amine, hence the enantiospecificity of the transaminase [21]. Then, by imine-amine exchange, the amine function (from the amino donor) substitutes the lysine residue (bounded to PLP), and binds the cofactor as an imine intermediate (the lysine anchoring point is then released). In the next step (Figure i-10c), a basic residue located in the active site tears off the proton located on the alpha-carbon and the pyridinium ring of the cofactor pulls the delocalized electrons. Electrons are then pushed back and the cofactor is protonated on the other side of the substrate nitrogen by acid catalysis. Hence, electron displacement and acid/base catalysis result in the isomerization of the imine intermediate into a so-called external imine formed between the nitrogen and the alpha-carbon of the amino donor. As a last step of the first half-reaction (Figure i-10d) the external imine is hydrolyzed, releasing a carbonyl compound as a by-product (here, an α-keto acid). The cofactor stays in the active site in an aminated form, namely pyridoxamine 5'-phosphate (PMP). Thus, the first half-reaction consists in the deamination of the amino donor (transformed into a keto derivative) and the amination of the PLP (into PMP). Then, the second half-reaction occurs in the exact reverse sequence of events (Figure i-10 from e to h), but using a keto-substrate as amino-acceptor and releasing a chiral amine [80–82]. As the transamination reaction is an equilibrated chemical reaction, this mechanism can be read in both ways.

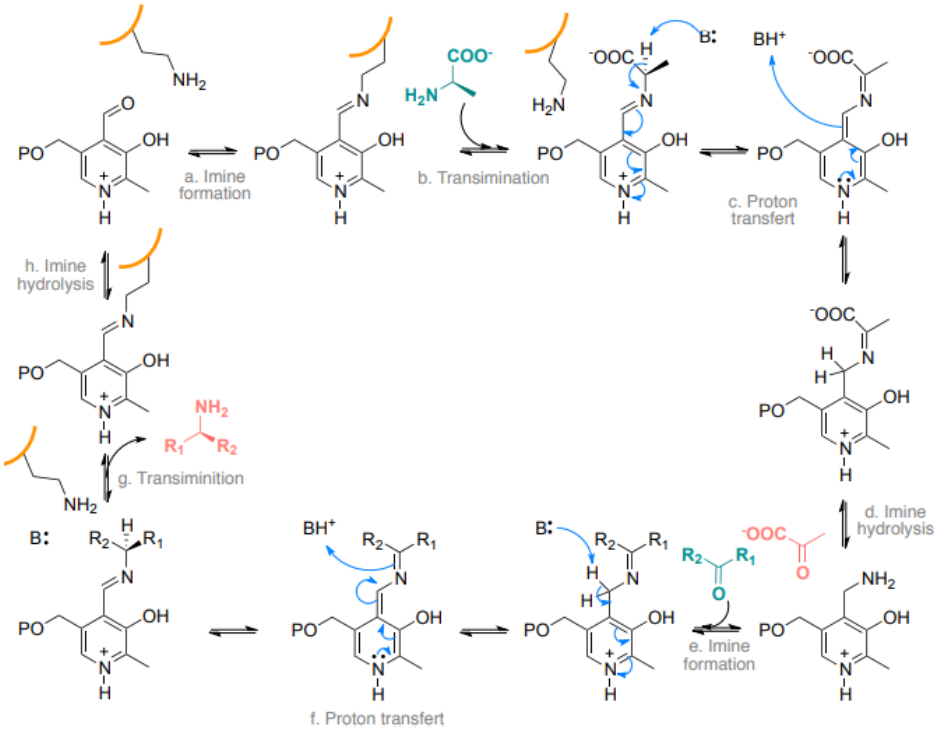

Figure i-10 – Transamination mechanism. Substrates and products of the reaction are depicted in green and red respectively. Two half-reactions execute the ping-pong bi-bi mechanism: from (a) to (d), the amine substrate reacts with the PLP cofactor to form the ketone by-product and a PLP amine-derivative (PMP, Pyridoxamine phosphate); from (e) to (h), the ketone substrate reacts with the PMP to form the PLP and release the amine product. PO stands for phosphate, and B for base. Adapted from [80–82].

1.4 Transaminase-catalyzed synthesis of amines: industrial relevance, challenges and opportunities

Chiral amines can be produced via three different types of enzymatic reactions using ω-transaminases [71,83] (Figure i-11): (i) kinetic resolution, (ii) asymmetric synthesis, and (iii) deracemization.

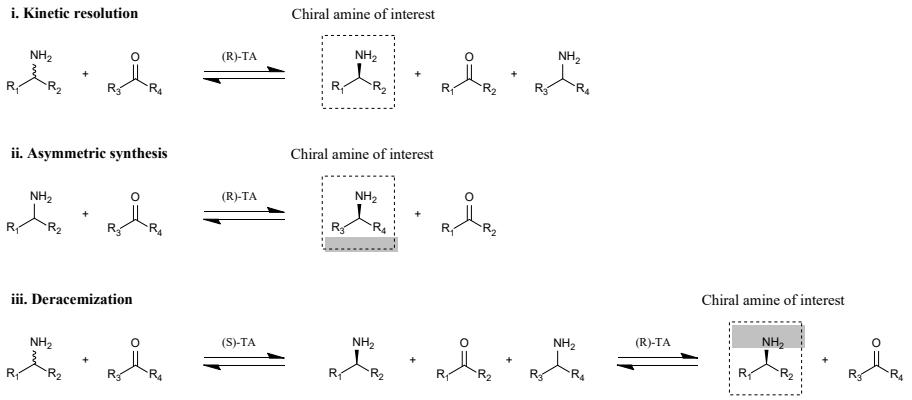

Figure i-11. Reactions catalyzed by transaminases for the production of chiral amines.

The kinetic resolution starts with a racemic mixture of enantiomers, and the enantioselective enzyme converts only one enantiomer into the corresponding keto-compound. At the end of the kinetic resolution, one enantiomer of the racemic mixture has been converted into ketone, the other one stays unconverted. An aminated by-product is also present in the final mixture. Thus, the maximal yield for the production of chiral amines using kinetic resolution is only 50 %. Also, when using amines (not amino acids) as amino donor, the co-product is a ketone (not a keto acid as in the biological systems) that can inhibit the transaminase if it accumulates in the medium [21,71,84]. The main advantage of the kinetic resolution is that it only requires one enantioselective enzyme [80].

In the asymmetric synthesis, a pro-chiral ketone is converted into a chiral amine using an amino donor and producing a ketone by-product. If the enzyme is perfectly enantioselective and the chemical equilibrium position is favourable, the maximal yield is 100 % as all the pro-chiral ketone is stoichiometrically transformed into chiral compound. Moreover, this method only requires one enzyme. However, the asymmetric synthesis *via* transamination suffers from two severe limitations: first, most transaminases are inhibited by ketones (*e.g.* acetone when the amino donor is

isopropylamine, ISO). Second, the asymmetric synthesis of chiral amines (that are not amino acid) is not favoured thermodynamically [71,80]. In Nature, transaminations between α-keto acids and α-amino acids are fairly equilibrated reactions (Figure i-12, top), because α-keto acids and α-amino acids substrates and products have similar free energies [21]. However, thermodynamically, amines (*i.e.* not amino acids) are less stable than amino acids, while ketones (as compared to α-keto acids) are more stable than α-keto-acids (Figure i-12, bottom). Thus, the chemical equilibrium is driven in the unwanted direction [21]. Employing amines as amino-donor (*e.g.* ISO) instead of amino-acids allows benefiting from a less unfavourable thermodynamic equilibrium.

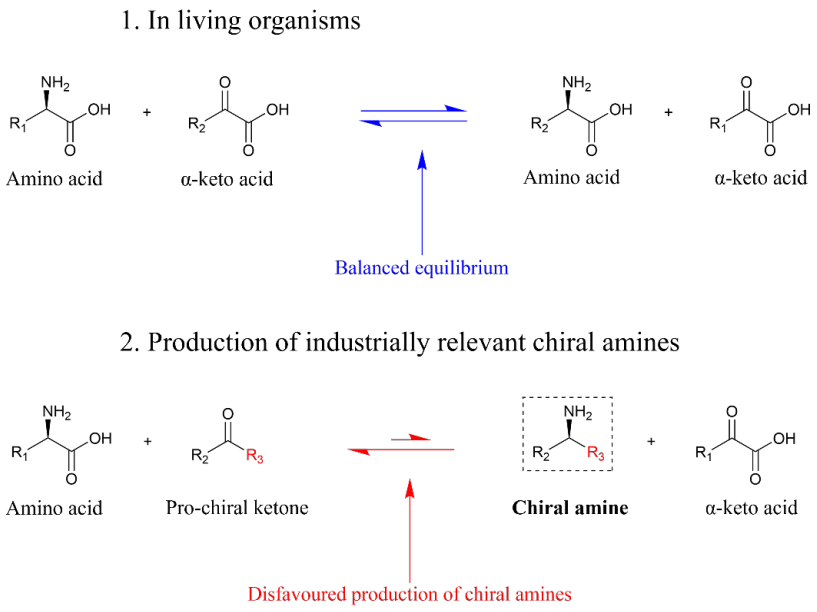

Figure i-12. Transamination for the production of chiral amines. Transaminations that involve only α-amino acid and α-keto acids (as mostly the case in living organisms) are governed by a well-balanced equilibrium. As the chemical and pharmaceutical industries need to produce chiral amines that are not amino acids (*i.e.* R is not a carboxylic acid), the transamination requires the use of ketones that are not α-keto acids. However, ketones are not easily aminated. Thus, the equilibrium reaction to produce chiral amines is not favoured.

Deracemization involves a kinetic resolution, starting with a racemic mixture, followed by an asymmetric synthesis. First, an enantioselective transaminase (*e.g.* S-selective TA) converts the distomer from the racemic mixture into the corresponding ketone, leaving the eutomer untouched. Then, a second transaminase of reversed enantioselectivity (*e.g.* R-selective TA) back-converts the ketone into the eutomer. Thus, by this method, the maximal theoretical yield is 100 % [85], and no inhibiting ketone is accumulated, as only α-keto acid is accumulated at the end of deracemization (if starting from α-keto acid as amino acceptor). However, this method requires two enzymes (and suffers from unfavourable thermodynamics in the asymmetric synthesis reaction) [86].

1.4.1 Industrial relevance

Some transamination reactions are already developed at kilo- and pilot-scales for drug manufacture in batch reactors [87], *e.g.* Sitagliptin (anti-diabetic drug), Suvorexant (sleep regulation) and Ivabradine (heart-rate regulation) production. R-Sitagliptin is produced by Merck at high concentration (250 g/L), in 50 % DMSO at 50 °C, using the engineered transaminase ATA-117-11Rd (Figure i-13a). In 2009, Merck scaled up the new process to pilot scale, and plans to commercialize this technology are now moving forward [88]. Thus, the transamination reaction should be implemented instead of the chemocatalytic synthesis involving a rhodium catalyst and high-pressure hydrogen [18,19]. The product obtained by the biocatalytic approach had higher optical purity which made further crystallization steps unnecessary; the total waste production was cut by approximately 20% and the productivity of the global process was increased by ca. 53% [89].

The same enzyme is used by Merck to produce Suvorexant (MK-4305) at kg scale: the biocatalytic transamination reaction uses ISO as the amino donor

and significantly shortens the synthetic pathway by leading to a key-intermediate (Figure i-13b). The entire synthesis requires only four linear steps for completion and proceeds in 43% overall yield [90,91].

ATA-117 is also employed to produce a key building block in the synthesis of another candidate for the treatment of insomnia: Filorexant (MK-6096) [75]. Performed in a 100 L total volume and starting from 4.5 kg keto-diester substrate, the transamination reaction uses D-alanine as amino donor and a coupled Lactate dehydrogenase/Glucose dehydrogenase (LDH/GDH) regeneration system. It resulted in 74% yield and 99% enantiomeric excess. This transamination reaction was integrated in the nine-steps chemoenzymatic synthesis of MK-6096 (at kg-scale). A 13% overall yield was first achieved. Improvements of the biocatalytic system (*i.e.* CDX-010 transaminase employing ISO and a different keto-diester precursor, enabling the use of a single-enzyme system) allowed further increasing the synthesis efficiency [92,93] (Figure i-13c). The MK-6096 target is now synthesized through a four-step process based on crystallization-induced dynamic resolution (CIDR) of the chiral intermediate, reaching 40% overall yield.

Another remarkable example is the use of ATA from *Vibrio fluvialis* (*Vf*-ATA) in a pre-industrial process developed by AstraZeneca for the production of a key intermediate in the synthesis of a kinase (*i.e.* JAK2) inhibitor, AZD1480 (used for the treatment of idiopathic myelofibrosis) [94,95] (Figure i-13d). S-MBA was used as amino donor and an in-situ co-product removal (IScPR)-based strategy was employed to push the equilibrated reaction towards the formation of the targeted intermediate [96]. Briefly, the acetophenone co-product was extracted from the aqueous phase by the use of a biphasic system (20 % (v/v) toluene). Subsequent scale-up of the biotransformation allowed reaching 68% yield and 99% enantiomeric excess when employing the Codexis enzyme, TA-P1-A06. The intermediate has been then used in the chemoenzymatic synthesis of AZD1480 on a 100 L scale, which resulted in > 30% overall yield.

In 2017, Burns et al. (Pfizer Inc.) reported a chemo-enzymatic route for the synthesis of key chiral intermediates of a γ-secretase inhibitor, employing a transaminase and an alcohol dehydrogenase [97] (Figure i-13e). The researchers performed a screening of a relatively large enzyme library for the conversion of a substituted tetralone to the corresponding S-amine intermediate. ATA-47 from LCeta, was selected to run the reaction at large scale. The scaled-up transamination enabled the production of nearly 40 kg of enantiopure amino-compound, in a 94% isolated step yield.

In 2021, an efficient large-scale production of a chiral precursor of Sacubitril (a key component of the heart failure drug Entresto), was reported by researchers at Codexis Inc [98] (Figure i-13f). Starting from a *Vf*-ATA variant (ATA-217) displaying unsatisfactory biocatalytic performance, 11 rounds of directed evolution were performed to obtain a more active mutant. Additionally, an IScPR strategy based on acetone evaporation was employed to drive the thermodynamic equilibrium (by running the reaction at as high as 58 °C). In lab-scale assays, the final variant (CDX-043) reached 90% conversion at high ISO (1 M) and ketone substrate concentration (75 g/L) within 24h at 58 °C. CDX-043 was subsequently selected for the multi-kg scale sacubitril production. To this end, a large-scale fermentation was implemented to produce c.a. 200 kg of CDX-043 (lyophilized clarified cell lysate), which was in turn used to produce a total amount of c.a. 20 kg of the sacubitril precursor.

A novel synthesis pathway featuring a transamination reaction leading to MK-7246 drug (used for the treatment of respiratory disease) was recently implemented at pilot-plant scale production (> 100 kg). This route proceeds in eight steps, requires no chromatographic purification and features a dramatically improved overall yield and productivity with respect to the previous reported chemo-catalytic syntheses. CDX-017 transaminase, with ISO as amino donor, were employed for the transamination reaction [76] (Figure i-13g).

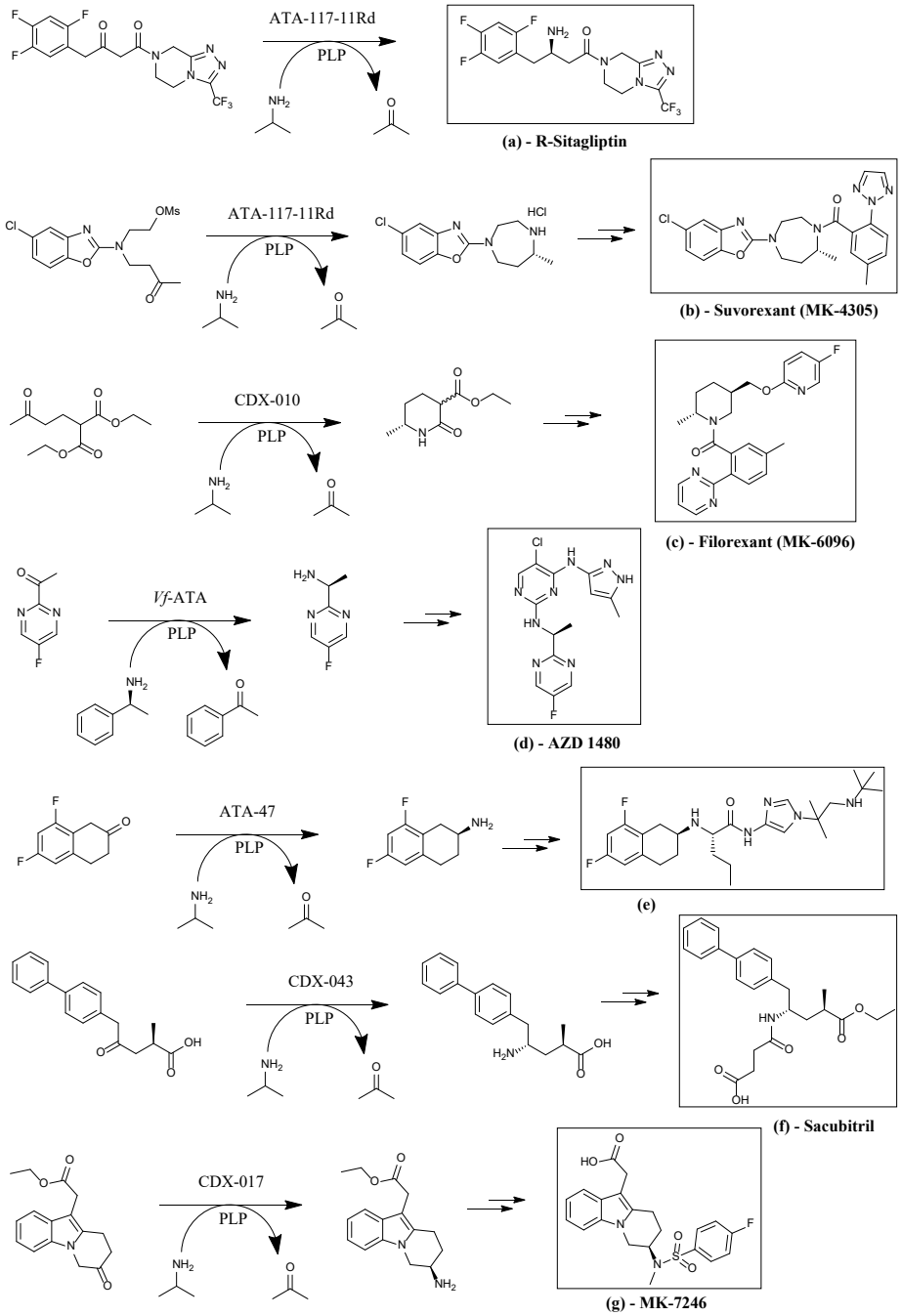

Figure i-13. Selected applications including transaminations implemented at large-scale (industrial and multi-kg scale) in batch. OMs stands for methanesulfonate (mesylate) group. Framed compounds represent the target chiral amine of interest.

Other interesting examples were reported using commercially available ATAs, although on a smaller scale (> 100 mg to g scale) [66,99]. Typically, a *Vf*-ATA variant (*Vf*-TA r414) displaying a 60-fold increase in activity toward the oxooctanoate substrate with respect to its wild-type counterpart, allowed the straightforward synthesis of Imagabalin (277 mg, 95% diastereomeric excess) [100]. Similarly, S-Ivabradine was successfully synthesized at a preparative scale, by means of a four-step sequence including transamination reaction (i.e. using transaminase from Codexis with ISO as amino donor). A 50% overall yield and excellent enantioselectivity were obtained [19,101]. Besides, an ATA from *Chromobacterium violaceum* (*Cv*-ATA) was employed to efficiently perform the asymmetric synthesis of a key intermediate for the production of the anti-allergic drug Ramatroban. The practical applicability of this transamination reaction was demonstrated on a 500-mg scale. Excellent yield (96%) of the R-amine (in enantiopure form) was obtained [102].

In 2021, von Langermann *et al.* [103] implemented a crystallization-assisted semi-continuous transamination for the gram-scale preparation of S-(3-methoxyphenyl)ethylamine, a valuable intermediate of Rivastigmine. Briefly, the authors leveraged on an *in-situ* product crystallization (assisted by the evaporation of the by-product, acetone, under mild vacuum) to shift the transamination reaction towards completion. The resulting crystal was easily recovered via filtration, and the enantiopure amine product was obtained at high concentration (> 1 M). The transaminase from *Silicibacter pomeroyi* (*Sp*ATA) was employed for this study. Kohrt and co-workers demonstrated the synthesis of a valuable chiral spirocyclic intermediate (1-Oxa-8-azaspiro[4.5]decan-3-amine) at the gram scale (580g), employing Codexis ATA-200.

Such biocatalytic reaction reached 82% yield and allowed boosting the enantiomeric excess from 70% to 97.8% with respect to the chemocatalytic route (*i.e.* a hazardous azide-mediated S_N2 reaction followed by a Staudinger reduction) [104].

Last but not least, we must mention the production of S-methoxy-isopropylamine by an optimized transaminase from *Bacillus megaterium*, using ISO as the amino donor [105]. The product is a key-intermediate for the production of Metolachlor, a widely used herbicide [34].

1.4.2 Challenges and mitigation strategies

Despite the successful examples cited in the previous section, the use of transaminases for the production of chiral amines suffers from two major limitations: (i) when using amines as amino donor, the transaminases are strongly inhibited by the ketone by-product; and (ii) the thermodynamics does not favour the production of chiral amines that are not amino acids. Those limitations hamper the enzymatic production of chiral amines at industrial scale. Therefore, strategies have been developed to obtain chiral amines at high yield, and high concentration. They can be split in three categories (Figure i-14): (i) strategies aiming at enhancing the enzyme performance or robustness, (ii) strategies aiming at shifting the equilibrium by physico-chemical effects (mono-enzymatic methods) or by combining several enzymes in addition to TA (multi-enzymatic methods) [21,106], and (iii) strategies aiming at enhancing the enzyme recoverability by immobilization in/on solid supports. In practice, many studies have combined several strategies [7], and the classification is not so straightforward.

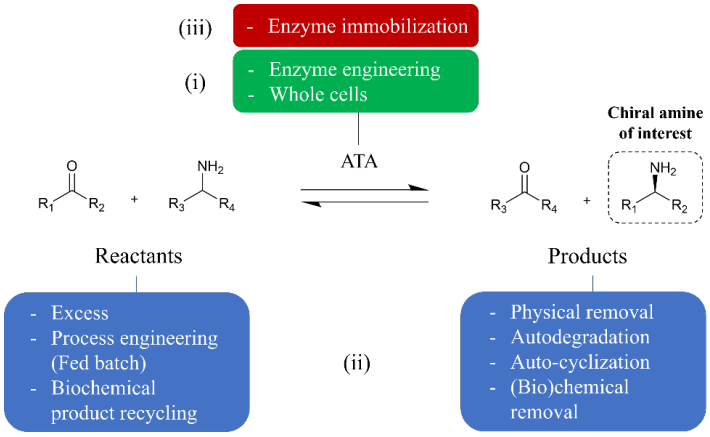

Figure i-14. Enhancement strategies. Strategies addressing the issues of ketone inhibition and unfavourable thermodynamics.

1.4.2.1 Enhancing enzyme scope and robustness

At the enzyme scale, there are three approaches to prevent enzyme inhibition by ketone compounds: applying enzyme engineering techniques on available enzymes, using whole cells, and exploiting extremophiles-derived enzymes.

The enzyme engineering strategy allows the production of enzyme mutants that exhibit new properties as compared to the wild type enzyme. For example, engineered transaminase could be more tolerant to high substrate and/or product concentrations. The resulting enzyme would not be inhibited anymore (or at a lower level) [21]. This strategy allows getting enzymes that are more suitable for industrial applications: stable under non-physiological conditions (high concentrations, organic solvent), increased working and storage duration [21,107]. In practice, there are two ways to produce mutated enzymes [71].

First, directed evolution approaches based on iterative cycles of random mutagenesis and variant screening can be envisioned [108]. In this strategy, the enzyme structure is not necessarily known and mutations are introduced in the gene encoding the enzyme of interest in a random or partially random manner.

A library of microorganisms expressing the enzyme variants is then created. Then, the library is screened to identify the colonies that express the enzyme exhibiting the interesting properties. The interesting colonies are then selected. For example, Kim *et al.* [109] created and identified a mutated version of *Vibrio fluvialis* transaminase that shows better tolerance to aliphatic ketones (as compared to the wild-type transaminase).

The second method for mutated enzymes production is based on site-specific mutagenesis. This requires knowing the enzyme structure. By a rational design approach (identifying the link between amino acid sequence and enzyme 3D structure), it is possible to predict the properties of a desired mutant where a specific amino acid would be replaced by another (predictions and modelization *in silico*) [71]. However, our capacity to rationally predict mutations that will modify the properties of an enzyme in a desired way is still very limited and many strategies are combining rational and random approaches. For example, Savile *et al.* [18] used a substrate walking approach to predict the effects of mutations of the active site on the substrate pocket affinity. The wild type enzyme (ATA-117) does not accept large substrate in its pocket. After 11 rounds of mutations (a combination of site-directed and random mutations), a mutated enzyme (ATA-117-11Rd, exhibiting 27 mutations) was able to accept larger substrate in its active site pocket. Then, the mutated enzyme was able to catalyze the synthesis of Sitagliptin, an anti-diabetic drug (see Figure i-1), with excellent yield (92%) and enantioselectivity (> 99%). Moreover, the mutated enzyme exhibited better tolerance to the organic solvent (DMSO) and amino donor (ISO). Besides engineering known enzymes, the availability of genome sequences has been increasing exponentially, giving straightforward access to large diversities of genes encoding natural enzymes including ATAs that can be screened for specific activities and used as starting points in directed evolution campaigns [7]. These novel biocatalysts represent a massive addition to the application of ATAs for the industrial synthesis of enantiopure amines [110]. Nevertheless,

high cost, time consumption and uncertainty are intrinsically associated with the engineering of enzymes featuring desired properties [21].

In addition to enzyme engineering, the sourcing of biocatalysts from extremophilic organisms also taps into key strategies to address the insufficient stability of ATAs [111–113]. Extremophiles are microorganisms that are adapted to survive in ecological niches such as extreme temperatures (– 5 and 130°C) and pH (0–12), high salt concentrations (3-35%) and high pressure (up to 1000 bar) [114]. The adaptation process of extremophiles has affected the features of their enzymes providing them remarkable properties with respect to their mesophilic counterparts. Although these natural organisms are often difficult to cultivate in large quantities in the laboratory, their genes can be cloned and the corresponding enzymes overexpressed in large amounts, for example in *Escherichia coli* [115]. Accordingly, extremophile enzymes often result in more robust biocatalysts, that offer versatile tools for a variety of industrial applications. For example, halophilic enzymes remain active under extremely high salt concentration and have been reported to be stable under ''dry condition'' (low water concentration) [116,117]. As salt greatly reduces water activity of the medium, halophilic enzymes might become the choice for biocatalytic processes performed in low water activity environments like aqueous/organic and non-aqueous media [118,119]. Similarly, thermophilic strains provide a rich library of proteins with increased stability not only to high temperatures, but also to organic solvents and proteolytic enzymes [115,120,121].

In 2015, the Paradisi group cloned and expressed the first ATA from a halophilic bacterium, *Halomonas elongata* (HeWT) [122]. HeWT showed good tolerance to a series of co-solvents up to 20% (v/v), and optimum activity at pH 10. It was highly S-selective and showed broad substrate scope, making it a promising candidate for industrial applications [123]. New ATAs have been recently identified from thermophilic microorganisms [124,125], including *Geobacillus thermodenitrificans* and from *Thermomicrobium roseum* [126,127].

These biocatalysts display optimal temperatures at 65 and 80 °C, respectively, and their activity increases after thermal pre-treatment at 60–65 °C. Arguably, the development of novel ATAs based on extremophiles enzymes that are be further improved through enzyme engineering is currently emerging as major playground researchers who can start exploring pristine chemical spaces [128,129].

Another strategy consists in the use of whole cells. In this case, the interesting transaminase is overexpressed in living cells, which are then used as such as living catalysts. In this way, the enzymes are protected against extreme environment conditions by the natural cytoplasmic membrane. For example, Kroutil *et al.* [130] used *Escherichia coli* cells (containing an over-expressed transaminase) to produce aliphatic chiral amines by kinetic resolution. The main disadvantages in the use of whole cells are (i) substrates and products must be able to penetrate and come out of the cells; (ii) the need to feed the living cells, and the potential interferences with other metabolic pathways [131].

1.4.2.2 Enhancing reaction yield by shifting the equilibrium

The equilibrated transamination reaction that is catalyzed by the transaminase is often unfavourable, and should be pushed towards the product side either by using an excess of substrate, or removing a product. This can be achieved by chemical, biocatalytic, or engineering strategies.

An excess of ISO (50-fold excess) has been successfully used by Truppo *et al.* [132] in the amination of acetophenone, using ATA-117. The product, R-methylbenzylamine (R-MBA) was obtained at high yield (95 % conversion) and high enantiomeric excess (> 99%). However, most wild-type ATAs do not accept ISO under standard conditions, and need thus to be engineered to display such desirable property [12,122].

Inhibition caused by the substrate (in high concentration) can be avoided by process engineering: a fed-batch strategy allows feeding progressively the reaction medium with the substrate, so that its concentration remains below the inhibition limit. Lye *et al.* [133] used such fed-batch strategy for the progressive addition of ISO in a bioreactor (containing a transketolase and a transaminase). They synthesized a chiral amino-alcohol product ((2S,3S)-2-aminopentane-1,3-diol) with satisfying yield (70 %), avoiding the inhibition caused by high ISO concentration (due to alkaline properties of ISO).

Another strategy used to shift the equilibrium towards the asymmetric synthesis consists in the removal of products and by-products [21]. Shin *et al.* [134] used ISO as amino donor for the production of L-homoalanine (from 2-oxobutyric acid, previously synthesized from L-threonine), leading to the co-production of acetone that was easily eliminated from the reaction medium by evaporation. Products and co-products can also be extracted from the reaction medium by liquid-liquid or liquid-solid extractions [135–138]. Noteworthily, as previously mentioned, researchers from von Langermann group implemented an *in-situ* product crystallization (ISPC) assisted by co-product (acetone) evaporation to perform the synthesis of S-methylbenzylamine derivatives, such as S-(3-methoxyphenyl)ethylamine (S-MEA) [103,139]. Such an elegant strategy relied on the use of crystallization agent (i.e. bulky carboxylic acid such as 3-diphenylpropionic acid) able to form poorly soluble crystalline salts with S-MEA, hereby driving the transamination equilibrium.

Products can also be removed from the system by an auto-conversion pathway. Green *et al.* [140] propose the use of ortho-xylylenediamine as amino donor for the transamination (using ATA-113).

The by-product (1H-isoindole) spontaneously undergoes tautomerization, leading to the formation of 2H-isoindole that polymerizes and precipitates into a blue compound.

This spontaneous product tautomerization and subsequent precipitation drives the chemical equilibrium towards the production of S-1-(4-fluorophenyl)propan-2-amine (from (4-fluorophenyl)acetone). However, it should be noted that the amino donor employed in this study is more expensive than alanine or isopropylamine.

Product removal has also been conducted through co-product cyclization. For example, by using lysine as amino donor, Hsu *et al.* [141] produced L-homophenylalanine (from 2-oxo-4-phenylbutanoic acid) in high yield (97 %) and with high enantiomeric excess (> 99.9 %), as the by-product (2-keto-6-aminocaproate) spontaneously cyclizes and then, drives the equilibrium. Also, this cyclization allows avoiding the inhibition by the by-products.

In multi-enzymatic approaches, another enzyme is used in conjunction with the transaminase, either to consume the by-product, or to recycle the by-product into fresh substrate. By using enzymes purified from similar cell media, multi-enzymatic methods (also called enzymatic "cascades") are easily practicable in one-pot system [50] (Figure i-15). While several types of cascade have been defined in the field of biocatalysis (linear, parallel, orthogonal, and cyclic) [50], the one that is the most relevant in the field of chiral amine synthesis using transaminase is the orthogonal cascade. In the latter, a first reaction allows the production of a product of interest and a by-product (or intermediate) that is transformed in a second reaction. This kind of cascade allows the equilibrium displacement (by withdrawing the by-product) towards the formation of the product of interest. When alanine is used as amino donor, the transamination leads to the production of pyruvic acid (or pyruvate salt) as the by-product. Several strategies have been implemented to catalyze the consumption of pyruvate to shift the equilibrium.

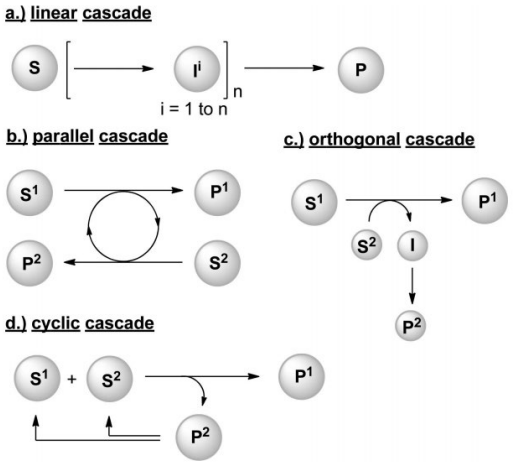

Figure i-15. Overview of different types of enzymatic cascades. S, I and P respectively stand for starting material, intermediate, and product. P^1 is the desired product. Figure reproduced from [50].

For example, lactate dehydrogenase (LDH) allows converting pyruvate into lactic acid, using NADH as the cofactor (Figure i-16) [83,132,142,143]. This strategy has been successfully used by Meadows *et al.* [135] for the production of S-1-(5-fluoropyrimidin-2-yl)ethylamine. Moreover, the amine of interest was extracted in an *in situ* product removal (ISPR) approach by supported liquid membrane (SLM), leading to a final 98 % yield, and high amine purity.

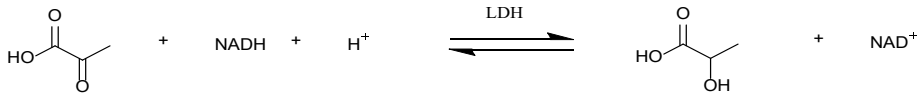

Figure i-16. Reaction catalyzed by lactate dehydrogenase. Lactate dehydrogenase (LDH) allows to transform pyruvic acid into lactic acid, using NADH.

Other enzymes allow converting pyruvic acid. For example, pyruvate decarboxylase catalyzes the decarboxylation of pyruvate into acetaldehyde and CO_2 [144]; and alanine dehydrogenase allows the recycling of pyruvate into alanine (the amino donor), using ammonia and NADH as a cofactor [145].
If ISO is used as amino donor, acetone is produced as by product. Then, alcohol dehydrogenases (*e.g.* yeast alcohol dehydrogenase, YADH) can

catalyze the reduction of acetone into isopropyl-alcohol, as proposed by Berglund *et al.* [146] (Figure i-17).

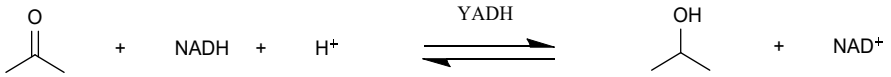

Figure i-17. Reaction catalyzed by yeast alcohol dehydrogenase. Yeast alcohol dehydrogenase (YADH) catalyzes the reduction of acetone in the presence of NADH.

Many of those enzymes are using NADH as reducing agent, in stoichiometric amount. However, this reagent is highly expensive and thus, needs to be recycled. Two main enzymes allow the recycling of NADH (towards the implementation of parallel cascades): glucose dehydrogenase (GDH) and formate dehydrogenase (FDH). GDH catalyzes the oxidation of D-glucose by NAD^+ (the oxidized form of NADH) into ∂-gluconolactone (releasing NADH; Figure i-18). This method has been extensively studied [86,132,145,147]. Formate dehydrogenase catalyzes the oxidation of formic acid in the presence of NAD^+, into CO_2 and allows the recycling of NADH [146,148].

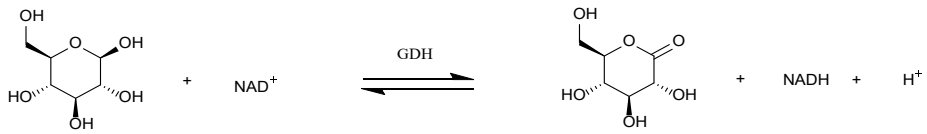

Figure i-18. Reaction catalyzed by glucose dehydrogenase. Glucose dehydrogenase (GDH) catalyzes the oxidation of glucose by NAD^+ to form ∂-gluconolactone and NADH.

1.4.2.3 Enhancing recoverability and reusability: the key role of immobilization

The great efficiency of enzymes is well established. Once the gene coding for the enzyme of interest is known, it is usually possible to produce the latter at large scale and to isolate it. It may be noted that technical difficulties can

be encountered, related to the lack of stability for highly engineered enzymes, or with purification (e.g. filtration is not straightforward; ATA-117 monomer is 3 nm in size [74]). More significantly, for the subsequent use of the free enzymes in industrial processes, poor long-term stability and difficult recovery and recycling often represent the most important shortcomings [149–151].

Immobilizing the enzymes on solid carriers allows envisaging a facile recovery of the biocatalysts at the end of the reaction. Thanks to immobilization, it can be envisioned to reuse the enzymes, or to implement continuous processes, where the enzymes are maintained in the reactor while the reaction medium is flowed through (*vide infra*, see state of the art about flow transaminations exposed in Chapter I) [151–153]. The facile separation of the solid biocatalyst from the reaction medium also allows minimizing or avoiding protein contamination of the product [154,155]. Furthermore, some immobilized enzymes have shown remarkable enhancement of their properties as compared to the free enzyme: *e.g.* enhanced selectivity [156], improved stability towards storage and operational conditions [157,158]. While most enzymes are inactive or perform poorly in organic solvents, immobilized enzymes may exhibit a higher activity in organic [159]. However, despite all the potential advantages offered by enzyme immobilization, it was estimated in 2009 that only 20% of industrial biocatalytic processes employ immobilized enzymes in their processes [160], resulting in a very modest market share (20%) of immobilized enzymes relatively to the total enzyme market [161,162]. Hence, there is still room for improvements in the development and application of immobilized enzyme products, which requires an accurate understanding of both technical and economic factors.

1.5 Towards the use of membrane-immobilized transaminases

Enzyme immobilization on solid carriers has been extensively studied during the past decades, on a wide variety of carriers, such as inorganic powders or monoliths, polymeric resins, biopolymers (see section 1.2 of Chapter I) [152,163,164]. As far as transaminases immobilization is concerned, ready-to-use synthetic resins (e.g. Relizyme) are the most commonly employed supports [163,165], enabling high immobilization yields, easy recovery and reuse of biocatalysts. However, given the limitations faced by transamination reactions, enzyme immobilization on membranes should also be considered, as it offers the added benefit of performing biocatalytic reactions alongside membrane operation in a single step. For instance, removing a product can shift the reaction equilibrium toward the product side, thereby increasing the product yields [166]. Additionally, membranes can also allow for controlled reagent introduction, which is of particular interest to prevent ATAs inhibition by their keto-substrates.

Thus, the combination of biocatalytic reactions and membrane operations in "enzyme-membrane-reactors" (EMR) holds significant potential for enhancing biocatalytic processes. Such integrated systems, simultaneously combining biocatalytic reactions and membrane operations, allow for more productive flow processes displaying enhanced products yield (by increasing the conversion and/or the selectivity of the process, via e.g. membrane-assisted product separation) and boosted enzyme kinetics (by preventing enzyme inhibition via controlled reagent introduction). We argue that several enzymatic processes, including transaminations, can benefit from such cross-fertilization between membrane technology and heterogeneous biocatalysis. Integrated hybrid processes that enable simultaneous flow biocatalytic reactions and product separation (e.g., to shift equilibrium) or controlled substrate addition, are particularly valuable in organic syntheses, notably for

the production of pharmaceutical intermediates and fine chemicals (e.g. chiral amines).

2. Objectives

As exposed in the general context of the thesis, the coupling between transamination reactions and membrane technology can be highly beneficial, as it may address several limitations faced when targeting the asymmetric synthesis of enantiopure amines. In this work, we focus on this specific case-study by looking to master the immobilization of transaminases onto membranes, and by exploiting the resulting biocatalytic membranes in challenging asymmetric synthesis of enantiopure amines.

Thus, the general aim of this PhD thesis is the obtention of efficient lab-scale membrane-immobilized transaminase reactors for the intensified production of industrially relevant chiral amines in continuous flow mode. To this end, we set the following specific objectives:

(i) producing a precise overview of existing, recent, pertinent knowledge about continuous flow-mode synthesis of chiral amines using immobilized transaminases on one side, and of enzyme-membrane-reactors applications on the other side.

(ii) controlling immobilization of transaminases enzymes on polymeric membranes (i.e. avoid enzyme leaching from the carrier, maximize the specific activity and the stability). This entails the study and optimization of transaminases membrane-immobilization to obtain enantioselective, robust and reusable biocatalytic membranes (by determining optimal conditions for their controlled development (membrane surface functionalization process, enzyme immobilization));

(iii) displacing the chemical equilibrium towards the asymmetric synthesis of industrially relevant chiral amines via product separation. This implies the

implementation of those membrane-immobilized biocatalysts towards an industrially relevant transamination coupled with an *in situ* product separation (i.e. crystallization) to shift the equilibrium of the transamination. This proof of concept will allow to demonstrate the feasibility of performing high-yield asymmetric amine synthesis using membrane-immobilized ATAs in batch mode

(iv) producing chiral amines in high yields in continuous flow. This will be done *via* the transfer of this technology from batch to continuous flow mode in a lab-scale enzyme-membrane-reactor, for the intensified biocatalytic production of enantiopure amines. This will allow to pave the way for the set-up of upcoming hybrid flow processes, in which membrane operation allows to enhance the productivity of the heterogeneous transamination.

3. Strategy

The strategy that was used in this research to answer the objectives raised in the previous section can be articulated around two main parts, as outlined below.

Through the scientific reviews exposed in the first two parts (Chapters I and II), we aim to provide extensive and comprehensive state-of-the-art about flow transaminations and EMR, as well as recent trends and applications for the production of value-added chemicals.

The third chapter is dedicated to the optimization of transaminases immobilization on conventional polymeric membrane supports. This approach aims to create robust and reusable biocatalysts that stabilize transaminases and which display satisfying catalytic performance. Two transaminase immobilization strategies were investigated, leveraging prior membrane surface functionalization. Two different transaminases (one R-selective and one S-selective) were studied in this work. Polyacrylonitrile

(PAN) and polypropylene (PP) membranes were selected as commercially available and industrially relevant membrane carriers. We leverage electrostatic interactions (on functionalized PAN) or covalent grafting (on functionalized PP) strategies to avoid undesired enzyme leaching. The membrane carriers are characterized at different stages of the preparation to ensure the successful surface functionalization steps. After transaminase immobilization, the obtained membrane-immobilized transaminases are tested in a model reaction (i.e. kinetic resolution of a racemic mixture of 4-bromo-α-methylbenzylamine (BMBA)). This reaction consumes a chiral amine, and may therefore appear economically irrelevant but (i) allows us assessing enzyme activity in the elementary transamination act since it is not limited by the thermodynamic equilibrium, and (ii) is relevant in the context of production of complex ketones. An iterative research strategy is implemented: polymeric membranes are functionalized and subsequently characterized to assess the course of their modification; biocatalytic membranes are then obtained by immobilizing transaminases on the functionalized membranes; their catalytic efficiency is assessed by a kinetic resolution in batch mode. The results of this test reaction are used to feed a retroactive loop, with the idea to improve the steps of functionalization and immobilization, and therefore optimize the process.

In Chapter IV, the best performing immobilized ATAs (obtained in chapter III) are implemented towards an industrially relevant transamination, namely the asymmetric synthesis of R-2-fluoromethylbenzylamine (R-FMBA). After demonstrating the successful application of the membrane biocatalysts, we proceed to improve the productivity of the synthesis process. First, we rely on the use of production separation method in order to enhance the final amine yields.

To shift the equilibrium towards the product side, in-situ product crystallization is attempted while performing the biocatalytic reaction. Second, the transaminase immobilization and subsequent asymmetric synthesis are implemented in a flow reactor. By this way, the impact of such transition from batch to continuous flow mode on the ATA immobilization efficiency and on transamination productivity, is studied and assessed. The aim of this last step is to demonstrate the applicability of a membrane-immobilized ATA to catalyze an asymmetric synthesis in continuous flow-mode (which, to our best knowledge, has never been done so far).

Chapter I – State of the art of flow transaminations for (chiral) amines synthesis

The content of this chapter is entirely reported in our following publication (review) :

"Continuous flow-mode synthesis of (chiral) amines with transaminase: a strategic biocatalytic approach to essential building blocks". H. M. Arango, L. van den Biggelaar, P. Soumillion, P. Luis, T. Leyssens, F. Paradisi and D. P. Debecker, *React. Chem. Eng.*, 2023, **8**, 1505–1544.

ABSTRACT

As presented in the Context part, greener synthesis processes of enantiopure amines are needed for the manufacture of active pharmaceutical ingredients (APIs). Amine transaminases (ATAs) can catalyze the production of chiral amines through transaminations with perfect enantioselectivity and in mild conditions. Industrial applications of transaminations, however, remain scarce as the free enzymes often operate in restricted operational conditions and display limited stability. Batch reactors utilizing the free enzyme in solution also face issues regarding catalyst separation, recovery, and reuse. Moreover, the synthesis of most compounds of interest is thermodynamically unfavoured. Taking a side step, catalysis scientists design heterogenized biocatalysts that are more versatile and amenable to more productive continuous flow processes. A number of improvement strategies have been deployed, and these were exposed in the Context part. Here, we summarize and exemplify the advances (optimization of immobilization strategies, design of structured supports, development of integrated equilibrium shifting strategies, concatenation with purification, etc.) leading to more efficient heterogeneous biocatalytic systems based on transaminases operating in continuous flow mode.

1 Continuous flow-mode synthesis of (chiral) amines with transaminase: a strategic biocatalytic approach to essential building blocks

1.1 Introduction

As exposed in the Context part of the thesis, chemical processes dedicated to the production of active pharmaceutical ingredients (APIs) are known to generate significant amount of waste per unit mass of product (high E-factor) [6]. The specific case of the synthesis of chiral amines, which are essential building blocks for the pharmaceutical industry [7,8,167], is a prominent illustration of this issue. Industrially, the synthesis of chiral amines is operated via multi-step batch processes which usually feature low overall yield, produce large amounts of waste, and are energy-intensive. They are typically catalyzed by organometallic homogeneous catalysts based on toxic and depleted heavy metals (Ru, Rh, Pd) which usually operate at relatively high temperature, are not 100% enantioselective, and are difficult to recover [11,12]. In this context, it is of particular interest to develop more sustainable chiral amines synthesis methods [13,14].

Biocatalytic routes have gained considerable attention in the last decades as potentially effective and sustainable alternatives. Remarkably, amine transaminases (ATAs) catalyze the direct synthesis of chiral amines from pro-chiral ketones, using cheap and readily available amino donors (*e.g.* amino-acids) through transamination, with excellent enantioselectivity and in mild conditions. ATAs are catching the eye as tremendous achievements have been made recently, both at the fundamental and applied levels [18,19,91,95,97–99,168,169]. Industrial applications of biocatalytic transamination, however, remain scarce

for ATAs since they are usually employed as free enzymes in solution, which display limited stability. Batch processes utilizing such free enzymes do not allow easy catalyst separation, recovery, and reuse [163,170,171]. Additionally, thermodynamic limitations and substrate/product inhibitions tend to limit the applicability of transaminases in asymmetric synthesis of enantiopure amines [66].

To overcome these limitations, scientists aim at developing equilibrium shifting strategies and at enhancing the ATA robustness. This includes methods to (i) shift the thermodynamic equilibrium, (ii) expand the substrate scope and robustness, and (iii) enhance recoverability and reusability. For the last point, immobilization strategies are often proposed [165,172–174]. Enzyme immobilization has proven effective in generating heterogeneous biocatalysts that are often more versatile and amenable to more productive flow processes [163,167,170,171,175,176]. Importantly, the transition from homogeneous batch processes – where the enzyme is free in the liquid phase – to heterogeneous flow processes – where the enzyme is immobilized on a suitable carrier – is identified as a key to develop greener processes [161,177]. Continuous flow processes will allow envisaging more robust, green, and productive syntheses [178]. Thus, the state of the art on the immobilization of transaminases and their implementation in flow transamination processes is presented.

1.2 Transaminases immobilization onto solid supports – general overview

Immobilizing the enzymes on solid carriers allows envisaging the reuse of enzymes and or their implementation in continuous processes (where the enzymes are maintained in the reactor while the reaction medium is flowed through) [179].

Since one particular challenge is to make the enzymes recyclable while maintaining their activity, the enzyme leaching from the surface of the support during operation must be prevented. Avoiding enzyme leaching is of upmost importance regarding process sustainability and can be more challenging to achieve in continuous flow-mode as compared to batch. In most cases, a compromise has to be found between a good immobilization and a good retention of enzyme activity [180]. Indeed, the immobilization can strongly affect the enzyme structure or/and reduce the accessibility to active sites, and therefore, the enzymatic activity [157,181]. Therefore, the main challenges of immobilizing enzymes are: (i) getting an efficient attachment of the enzymes on the carrier to avoid the enzyme leaching, while concomitantly (ii) retaining the enzymatic activity.

It is generally admitted that enzyme immobilization has to be envisaged case-by-case, as a function of the enzyme properties (surface composition, charge, active site location), of the reaction of interest (operating conditions), of the solid carrier that is envisaged, and depending on the targeted improvements (stability, activity, substrate specificity, product selectivity, etc.). Immobilization methods are generally sorted in three categories: (i) Enzyme hooked at the surface of a support (either by adsorption, site-specific affinity attachment or covalent grafting), (ii) enzyme entrapment (i.e. the physical confinement of the enzyme within a porous matrix) and encapsulation (i.e. enclosure of the enzyme within a membrane or shell), (iii) enzyme cross-linking. Noteworthily, a combination of two immobilization strategies is often implemented in order to overcome the drawbacks presented by one immobilization strategy (*e.g.* cross-linking of encapsulated enzymes to prevent their leaching from the carrier porosity) [154,182,183].

Many excellent reviews cover extensively enzyme immobilization methods [154,159,163,181,184,185]. Here, we provide the reader with a concise summary in Table I-1 with the aim to highlight, for each immobilization strategy, the type

of interactions that are involved, the spatial localisation of the enzyme, and the pros and cons.

Focusing specifically on transaminases, Table I-2 highlights examples of the strategies that have been reported to prepare efficient heterogeneous biocatalysts for transamination reactions. Most of the time, immobilization allowed improving the performance of the transaminase, either in terms of stability or activity.

Table I-1. Summary of enzyme immobilization strategies and some of their main features.

	Entrapment and encapsulation	**Adsorption (electrostatic or hydrophobic interactions)**	**Site-specific affinity attachment**	**Covalent grafting**	**Cross linked enzyme aggregates or crystals (CLEAs or CLECs)**
Type of interactions involved	Reversible (Van der Waals, H-bonds)	Reversible (hydrophobic interactions)	Reversible (electrostatic interactions)	Reversible or irreversible	Reversible or irreversible
Enzymes localization	Carrier matrix or porosity	Carrier surface	Carrier surface	Carrier surface	Carrier-free

Features	**pros**	Mild enzyme distortions Enzyme protection by the carrier Direct assembly of the solid catalyst (carrier + immobilized enzyme in one pot)	Mild enzyme distortions Enzyme immobilization is tuneable (adapting carrier hydrophobicity or pH and pI during adsorption)	Mild enzyme distortions Possibly combined with enzyme purification Controlled enzyme orientation	Enzyme leaching prevention (strong interactions)	No need for enzyme carrier High catalyst productivity (kg product per kg catalyst) Enzyme leaching prevention (strong interactions)
	cons	Enzyme leaching (low stability) Possible diffusional limitations through carrier's pores	Enzyme leaching (low stability)	Enzyme leaching (low stability)	Possible rigidification of the enzyme structure	Possible diffusional limitations Possible rigidification of the enzyme structure

Typical immobilized enzymes formulations	Entrapment into a polymer or a sol-gel matrix	Adsorption onto hydrophobized silica (with carbon moieties) Electrostatic interactions with polyelectrolytes (*e.g.* chitosan), pristine silica, etc.	His-tag binding onto metal-derivatized carriers	Covalent grafting onto epoxy-resins Covalent grafting onto glutaraldehyde functionalized carriers	Enzymes aggregates cross-linked with glutaraldehyde
Useful ref.	186,187	183,188–191	192,193	131,194	195–197

Table I-2. Non-exhaustive list of examples of transaminase immobilization reported in the literature.

Method of Immobilization	Material	Enzyme and type of reaction catalyzed	Ref.
His-tag	Glass carrier	ω-TA (kinetic resolution)	198
Adsorption	Sepabeads® octadecyl-grafted resin	ATA-117-11Rd (asymmetric synthesis, excess of ISO and acetone removal)	199
Covalent grafting	Chitosan + glutaraldehyde	ω-TA (kinetic resolution)	200–202
Entrapment	Sol-gel matrix (+ celite)	ω-TA (kinetic resolution and deracemization)	186,203
CLEAs	Aggregation using glutaraldehyde	Glutamic transaminases	204

Lee *et al.* [200] have conducted the covalent immobilization of ATAs (from *Vibrio fluvialis* JS17) on chitosan beads, using glutaraldehyde as cross-linker agent. Residual activity of such heterogeneous catalyst reached 18 %. Similarly, Bornscheuer *et al.* [201,202] have covalently immobilized a series of ATAs (from *Giberella zeae*, *Neosartorya fischeri, Aspergillus fumigatus, Ruegeria pomeroyi* and *Rhodobacter sphaeroides*) on chitosan beads, using glutaraldehyde as crosslinking agent. In a model kinetic resolution reaction, an enhanced thermal stability was observed: when the enzymes were heated (to 60 °C for 4 hours) before reaction, the immobilized ones were more than twice more active than the free ones.

Entrapment of ATAs (ATA-113, ATA-117 and *Vf*-ATA) was successfully performed by Kroutil *et al.* [186], using a sol-gel matrix (with celite inclusion as porous additive). Entrapped enzymes exhibited activity even at pH 11 (whereas free enzymes were strongly deactivated in such extreme conditions), were stable over 5 cycles, and maintained their enantioselectivity (enantiomeric excess was over 99 %). Transamination reactions were performed both in the kinetic resolution mode, and in the deracemization (one-pot two steps) mode using lactate dehydrogenase or alanine dehydrogenase for driving equilibrium. This system was used to demonstrate the biocatalytic synthesis of pharmaceutically relevant chiral amines (S-Mexiletine and S-4-phenyl-2-butylamine). Kanerva *et al.* [203] recently performed the kinetic resolution of racemic amines, using ATA from *Arthrobacter* sp. (*As*-ATA) entrapped in sol-gel matrix (with controlled hydrophobicity, using Methyltriethoxysilane, MTES, during the sol-gel synthesis). Catalysts were shown to be reusable after 5 cycles.

Recently, Cassimjee *et al.* [198] achieved the immobilization of *Cv*-ATA through His-tag, on a glass carrier, derivatized with cobalt ions (EziG™ support). The catalyst was active in methyl *tert*-butyl ether as solvent and at 50 °C. *rac*-MBA was used as amino donor in the kinetic resolution mode, for the amination of 1-phenoxypropan-2-one.

Hydrophobic interactions for immobilization enhancement was also exploited by Truppo *et al.* [199] for the immobilization of engineered ATA-117-11Rd transaminase on Sepabeads® resin EXE 120 (polystyrene resin grafted with octadecyl moieties). The solid biocatalyst was active in an organic medium (water saturated isopropyl acetate as solvent), at high temperature (up to 60 °C) for the asymmetric synthesis of Sitagliptin. To reach high product yield, they used a large excess of ISO as amino donor and shifting the equilibrium by further converting acetone as proposed by Savile *et al.*[18].

To our knowledge, a simple physical adsorption was never reported as a successful immobilization strategy for transaminase. Concerning the immobilization through CLEA and CLEC formation, Patramani *et al.* [204] have tried to form transaminases (glutamic-transaminases) aggregates using glutaraldehyde as cross-linking agent, for antibody isolation. However, the CLEA were not active anymore after reticulation.

1.3 Continuous flow mode transamination reactions: literature survey

In general, batch processes involve significant maintenance time after each synthesis (for reactor washing and reconditioning for the next synthesis) during which synthesis is in pause. Also, reaction parameters (i.e. product and reagent concentrations) evolve with time, which implies that the catalyst is not running at full speed during the whole duration of the synthesis. Flow processes generally allow decreasing drastically the maintenance time and accelerating biotransformations due to enhanced mass transfer, making large-scale production more economically viable [170,205]. Moreover, flow processes afford a better control on conversion, as it is a function of reactor length (space-time yield) and not of reaction time. As a result, flow processing generally features increased scalability [176,206], higher space-time yields [175] and thus, enhanced productivity levels with respect to batch processes [163,174,207–212].

Finally, the outflows can be analysed in real time, and subsequent unit operations such as in-line liquid–liquid extraction, crystallization, membrane separation (*e.g.* for by-product elimination) can be integrated to the biotransformation [163,170].

Thus, performing biocatalytic transamination reactions in continuous flow mode is primed to solve many issues chemist and industrial chemists have to face when trying to design an efficient and green production process [165,213]. Table I-3 gathers the scholarly reports in which biocatalytic transamination reactions have been demonstrated in continuous flow mode. In the following sections, we discuss sequentially the cases where the enzyme is used in whole cells or as a stand-alone enzyme, in combination with other enzymes, and with co-immobilized cofactor. Figure I-1 shows the pictograms used to represent each component that are included in the process schemes discussed in the following section.

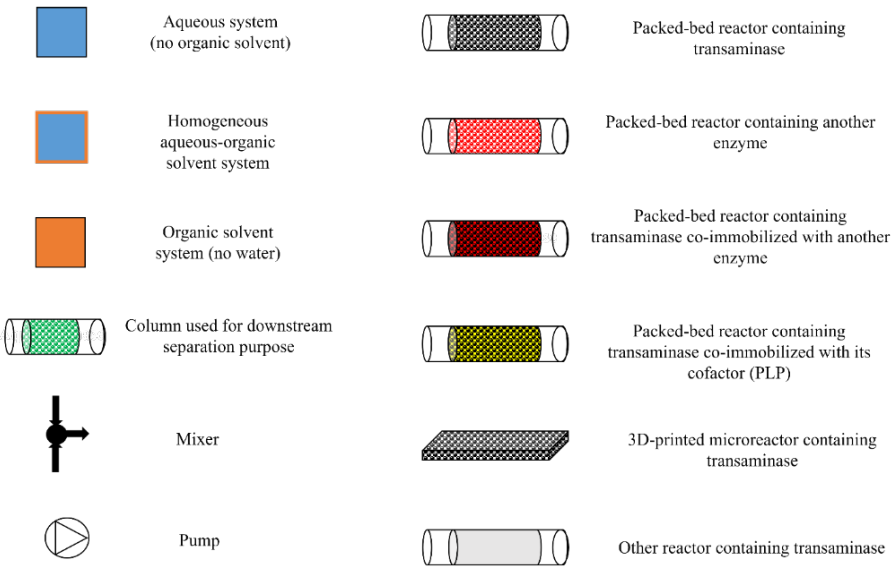

Figure I-1. Representation of each components featured in the transaminase-catalyzed continuous process schemes included in the following section.

Table I-3 – Overview of the reported examples of transaminations in continuous flow.

Immobilization	Materials	TA	Reaction	Ref.
TA in immobilized whole cells				
Entrapment	Ca-Alginate beads	Whole cells (*Vibrio fluvialis* JS17)	Kinetic resolution (continuous removal of ketone)	136
Entrapment	Chitosan	Whole cells (*Escherischia coli*)	Asymmetric synthesis (continuous removal of product, using SLM)	214
Entrapment	Hollow silica microspheres	Whole cells (*Escherischia coli*)	Kinetic resolution and asymmetric synthesis	215
Covalent grafting	Methacrylate beads	Whole cells (*Escherischia coli*)	Asymmetric synthesis (favourable thermo-dynamics)	216
Covalent grafting	Cycloolefin polymer microchannels + APTES[b] + Glutaraldehyde	Whole cells (*Escherischia coli*)	Deamination	217
Immobilized TAs				
His-tag immobilization	EziG™ supports + Fe^{3+} derivatization	ω-TAs	Kinetic resolution	218

His-tag immobilization	Derivatized EziG™ supports	*Aspergillus fumigatus* ω-TA mutant	Asymmetric synthesis (following a Suzuki–Miyaura reaction)	219
His-tag immobilization	EziG™ supports + Fe^{3+} derivatization	ω-TAs	Amination (in multi-enzymatic cascade reactions)	220
Covalent grafting (and His-tag driving)	Sepabeads® + Co^{2+} derivatization	*Halomonas elongata* ω-TA	Amination	131
Covalent grafting (and His-tag driving)	Sepabeads® + Co^{2+} derivatization	*Halomonas elongata* ω-TA	Asymmetric synthesis of cyclic chiral amines	221
Covalent grafting (and His-tag driving)	Sepabeads® + Co^{2+} derivatization	*Halomonas elongata* ω-TA	Asymmetric synthesis of 2-aminobutane	222
Covalent grafting (and His-tag driving)	Sepabeads® + Co^{2+} derivatization	*Halomonas elongata* ω-TA	Deamination	223
Covalent grafting (and His-tag driving)	Sepabeads® + Co^{2+} derivatization	*Halomonas elongata* ω-TA and Horse liver alcohol dehydrogenase	Deamination or kinetic resolution (followed by aldehyde reduction into alcohol)	224
Covalent grafting (and ionic driving)	Epoxy resin 107s (Xi'an Lan Xiao Technology Co. Ltd) + ethylenediamine derivatization	*Caulobacter sp.* ω-TA	Asymmetric synthesis of S-1-Boc-3-aminopiperidine	225

Covalent grafting	Aminoalkyl-functionalized resins (ReliZyme™ EA) + bisepoxides	*Chromobacterium violaceum* ω-TA mutant	Kinetic resolution	[226]
Covalent grafting	Glyoxyl-agarose beads	*Vibrio fluvialis* ω-TA	Asymmetric synthesis of AZD1480 intermediate	[227]
Hydrophilic interactions	DIAION HP2MG resin (Mitsubishi)	ω-TA mutant	Asymmetric synthesis of R-sitagliptin (in wet isopropylacetate, acetone evaporation by N_2 sparging)	[228]
Covalent grafting	Amine-functionalized beads (ReliZyme™ HA 403) + glutaraldehyde	*Silicibacter pomeroyi* ω-TA	Amination of furan aldehydes	[229]
Covalent grafting	Cellulose (+ APTES[b] + glutaraldehyde) or (+ GLYMO)	*Vibrio fluvialis* ω-TA	Asymmetric synthesis (using LDH and GDH)	[230]
Electrostatic interactions	Derivatized lignin + PEI[a]	*Halomonas elongata* ω-TA	Amination (of cynnamaldehyde) and deamination (of S-MBA)	[231]
Covalent grafting	Silica monolith + APTES[b] + glutaraldehyde	ATA-117	Kinetic resolution	[194] and [172]

His-tag immobilization	Silica capillary + Ni^{2+} derivatization	Immobilized ω-TA and transketolase	Asymmetric synthesis (following formation of chiral ketone)	232
His-tag immobilization	Agarose beads + Ni^{2+} derivatization	Immobilized ω-TA and transketolase	Asymmetric synthesis (following formation of chiral ketone)	233
Covalent grafting	3D-printed Nylon matrix (Taulman) + Glutaraldehyde + PEI[a]	ω-TAs	Kinetic resolution	234
Entrapment	Lentikats® (polyvinyl alcohol gel)	ω-TA	Deamination	235
Co-immobilized TAs and cofactor (PLP)				
Covalent grafting (and His-tag driving)	Epoxy-activated methacrylate beads + PEI[a]	Co-immobilized ω-TAs and PLP	Amination (of cynnamaldehyde) and deamination (of S-MBA)	236
Covalent grafting (and His-tag driving)	Epoxy-activated methacrylate beads + PEI[a]	Co-immobilized H*alomonas elongata* ω-TA and PLP	Deamination	237
Covalent grafting	Epoxy-resin (Xi'an Lan Xiao Technology Co. Ltd)	Co-immobilized ω-TA and PLP	Asymmetric synthesis of R-sitagliptin	238

Entrapment	Copolymer hydrogel of polyvinyl alcohol and sodium alginate	Co-immobilized ω-TA and PLP	Deamination	[187]
Combining TAs with other enzymes				
Covalent grafting	Silica capillary + APTES[b] + Glutaraldehyde	Co-immobilized glutamic-pyruvic transaminase, glutamate dehydrogenase	Asymmetric synthesis	[148]
Covalent grafting	Polymethacrylate-based porous beads Relisorb® EP400SS	Co-immobilized H*alomonas elongata* ω-TA with Horse liver alcohol dehydrogenase and NADH oxidase	Amination (following the oxidation of alcohol into aldehyde)	[239]
Covalent grafting	Polymethacrylate-based porous beads Relisorb® EP400SS	Co-immobilized H*alomonas elongata* ω-TA with Horse liver alcohol dehydrogenase and NADH oxidase	Amination (following the oxidation of alcohol into aldehyde)	[240]

Combining TAs with other enzymes in whole cells				
Entrapment	Hollow silica microspheres	Co-immobilized Whole cells (*Escherischia coli*) and *Lodderomyceselongisporus* yeast with ketoreductase activity	Kinetic resolution (followed by ketone reduction into chiral alcohol and amines) - one-pot cascade	241

[a] PEI = polyethyleneimine

[b] APTES = (3-aminopropyl)triethoxysilane, respectively.

1.3.1 Flow mode transamination with ATAs in immobilized whole cells

Shin *et al.* [136] were the first to report a biocatalytic transamination reaction in flow mode. Whole cells of *Vibrio fluvialis* JS17 containing overexpressed transaminases were entrapped in calcium-alginate beads, and used to form a packed-bed reactor (PBR). As compared to the cell-free extract, a change in the pH optimum was observed (from 9 to 8) and the substrate and product inhibition was lower. They successfully perform the kinetic resolution of *rac*-MBA, using alanine as the amino donor. The ketone product (acetophenone) was continuously removed using a hydrophobic membrane contactor (Figure I-2). Noteworthily, the authors also performed such continuous transamination process using an enzyme membrane reactor (EMR) in place of a PBR. In this case, the *Vibrio fluvialis* whole cells were encapsulated in a hydrophilic ultrafiltration membrane [242].

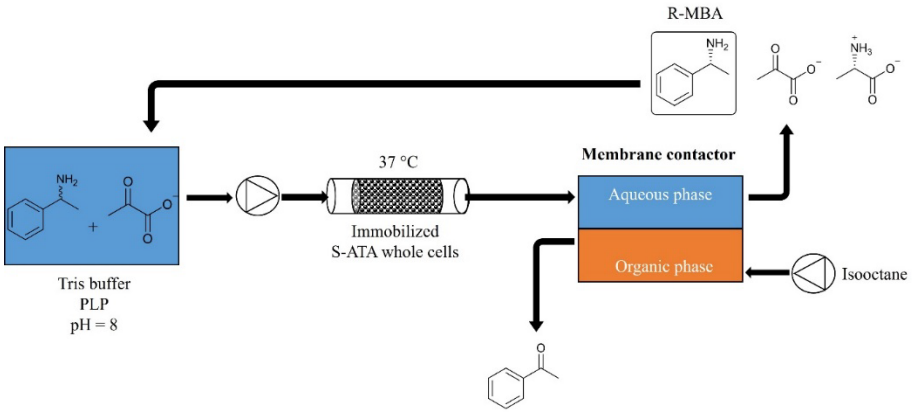

Figure I-2. Schematic representation of the continuous transamination process described by Shin *et al.* [136].

Escherichia coli whole cells containing over-expressed ATA from *Arthrobacter citreus* were also entrapped in chitosan matrix and placed in a PBR by Rehn *et al.* [214] for the asymmetric synthesis of S-MBA (Figure I-3). Large excess of amino donor (ISO) was employed, and the equilibrium was additionally shifted towards completion through a continuous and selective

extraction of MBA using a SLM contactor (*i.e.* a porous membrane, with pores filled with undecane allowing the transfer of the amine). This system led to 98 % conversion in flow mode. Final product concentration was as high as 55 g/L (obtained by processing the flow setup for 80 h).

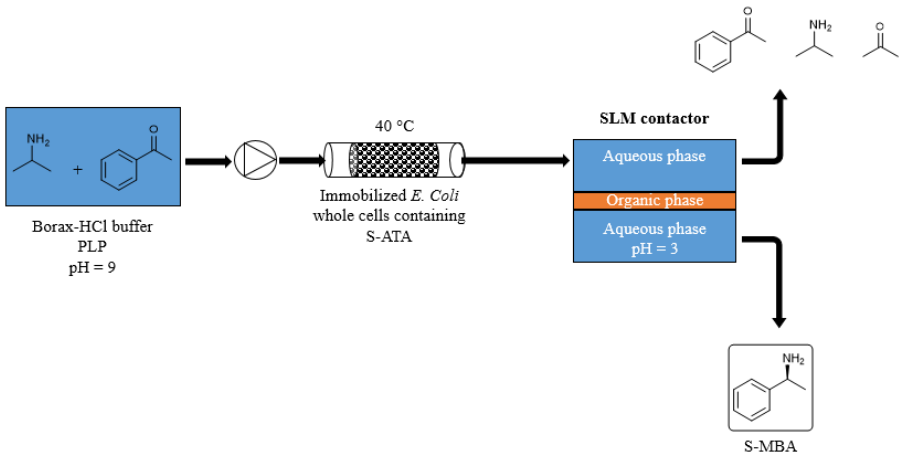

Figure I-3. Schematic representation of the continuous transamination process described by Rehn *et al.* [214].

In 2019, the Poppe group [215] performed the immobilization of six different ATAs (three S-selective and three R-selective) overexpressed in *Escherichia coli* whole cells entrapped into hollow silica microspheres forming a sol-gel matrix. The resulting sol-gel system allowed quantitative immobilization (~100 % immobilization yield) even at high enzyme loading. Notably, ~9 g of dry heterogeneous TA biocatalyst could be produced from 10 g of wet cells. Moreover, despite the harsh immobilization conditions, ATAs-containing whole cells were able to efficiently catalyze the kinetic resolution of various amines in batch. Interestingly, they remained catalytically active even after many months of air-storage. Subsequently, the most efficient S and R-selective immobilized ATAs were selected to run the kinetic resolution in continuous flow mode, in a PBR. Both solid biocatalysts exhibited excellent yield and good enantiomeric excess under various flow rates and substrate concentrations. Eventually, the continuous production of the two pure

enantiomers of the drug-like 1-(3,4-dimethoxyphenyl)ethan-1-amine (DMPEA) (Figure I-4) was demonstrated, with space-time yields of 1.8 $g.L^{-1}.h^{-1}$ and 4.8 $g.L^{-1}.h^{-1}$ for S- and R-enantiomers, respectively, and showed remarkable operational stability.

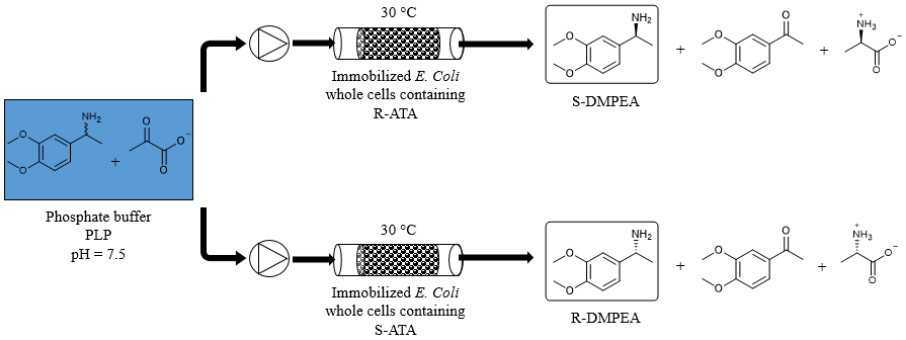

Figure I-4. Schematic representation of the continuous kinetic resolution of *rac*-1-(3,4-dimethoxyphenyl)ethan-1-amine (DMPEA) described by Poppe *et al.* [215].

In another study, Jamison *et al.* [216] reported on the flow transamination for the thermodynamically favourable asymmetric synthesis of non-natural amines in organic solvent (methyl *tert*-butyl ether). *Escherichia coli* whole cells containing both over-expressed R-selective transaminases and entrapped PLP cofactor were grafted on methacrylate beads (*via* grafting of the peptidoglycan layer present in the cell wall). The API R-mexiletine was synthesized in 94 % yield using ISO as the amino donor (residence time was 60 min). PLP leaching was avoided thanks to the organic solvent (the cofactor stayed in the aqueous phase entrapped in the beads). The biocatalysts were stable up to 10 days. The continuous reaction was followed by a downstream purification step (*i.e.* a catch-and-release system), allowing the recovery of highly pure chiral amine products (Figure I-5).

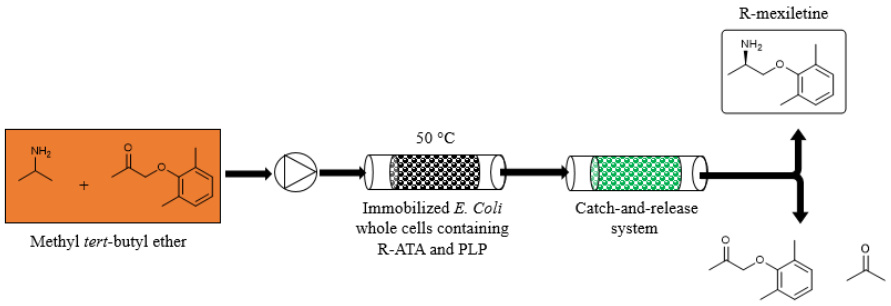

Figure I-5. Schematic representation of the continuous process leading to the asymmetric synthesis of R-mexiletine in organic solvent, described by Jamison *et al.* [216].

Žnidaršič-Plazl *et al.* [217] developed three microscale reactors containing ATAs immobilized on the inner wall surface, using different immobilization strategies. On the one hand, *Escherichia coli* whole cells (overexpressing the ATA) were immobilized on the surfaces of cycloolefin polymeric microchannels (COP, Zeonor®) through surface silanization (with APTES) and glutaraldehyde coupling. On the other hand, a glass microchannel reactor was used for the immobilization of a genetically engineered ATA featuring a silica-binding module tag (SBM tag) at the N-terminus (N-SBM-ATA), leading to immobilization *via* electrostatic interactions. The catalytic performance of the resulting biocatalytic microreactors were evaluated towards the continuous deamination of S-MBA into acetophenone using pyruvate as the amine acceptor. Both whole cells (overexpressing ATA) and N-SBM-ATA were efficiently immobilized and displayed high productivities (space time yields were 11.53 $g.L^{-1}.h^{-1}$ and 14.42 $g.L^{-1}.h^{-1}$, respectively). However, whole cells showed negligible leaching and enhanced operational stability while N-SBM-ATA productivity dropped quickly, which was suggested to indicate rapid leaching from the reactor.

1.3.2 Flow mode transamination with immobilized ATAs

Among the different reported supports hosting immobilization of stand-alone ATAs used in flow applications, porous glass-based materials and functionalized polymeric resins are the ubiquitous supports. For example, EziG™ materials are based on controlled porosity glass (featuring additional polymer coating in some case) that easily chelate metal cations and therefore can also bind proteins equipped with affinity tags [198]. This allows combining enzyme purification and immobilization in a straightforward manner.

Mutti et al. [218] achieved the immobilization of two His-tagged ATAs (*As*-ATA and *Cv*-ATA) on different EziG™ supports, loaded with iron ions. Three types of EziG carrier material possessing distinct surface polarities were tested: EziG1 (Fe-Opal, hydrophilic derivatized silica surface), EziG2 (Fe-Coral, coated with hydrophobic polymer), and EziG3 (Fe-Amber, covered with semi-hydrophobic polymer). The impact of immobilization conditions (buffer composition, concentration, pH and PLP concentration) on immobilization efficiency was assessed. EziG3 provided the highest immobilization yield when performing immobilization in optimal conditions, and *As*-ATA showed highest specific activity in batch experiments. Thus, EziG3-*As*-ATA (with 20 wt % ATA) was selected to run the flow kinetic resolution of *rac*-MBA (Figure I-6). The resulting PBR was operated for 96 hours without any detectable loss of activity nor enantioselectivity, and high space-time yield (335 $g.L^{-1}.h^{-1}$) was achieved.

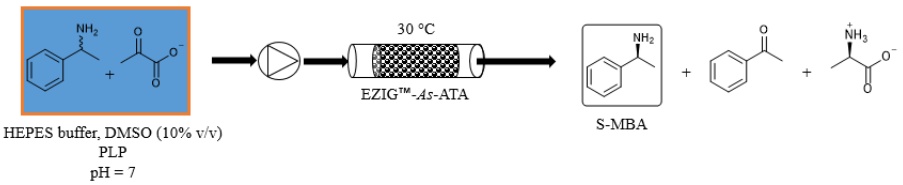

Figure I-6. Schematic representation of the continuous kinetic resolution of *rac*-methylbenzylamine (MBA) described by Mutti *et al.* [218].

Bornscheuer *et al.* [219] also immobilized a variant ATA from *Aspergillus fumigatus* (*Af*-ATA) on an EziG™ support to perform a cascade combining chemo- and biocatalytic reactions in continuous flow mode. More precisely, the cascade featured a combination of the palladium-catalyzed Suzuki–Miyaura coupling producing biphenyl ketones followed by transamination (*i.e.* asymmetric synthesis of high-value chiral biaryl amines). The soluble Pd species ($PdCl_2$, as a homogeneous coupling catalyst) was continuously fed but the enzyme was fixed in a single PBR. In other words, two reaction solutions (the crude Suzuki–Miyaura reaction mixture producing the ketone, and an ISO/PLP-containing solution) were pumped through the PBR (Figure I-7). The cascade resulted in 43% overall conversion at a flow-rate of 0.1 $mL.h^{-1}$ (210 minutes residence time) when employing 30% (v/v) DMF for transamination reaction. Such an achievement highlights the excellent compatibility of chemo- and biocatalysis for such cross-coupling reaction in DMF/water mixtures as well as the robustness of the employed ATA variant in the presence of reagents required for the chemocatalytic reaction (*e.g.* $PdCl_2$).

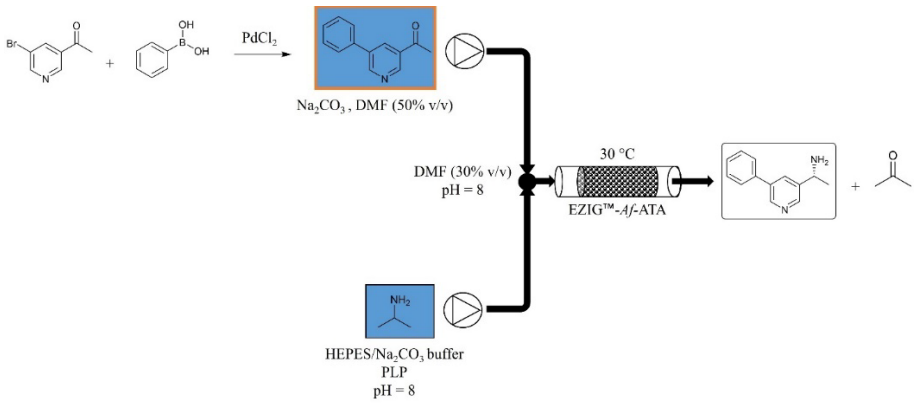

Figure I-7. Schematic representation of the continuous process leading to the asymmetric synthesis of R-1-(5-phenylpyridin-3-yl)ethan-1-amine (framed compound), described by Bornscheuer *et al.* [219]. Suzuki–Miyaura reaction by-products were intentionally omitted for clarity purpose.

Flitsch *et al.* [220] exploited the combined use of alcohol oxidase, transaminase, and imine reductase (IR) to synthesize various primary and secondary amines. Such a three enzymes system is not viable in batch mode, due to incompatible substrates or enzyme combination (*e.g.* cross-reactivity and inhibition issues). Thus, as a proof-of-concept, they designed a sequential flow mode process. A first reaction involved an alcohol oxidase to form aldehyde intermediates from alcohols, using catalase-generated oxygen (from the decomposition of hydrogen peroxide). The reactive aldehyde were then passed through a series of packed-bed modules loaded with ATA or IR immobilized on EziG™ amber based-carriers. ATA, fed with alanine, was used to generate primary amines (Figure I-8**a**) or intermediate amines that were subsequently non-catalytically carbonylated (into imines) and then reduced on the IR (using glucose as co-substrate and Nicotinamide Adenine Dinucleotide Phosphate ($NADP^+$) as the cofactor) into the targeted secondary amines (Figure I-8**b**). This method proved to greatly improve the overall yields and the biocatalytic productivity with respect to the equivalent sequential batch reactions.

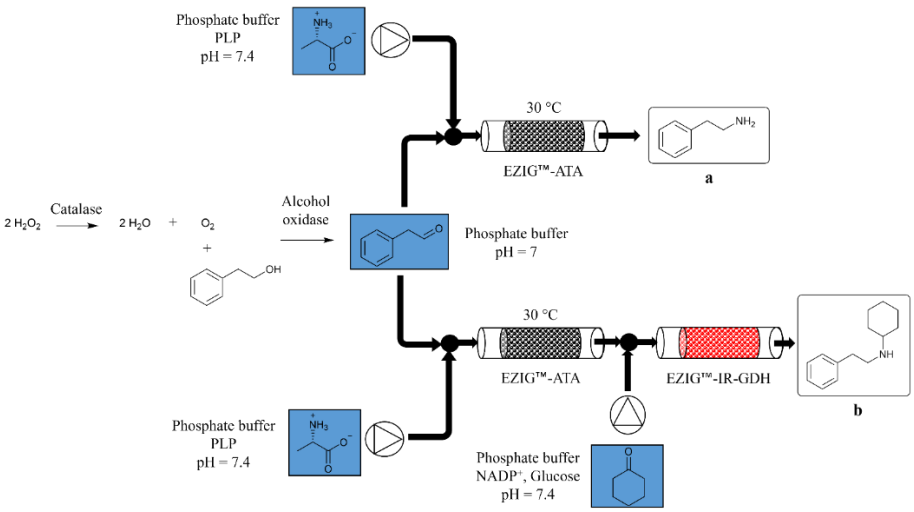

Figure I-8. Schematic representation of the continuous transaminase-mediated process leading to primary (a) and secondary (b) amines, described by Flitsch *et al.* [220]. The first cascade reaction (involving soluble catalase and alcohol oxidase) was performed in a multipoint injection reactor. By-products of transamination (pyruvate) and glucose dehydrogenation (gluconolactone) were intentionally omitted for clarity purpose.

Commercial epoxy-activated (usually made of methacrylate or polyacrylic matrix) resins such as Sepabeads® are also widely employed as carrier for TA immobilization. Their surface epoxy-groups are especially useful as they afford the coupling with different nucleophilic species. As ready-to-use carriers they directly bind to the nucleophilic groups on the enzyme surface (i.e. Lys or Cys residues). However, due to the low reactivity of the epoxy groups, a second functional group (*e.g.* amines or metal chelates) is frequently added to the support to drive the enzyme toward the epoxy-carrier surface [225,231,243].

As matter of illustration, a metal-derivatized epoxy-resin (Sepabeads® EC-RP/S) was used by Paradisi *et al.* [131] for the continuous flow synthesis of a range of achiral amines, using immobilized *Halomonas elongata* ω-transaminases (HeWT). The beads were activated with iminodiacetic acid (IDA) and $CoCl_2$ solutions, resulting in cobalt chelates able to drive the covalent immobilization of HeWT (by His-Tag binding). The resulting

immobilized enzyme retained 40% activity and displayed increased organic solvent tolerance (with respect to the free form). The amination of *p*-NO_2-benzaldehyde into *p*-NO_2-benzylamine was successfully performed (> 99% yield in 2 minutes residence time) and coupled to on-line product purification device (*i.e.* basification of the reaction stream followed by extraction with ethyl acetate). Additionally, cinnamylamine (a valuable building block for the synthesis of biologically active material) was efficiently produced through amination (90% yield in 2 minutes residence time) using alanine as the amino donor (Figure I-9).

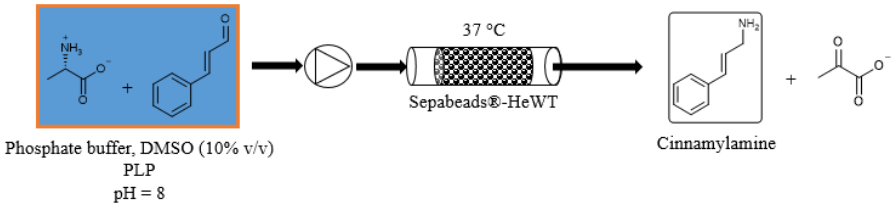

Figure I-9. Schematic representation of the continuous transaminase-mediated production of cinnamylamine, described by Paradisi *et al.* [131].

Similarly, the Paradisi group relied on the same biocatalytic system for different applications. For example, they exploited this system to produce a range of small cyclic chiral amines in continuous flow. [221] Cyclic pro-chiral ketones were used as starting reagent, along with along with S-MBA, and no particular equilibrium shifting strategy was used for this synthesis. Remarkably, complete conversion of tetrahydrofuran-3-one and tetrahydrothiophene-3-one was achieved in 5- and 10-min residence times, respectively. However, the enantiomeric excess for these rapid transamination reactions did not exceed 30 % (while soluble HeWT reached 60 to 70 %). Molecular docking studies suggested that the rigidification imposed by the immobilization of HeWT could explain the relatively lower selectivity displayed by the heterogeneous biocatalyst for the conversion of such small cyclic ketones. Nevertheless, the efficient production of bulkier cyclic chiral

amines such as S-1-methyl-piperidin-3-ylamine (MPPA; Figure I-10) with enhanced enantioselectivity (90%) was achieved with longer contact times (30 to 45 minutes).

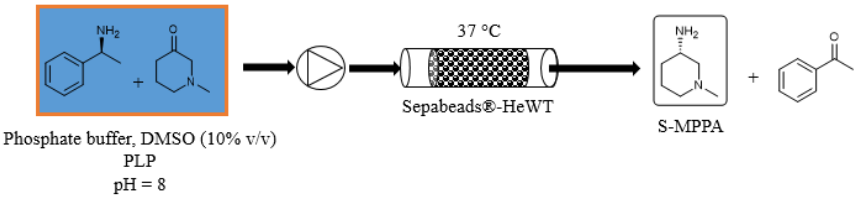

Figure I-10. Schematic representation of the continuous asymmetric synthesis of S-1-methyl-piperidin-3-ylamine (MPPA) using immobilized transaminase, described by Hegarty and Paradisi [221].

The flow asymmetric synthesis of both enantiomers of 2-aminobutane from butanone was also reported,[222] using the same immobilized transaminases system as described above. Notably, R-2-aminobutane is a sub-unit of drug candidate XL888, which is currently used in clinical trials for cancer treatment [244]. After screening a panel of ATAs, two candidates were identified: the S-selective HeWT and a commercial R-selective ATA (*RTA-X43, from Johnson Matthey). Notably, a single strategic point mutation enhanced the enantioselectivity of HeWT from 45 to > 99.5% enantiomeric excess. Once immobilized, the resulting HeWT mutant (HeWT-F48W) and RTA-X43 enabled the multi-gram production of S- and R-2-aminobutane at high concentration (Figure I-11), which were subsequently purified by three fractional distillations under atmospheric pressure. Both biocatalysts displayed excellent stability, especially the immobilized HeWT-F48W which did not show any activity loss over 7 days of operation. As a result, it achieved a space-time yield of 3.6 $g.L^{-1}.h^{-1}$. ISO (1.5 M) was employed as amino donor.

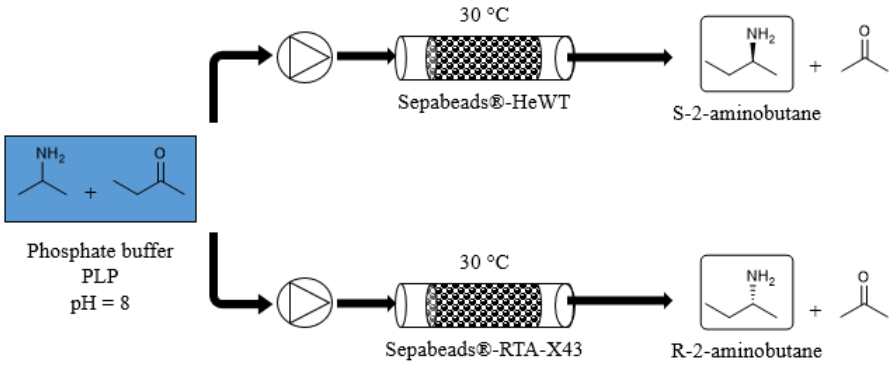

Figure I-11. Schematic representation of the continuous asymmetric synthesis of R- and S-2-aminobutane using immobilized transaminase, described by Paradisi *et al.* [222].

HeWT immobilized on this metal-derivatized epoxy resin was also used for the flow production of aromatic primary and secondary alcohols starting from aromatic amines. [224] The flow-mode transamination reactions (*i.e.* deamination or kinetic resolution) were followed by the reduction of the aldehyde product into the targeted alcohol in a subsequent PBR, *via* immobilized Horse liver alcohol dehydrogenase (HLADH) or ketoreductase (KRED). For example, starting from dopamine (biologically available substrate) and using a biphasic stream (HEPES buffer/toluene 85:15), the authors successfully synthesized hydroxytyrosol (an antioxidant compound) in high yield (82 %). The flow setup was connected to an in-line purification device, allowing cofactor recycling and product isolation (Figure I-12).

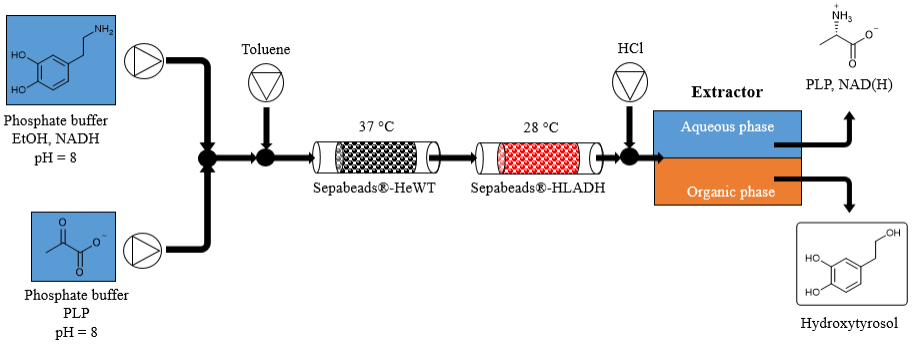

Figure I-12. Schematic representation of the process leading to the continuous multienzymatic synthesis of hydroxytyrosol, described by Contente and Paradisi [224]. NADH cofactor was regenerated in-situ by ethanol (EtOH) dehydrogenation into acetaldehyde. By-products of alcohol dehydrogenations (acetaldehyde and 2-(3,4-dihydroxyphenyl)acetaldehyde) were intentionally omitted for clarity.

Employing such immobilized HeWT, Paradisi *et al.* [223] also performed the flow synthesis of a plethora of valuable aromatic aldehydes (featuring key applications as components of flavours and fragrances). Using very short residence times (3-15 min), the biocatalyst allowed obtaining at least 90% yield (with pyruvate as amino acceptor). An elegant in-line extraction step was implemented, which afforded the recovery of the targeted pure aldehydes in the organic stream.

Wang *et al.* [225] also managed to covalently immobilize an ATA from *Caulobacter* sp. (ATA-W12) on derivatized epoxy resins. Here, the resin was partially aminated with ethylenediamine (EDA) in order to drive the adsorption of ATA *via* electrostatic interactions, and thus to favor its subsequent covalent anchoring on the epoxide functions. Such derivatization enabled to improve the heterogeneous biocatalyst residual specific activity and stability. Indeed, after 15 consecutive cycles in batch, the EDA-treated biocatalyst retained >90 % of specific activity, while the ATA immobilized on the pristine epoxy resin lost half of its specific activity. The resulting immobilized ATA was used to run the flow asymmetric synthesis of S-1-Boc-3-aminopiperidine (a key intermediate for the synthesis of CHK1 inhibitor),

in a PBR (Figure I-13). After 24 h of continuous operation at 0.4 mL.min^{-1}, the conversion rate was maintained at > 90 %, resulting in a space-time yield of 38.8 g·L^{-1}·h^{-1}.

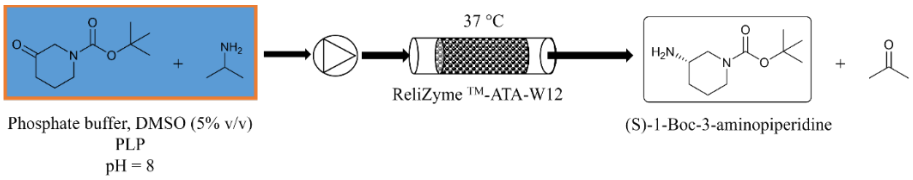

Figure I-13. Schematic representation of the continuous synthesis of S-1-Boc-3-aminopiperidine using immobilized transaminase, described by Wang *et al.* [225]

Poppe *et al.* [226] successfully immobilized a *Cv*-ATA mutant through covalent attachment on bisepoxide-activated aminoalkyl resins (ReliZyme™ EA403/S) for the kinetic resolution of racemic amines in continuous flow mode. The impact of the hydrophilicity and length of the linker arm (i.e. bisepoxide coupling agents) on ATA specific activity was assessed. It was found that the specific activity is boosted when the enzyme is attached to the polymeric resin *via* short and hydrophilic linkers, such as glycerol diglycidyl ether. With this optimized biocatalyst in hand, the authors carried out a recycling study in batch mode and proved its high operational stability (98% retained activity over 19 consecutive cycles). Subsequently, a kinetic resolution was efficiently achieved in flow mode, resulting notably in pure R-4-phenylbutan-2-amine, a precursor of antihypertensive drug Dilevalol (Figure I-14**a**). Space-time yield was 45.8 g.L^{-1}.h^{-1} (0.5 mL.min^{-1} contact time, without organic solvent). Additional flow experiments performed in water/DMSO systems (50% v/v) further allowed producing R-1-aminotetraline (a component used in the synthesis of Sertraline) with an enantiomeric excess > 95% at 0.1 mL.min^{-1} (Figure I-14**b**). Such result highlights the enhanced solvent tolerance of such immobilized *Cv*-ATA mutant with respect to its free form, which could be attributed to a significant

stabilization of its tertiary structure upon immobilization (due to multipoint covalent fixation).

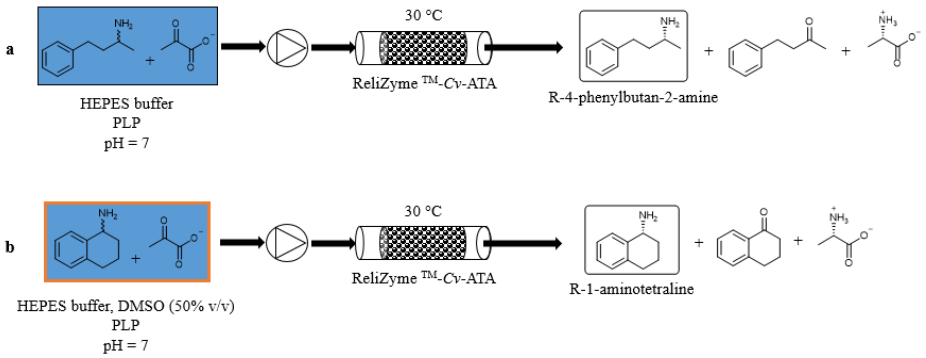

Figure I-14. Schematic representation of the continuous kinetic resolution of *rac*-4-phenylbutan-2-amine (a) and *rac*-1-aminotetraline (b) using immobilized transaminase, described by Poppe *et al.* [226].

Ubiali *et al.* [227] reported on the covalent immobilization of *Vf*-ATA on glyoxyl-agarose beads, by exploiting the reactivity of the lysine residues of the enzyme towards the aldehyde groups of the carrier. The formed imine bond was further reduced to stabilize the anchoring and avoid leaching. Two reducing agents ($NaBH_4$, $NaBH_3CN$) were used in under different conditions, in attempts to minimize the negative impact of this reduction on the enzyme activity. The optimal immobilized biocatalyst (obtained using $NaBH_3CN$ at 4°C) retained c.a. 30% of activity and similar stability with respect to its free form. The immobilized biocatalyst was tested in batch and flow mode (in a PBR, using 10 minutes residence time) for the synthesis of S-1-(5-fluoropyrimidin-2-yl)-ethanamine, a key intermediate of AZD1480 kinase inhibitor. For a similar degree of conversion, the specific reaction rate of the flow reaction resulted to be about 22-fold higher than the batch reaction. Moreover, DMSO could be replaced by dimethyl carbonate (5% v/v) as a greener co-solvent, further enhancing the sustainability performance of the process. An in-line downstream purification was developed for product

isolation using an ion-exchange resin. Using S-MBA as the amino donor, optically pure S-1-(5-fluoropyrimidin-2-yl)-ethanamine (enantiomeric excess > 99%) was isolated in 35% yield (Figure I-15).

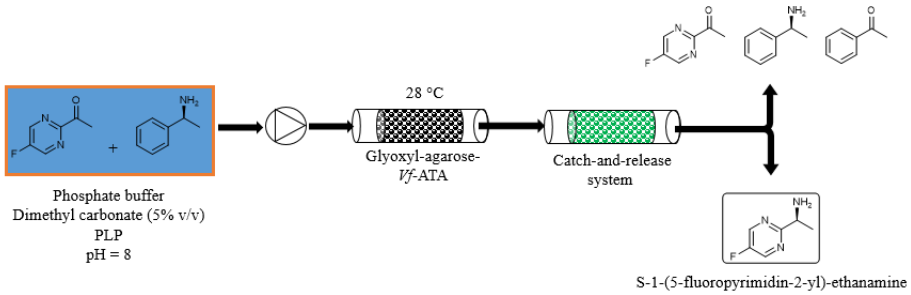

Figure I-15. Schematic representation of the process leading to the continuous asymmetric synthesis of S-1-(5-fluoropyrimidin-2-yl)-ethanamine using immobilized transaminase, described by Ubiali *et al*. [227].

In a recent patent, Truppo and co-workers at Merck [228] demonstrated the use of immobilized recombinant transaminases to manufacture R-sitagliptin in batch and continuous flow mode. The employed immobilized ATA consisted in commercial methacrylate-based carrier (DIAION HP2MG resin (Mitsubishi)) linked to the recombinant ATA through hydrophilic interactions. Impressively, such biocatalyst remained highly active and stable in organic solvent systems (i.e. comprising at least 90% of organic solvent). Isopropylacetate (IPAc) was used as main solvent for the reaction and isopropylamine as the amino donor. Acetone evaporation (high temperature and N_2 sparging) enabled to displace the position of the transamination equilibrium towards the formation of products. In the continuous operation, the immobilized ATA was packed into a column (as a PBR). At 60 °C and with a flow rate of 63 µL.min^{-1} (corresponding to 1h of residence time), the conversion was 45%; it reached 85% when the residence time was set to 4h. Optically pure R-sitagliptin (enantiomeric excess > 99.5%) was successfully obtained (Figure I-16).

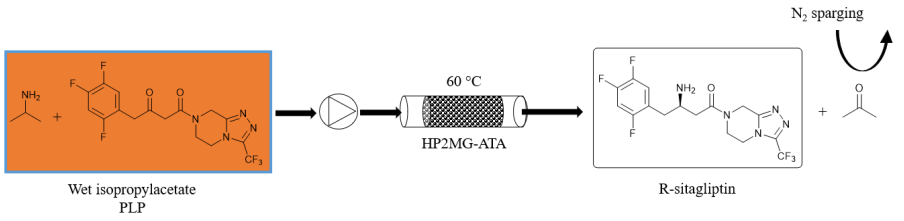

Figure I-16. Schematic representation of the process leading to the continuous asymmetric synthesis of R-sitagliptin using immobilized transaminase, described by Truppo *et al.* [228].

In 2023, the Berglund and Bornscheuer groups [229] demonstrated the reductive aminations of biobased furan aldehydes, namely 5-(hydroxymethyl)furfural (HMF) and 2,5-diformylfuran (DFF), in batch and flow mode using immobilized ATAs. To this aim, different ATAs were immobilized on glutaraldehyde-functionalized amine beads (ReliZyme™, HA 403), and both alanine and isopropylamine were tested as amino-donors. Among the different heterogeneous biocatalysts developed, the ATA from *Silicibacter pomeroyi* (*Spo*-ATA) exhibited enhanced recyclability towards the different aminations in batch experiments. It was therefore selected to run the reductive amination of HMF into 5-(hydroxymethyl)furfurylamine (HFMA) in continuous flow-mode, with alanine (Figure I-17**a**) or isopropylamine (Figure I-17**b**) as co-substrate. After 12 days of continuous operation at a flow rate of 0.05 mL.min^{-1} (4 minutes residence time), the heterogenous biocatalyst lost c.a. half of its initial activity, but still showed high HMF conversions (i.e. 48% and 41%, with alanine and isopropylamine, respectively).

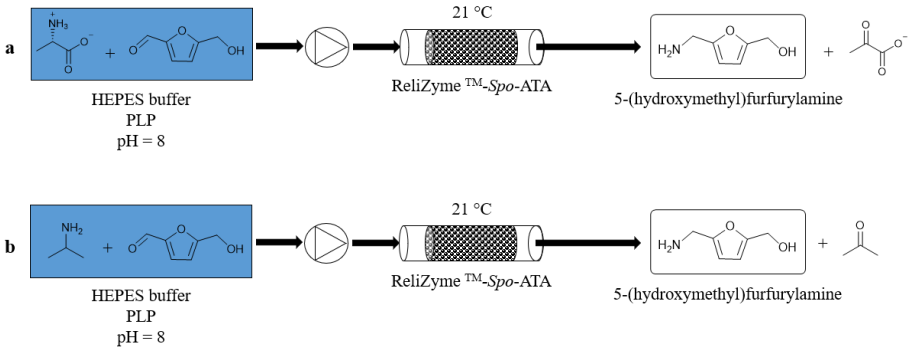

Figure I-17. Schematic representation of the process leading to the continuous reductive amination of 5-(hydroxymethyl)furfural into 5-(hydroxymethyl)furfurylamine (HFMA) using immobilized transaminase, described by Berglund *et al.* [229].

Other carriers were also employed as enzyme support to run transamination reactions in continuous flow-mode. For example, de Souza *et al.* [230] managed to covalently immobilize *Vf*-ATA onto two distinct functionalized cellulose. To provide the anchoring points for covalent grafting, the hydroxyl groups of cellulose were silanized either using APTES (followed by glutaraldehyde activation) or by (3-glycidyloxypropyl)trimethoxysilane (GLYMO), prior enzyme immobilization to ensure the covalent grafting. This epoxy-modified cellulose gave rise to high enzyme loading (40 mg.$g_{carrier}^{-1}$) and the resulting immobilized *Vf*-ATA demonstrated good catalytic activity and recyclability in batch (towards the kinetic resolution of *rac*-MBA). Subsequently, the biocatalyst was employed for the asymmetric synthesis of S-MBA (using the multienzymatic LDH-GDH system to shift the equilibrium) in continuous flow-mode, in a PBR (Figure I-18). LDH and GDH enzymes were continuously fed in the free form (in a buffered solution containing also alanine and acetophenone) to the PBR. The continuous operation resulted in enhanced productivity with respect to batch processes: the reaction time was reduced from 48 h to 90 min, while the conversion was increased from 30% to 80%.

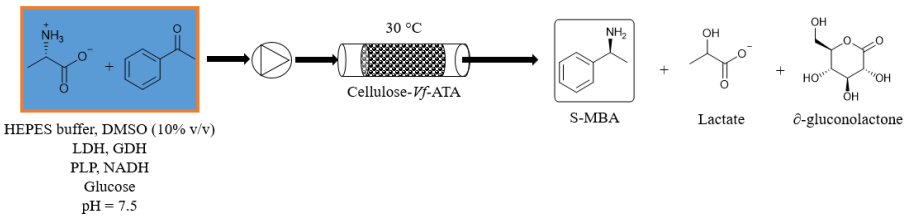

Figure I-18. Schematic representation of the process leading to the continuous asymmetric synthesis of S-methylbenzylamine (S-MBA) using immobilized transaminase, described by de Souza *et al.* [230]. The LDH-GDH system was employed to shift the thermodynamic equilibrium (and for NADH cofactor regeneration).

Very recently, lignin derivatives were valorised as carrier for the immobilization of a battery of enzymes, including transaminases [231]. A number of lignin functionalization strategies were attempted to provide various anchoring points (namely aldehydes, epoxy, cobalt chelates and amines) for the subsequent ATAs immobilization. Among all the screened enzymes and activated supports, the HeWT transaminase reversibly immobilized on PEI-derivatized lignin showed the highest immobilization and catalytic performance (17% retained specific activity). Importantly, despite the weak ionic interactions between HeWT and the PEI-lignin, no enzyme leaching was detected after 8 catalytic cycles in batch. Owing to its enhanced efficiency and recyclability, such heterogeneous biocatalyst was integrated to a PBR to run the flow amination of cinnamaldehyde into of cinnamylamine (Figure I-19). At a flow rate of 0.35 mL.min^{-1} (2 minutes retention time), ≥80% conversion was achieved during the 100 minutes of continuous operation.

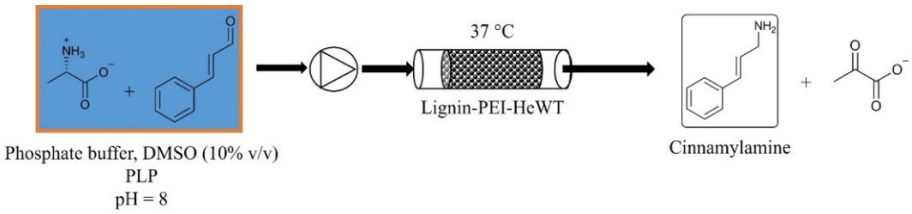

Figure I-19. Schematic representation of flow synthesis of cinnamylamine using PEI-lignin-immobilized transaminase, described by Luterbacher *et al.* [231].

In 2017, Žnidaršič-Plazl *et al.* [235] successfully achieved the flow transamination of S-MBA (deamination) with pyruvate using ATAs entrapped in a polyvinyl alcohol matrix (Lentikatz®) placed in a PBR. After 21 days of process (at flow rate of 0.5 µL.min^{-1}), the catalyst still exhibited up to 80 % initial activity.

Debecker *et al.* [194] recently reported on the use of ATA-117 transaminase, covalently immobilized on a macroporous silica monolith prepared by emulsion-based sol-gel method (denoted "Si(HIPE"), in flow. To this aim, the Si(HIPE) was first aminated through silanization using APTES and further modified by glutaraldehyde, which provided suitable anchoring points for the ATA. The resulting bioreactor was then to run the kinetic resolution of racemic bromo-α-methylbenzylamine (*rac*-BMBA) in continuous flow-mode (Figure I-20). This texture of the Si(HIPE) ensured a plug-flow regime through the macroporous support. The most productive biocatalyst yielded 6.2 % of BAP with 10 minutes contact time (corresponding to 16 % residual activity with respect to free enzymes in batch reactor). Simply placing 8 monoliths in series (to increase the contact time) allowed pushing the reaction to completion (i.e. ~50% conversion). In a second work [172], the APTES silanization and enzyme grafting steps were improved by optimizing some technical parameters (humidity, temperature, concentrations) which resulted a significant specific activity boost. The optimized immobilized biocatalyst reached 30 % conversion with 10 minutes contact time.

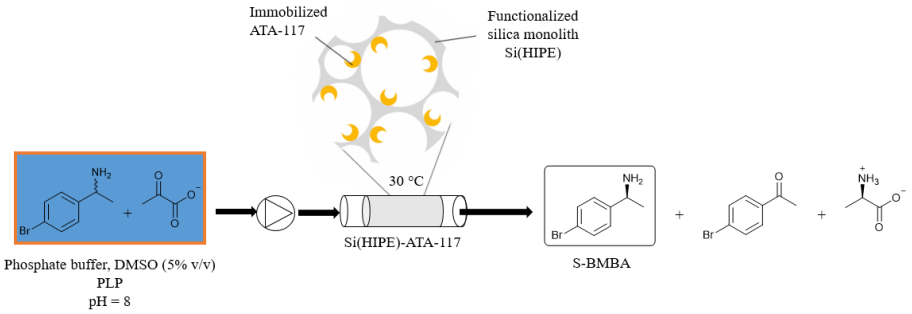

Figure I-20. Schematic representation of the continuous kinetic resolution of *rac*-bromo-α-methylbenzylamine (*rac*-BMBA) using immobilized transaminase described, by Debecker *et al.* [194].

Very recently, Corma *et al.* [245] managed to immobilize an ATA on 2D ITQ-2 zeolites, for the obtention of valuable chiral amines from prochiral ketones derived from biomass through a chemo-enzymatic cascade in continuous flow-mode. The zeolite surface was functionalized with amino groups (using APTES, through silanization) in order to reversibly immobilize the ATA (*via* electrostatic interactions). The resulting heterogeneous biocatalyst showed enhanced stability in batch and flow model transamination experiments, and no enzyme leaching was detected. The solid was exploited to run the chemo-enzymatic production of S-4-(4-methoxyphenyl)-2-butananamine production from 4-(4-methoxyphenyl)-2-butanone and acetone. Two reactors were placed in series: the first step of the cascade, a chemo-catalytic aldol-reduction, was performed in a semi-continuous batch reactor (in presence of Pd/MgO catalyst and under pressurized hydrogen) while the subsequent transamination took place in a fixed-bed reactor, in flow mode (Figure I-21). At a flow rate of 0.25 mL.h^{-1}, the S-4-(4-methoxyphenyl)-2-butanamine yield was maintained over 90% during the 160 hours of operation.

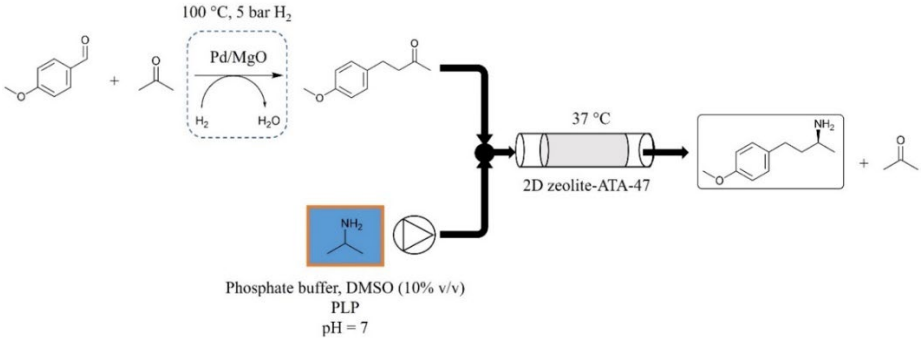

Figure I-21. Schematic representation of the chemo-enzymatic process involving a flow asymmetric synthesis of S-4-(4-methoxyphenyl)-2-butanamine (framed compound), described by Corma *et al.* [245]. The dotted area represents the semi-continuous batch reactor hosting the chemocatalytic step of the cascade (aldol-reduction).

Silica-based micro-reactors also were handled by Baganz *et al.* [232] for the immobilization of transaminase and transketolase (TK) enzymes, and exploited for the flow cascade synthesis of a valuable chiral amino-alcohol: (2R,3S)-3-aminobutane-1,2,4-triol (a building block used in pharmaceutical industry). Nickel-derivatized silica (previously made more hydrophobic *via* MTES grafting) was employed for His-tag affinity immobilization. To perform the multi-enzymatic cascade, two separated micro-reactors containing the respective enzymes were placed in series. The first immobilized enzyme (TK) catalyzed the model conversion of lithium-hydroxypyruvate and glycolaldehyde to L-erythrulose (ERY), while the second micro-reactor unit (loaded with immobilized ATA) converted ERY into aminobutanetriol. Transamination was conducted in the asymmetric synthesis mode, using S-MBA as amino donor. Similarly, authors from the same group [233] achieved such flow mode synthesis of chiral aminobutanetriol amino-alcohols, but with a different support for the immobilized ATA and TK enzymes (i.e. Ni-NTA derivatized agarose beads ; Figure I-22).

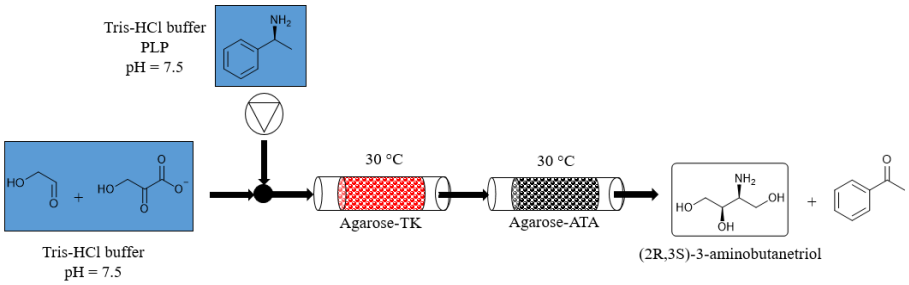

Figure I-22. Schematic representation of the process leading to the continuous multienzymatic synthesis of (2R,3S)-3-aminobutanetriol, described by Baganz *et al.* [232]. By-product (CO_2) and intermediate compound (L-erythrulose) generated by transketolation were intentionally omitted for clarity purpose.

In 2017, Sans *et al.* [234] demonstrated the first example of modified 3D-printed devices for the immobilization and application of ATAs in continuous flow-mode. A commercially available Nylon (Taulman 645 and 618) was 3D-printed and chemically modified in order to ensure subsequent covalent grafting of ATAs. More precisely, Nylon was treated with HCl in order to generate superficial amine groups, which were then modified with alternated glutaraldehyde-polyethyleneimine (PEI) layers to provide covalent anchoring points for the enzymes. The authors first used the transamination of S- and R-MBA with pyruvate in batch mode, using both S- and R-selective commercial ATAs to showcase the technology. The immobilized R-selective ATA-117 was then selected for the continuous flow experiment (*i.e.* flow kinetic resolution of *rac*-MBA Figure I-23). When working with a residence time of 50 min, almost full conversion and enantiomeric excess were observed. Moreover, the immobilized biocatalyst showed good operational stability as it displayed stable performance during ~100 hours of time on stream.

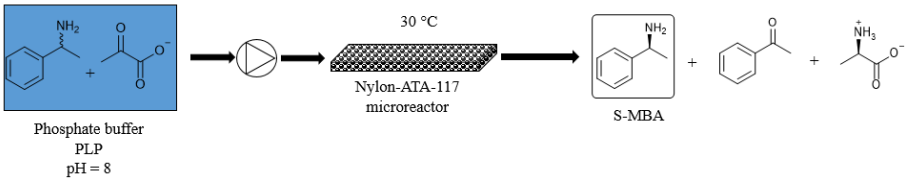

Figure I-23. Schematic representation of the continuous kinetic resolution of *rac*-methylbenzylamine (*rac*-MBA) using immobilized transaminase, described by Sans *et al.* [234].

1.3.3 Flow mode transamination with ATA co-immobilized with its cofactor (PLP)

Sticking to the aim of developing more robust biocatalysts with enhanced operational life-span and enhanced cost efficiency, the López-Gallego and Paradisi groups have developed novel strategies to co-immobilize enzymes and their phosphorylated cofactors (e.g. PLP and NADH onto a plethora of porous beads) [171,246]. Such novel biocatalyst formulation should allow processing flow enzymatic reactions without additional (exogeneous) feed of the cofactor during operation. The authors managed to demonstrate such model of self-sufficient heterogeneous biocatalysts by co-immobilizing ATAs and PLP onto metal derivatized commercial epoxy-activated methacrylate beads (Lifetech Purolite® ECR and Sepabeads® EC-EP/S) [236]. The metal derivatization (leading to cobalt chelates) was first performed as described by Paradisi *et al* [131]. A fraction of the remaining epoxy-groups of the carriers were subsequently modified with amine groups (reaction with ethanolamine (eA), hydroxylamine (hA) or polyethyleneimine (PEI)). Modification with eA and hA provide electrostatic interaction points for PLP adsorption. Modification with PEI additionally allows establishing reversible covalent (imine) bonds between the carrier and PLP (Figure I-24). ATA immobilization was promoted by His-tag affinity and consisted in a multi-covalent attachment on the residual epoxy groups present on the carriers.

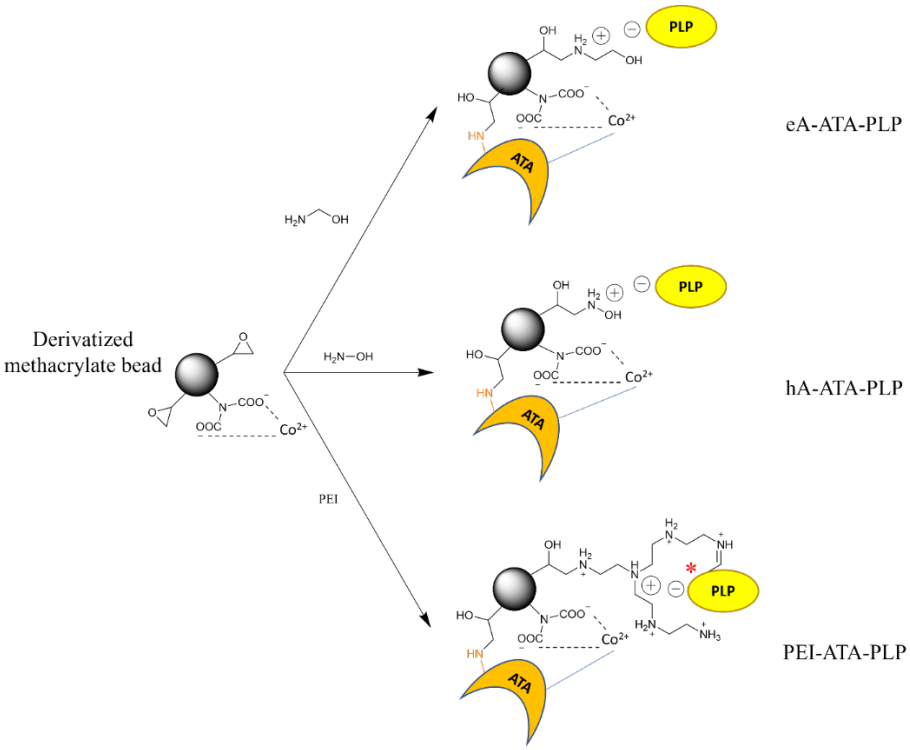

Figure I-24. Preparation of self-sufficient biocatalysts. Methacrylate-based carriers activated with epoxy groups were first pre-functionalized (not shown) with cobalt chelates able to drive the His-tagged ATA immobilization. The resulting carrier was further activated with amine groups from ethanolamine (eA), hydroxylamine (hA) and polyethyleneimine (PEI) for the PLP co-immobilization. Red asterisk highlights the dual binding of PLP on the PEI layer. Note that the orange bonds represent the ATA lysine groups involved in the covalent attachment (with the residual epoxy groups of the carriers). Adapted from [236].

The catalytic performance of the resulting self-sufficient heterogeneous biocatalysts were evaluated towards the flow deamination of S-MBA into acetophenone (in a PBR), without exogenous addition of PLP. The beneficial impact of such dual PLP binding (enabled by the PEI) on catalytic performance was clearly highlighted by the greater operational stability displayed by the PEI-coated biocatalyst, EC/PEI-HeWT-PLP. Pleasingly, EC/PEI-HeWT-PLP even displayed higher stability than the corresponding biocatalytic system continuously supplied with exogenous PLP, for 100 minutes of time on stream (in the flow synthesis of cinnamylamine ; Figure I-

25). Finally, the authors expanded this concept of self-sufficient heterogeneous biocatalysts to other ATAs: *Cv*-ATA and the ATA from *Pseudomonas fluorescens, Pf*-ATA. Interestingly, clear differences in terms of operational stabilities were observed between the ATAs when performing the deamination of S-MBA into acetophenone in flow. The obtained trend was as follow: HeWT > *Pf*-ATA > *Cv*-ATA. The cofactor loading was around 7.5 µmol.g^{-1} on all the EC/PEI-ATA-PLP catalysts.

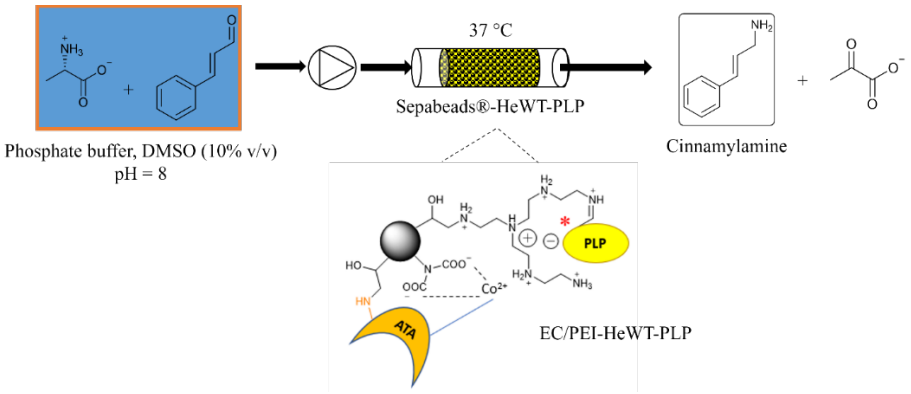

Figure I-25. Schematic representation of the continuous production of cinnamylamine (employing self-sufficient immobilized transaminase, without exogeneous PLP addition), described by Lopez-Gallego *et al.* [236].

This self-sufficient co-immobilized biocatalyst system was also used for the synthesis of high value biogenic aldehydes in a PBR (using HeWT) [237]. The packed enzyme column was fed by a segmented biphasic flow stream (80:20 buffer/toluene) formed through toluene addition at the entrance of the reactor. Such biphasic system allowed an in-line separation of pure aldehydes (recovered in the toluene stream) from L-alanine and unreacted amines (that remained in the aqueous phase) without affecting the biocatalyst's activity. Similarly, Liu and co-workers managed to covalently co-immobilize both an ATA and PLP on functional epoxy resins [238]. Thus, compared to the previously reported self-sufficient ATA catalysts (on which PLP is

immobilized through reversible covalent interactions) [236], here, the epoxy groups of the resin formed irreversible covalent bonds with the phosphate group of the PLP. They also afforded the covalent immobilization of the ATA *via* grafting of its lysine residues. A linker, with appropriate length (12 carbons), ensured a high PLP-epoxy binding efficiency and did not alter PLP conformation. Similar cofactor loadings to those previously obtained on epoxy-activated methacrylate beads (c.a. 7 µmol.g^{-1}) were achieved through this protocol. This self-sufficient biocatalyst was employed in the flow asymmetric synthesis of R-sitagliptin in a PBR for > 500 hours of time of stream, without exogenous addition of PLP (Figure I-26). ISO (35 g/L) was used as amino donor. For each column volume (*i.e.* 45 min residence time), the yield and enantiomeric excess of R-sitagliptin reached at least 90% and 99%, respectively. An overall space-time yield of 40.0 g.L^{-1}.h^{-1} was obtained.

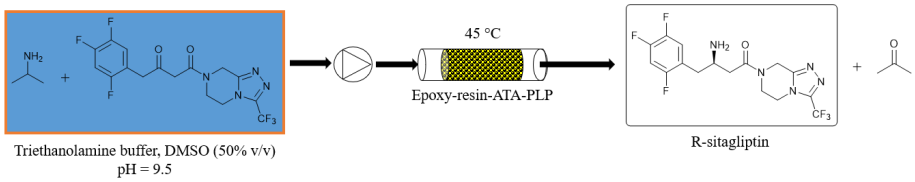

Figure I-26. Schematic representation of the continuous asymmetric synthesis of R-sitagliptin (employing self-sufficient immobilized transaminase, without exogeneous PLP addition), described by Liu *et al.* [238].

Noteworthily, the PEI-derivatized lignin carrier discussed above [231] (see section 1.5.2) also enabled the co-immobilization of ATA and PLP. The cofactor was immobilized by dual reversible interactions on the PEI layer, which allow it to travel to the enzyme active site without diffusing through the lignin network. PLP loading yielded c.a. 7 µmol.g^{-1}, like on others self-sufficient biocatalysts [236,238]. Such biocatalyst was integrated in a PBR to perform the flow synthesis of cinnamalylamine. At a flow rate of 0.35 mL.min^{-1}, the self-sufficient biocatalyst showed stable performance and maintained > 50% conversion during the 100 minutes of operation.

Independently, Menegatti and Žnidaršič-Plazl [187] also demonstrated the possibility to obtain such self-sufficient heterogeneous biocatalyst *via* enzyme and cofactor entrapment into a microreactor containing a polyvinyl alcohol (PVA) and sodium alginate copolymer hydrogel. The microreactor was composed of two PMMA rectangular plates (200 μm thick, 25 mm wide, 50 mm long), filled with the hydrogel. The ATA and PLP were first immersed into the polymeric network, and a $CaCl_2$ post-treatment was eventually applied to reduce the pore size to <5 nm. The resulting biocatalytic microbioreactor was employed to run the model deamination of S-MBA and pyruvate into acetophenone and L-alanine in flow mode. 92% of the initial productivity was retained and no leaching of PLP or enzyme from the hydrogel was observed after 10 days of continuous operation. Similar performance was obtained with and without addition of exogenous PLP, suggesting an efficient cofactor immobilization. The space-time yield was 19.91 g L^{-1} h^{-1}.

1.3.4 Flow mode transamination with ATA co-immobilized with other enzymes

Enzymatic cascade reactions exploiting multi-enzyme systems appear a highly attractive solution for the design of greener synthesis processes. Here too, (co)-immobilization is considered as the key, allowing to envisage robust processes where (multi)-functional biocatalysts can be (i) recovered and reused in batch mode, or (ii) exploited in continuous flow mode. Materials featuring several co-immobilized enzymes are primed to simplify and intensify continuous processes, *e.g.* by using a single PBR, avoiding transitional separation and purification of intermediates, and displacing equilibria towards product formation [247,248]. Examples of multi-enzyme heterogeneous biocatalysts featuring immobilized ATA operating in continuous flow are discussed below.

In 2009, Yang *et al.* [148] reported on the combined use of transamination and dehydrogenation, for the flow mode glutamate quantification in rat plasma. Glutamic-pyruvic transaminase (GPT) and glutamate dehydrogenase were co-immobilized into a glass micro-capillary previously functionalized with APTES and glutaraldehyde. The transaminase was used for the recycling of α-keto-glutarate (previously produced by glutamate dehydrogenation) into glutamate, as shown in Figure I-27. Glutamate concentration was indirectly monitored through NADH product quantification. As the transaminase catalyzes the reaction between the natural amino acid and α-keto acid, the chemical equilibrium was highly favourable.

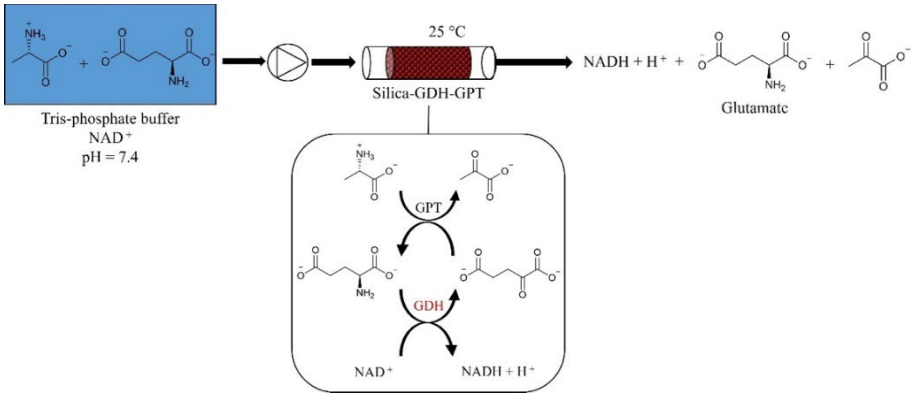

Figure I-27. Schematic representation of the multienzymatic one-pot process described by Yang *et al.* [148] (including flow transamination, in combination with a flow glutamate dehydrogenation) resulting in the continuous blood glutamate determination. The complete cascade reaction is highlighted in the frame. GPT and GDH stand for glutamic-pyruvic transaminase and glutamate dehydrogenase, respectively.

In 2021, Romero-Fernandez and Paradisi [239] synthesized the drug betazole by co-immobilizing alcohol dehydrogenase, HLADH (i.e. a NADH-dependent enzyme that oxidizes alcohols into aldehydes) and HeWT onto functionalized epoxy-activated methacrylate beads (Relisorb® EP400SS). In order to shift the equilibrium of the alcohol oxidation (and thus, of the entire cascade) and enable the *in-situ* continuous recycling of the NADH cofactor, a

third enzyme was grafted on the carrier: the NADH oxidase (NOX). Since NOX uses O_2 as oxidant (generating H_2O as by-product), the multifunctional heterogeneous biocatalyst a constant supply of oxygen was fed through a segmented air-liquid flow. The resulting multifunctional biocatalyst allowed performing a flow-cascade in a PBR, starting from 2-(1H-pyrazol-3-yl)ethanol and yielding betazole in good yields (73 %) (Figure I-28). A space-time yield up to 2.59 $g.L^{-1}.h^{-1}$ with 15 min residence time was achieved.

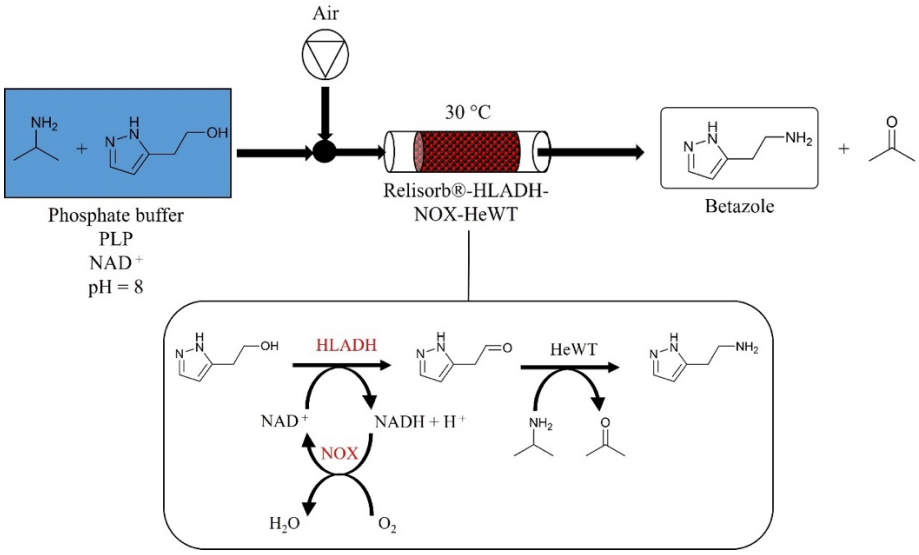

Figure I-28. Schematic representation of the one-pot multienzymatic production of betazole drug described by Romero-Fernandez and Paradisi [239] (including flow transamination, in combination with flow alcohol dehydrogenation and NADH oxidation). The complete cascade reaction is highlighted in the frame. NOX cofactor (FAD) was intentionally omitted for clarity.

Paradisi et al. [240] employed this same co-immobilized HLADH-NOX-HeWT biocatalysts system to access the flow cascade synthesis of 6-aminocaproic acid (a Nylon 6 precursor) from ϵ-caprolactone. The enzymes were combined with commercially available *Candida antarctica* lipase B (CalB, Novozym® 435), which performed the first step of the cascade (i.e. hydrolysis of ϵ-caprolactone into 6-hydroxycaproic acid). A substrate solution was flowed into the two sequential PBRs, respectively containing

immobilized CalB (10 min residence time) and co-immobilized HLADH-HeWT-NOX (15 min residence time). A segmented air-liquid flow was also fed into the second PBR, in order to feed oxygen to the NOX enzyme for the *in-situ* continuous recycling of the NADH (Figure I-29). A final conversion of 34 %, associated with a space-time yield of 3.31 $g.L^{-1}.h^{-1}$, was achieved. Remarkably, this study represents the first biocatalytic synthesis route of 6-aminocaproic acid from ϵ-caprolactone, which can be derived from lignocellulosic biomass. It is also the first synthesis of this platform chemical in continuous flow-mode.

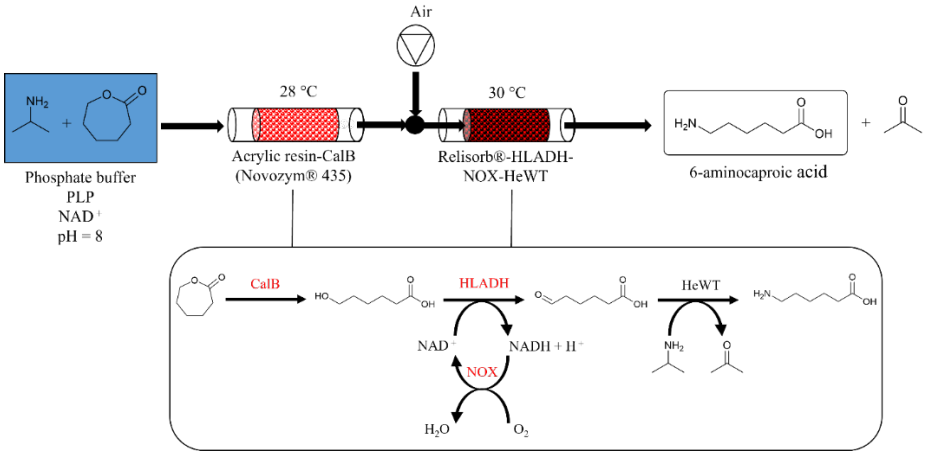

Figure I-29. Schematic representation of the one-pot multienzymatic production of 6- aminocaproic acid (a Nylon 6 precursor), including flow transamination, in combination with flow alcohol dehydrogenation and NADH oxidation [240]. The complete cascade reaction is highlighted in the frame. NOX cofactor (FAD) was omitted for clarity.

It should be noted that the combination of several enzymes in one continuous flow process can also be applied with whole cells biocatalysts. A sol–gel process was exploited by Poppe *et al.* [241] to co-immobilize *Escherichia coli* whole cells with *Cv*-ATA activity and *Lodderomyceselongisporus* yeasts with ketoreductase activity (*Le*KRED) in hollow silica microspheres. The bifunctional biocatalyst allowed performing a cascade of reactions to convert racemic amines into a mixture of the corresponding enantiomerically pure R-

amine and S-alcohol in continuous flow mode. In other words, the kinetic resolution catalyzed by *Cv*-ATA let enantiopure R-amine unreacted as it enabled the bioconversion of the S-amine into the corresponding ketone, which was subsequently reduced into the corresponding S-alcohol by *Le*KRED (Figure I-30). Notably, the authors managed to obtain simultaneously two different APIs : R-4-phenylbutan-2-amine (a constituent of Dilevalol drug) and S-4-phenyl-2-butanol (a precursor to antiepileptic agents). Moreover, they demonstrated that the use of such bifunctional heterogeneous biocatalyst containing both co-immobilized whole cells (with overexpression of the enzyme) in a single reactor enhances the activity and the operational stability of the system compared to that of the cascade featuring single-cells immobilized in separated reactors (placed in series).

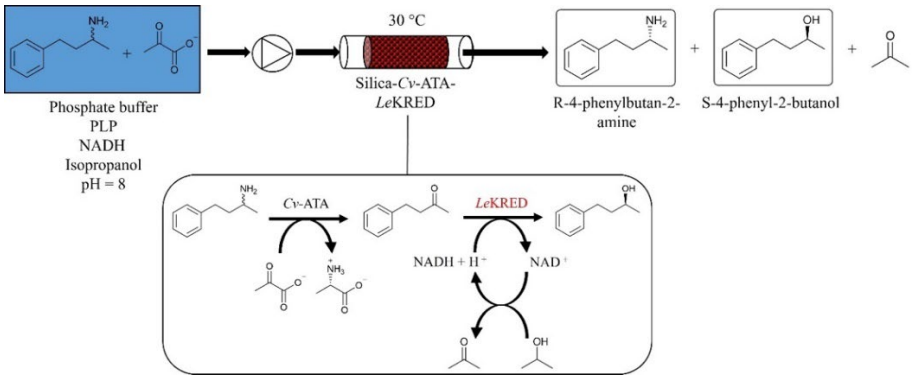

Figure I-30. Schematic representation of the one-pot multienzymatic production of R-4-phenylbutan-2-amine and S-4-phenyl-2-butanol (including flow transamination, in combination with flow ketone reduction) described by Poppe *et al.* [241]. The complete cascade reaction is highlighted in the frame. *Le*KRED stands for *Lodderomyceselongisporus* yeast displaying ketoreductase activity.

1.4 Conclusion

Transaminases have gained immense interest lately as their potential to produce enantiopure amines at a lower environmental cost is now well-established. Considerable efforts have been deployed to mitigate the limitations that used to hinder their application at large-scale. In particular, implementing equilibrium displacement methods and leveraging effective enzyme immobilization strategies made the application of transaminases more realistic. Moving further, we argue that embracing a transfer from batch processes – where the enzyme is soluble in the liquid phase – to heterogeneous flow processes – where the enzyme is immobilized on a solid carrier, is a key step in the development of biocatalytic transamination for organic synthesis.

The present review extensively covers and discuss applications featuring immobilized transaminases in continuous flow-mode. As illustrated with a variety of successful examples, the opportunities offered by continuous flow mode processing for the biocatalytic production of chiral amines are multiple: in addition to enhance their productivity as well as scalability (due to improved mass transfer and biocatalyst reusability), it facilitates the combination with other reactions, it is amenable to multi-enzymatic cascade reactions and it allows envisaging useful in-line separations such as product purification (*e.g. via* catch-and-release systems, membrane separation, etc.). Integrated processes allowing to simultaneously perform flow transamination reactions and product separation (to drive the equilibrium), are of particular interest [103,249]. We argue that the implementation of novel hybrid reactors which simultaneously host the immobilized enzymes and perform product separation (*e.g.* in membrane reactors), will foster further advances in the field of greener chiral amine synthesis.

It appears undisputable that continuous flow mode biocatalytic processes pave the way for the development of more efficient, industrially relevant,

greener, and intensified organic synthesis [250]. This report should provide useful guidelines to industrial chemists who envisage turning to flow biocatalysis for their drug production, but also academic researchers who will keep inventing greener routes to high-value molecules. The deployment of flow biocatalysis is a multidisciplinary challenge that requires various expertise. Arguably, the "cross-fertilization" – illustrated in this review – between the fields of biocatalysis and organic synthesis on the one hand, and process and materials engineering on the other hand, is crucial for both academic and industrial developments.

Chapter II – State of the art on enzyme-membrane-reactors

The content of this chapter is submitted for publication in *Comptes Rendus Chimie*.

"Enzyme-membrane-reactors: recent trends and applications for the production of fine chemicals and pharmaceuticals". H. M. Arango, P. Luis, T. Leyssens and D. P. Debecker, 2024.

ABSTRACT

Biocatalysis has gained considerable attention lately as a potential greener method for producing high-value compounds. Enzymes, notably due to their high selectivity, offer significant advantages for organic synthesis. However, industrial implementation remains limited due to challenges such as free enzyme instability, inhibition, and issues in recovery and reuse. The coupling of biocatalysis with membrane technology in enzyme-membrane-reactors (EMR) holds significant potential for process intensification, as it enables continuous flow synthesis concatenated with product purification, and biocatalyst recovery. By allowing flow hybrid processes (i.e. simultaneous biocatalytic reactions and membrane operations in one-pot), EMR have the potential to increase reaction yields and kinetics, as well as reducing downstream processing requirements. This review explores recent trends and advances in EMR for the production of pharmaceutical building blocks and fine chemicals. We examine the combination of enzymes with both polymeric and ceramic membranes, highlighting their respective benefits and limitations. Importantly, this review also distinguishes EMR processes where free enzymes are used separately from membrane devices, and those employing membrane-immobilized enzymatic reactors. As enzyme immobilization in/on solid supports has emerged as an effective approach for enhancing enzyme stability and reusability, we argue that the development of such membrane-immobilized enzyme reactors is of prime importance in organic synthesis. These insights aim to provide a comprehensive overview of the role and recent applications of EMRs in advancing biocatalytic processes within the pharmaceutical industry.

1. Enzyme-membrane-reactors: recent trends and applications for the production of fine chemicals and pharmaceuticals

1.1 Introduction – membranes as practical tool to intensify biocatalytic processes

Over the past decades, biocatalysis has emerged as a promising and potentially greener approach to produce value-added molecules [167]. Owing to their unique characteristics, such as their high (enantio)selectivity and stereospecificity, non-toxicity (biodegradable), and their ability operate under mild conditions (e.g., aqueous media, low temperatures), enzymes have gained significant interest in organic synthesis and pharmaceutical industry [251]. Hence, biocatalytic processes have the potential to rapidly become a powerful synthetic tool for the industrial preparation of valuable compounds, such as pharmaceuticals and fine chemicals [8,65,252].

However, despite multiple benefits and advantages they offer, their implementation at the industrial level in the pharmaceutical industry is not straightforward and remains limited [2], due to several challenges. These are generally related to the fact that enzymes are often used in their "free" form, functioning as soluble homogeneous biocatalysts that are difficult to reuse, restricted to batch reactors, and which typically exhibit limited stability [168]. Additionally, enzymes tend to suffer from substrate and/or product inhibition, and – in some cases – unfavorable thermodynamic equilibria for the targeted reactions. The quality of the final product can also be compromised by free enzyme deactivation, resulting in complex purification processes [166].

Some of these challenges can be mitigated by immobilizing enzymes on solid supports [177,253], which allows for their recovery and reuse, as well as their implementation in continuous flow processes [174]. Moreover, immobilization

often results in enhancing the enzyme stability and tolerance to organic solvents [163,254]. The transfer from batch to continuous-flow processing is of major industrial interest as it increases the productivity of (bio)catalytic transformations and the efficiency of subsequent/coupled unit operations (e.g. crystallization), thus improving the overall process's economic viability [165,167,170,172,173,175,209,255–258]. Flow enzymatic processes arguably pave the way for the development of intensified industrially relevant organic synthesis [250].

Enzyme immobilization can be performed in various ways, and on a wide range of functional materials such as polymeric resins, inorganic powders, biopolymers, or membranes [152,163,164]. Ready-to-use synthetic resins are the traditional ubiquitous carrier, allowing to run biocatalytic reactions in heterogeneous catalysis mode, and to easily recover and reuse the biocatalysts. However, enzyme immobilization on membranes should be considered as well, as it additionally offers the possibility to perform biocatalytic reactions along with membrane separation, in a one-pot fashion. For example, the removal of a product can favorably shift the biocatalytic reaction equilibrium toward product formation and hence increase the reaction yield. Also, membranes can be used to introduce one of the reagents at a controlled rate, to avoid enzyme inhibition. The coupling of biocatalytic reaction with membrane operation in so-called "enzyme-membrane-reactors" (EMR) have great potential to intensify biocatalytic processes. Typically, membrane separations have the advantage of requiring only a limited amount of energy with respect to other unit operations [259–261]. Furthermore, membrane-reactors also display relatively easy reactor operation and modulation, as well as straightforward scale-up to large systems [166,262–264].

Integrated hybrid processes allowing to simultaneously perform flow biocatalytic reactions and product separation (e.g. to drive the equilibrium) or controlled substrate addition, are of particular interest for the pharmaceutical industry [103,249,265]. Through this report, we aim at gathering a useful and exhaustive list of recent examples employing enzyme-loaded membrane

technologies for the production of pharmaceutical building blocks and fine chemicals.

It must be noted that the concatenation of reaction and membrane separation on catalytically active membranes is already well established, and has been reviewed extensively. For example, Zhang et al.[266] reviewed the applications of a wide range of polymeric catalytic membranes to intensify chemical processes. Also, conventional enzyme immobilization methods and strategies have already been extensively and thoroughly reviewed [107,160,166,267–269]. These accounts focus on the detailed preparation and/or functionalization of various supports – including membranes – for enzyme immobilization. Also, some excellent reviews [166,265–267,270–272] cover the interests of implementing EMR in organic synthesis, by gathering scholarly examples and/or providing useful insights on industrial process considerations. For example, the tutorial reviews by Sitanggang et al. [272] and Dejonghe et al. [265] summarize the interest of coupling enzymes (free or immobilized) with membrane reactors and exemplified their use in a selection of chemical processes.

In this review, we aim to discuss the recent trends (i.e. 2010 or later) of EMR processes applied specifically for the production of valuable (chiral) building blocks for the pharmaceutical industry. We cover both ceramic and polymeric membranes applications. Polymeric membranes are most commonly employed support to develop biocatalytic membrane reactors, and present an array of advantages with respect to their ceramic counterparts. For example, polymeric membranes tend to be generally cheaper and offer a wider range of manufacturing techniques have been developed to enable better control and tailoring of the final membrane properties [251,266]. Yet, their organic nature often hampers their chemical stability, which could be an issue when such membranes are put in contact with organic solvents and hence, limit their applicability in multiphasic membrane reactors [273]. On the other hand, ceramic membranes are able to overcome these drawbacks thanks to their inherent

outstanding chemical and thermal stability [273,274], hence we consider that it is also important to cover their applications.

1.2 Main synthetic routes that can benefit from the synergistic use of enzymes and membranes

Chiral compounds are the most important building blocks in the chemical and pharmaceutical industry, as they are widely employed for the production of fine chemicals and drugs [275,276]. Moreover, it is increasingly important to synthesize enantiopure drugs for the pharmaceutical industry [277,278]. More precisely, enantiopure alcohols [85] and amines [5,8,167] are key examples of prime importance in the synthesis of pharmaceuticals, but also in the flavours and fragrances industry. Here, we first define the scope of this study, by selecting the main targeted biocatalytic reactions that we will cover in this work.

Using transaminases (Figure II-1a) and alcohol dehydrogenases (Figure II-1b) is a conventional biocatalytic strategy to produce chiral amines and alcohol, respectively. [18,279,280] Most industrially relevant transaminations suffer from unfavourable thermodynamics, and transaminases tend to be inhibited by their keto substrate (amino-acceptor) and by-products. To achieve high transamination yields while avoiding transaminase inhibition, in situ (co)-product removal and/or controlled substrate addition can be performed using membrane technologies [214,281,282]. One possible strategy is the use of pervaporation to remove acetone (i.e. the most common co-product of transamination reactions). Pervaporation is especially attractive for the temperature-sensitive processes because it can be operated at moderate temperatures.

Dejonghe et al. [282] implemented a hydrophobic pervaporation at the outlet of a transamination reactor (running the S-MBA asymmetric synthesis employing free enzymes) in order to remove the acetone by-product from the biocatalytic system. A PolyDiMethylSiloxane (PDMS) membrane module,

was used as pervaporation unit. Such transamination coupling with pervaporation resulted in a 13% increase in product yield after 9 hours of reaction, compared to the standard transamination process (where no pervaporation was performed). However, it was also observed that the effect of acetone removal by pervaporation is minimal at low acetone concentrations (in the biocatalytic system). This highlights the need to work at high substrate concentrations and possibly to couple pervaporation to another product separation technique (which would allow to primary push the transamination towards high product yields). This other product separation technique should target the amine product, and may be also performed via membrane technology (e.g. via membrane-extraction). Notably, Dejonghe et al. [283] conducted the flow asymmetric synthesis of 1-methyl-3-phenylpropylamine (MPPA) from benzyl acetone using free ATA-v2 mutant enzyme in organic solvent (n-heptane), and employed polypropylene (PP) membranes contactor for the *in situ* amine product removal. An acidic aqueous solution (pH = 3) was used to efficiently extract the amine product via membrane-assisted extraction. In this study, the use of an organic solvent as reaction medium was found beneficial in the sense that it allowed to increase the optimal keto-substrate concentration (by 2.5-fold with respect to its aqueous solubility) without triggering inhibition. This approach resulted in a significant increase in terms of final product yield (i.e. 99% yield) with respect to the standard transamination process (i.e. 69% yield when run without membrane-assisted extraction). Additionnally, by demonstrating the intensified asymmetric synthesis of the R-sitagliptin drug, Yang et al. [284] successfully expanded the applicability of such synergistic coupling between transamination and membrane-assisted product separation. In this case, transamination was conducted in aqueous medium (pH = 9) and PDMS was used as membrane contactor for the solvent extraction. In all these examples, the use of membrane operations offers avenues to intensify the synthesis process.

Other (chiral) molecules such as carboxylic acids or esters can lead to the obtention of valuable compounds, including chiral intermediates [264,285–287]. To this aim, lipases have gained much attention lately as they allow for the enantioselective hydrolysis/esterification (Figure II-1c) and transesterification (Figure II-1d) of poorly water-soluble compounds (i.e. in biphasic media or in organic solvents) [288,289]. Enzymatic esterification reactions are commonly conducted in non-aqueous solvents, as water accumulation in the reaction medium can promote side reactions (e.g. hydrolysis) and hamper the final esterification yields [290,291]. Additionally, for enzymatic process, it is well-known that excess water should be avoided to preserve high lipase activity [292,293]. In lipase-catalyzed esterification, for example, water by-product can be removed *in situ* from the reactor using membrane technologies. Pervaporation seems particularly suited for such purpose, since it requires significantly lower energy consumption and operating costs with respect to distillation processes [294]. Notably, the pervaporation-aided enzymatic production of monoacylglycerols from lauric and caprylic acid with glycerol, in solvent-free medium, was demonstrated by Satyawali et al. [295] in 2021. Lipases immobilized on polymeric resins in packed-bed reactor (3 kg scale) operating in recirculation mode, were coupled with two zeolite membranes (in series, 56.5 cm^2 total area) for pervaporation. Such coupled esterification-pervaporation process not only allowed to push the fatty acids conversion towards completion (> 95% after 256 hours), but also afford to increase the relative monoacylglycerols content in the final product (with respect to di- and triacylglycerols). Such study demonstrates the practical applicability of zeolite based membranes for *in situ* water removal.through hydrophilic pervaporation.

Various functional oligosaccharides, such as lactulose, galacto-oligosaccharides (GOS) [296], cyclodextrins [297] or oligodextran (5-8 kDA) [298,299], are known to have potential applications in the fine chemicals and pharmaceutical industries. β-galactosidase can catalyze the direct obtention of

GOS (Figure II-1e) and lactulose from lactose via transgalactosylation reactions [296,300,301]. Lactose (a disaccharide composed of glucose and galactose) is generated in high contents in the dairy by-product of many (bio)chemical processes [302,303], and acts as a renewable feedstock to produce such building blocks. Cyclodextrin glycosyltransferase and dextranase catalyze the conversion of starch into mixtures of (cyclo)dextrins and the hydrolysis of dextran into oligodextrans of various molecular weights, respectively.

A severe limitation in transgalactosylation reactions is that the targeted products tend to spontaneously undergo undesired consecutive reactions (i.e. hydrolysis reactions to monosaccharides glucose and galactose) [304]. Besides, it has been observed that such monosaccharides formation inhibits the β-galactosidase (i.e. inhibition of transgalactosylation reaction) [265], which further highlights the need of a product separation in these processes. Finally, selecting producing oligodextran of tailored molecular weight is also a complicated task. Hence, it clearly appears that, in all these biocatalytic reactions, the coupling with membrane technology is of particular interest, since it would afford to enhance the selectivity of the process, and the purity of the targeted product (i.e. desired molecular weight) by operating adequate size-exclusions membrane operations.

Peptides are another class of target compounds exhibiting biological activities (e.g. antihypertensive, antioxidant), which find nutritional, cosmetic, pharmaceutical applications [265,305]. Peptidases catalyze their production through protein hydrolysis (Figure II-1f). However, it is established that the efficiency of peptidases decreases upon accumulation of the hydrolysis products (i.e. soluble peptides and amino acids) in the medium [265,306]. Here, conducting protein hydrolysis in continuous membrane reactors (i.e. through size-exclusion membrane operations) enables the separation of low-molecular-weight peptides from protein hydrolysates, thereby overcoming the drawbacks of batch reactions, such as product inhibition, low process

productivity, and excessive hydrolyses (i.e., prevention of side reactions) [265]. Additionnally, the continuous feeding of substrates (e.g. water in this case) to the reactor is advantageous as it allows to enhance the reaction kinetics, and to maintain a constant volume in the reactor by compensating the permeate flux. Such beneficial substrate addition was demonstrated by Ma et al.[307], which conducted the membrane-assisted enzymatic protein hydrolysis for the tailored production of antihypertensive peptides. First, the membrane ultrafiltration unit was implemented at the outlet of the reactor tank, which allowed to recycle the free enzymes (retained in the retentate) and prevent undesired product inhibition (*via* product separation). When further coupling the enzymatic hydrolysis (performed in recirculating mode) with continuous feeding of water to the reactor, the yield and productivity were respectively enhanced by 62.7% and 22.1% when compared to the standard batch operation (i.e. run without membrane separation and substrate feeding). The continuous addition of the protein substrate (in addition to water feeding) enabled to further boost the peptides productivity.

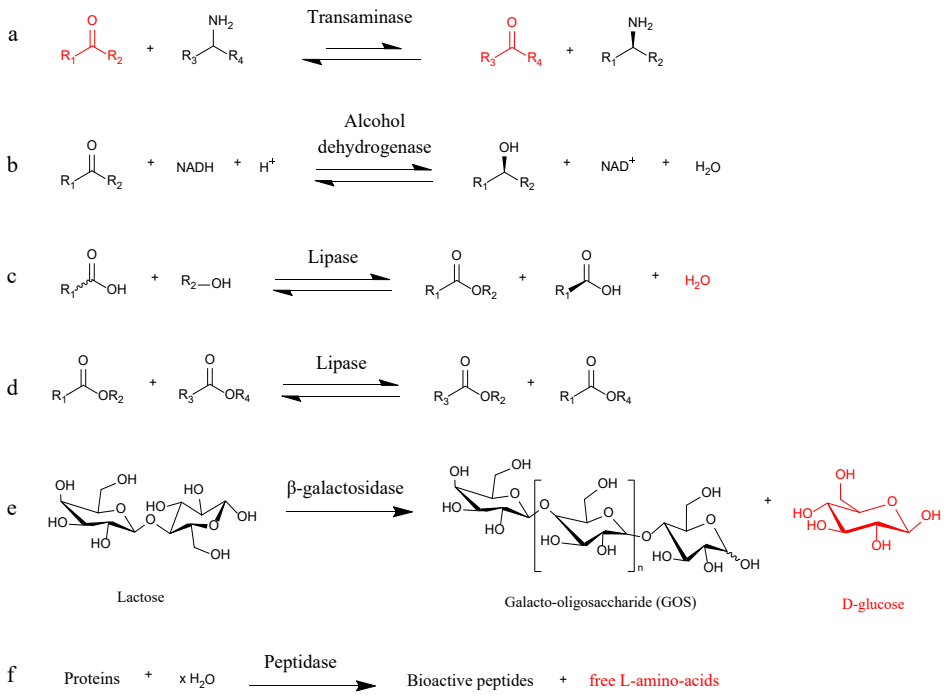

Figure II-1. Main enzymatic transformations leading to pharmaceuticals and fine chemicals, and susceptible to be coupled with membrane reactors, studied in this work. Products highlighted in red are responsible for enzyme inhibition.

Overall, one of the key advantages of coupling biocatalysis with membrane technology is the ability to run biocatalytic reactions while simultaneously performing product/substrate separation from the enzymes, and from the reaction medium. Furthermore, it allows operating the synthesis process in continuous flow mode, which enhances productivity and economic feasibility of the process. Using multiple membranes in series with different molecular weight cut-offs (MWCO) can also enhance product selectivity, and the final step of membrane separation allows the concentration of the non-permeable product. The selected membrane material must be stable under the conditions (temperature, pH, presence of organic solvent) that optimize the enzyme's catalytic activity. Enzymes can be used either in their soluble (freely dispersed) or immobilized forms when being coupled with membrane

reactors. This defines two categories of hybrid processes that are consecutively discussed in the next sections.

1.3 Free or immobilized enzymes combined with membrane technology

When working with free enzymes in solution, size-exclusion membrane operations are often chosen to separate the soluble biocatalyst [270] (retained in the retentate in cross-flow operations, see Figure II-2) while isolating the product in the permeate [272]. In such size-exclusion operations, the membranes porosity – which defines its molecular weight cut-off (MWCO, in kDA) – has to be carefully chosen based on the molecular size of the enzyme (if present in free form), substrate(s), and product(s). Given that enzyme molecular weights typically range from 10 to 150 kDa, ultrafiltration (UF) membranes are commonly used in various membrane reactors designs. The UF membrane pore size must ensure complete enzyme retention while ensuring unobstructed product transport. Nanofiltration (NF) membranes can also be employed in size-exclusion membrane operations design, especially for biocatalysts displaying small molecular weights (typically 0.2 to 10 kDA, such as for example some cysteine proteases [308]) [309,310]. Additionally, NF membranes are effective in concentrating target compounds as a secondary separation step [311]. As product purification is known to be a major driver of the cost of drugs manufacturing, this is a crucial point.

Further than facilitating product separation, membranes-based operations are particularly helpful to displace the thermodynamic equilibrium and enhance synthesis yields. Table II-1 gathers a list of examples (as exhaustive as possible among the selected biocatalytic transformations listed in the Figure II-1) of membrane-induced equilibrium-shifting strategies have already been applied in combination with soluble or immobilized enzymes, in order to

intensify biocatalyzed reactions. Here, soluble enzymes were typically employed separately from the membrane devices (i.e. membranes were at the boundary or at effluent of the enzymatic reactors, acting as separation units) as represented in Figure II-2, and not in a one-pot fashion. Note that other membrane-intensified transaminations employing heterogenized biocatalysts were also reported [214,242,249,281], yet these studies fall outside of the scope of such report as they involved whole-cells (instead of enzymes) as biocatalysts.

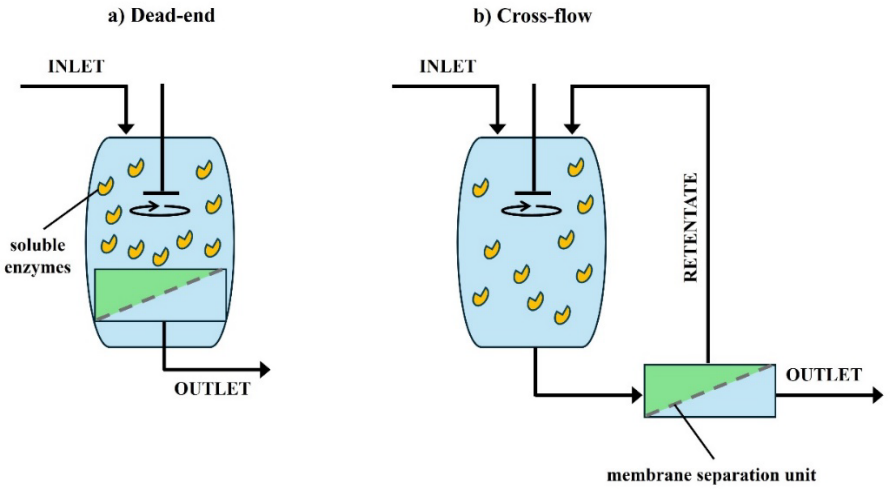

Figure II-2. Schematic representation of biocatalytic processes involving free enzymes in combination with membrane separation units. In case **b)** enzymes are recycled (retained) in the retentate through membrane separation. Reproduced from Sitanggang et al (2022) [272], with permission.

Table II-1 – Exhaustive list of recent (2010-2024) examples of enzymes combination with membrane technologies for the considered biocatalytic processes intensification

Reaction(s)	Substrate	Product	Enzyme	Immob. (carrier)	Membrane	Operation	Mode	Refs
Carboligation	Benzaldehyde + acetaldehyde	(S)-2-hydroxypropiophenone	Benzoylformate decarboxylase	/ (free)	Polymeric (N.D., 10 kDA)	UF (dead-end)	Flow	[312]
Cascade (De)hydrogenation	Octanone + D-glucose	R-octanol + D-gluconolactone	Alcohol dehydrogenase + glucose dehydrogenase	/ (free)	N.D. (10kDA)	UF (dead-end)	Flow	[313]
Hydrolysis	Phenylethanol + vinyl butyrate	Phenylethyl butyrate + acetaldehyde	Lipase (in water-oil emulsions)	/ (free)	Polymeric (PES, 10 kDA)	UF (dead-end)	Flow	[314]
Esterification	Fatty acids + glycerol	Monoacylglycerols	Lipase	Immob. (acrylic resin)	Ceramic (zeolites type T, N.D.)	Pervaporation	Recirc.	[295]
Esterification	Fatty acids + glycerol	Isopropyl esters	Lipase	Immob. (acrylic resin)	Ceramic (zeolites type T, N.D.) and polymeric (PVA, N.D)	Pervaporation	Recirc.	[315]
O-glycosylation	Resveratrol	Resveratrol *O*-glycosides	β-cyclodextrin–resveratrol	/ (free)	Polymeric (N.D., 0.9 or 1.4 kDA)	NF	Recirc.	[316]

Transgalactosylation	Lactose	GOS	β-galactosidase	/ (free)	Polymeric (Cellulose, 50kDA)	UF + NF	Flow	[317]
Transgalactosylation	Lactose	GOS	β-galactosidase	/ (free)	Polymeric (PES, 10 kDA)	UF	Recirc.	[318]
Transgalactosylation	Lactose	GOS	β-galactosidase	/ (free)	Ceramic (TiO_2, 20 kDA)	UF	Flow	[319]
Transgalactosylation	Lactose	GOS	β-galactosidase	/ (free)	Ceramic (50 kDA)	UF	Recirc.	[320]
Transgalactosylation	Lactose	GOS	β-galactosidase	/ (free)	Polymeric (cellulose acetate, N.D.)	UF	Recirc.	[321]
Transgalactosylation	Lactose	GOS	β-galactosidase	/ (free)	Polymeric (PES, 10 kDA)	UF	Recirc.	[322]
Transgalactosylation	Lactose + fructose	Lactulose	β-galactosidase	/ (free)	Polymeric (PES, PS, cellulose acetate, fluoro polymers 10 kDA)	UF (dead-end)	Flow	[323–325]
Hydrolysis	Starches	Cyclodextrin	Cyclodextrin glycosyltransferase	/ (free)	Polymeric (Cellulose, 10 kDA)	UF	Flow	[326,327]

Hydrolysis	BSA	Bioactive peptides	Peptidase	/ (free)	Polymeric (PES, 3 or 10 kDA) or ceramic (ZrO_2/TiO_2, 15 kDA)	UF	Recirc.	[328]
Hydrolysis	*P. yezoensis* protein	Bioactive peptides	Peptidase	/ (free)	N.D. (3 kDA)	UF	Flow	[307]
Hydrolysis	Egg white protein	Bioactive peptides	Peptidase	/ (free)	Polymeric (PES, 10 kDA)	UF	Flow	[329]
Hydrolysis	Casein	Bioactive peptides	Peptidase	/ (free)	Polymeric (PES, 1 to 10 kDA)	UF	Recirc.	[330]
Hydrolysis	Corn gluten meal	Bioactive peptides	Peptidase	/ (free)	Polymeric (Cellulose, 1 to 5 kDA)	UF	Flow	[331]
Hydrolysis	Casein	Bioactive peptides	Peptidases	/ (free)	Polymeric (PES, 10 kDA) and ceramic (Al_2O_3, 10 kDA)	UF	Flow	[332]
Hydrolysis	Wheat gluten	Protein hydrolysate	Peptidases	/ (free)	Ceramic (hollow fibers Al_2O_3, 5 or 10 kDA)	UF	Flow	[333]
Hydrolysis	Sesame seeds	Bioactive peptides	Peptidases	/ (free)	Polymeric (PES, 5 kDA)	UF	Flow	[334]
Hydrolysis	Milk	Bioactive peptides	Peptidases	/ (free)	Polymeric (Cellulose, 5 kDA)	UF	Flow	[335]

Hydrolysis	Whey	Inhibitory peptides	Peptidase	/ (free)	Polymeric (PES, 3 kDA)	UF	Flow	[336]
Transamination	Pro-sitagliptin ketone + ISO	R-Sitagliptin + acetone	TA	/ (free)	Polymeric (Psf, 10 kDA) + dense PDMS	UF (for enzyme retention) + solvent extraction	Recirc.	[284]
Transamination	Benzyl acetone + ISO	R-1-methyl-3-phenylpropylamine + acetone	TA	/ (free)	Polymeric (PP, N.D.)	Solvent extraction	Recirc.	[283]
Transamination	Acetophenone + ISO	R-MBA + acetone	TA	/ (free)	Dense PDMS	Pervaporation	Batch	[282]

N.D. – non-specified ; PVDF - polyvinylidene fluoride ; PES – polyethersulfone ; Psf – polysulphone ; PS – polystyrene ; BSA – Bovine Serum Albumin ; MBA – methylbenzylamine ; PDMS – Polydimethylsiloxane ; UF – ultrafiltration ; NF – nanofiltration ; GOS – galacto-oligosaccharides ; ISO – isopropylamine ; TA – transaminase.

1.4 Membrane-immobilized enzymatic reactors

The incentives for immobilizing enzymes to intensify biocatalytic processes are evident. Enzyme immobilization is a prerequisite to envisage recovery and reuse. Immobilization usually tends to enhance enzyme stability and tolerance to organic solvents, and to allow for the use of different reactor configurations [272], which are key features industrial processes. It also paves the way to the integration of enzymes within heterogeneous catalysts, forming so-called hybrid chemo-enzymatic catalysts that are excellent candidates to run intensified cascade reactions [150,182,183]. A potential downside of enzyme immobilization is that enzymatic activity may – in some cases – be decreased through the immobilization process (due to active site blockage, for example). Nevertheless, free enzymes can also experience activity reduction over time due to heat and mechanical stresses during extended biocatalytic processes [337].

Immobilization on membranes is going one step further in the direction of process intensification, as it implies fixing the enzyme on a material that it itself functional in the sense that it is able to perform tailored compounds separation. As in the previous section, the membrane can be used to remove products during reaction, to inject reagents in a controlled way, etc. In some cases, the membrane itself can also be chemo-catalytically active. However, prior to enzyme immobilization on a membrane, the membrane surface often needs to be functionalized or chemically modified. Indeed, appropriate membrane materials which are directly amenable to enzyme immobilization are very rare [166]. A plethora of different surface functionalization techniques (e.g. wet chemical modifications,, plasma or UV exposure) have been reported in the literature [166,267,338,339], showing a variety of approaches, depending on the substrate chemical nature. The implementation of such surface modifications depends on the type of enzyme immobilization (e.g. covalent

grafting, electrostatic-assisted adsorption, site-specific immobilization through coordination) that is envisaged, as well as the membrane operation which are targeted in the intensified biocatalytic process. Among the different existing strategies, silanization of inorganic membrane surface using (3-aminopropyl)triethoxylsilane (APTES) and polydopamine (PDA) coating deposition on polymeric membranes have been widely employed over the recent years [172,173,340–343] to confer amino-groups at their surfaces, serving as anchoring points for grafting. In these cases, glutaraldehyde (GA) is most conventionally used as a coupling agent between the enzyme and the functionalized membrane. Another general trend is to try and stabilize the immobilized enzymes via electrostatic interactions; polyelectrolytes such as polyethyleneimine (PEI) are often employed with this aim.

Table II-2 gathers an exhaustive list of examples of membrane-immobilized enzymes exploited for the production of fine chemicals and pharmaceuticals, among the selected biocatalytic transformations listed in the Figure II-1. Enzymes are immobilized either in the membrane (i.e. encapsulated in the membrane pores) or onto the membrane surface, In these examples, the membrane can either be employed as a mere solid support (i.e. not exploited to perform membrane operations), or as a functional support forming an enzyme-membrane-reactor which acts as a combined reaction-separation unit (Figure II-3).

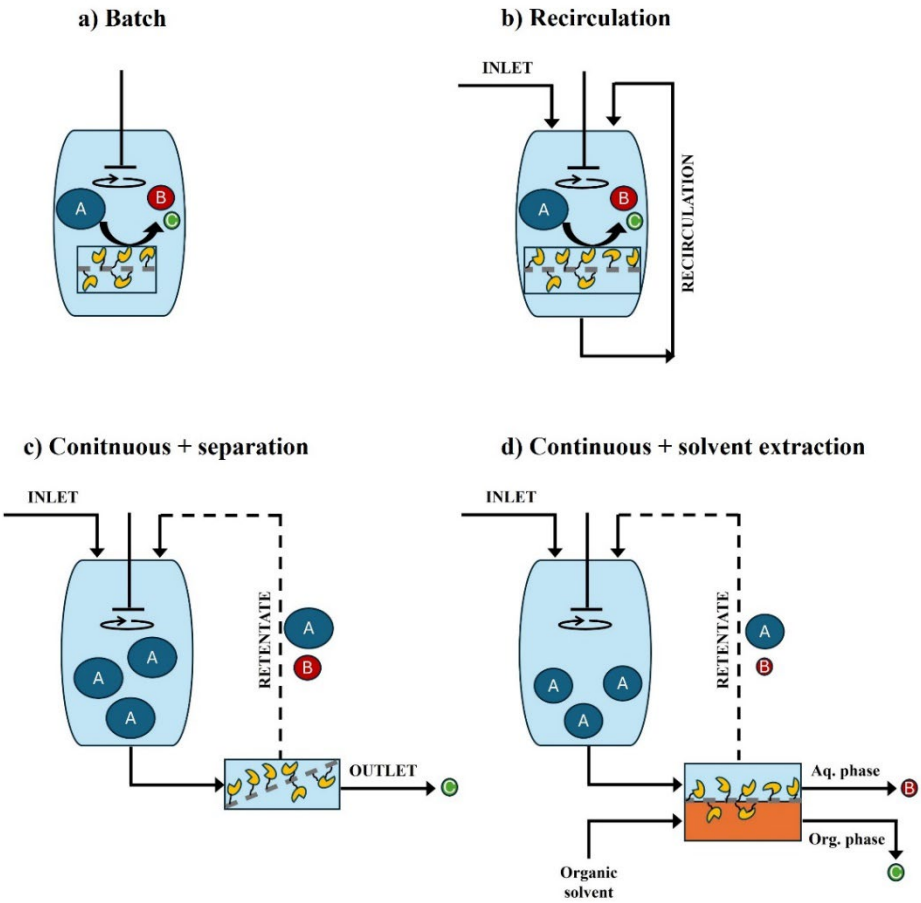

Figure II-3. Schematic representation of membrane-immobilized enzymes, acting as simple heterogeneous membrane-immobilized biocatalysts (i.e. not performing membrane operations) operating in **a)** batch or **b)** in recirculating mode, or as enzyme-membrane-reactors (i.e. reaction-separation unit) in **c)** compounds separation (e.g. via size-exclusion, ion-exchange, etc.) or **d)** solvent extraction operations. Note that, by removing the recirculations, **c)** and **d)** become continuous flow operations

Table II-2 - Exhaustive list of recent (2010-2024) examples of membrane-immobilized enzymes, acting as simple heterogeneous membrane-immobilized biocatalysts (i.e. not performing membrane operations, operating in batch or in flow mode, with or without recirculation), or as enzyme-membrane-reactors (i.e. a reaction-separation unit), for the production of fine chemicals and pharmaceutical building blocks.

Reaction	Substrate	Product	Enzyme	Immob. (R. Sp. act)	Comments	Membrane	Separation	Mode	Refs
DKR	Ibuprofen ester	S-ibuprofen acid	Lipase	Encapsul. (90%)	Retained 53% of initial sp. activity after 120 h of operation	Polymeric (PAN, 50 kDA)	Solvent extraction (interfacial; OP = isooctane)	Recirc.	344,345
Esterification (lipophilization)	Hesperidin + lauric acid	Hesperidin laurate	Lipase	Covalent grafting + cross-linking (c.a. 900%)	/	Polymeric (PDA + GA modified PES, 30 kDA)	/	Batch	346
Esterification	Stearic acid + lauryl alcohol	Lauryl stearate	Lipase	CLEAs + entrapment (142 %)	/	Polymeric (CLEAs in PVA matrix, on PVA/PES dense layer)	Pervap.	Recirc.	292

Esterification	Ethanol + lactic acid	Ethyl lactate	Lipase	Entrapment (c.a. 100%)	Preserved 90% of sp. activity upon 6 cycles (i.e. 36 h of operation)	Polymeric (Sodium alginate network)	Pervap.	Recirc.	[347]
Esterification	Valeric acid + ethanol	Ethyl valerate	Lipase	Covalent grafting (76%)	/	Polymeric (PPC, 150 kDA)	/	Batch	[348]
Transesterification	Rac-phenylethanol	S-phenylethanol + R-phenylacetate	Lipase	Covalent grafting (/)	/	Ceramic (ZrO_2, 300 kDA)	/	Recirc.	[349]
Trans-galactosylation	Lactose	GOS	β-galactosidase	Covalent grafting (c.a. 75%)	Retained 50% of its initial sp. activity after 30 days of storage	Polymeric (GA-modified PVDF)	Filtration	Recirc.	[350,351]
Trans-galactosylation	Lactose	GOS	β-galactosidase	Covalent grafting + cross-linking (/)	/	Polymeric (PES, 5-50 kDA) and NF (0.4 kDA)	UF or NF	Flow	[352,353]

Trans-galactosylation	Lactose	GOS	β-galactosidase	Covalent grafting (104 %)	Maintained 54% of its initial sp. activity after 20 cycles	Polymeric (GO + APTES modified electrospun PS nanofibers)	/	Batch	354
Trans-galactosylation	Lactose	GOS	β-galactosidase	Adsorption (95 %)	/	Mixed matrix (PSf + ZrO_2, 13.8 kDA)	/	Batch	355
Trans-galactosylation	Lactose	GOS	β-galactosidase	Covalent grafting (/)	Maintained 91% of its sp. activity after 16 h of operation	Magnetic-responsive on polymeric membrane (PES, UF 50 kDA)	UF	Flow	356
Trans-galactosylation	Lactose	GOS	β-galactosidase	Covalent grafting + cross-linking (140 %)	/	Polymeric (PEI + GA-modified PSf, 10 kDA)	UF	Recirc.	357
Hydrolysis	Oleuropein	Oleuropein aglycon	β-glucosidase	Encapsul. (c.a. 100%)	Activity was unchanged after 30 h of continuous operation	Polymeric (Psf and cellulose, 30 kDA)	Solvent extraction of product (OP = Limonene)	Flow	358–361

Hydrolysis	Oleuropein	Oleuropein aglycon	β-glucosidase	Covalent grafting (c.a. 100%)	/	Ceramic (APTES + GA-modified Al_2O_3 capillary, 30 kDA)	Solvent extraction of product (OP = Ethyl acetate)	Recirc.	273
Hydrolysis	Dextran	Oligodextran	Dextranase	Covalent grafting (/)	/	Polymeric (Tannic Acid + APTES-modified PES (30 kDA) or cellulose (10 kDA))	UF	Flow	362
Hydrolysis	Dextran	Oligodextran	Dextranase	Adsorption (/)	/	Polymeric (PES, 20 or 30 kDA)	UF	Flow	299
Hydrolysis	Wheat gluten	Protein hydrolysate	Peptidase	Encapsul. (/)	/	Polymeric (UF) (PES, 10 kDA)	Filtration (dead-end)	Flow	363
Hydrolysis	BSA	Bioactive peptides	Peptidase	Electrostatic interactions	/	Polymeric (PDA + PEI modified PES, 50 kDA)	UF	Flow	364
Hydrolysis	BSA	Bioactive peptides	Peptidase	Covalent grafting (/)	50% initial sp. activity retained	Polymeric (EDC/NHS-modified	/	Batch	365

					after 6 cycles of 1h	PVDF, Nylon 6,6, chitosan composite)			
Hydrolysis	Whey protein	Bioactive peptides	Peptidase	Electrostatic interactions (80 %)	/	Polymeric (PDA + PEI modified PES, 30 kDA)	/	Batch	366
Oligomerization	Rutin	Oligorutin	Laccase	Encapsul. (/)	90% of initial sp. activity after 3 cycles of 24 h	N.D. (10 kDA)	Filtration (dead-end) of product	Batch	367
Oxidation	Tyrosine	L-DOPA	Tyrosinase	Encapsul. (183%)	Unaltered initial sp. activity for 30 h of continuous operation	Polymeric (polyamide, 20 kDA)	UF	Flow	368
Oxidation	Tyrosine	L-DOPA	Tyrosinase	Covalent grafting (276%)	/	Ceramic (GA-modified NaY zeolite)	/	Recirc.	369
Oxidation	Tyrosine	L-DOPA	Tyrosinase	Covalent grafting (87%)	Unaltered initial sp. activity after 5 catalytic cycles (c.a.	Polymeric (DAB + GA-modified PVDF)	/	Batch	370

					24 h operation)				
Transamination (deamination)	S-MBA + pyruvate	Acetophenone + L-alanine	TA	Coordination (His-tag) (23%)	Retained productivity after 5 days of continuous operation was 81 %	Polymeric blend (Cu-functionalized fibers)	/	Flow	371
Transamination (deamination)	S-MBA + pyruvate	Acetophenone + L-alanine	TA	Covalent grafting + His-tag driving (43.6%)	/	Polymeric blend (Co-derivatized PCADE/PVDF)	/	Batch	372
Cascade (transamination + (de)hydrogenation)	Cinnamaldehyde	Cinnamyl amine	TA + alanine dehydrogenase + formate dehydrogenase	EPC encapsul.	/	N.D. (12 kDA dialysis membrane)	/	Batch	373

R. Sp. act. – Recovered specific activity (with respect to free enzymes) ; N.D. – non-determined ; Pervap. – pervaporation , DKR – dynamic kinetic resolution ; OP – organic phase ; PAN – polyacrylonitrile ; PDA – polydopamine ; GA – glutaraldehyde ; PVA – polyvinyl alcohol ; PVDF - polyvinylidene fluoride ; CLEAs – cross-linked enzyme aggregates ; Encapsul. – encapsulation ; PES – polyethersulfone ; Psf – polysulphone ; PS – polystyrene ; GO – graphene oxide ; PPC – polypropylene chloride ; APTES - (3-aminopropyl)triethoxylsilane ; EDC/NHS -(1-ethyl-3-(3-dimethylaminopropyl)carbodiimide/N-hydroxysuccinimide) ; BSA – Bovine Serum Albumin ; PP – polypropylene ; PEI – polyethyleneimine ; DAB - 1,4-diaminobutane ; PCADE - polycarvone acrylate di-epoxide ; Rac-MBA – Racemic methylbenzylamine ; Rac-BMBA – Racemic bromo-α-methylbenzylamine ; BAP – bromoacetophenone ; UF – ultrafiltration ; NF – nanofiltration ; GOS – galacto-oligosaccharides ; encapsul. – encapsulation ; TA – transaminase.

The dynamic kinetic resolution of ibuprofen ester is a great example of how the use of a lipase-membrane-reactor can intensify a chemo-enzymatic process and push such technology to the next level (Figure II-4) [344,345]. In this example, a lipase was encapsulated in the porosity of a polyacrylonitrile (PAN) membrane contactor. Such EMR allowed to simultaneously perform the continuous ibuprofen ester hydrolysis and the resulting S-ibuprofen product separation (i.e. extraction into the aqueous phase). The unreacted R-ibuprofen ester was then recirculated into a chemocatalytic racemization unit (i.e. Amberlist OH^- coated-resin) [344,345]. The resin is an excellent racemization catalyst due to its strong basicity and to its macro-reticular network, which provides high surface-to-volume ratio. Its large pores allow bulky molecules, such as (R)-ibuprofen ester, to diffuse and interact with the encapsulated hydroxyl ions in the matrix. This feature, combined with its strong basic properties, enables the rapid racemization of the ester through ketol-enol tautomerism mechanism [374]. The racemized ibuprofen ester substrate is then recirculated to the organic tank, and fed again to the enzyme-membrane module. Compartmentalization of the heterogeneous bio- and -chemocatalysts allows protecting the lipase from the basic catalyst and from inhibition that would otherwise happen under the effect of unreacted substrate and by-product (2-ethoxyethanol, which is absorbed by the OH^- resin).

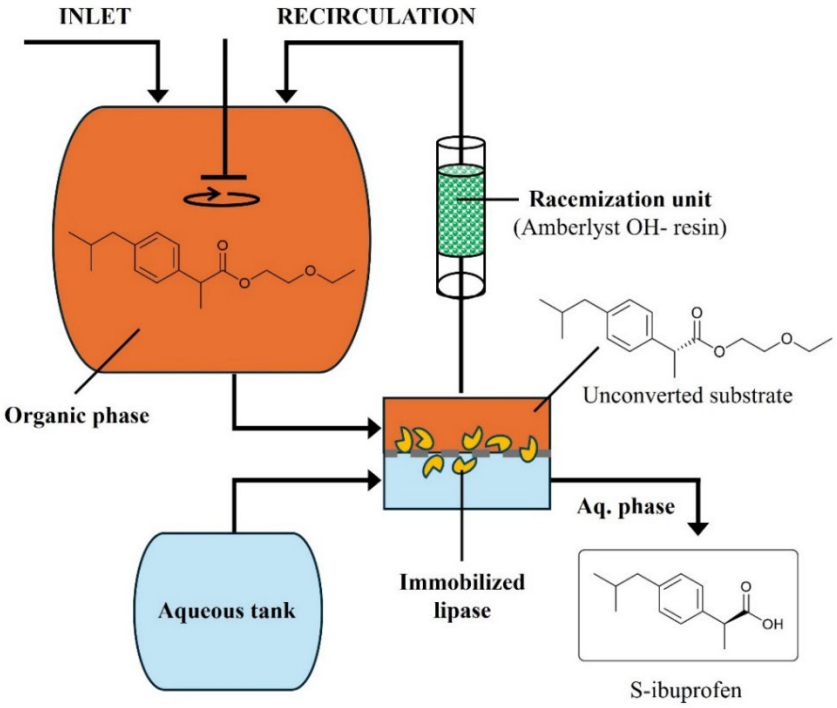

Figure II-4. Schematic representation of the dynamic kinetic resolution of ibuprofen ester catalyzed by lipase-membrane-reactor (Uzir et al., 2011) [344,345].

Interestingly, the same kind of approach (membrane-assisted extraction strategy) allowed achieving high product purity in the synthesis of oleuropein aglycone (an important antioxidant) through enzymatic hydrolysis in an enzyme-membrane-reactor. To this aim, β-glucosidase was covalently immobilized onto ceramic membrane surfaces, and employed to hydrolyze oleuropein into oleuropein aglycone and glucose (this time, in aqueous medium, see Figure II-5) [273]. Given the differences in polarities between oleuropein aglycone and the other compounds involved in the process, a membrane-assisted solvent extraction was chosen to intensify the process. The aglycone produced in the membrane contactor was continuously extracted with an organic solvent (ethyl acetate), which allowed its separation and purification from the reaction medium. The identical strategy was also implemented with polymeric (Psf) membranes containing encapsulated β-

glucosidase in its pores, and using limonene as organic solvent [358–360]. Yet, the use of such polymeric materials as aqueous-organic contactor for such solvent extraction processes might be less suitable than ceramic membranes, given their limited chemical stability.

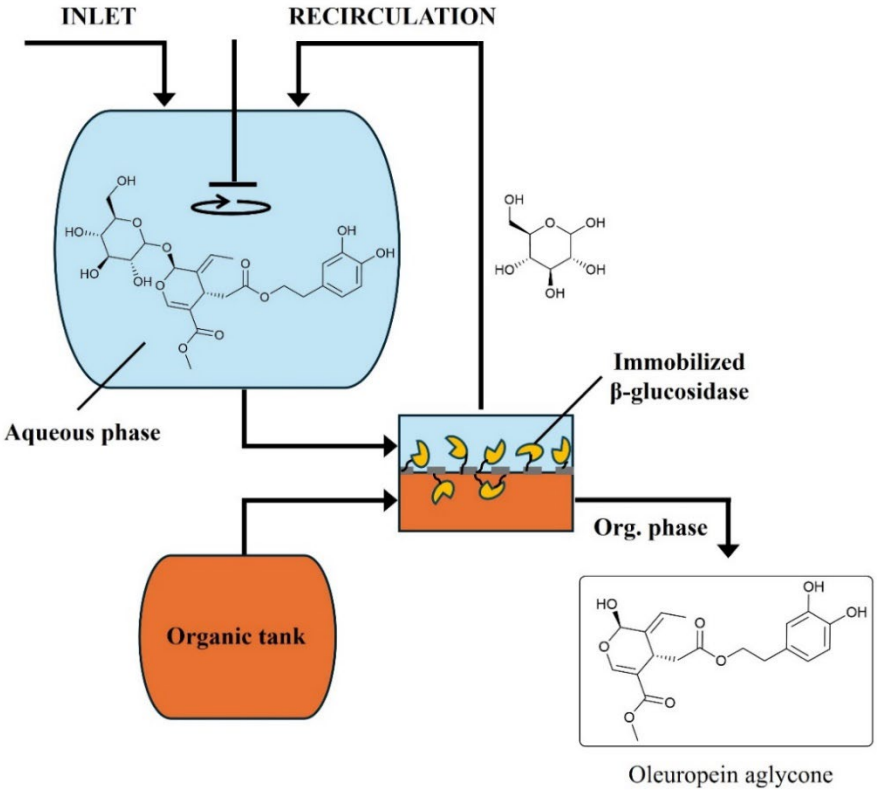

Figure II-5. Schematic representation of the oleuropein aglycone production through simultaneous hydrolysis and solvent extraction using an enzyme-membrane-reactor (Giorno et al., 2018) [273].

Another elegant example of membrane-immobilized enzyme reactors applications is the *in situ* removal of the water by-product through pervaporation, as in the intensified production of lauryl stearate (which is often used as emollient and excipients in cosmetics and pharmaceuticals [375]) [292]. In this work, a "sandwich-like" membrane structure, made of a porous lipase-PVA catalytic layer coated on a polyvinyl alcohol

(PVA)/polyethersulfone (PES) matrix, was employed as enzymatic-pervaporation reactor. Interestingly, the immobilized lipase exhibited enhanced specific activity and stability compared to the soluble enzyme. This improvement was attributed to the hydrophilic microenvironment created by the hydrophilic PVA carrier, which probably absorbs excess water produced during the enzymatic esterification, thereby shielding the lipase from adverse effects like enzyme inactivation. The implementation of this catalytically active membrane in a pervaporation reactor resulted in a substantial increase in conversion (i.e. from 60% to 83%) compared to the equilibrium-limited esterification process (conducted without pervaporation).

A similar strategy was applied for the synthesis of ethyl lactate (a pharmaceutical-grade excipient [376]), in which a lipase entrapped in sodium alginate membrane was as enzymatic-pervaporation unit [347].

Eventually, immobilizing enzymes such as β-galactosidase, peptidase and dextranase on membranes featuring adequate MWCO, is a practical tool to intensify the production of value-added compounds with tailored molecular weight via size-exclusion operations. For example, the production of galacto-oligosaccharides (GOS) from lactose is hindered by hydrolytic side reactions, and by enzyme inhibition caused by such monosaccharides formation and accumulation. To improve reaction yield and productivity, the continuous coupled GOS purification and monosaccharides elimination from the reaction mixture is of particular interest. Considering the molecular weight distribution of the carbohydrate mixture obtained after enzymatic reaction with lactose, ultrafiltration and/or nanofiltration are effective operations for GOS purification. Bhattacharjee et al. [352] immobilized β-galactosidase on nanofiltration (0.4 kDA) and ultrafiltration (5 to 50 kDA) membranes via covalent grafting, and compared their catalytic performance towards the continuous membrane-assisted GOS production. It resulted that a higher GOS yield was obtained when using the enzyme-loaded nanofiltration membrane, which aligns with the enhanced permeation of monosaccharides and improved

retention of GOS observed with the nanofiltration membrane. (compared to enzyme-immobilized ultrafiltration membrane). Furthermore, the nanofiltration process resulted in substantial retention of the lactose substrate, providing extended residence time and greater interaction between the substrate and immobilized enzyme, which contributed to the increased GOS production.

1.5 Conclusion

Among the existing methods capable of intensifying biocatalytic processes in an efficient way, enzyme-membrane-reactors (EMR) emerge as highly potent. Through this report, we aim at providing the recent trends and examples of the use of EMR for the intensified production of high-value chemicals, and in particular active pharmaceutical ingredients. It is clear that important enzymatic processes leading to the production of high-value chemicals, can benefit from the coupling between the fields of biocatalysis and organic synthesis on the one hand, and process engineering on the other hand, resulting in EMR. We argue that the implementation of such novel hybrid reactors which simultaneously host the immobilized enzymes and perform in-situ product separation, will catalyze and promote further advances in the field of greener fine chemicals and pharmaceuticals manufacturing.

Chapter III - Membrane-immobilized transaminases for the synthesis of enantiopure amines

This chapter is published as :
"Membrane-immobilized transaminases for the synthesis of enantiopure amines". H. M. Arango, X. D. L. Nguyen, P. Luis, T. Leyssens, D. Roura Padrosa, F. Paradisi and D. P. Debecker, *RSC Sustain.*, **2**, 3139-3152.

ABSTRACT

Transaminases (TAs) are able to produce chiral amines with excellent enantioselectivity and in mild conditions, and can be immobilized to target stability, recoverability, and reusability. In the perspective of process intensification, we propose to study TAs immobilization onto polymeric membranes. Two main immobilization strategies were investigated, requiring prior membrane surface functionalization. First, a polyacrylonitrile (PAN) membrane surface was partially hydrolyzed and coated with polyethyleneimine (PEI) to electrostatically trap TAs. Second, a polypropylene (PP) membrane was coated with polydopamine (PDA), which was subsequently modified with glycerol diglycidyl ether (GDE) in order to covalently graft TAs. The successful membrane functionalization was confirmed by surface characterization techniques (infrared spectroscopy, X-ray photoelectron spectroscopy, contact angle measurements, and scanning electron microscopy). Enzyme leaching was observed from the functionalized PAN membrane, highlighting the need to post-treat the reversibly immobilized TAs to improve their anchoring. The covalent coupling of TAs with PEI using glutaraldehyde (GA) was found highly effective to avoid leaching and to increase the enzyme loading, without affecting the specific activity of the biocatalyst. Similarly, the covalent grafting of TAs onto functionalized PP membranes yielded very efficient biocatalysts displaying perfect recyclability throughout successive cycles. Immobilizing either the S-selective HeWT or the R-selective TsRTA resulted in robust heterogeneous biocatalysts with antagonist enantioselectivities. Thus, chiral amine synthesis can be performed effectively with biocatalytic membranes, which paves the way to intensified flow processes.

1. Introduction

It appears undeniable that transaminases have the potential to provide greener routes to produce chiral amines with excellent enantioselectivity [167,168]. However, these biocatalytic strategies face important challenges such as unfavourable thermodynamics and poor stability of the soluble TAs. To overcome the main limitations faced by transaminations, scientists aim at enhancing the transaminase robustness and at developing equilibrium shifting strategies.

As exposed in the first chapters, the incentives of immobilizing transaminases on solid supports are evident to produce chiral amines in a greener way, as the resulting heterogeneous biocatalysts are often more versatile and amenable to more productive flow processes. On the other side, the development of equilibrium shifting strategies usually relies on using large amino donor excess or on consuming/removing the (co)product during reaction [377,378]. Besides the widely reported multi-enzymatic cascade reactions [379] or non-catalytic consecutive reactions [380] that can be used to push the equilibrium of the transamination reaction towards the production of the target amine, one alternative possibility is the physical separation of one of the transamination products towards another phase in the system. For example, *in-situ* (co)product removal (ISPR) strategies were recently employed in batch with free transaminases to drive the reaction towards the formation of valuable chiral molecules [94,139]. In these examples, the acetophenone co-product was removed from the aqueous phase reaction medium by liquid-liquid extraction (using an organic co-solvent), or the targeted chiral amine was selectively crystallized by salt formation.

When aiming to perform such reactions in continuous flow, possibly coupled with product separation, membrane technologies are of particular interest [175,259,260]. Membrane contactors are known to offer operational

flexibility, large and tunable interfacial area, modular linear scale-up which allows easy concatenation with other operations, compactness, and low energy consumption. Therefore, researchers have implemented membrane contactors at the outlet of the transamination flow reactor to separate their outputs [96,214,242]. In these processes, membranes are solely employed as separation unit for downstream processing and the transaminases are immobilized separately (onto classical supports) and packed into distinct fixed-bed reactors.

Taking this to the next level, it would be of particular interest to immobilize enzymes directly onto active membrane supports, and hence to develop bifunctional membranes allowing to simultaneously host the immobilized enzymes and perform the product separation to intensify the transamination process. Recently, Howdle et *al.* developed an electrospun polycarvone acrylate di-epoxide/polyvinylidene fluoride (PCADE/PVDF) membrane and exploited it for the immobilization of the TA from *Halomonas Elongata* (HeWT) [372]. This epoxy-functionalized membrane allowed 61.9 % immobilization yield and 43.6 % of specific activity recovery (no TA leaching), paving the way for potential application in combined reaction-separation processes.

In the perspective of designing effective hybrid chemical processes (i.e. combining reaction on immobilized enzymes and *in situ* separation through a membrane), it is essential to first master the step of enzyme immobilization on conventional polymeric membranes that are routinely employed industrially. Such supports differ from usual enzyme carriers such as porous silica, or resins beads (i.e. typically 100 µm particles, with average pore size of 20-60 nm [381]), in the sense that polymeric membranes tend to display lower specific surface area available for immobilization [382,383], resulting in potentially lower enzyme loadings [384]. Also, their surface is usually not directly amenable to enzyme grafting, so that chemical functionalization is needed. Thus, it is of prime importance to develop robust enzyme immobilization strategies on these membranes, with the aim to optimize

enzyme loading, preserve specific activity of immobilized enzymes, and avoid leaching.

In this context, we turned our attention to the immobilization of two transaminases (the S-selective TA from *Halomonas Elongata* (HeWT) [122] and the R-selective TA from *Thermomyces stellatus* (TsRTA) [129]) onto commercially available polymeric microporous membranes. Polyacrylonitrile membranes (PAN) and polypropylene (PP) were selected as commercially available and industrially relevant membranes showing good mechanical resistance and featuring respectively hydrophilic and hydrophobic surface chemistry. We leverage on electrostatic interactions and covalent grafting strategies to avoid leaching. The membrane carriers are characterized at different stages of the preparation. After TA immobilization, using a model kinetic resolution, we show that these functional materials exhibit high catalytic performance (specific activity), minor leaching and excellent reusability. This paves the way to a future use in flow mode hybrid processes, possibly concatenated with purification strategies.

2. Materials

4'-bromoacetophenone (BAP; ≥ 98 %), R-4-bromo-α-methylbenzylamine (R-BMBA; 99 %), S-4-bromo-α-methylbenzylamine (S-BMBA; 99 %), hydrochloric acid (37 wt %, aqueous solution), pyridoxal 5'-phosphate hydrate (PLP; ≥ 98 %), 4-bromo-α-methylbenzylamine (rac-BMBA; 98 %), dimethylsulfoxide (DMSO; ≥ 99.9 %), glycerol diglycidyl ether (GDE; technical grade), carbonate-bicarbonate buffer capsules, Bradford reagent were purchased from Sigma-Aldrich. Sodium hydroxide (NaOH; ≥ 99 %), N-2-Hydroxyethylpiperazine-N'-2-ethane sulphonic acid (HEPES; ≥ 99.5 %), HEPES sodium salt (≥ 99 %), pyruvic acid sodium salt (≥ 99.9 %), 2-(N-Morpholino)-ethane sulphonic acid sodium salt (MES sodium salt; ≥ 99%),

glutaraldehyde (GA; 25 wt % aqueous solution) were purchased from Carl Roth. Branched polyethyleneimine (PEI; 50 wt %, aqueous solution, M.N. 60,000) was purchased from Acros Organics. Dichloromethane (DCM; HPLC grade), ethanol absolute (EtOH) were purchased from VWR Chemicals. 1-Phenyl-2-propanol (> 98 %), Tris(hydroxymethyl)aminomethane (Tris; > 99 %), 3-hydroxytyramine hydrochloride (dopamine hydrochloride; 98 %), tert-butyl methyl ether (MTBE; > 99 %) were purchased from Tokio Chemical Industry. Commercial polyacrylonitrile membranes (PAN) were purchased from Snyder filtration company (USA). Commercial polypropylene membranes (PP) were purchased from 3M (USA).

Transaminases HeWT (from *Halomonas elongata*) and TsRTA (from *Thermomyces stellatus*) were expressed and lyophilized as previously described by Paradisi et al. [122,129], and then used as cell-free extracts. Distilled water was applied for all synthesis and treatment processes.

3. Methods

3.1 Transaminase immobilization onto polyacrylonitrile membrane (PAN)

3.1.1 PAN membrane surface functionalization

Figure III-1 describes the protocol – adapted from Shi *et al* [385] – used to immobilize transaminases onto PAN membranes. The PAN surface was partially hydrolyzed by dipping a 5 cm^2 disc of the PAN membrane in 50 mL of a 1.5 M NaOH solution for 2 hours at 50 °C under gentle stirring (as recommended by Pérez-Álvarez et al.[386]). The resulting hydrolyzed PAN membrane (HPAN) was then washed with 100 mL distilled water for 1 hour, and this washing step was repeated 3 times, before being dipped into 50 mL

of a 1 wt. % (unless stated otherwise) aqueous solution of branched polyethyleneimine (PEI) for 18 hours at 37 °C under gentle stirring. The resulting membrane was washed again 4 times, stored in distilled water and is denoted HPAN_PEI.

3.1.2 TA immobilization on functionalized PAN membranes

The functionalized membrane was transferred into round bottom glass flasks containing 5 mL of buffered solution (MES or HEPES 0.1 M buffer, PLP 1 mM, sodium pyruvate 10 mM) for enzyme immobilization. The latter contained the desired TA concentration (C_0) and was set either at pH 8 with the HEPES buffer or at pH 5.5 with the MES buffer. Incubation was done for 18 hours at 35 °C under gentle stirring. The resulting membrane-immobilized transaminase was either directly rinsed or post-treated and then rinsed. Post-treatment was done with glutaraldehyde (GA, 1 wt.%) or sodium alginate (SA, 0.2 wt.%) aqueous solutions for 1 hour (unless stated otherwise) at 25 °C in an attempt to prevent TA leaching [385]. Rinsing was done by suspending the membrane in 5 mL of rinsing solution (containing HEPES 0.1 M buffer, PLP 1 mM, sodium pyruvate 10 mM) for 30 minutes (repeated two times), to eliminate the loosely attached enzymes.

This TA immobilization was performed on each PAN membrane support employed in this study (i.e. PAN, HPAN, HPAN_PEI), in order to evaluate the impact of the different steps of functionalization on the catalytic performance of the resulting immobilized TAs. Depending on the immobilization pH, TAs immobilized on pristine PAN were labelled as TA_PAN$_a$ (if pH was 8) or TA_PAN$_b$ (if pH was 5.5). Similarly, TAs immobilized on HPAN were labeled as TA_HPANx$_a$ or TA_HPANx$_b$, where x = / stand for TAs immobilized on HPAN, x = 1 for HPAN_PEI (without

post-treatment), x = 2 for HPAN_PEI (with SA post-treatment) and x = 3 HPAN_PEI (with GA post-treatment), respectively.

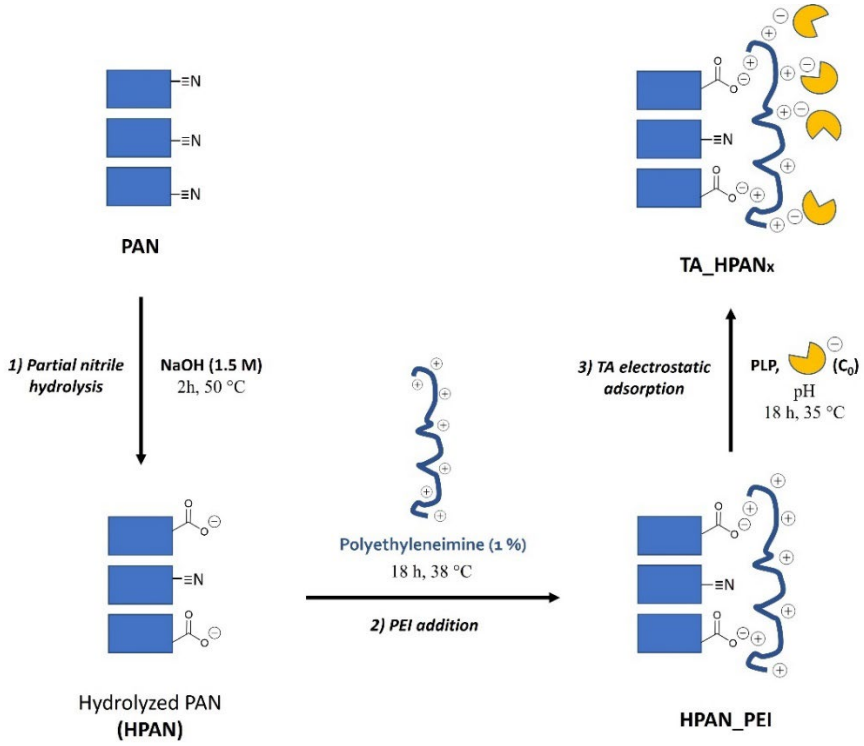

Figure III-1. Schematic representation of PAN functionalization and TA immobilization procedures, leading to TA_HPAN_xa or TA_HPAN_xb. In the case of TA_HPAN_2a, TA_HPAN_2b, TA_HPAN_3a and TA_HPAN3b, an additional post-treatment was applied (with SA or GA, respectively) before the rinsing step.

3.2 Transaminase immobilization onto polypropylene membrane (PP)

3.2.1 Functionalization of the PP membranes

PP membranes were functionalized in three steps. First they were coated with PDA with the aim to provide reactive amine functions for further functionalization of the PP support [340,387,388]. A 5 cm^2 disc of PP membrane was immersed into 10 mL of ethanol in order to wet its surface and pores.

Simultaneously, a dopamine (i.e. 3-hydroxytyramine) hydrochloride solution was prepared in a 10 mM Tris buffer (pH 8.5) at a concentration of 2 mg/mL, and left to stir. After about 15 min, dopamine started to self-polymerize and the colorless solution turned pale brown. At this stage, the wetted PP membrane was immersed in the dopamine solution and kept for 20 hours (unless stated otherwise) at room temperature, under gentle stirring (Figure III-2 [389]). The obtained PP_PDA membrane (dark brown to black) was then rinsed with 100 mL distilled water for 1 hour, and this washing step was repeated three times.

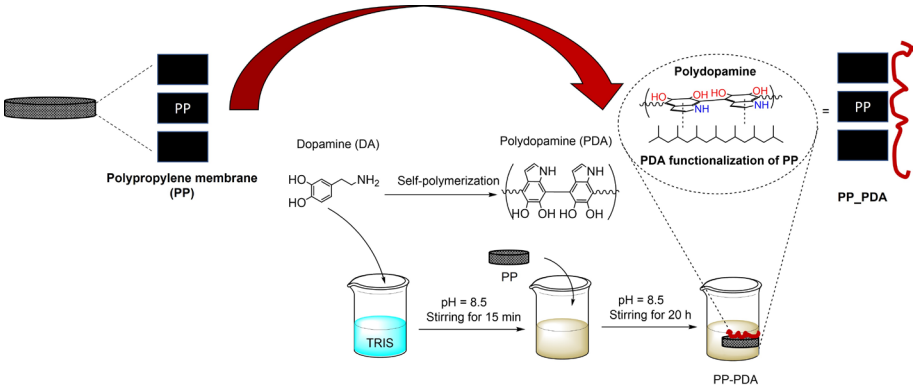

Figure III-2. Schematic representation of the PDA deposition on PP membrane surface, reproduced from [389].

Second, the obtained PP_PDA membrane was modified with a bisepoxide coupling agent (glycerol diglycidyl ether; GDE) to confer an appropriate linker arm for the subsequent covalent grafting of the enzyme [230] (Figure III-3, step 1). The PP_PDA was immersed in 50 mL of a 100 mg/mL GDE solution (in ethanol) and stirred for 18 hours (unless stated otherwise) at room temperature. The resulting PP_PDA_GDE membrane was then rinsed with 50 mL of ethanol for 1 hour first, then with 100 mL distilled water for 1 hour (repeated three times).

Third, in order to drive the covalent grafting of the transaminase on the epoxy linker arm, the PP_PDA_GDE membrane was partially functionalized

with polyethyleneimine (prior to enzyme immobilization; Figure III-3, step 2). Thus, the PP_PDA_GDE was immersed into 50 mL of a 5 mg/mL PEI solution in carbonate/bicarbonate 0.1 M buffer at pH 9.5 and stirred for 90 minutes (unless stated otherwise) at room temperature.

3.2.2 TA immobilization on functionalized PP membranes

3.2.2.1 Standard TA immobilization

The functionalized PP membrane was transferred into 5 mL of buffered solution (HEPES 0.1 M buffer, PLP 1 mM, sodium pyruvate 10 mM) containing the desired TA concentration (C_0) at pH 8, and incubated for 18 hours at 35 °C under gentle stirring (Figure III-3, step 3). After immobilization, the resulting membrane-immobilized transaminase was rinsed with 5 mL of rinsing solution (containing PLP 1 mM, sodium pyruvate 10 mM in HEPES 0.1 M buffer pH 8) for 30 minutes (repeated two times) to eliminate the loosely attached TAs. For comparison, this TA immobilization was also performed on each PP membrane support employed in this study (i.e. PP, PP_PDA, PP_PDA_GDE and PP_PDA_GDE_PEI). The resulting catalysts were denoted TA_PPy, where y = / stand for TAs immobilized on pristine PP, y = 1 on PP_PDA, y = 2 on PP_PDA_GDE and y = 3 on PP_PDA_GDE_PEI.

3.2.2.2 Dual TA and PLP immobilization

In a variation of this protocol, we attempted to prepare self-sufficient biocatalysts. Inspired López-Gallego *et al.* [236], we immobilized the enzyme onto PP_PDA_GDE_PEI (with either 0.1 mM or 1 mM PLP, sodium pyruvate 10 mM in HEPES 0.1 M buffer pH 8) and then rinsed the resulting membrane three time (5 mL sodium pyruvate 10 mM in HEPES 0.1 M buffer pH 8), and

directly incubated it with PLP (1 mM in HEPES 10 mM pH 8 for 90 minutes at room temperature under gentle stirring). Additional rinsing was applied again (four times 5 mL sodium pyruvate 10 mM in HEPES 0.1 M buffer pH 8, 30 minutes). The obtained membranes were denoted TA_PP3_SSz, where z is the concentration of PLP (in mM) used during the TA immobilization step. The amount of PLP effectively loaded onto the membrane was evaluated by UV absorption (see Supplementary informations of Chapter III).

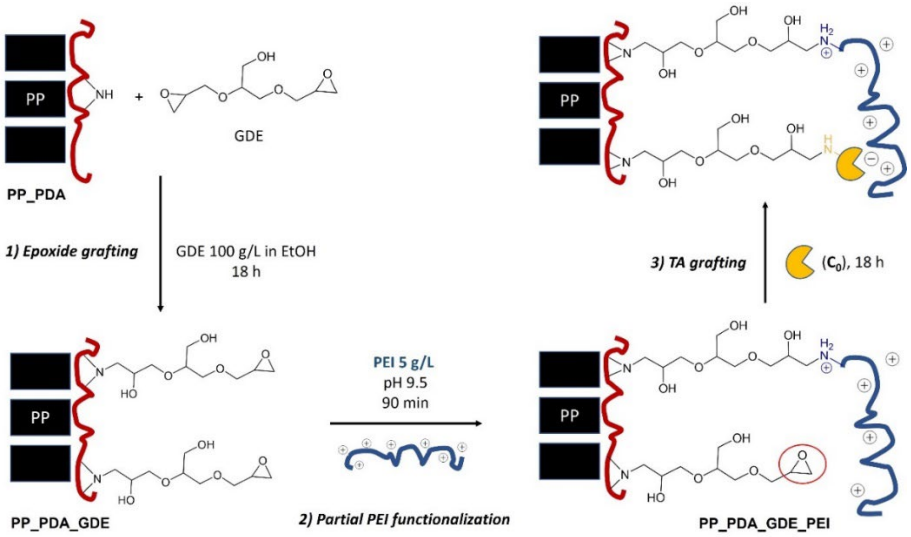

Figure III-3. Schematic representation of PP_PDA functionalization and TA immobilization procedures on PP-based membranes, leading to TA_PPy catalysts. In some cases, the protocole was modified by adding an additional step (i.e. PLP immobilization) after the third step.

3.3 Characterization of the membrane carriers

Both pristine and functionalized PAN and PP membranes were characterized by infrared spectroscopy, X-ray photoelectron spectroscopy, contact angle measurements, and scanning electron microscopy. Experimental

details on these characterization techniques are provided in the supplementary informations of Chapter III.

3.3.1 Attenuated Total Reflectance – InfraRed Spectroscopy (ATR-FTIR)

The presence of functional groups at the PAN and PP (pristine and functionalized) membrane surfaces was investigated by Attenuated Total Reflectance - InfraRed Spectroscopy (ATR-FTIR). Membrane surfaces were analyzed using a Bruker Equinox 55 with a Platinum ATR cell, with a diamond crystal, and Trans DTGS detector. 100 scans were taken for both background and samples, with a resolution of 2 cm-1. ATR correction was applied (number of ATR reflection is 1; angle of incidence is 45°; mean reflection index of sample is 1.5).

3.3.2 X-ray Photoelectron Spectroscopy (XPS)

Elemental surface compositions of PAN and PP (pristine and functionalized) membranes were assessed *via* X-ray photoelectron spectroscopy (XPS). XPS analyses were carried out in a SSX 100/206 photoelectron spectrometer from Surface Science Instruments (USA) equipped with a monochromatized micro focused Al X-ray source (powered at 20 mA and 10 kV). The pressure in the analysis chamber was around 10^{-6} Pa and the flood gun was set at 8 eV. The angle between the surface and the axis of the analyzer lens was 55◦. The analyzed area was approximately 1.4 mm^2 and the pass energy was set at 150 eV. Under these conditions, the full width measured at half maximum (FWHM) of the Au 4f7/2 peak for a clean gold standard sample was about 1.6 eV. Samples were prepared as 1x1 cm^2 squares and were fixed by using a piece of double-sided insulating tape, and

placed on a ceramic carousel with a Ni grid set above the sample surface for charge stabilization. The following sequence of spectra was recorded: survey spectrum, C 1s, O 1s, N 1s, Na 1s, F 1s, and C 1s again to check the stability of charge compensation with time. The C-(C,H) component of the C1s peak of carbon was fixed at 284.8 eV to calibrate the binding energy scale. Data treatment was performed with the CasaXPS program (Casa Software Ltd, UK). Carbon 1s peaks were decomposed with the least squares fitting routine provided by the software with a Gaussian/Lorentzian (85/15) product function and after subtraction of a non-linear baseline.

3.3.3 Water Contact Angle (WCA)

The hydrophobicity/hydrophilicity nature of the membranes was evaluated using the optical water contact angle (WCA) (DataPhysics OCA20). Three measurements were taken for each membrane sample using a sessile drop method with a 5 μL droplet of water.

3.3.4 Scanning electron microscopy (SEM)

The morphology and porosity of the membrane carriers were analyzed by performing Scanning Electron Microscopy (SEM) images (Ultra 55 Feg Sem, Zeiss, Zaventem, Belgium). The membranes cross-section were also observed. Prior to the SEM analysis, membranes were beforehand immersed into liquid nitrogen for a clean cross-sectional cut, and a thin layer of gold was deposited under vacuum with a sputter coater (Quorum Q150 RS) to make the samples conductive.

3.4 Characterization of the enzyme-loaded membranes

Enzyme loadings on the membranes were evaluated by mass balance. Typically, a functionalized membrane was incubated in a 5 mL (V_0) TA solution of known concentration, C_0 [mg.mL^{-1}]. After immobilization, the membrane was removed from the reactor and the TA concentration in the remaining solution (C_1) was measured by Bradford titration (see Supplementary informations of Chapter III). The membrane was then washed with 5 mL (V_0) of rinsing solution, and the enzyme concentration in the resulting solution was measured (C_2). The same procedure was applied to the next rinsing solutions, leading to measure C_3 and C_4. The immobilized enzyme loading (L) was determined by Eq. III-1. The immobilization yield (%) is defined as the ratio between immobilized TA (L) and the total TA mass introduced during the immobilization (5 x C_0).

$$L = V_0 \times (C_0 - C_1 - C_2 - C_3 - C_4) \ [mg] \qquad Eq.III-1$$

3.5 Biocatalytic testing

The kinetic resolution of BMBA was used as a model reaction to assess the catalytic activity of free and membrane-immobilized transaminases. Racemic BMBA was reacted with pyruvate, to produce BAP and either L-or D-alanine leaving unreacted R- or S-BMBA when using an S- or a R-selective TA, respectively (Figure III-4). When catalytic tests were run with immobilized transaminases, one disk of 5 cm^2 of membrane support was employed.

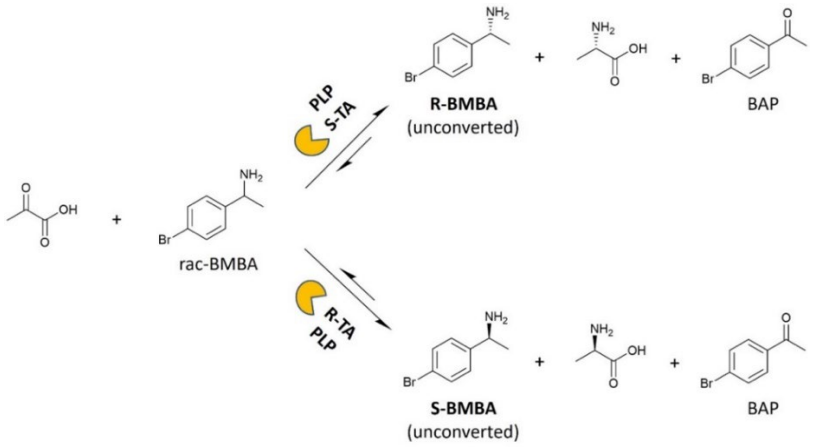

Figure III-4. Model transamination (kinetic resolution of racemic BMBA with pyruvic acid) implemented to study the membrane-immobilized TAs specific activity. Precisely, this represents a kinetic resolution performed by a S-selective TA (up) and a R-selective TA (down). Typical reaction conditions were 37 °C, HEPES buffer 0.1 M pH 8, PLP 1 mM (or in absence of PLP), sodium pyruvate 10 mM, racemic BMBA 10 mM, 1-phenyl-2-propanol 6 mM (as internal standard), DMSO 3 % (v/v), 5 mL total volume in a batch reactor (5 mL round bottom glass flask) under moderate magnetic stirring.

The progress of the reaction was followed by analyzing 100 µL samples taken from the reaction medium. 10 µL of sodium hydroxide (2 M) was added and the mixture was vortexed for 5 seconds. 400 µL of dichloromethane was then added to the aqueous phase, the sample was vortexed for 15 seconds and left to rest for 5 minutes to allow extraction of BAP, BMBA and 1-phenyl-2-propanol into the organic phase. This extraction step was repeated twice and the organic phases were pooled and analyzed by gas chromatography (see Supplementary Informations of Chapter III).

The yield is defined as the proportion of rac-BMBA converted into BAP (%). The maximum theoretical yield for the kinetic resolution is thus 50 %. The specific activity is defined as the number of µmol of 4'-bromacetophenone formed per minute per mg of immobilized enzymes (U.mg $_{TA}^{-1}$) and evaluated by Eq. III-2, where L is the immobilized enzyme loading

(determined by mass balance via the Bradford method (mg)) and, t is the reaction time (min). Specific activity was always determined in the kinetic regime (initial activity), after 15 minutes of reaction. The residual specific activity (%) is defined as the ratio between the specific activity of the immobilized TA and the specific activity of free TA (at identical enzyme concentration, in the same reaction conditions).

$$Specific\ activity = \frac{nBAP_{produced}}{t \times L}\ [U.mg^{-1}_{immob.\ TA}] \qquad Eq.III-2$$

After 24 hours of reaction, the solid membrane was removed and the concentration of leached enzyme was evaluated *via* the Bradford method (Supplementary Informations of Chapter III). The leached TA fraction (%) is defined as the ratio between the mass of leached TA after one catalytic test and the initial immobilized TA loading (L). 50 mM 3,3-diphenylpropionic acid (3-DPPA) was added to the reaction medium in order to crystallize with the remaining BMBA (in the form of a BMBA:DPPA salt).[139] After 20 hours of crystallization, crystals were filtered, washed twice with 5 mL distilled water, then once with 5 mL tert-butyl methyl ether (MTBE) to remove residual BAP, and then dried at room temperature overnight. Semi-quantification of BMBA enantiomers was then determined using Chiral High-Performance Liquid Chromatography (Chiral-HPLC), by dissolving the obtained crystals in the mobile phase (95% isohexane/5% 2-propanol/0.1% diethylamine) (see Supplementary Informations of Chapter III).

4. Results and discussion

4.1 Surface characterization of the pristine and modified membrane supports

The two membrane types (PAN and PP) have been modified and functionalized in order to bring the needed anchoring points for enzyme immobilization. Here, we describe these chemical modifications and provide detailed characterization of the membranes that are used in the next section to immobilize TA.

4.1.1 PAN membranes

The surface functionalities of the pristine and modified PAN membranes were analyzed by ATR-FTIR (Figure III-5). Table SIII-1 gathers the main infrared signature peaks of the different species of interest (i.e. amines, amides, carboxylic acids, alkanes, amides and nitriles) [386,390–392]. The spectra of the pristine PAN membrane (Figure III-5) featured the main characteristic peaks of nitriles (at 2240 cm^{-1}) and of alkanes (2925 and 1450 cm^{-1}). However, it also features a broad band in the 3200-3500 cm^{-1} region as well as additional peaks at 1730 and 1230 cm^{-1}, which suggest the presence of some impurities (such as hydroxyl or carbonyls functions) at the surface of the PAN membrane.

Based on previous reports [386,391], we applied a mild hydrolysis treatment (120 minutes with NaOH 1.5 M at 50 °C) in order to favor the formation of COO^- surface groups while preserving the HPAN membrane mechanical properties. Expectedly, new IR peaks highlighted the presence of carboxylic acid/carboxylate moieties at 1560, 1400 and around 3300 cm^{-1} [386,391], along

with amides groups (characteristic peak at 1670 cm^{-1}) coming from the partial surface hydrolysis of nitriles.

The subsequent addition of polyethyleneimine (HPAN_PEI1) was confirmed by the appearance of two small peaks attributed to amines and amine salts (at 1630 and 2850 cm^{-1}) [392]. Additional surface-sensitive *in-situ* infrared experiments (DRIFTS; see Figure SIII-1) were performed on HPAN_PEI1 at 120 °C (to get rid of the broad O-H stretching band from 2800 to 3600 cm^{-1} due to surface hydration). It revealed characteristic peaks of amine (3420 and 2850 cm^{-1}) as well as alkane (2925 and 1450 cm^{-1}) and nitrile (2240 cm^{-1}) moieties, which confirmed the results obtained from ATR-FTIR.

Characterization by XPS (Figure SIII-2) showed that the pristine PAN surface was partly oxidized (Table III-1, line 1), which confirmed the qualitative ATR-FTIR observations. Consequently, the N/C ratio obtained at the PAN surface is lower (0.25) than the theoretical one (0.33). As expected, the basic hydrolysis of PAN (Figure SIII-3) resulted in an increase of the O/C ratio and in a decrease of the N/C due to the conversion of nitrile moieties into amides and carboxylates moieties (Table III-1, line 2). Addition of PEI by electrostatic adsorption at the HPAN surface (Figure SIII-4) logically led back to an increase of the surface N content (Table III-1, line 3).

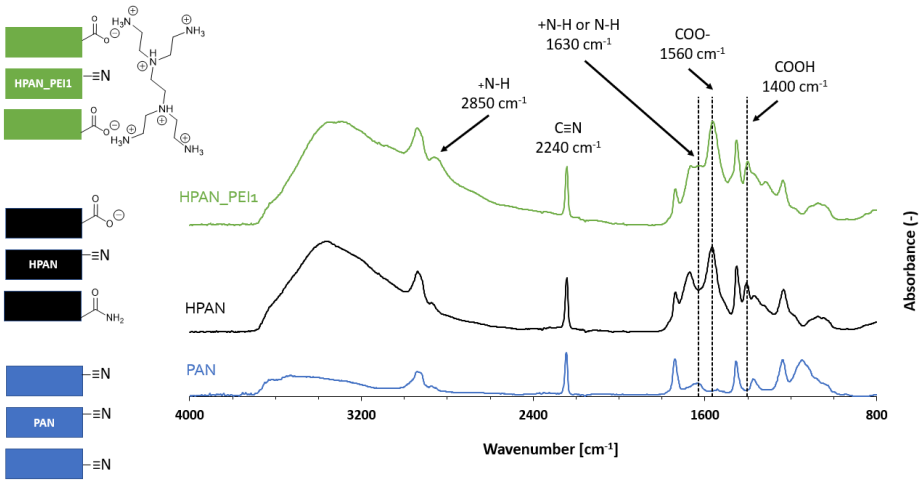

Figure III-5. ATR-FTIR spectra (and schematic representation) of the pristine (blue), hydrolyzed (black) and PEI-functionalized PAN (in green) membrane.

4.1.2 PP membranes

ATR-FTIR analysis on the pristine PP membranes showed only the expected signals of alkyl groups (Figure III-6) [392]. After dopamine polymerization (PP_PDA) the IR spectra showed an additional broad signal at 3200-3500 cm^{-1}, which can be attributed to the presence of hydroxyl (catechol) groups of PDA [393]. The mechanism of polydopamine adhesion on hydrophobic surfaces such as PP is not clearly understood, but it is believed to involve strong non-covalent (e.g. hydrogen bondings, hydrophobic) interactions [394,395]. The peak at around 1600 cm^{-1} may indicate the appearance of N-H (indole) groups generated by the PDA deposition [342], even though superposed with the O-H bending vibration mode of adsorbed water [396].

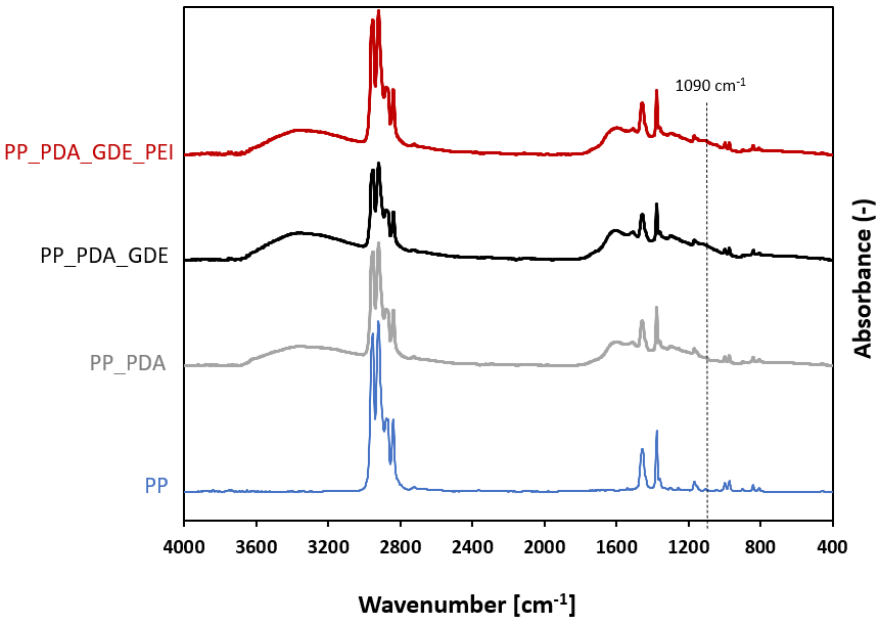

Figure III-6. ATR-FTIR spectra of the pristine PP (blue), of PP_PDA (grey), PP_PDA_GDE (black) and of PP_PDA_GDE_PEI (red).

In the next steps, the PP_PDA membrane was functionalized with GDE and then with PEI. The signature peak of the epoxy groups (i.e. symmetric ring stretching, expected at 1250 cm^{-1}) was not clearly observed on the PP_PDA_GDE spectrum, which might suggest an opening of the epoxy rings prior to the grafting of GDE, resulting in the presence of diol groups. Consistently, the small shoulder observed at 1090 cm^{-1} may correspond to the C-C-O symmetric stretch of secondary alcohols present in the diols. However, upon functionalization the membrane was turned hydrophilic (see water contact angle (WCA) analyses, Figure SIII-5) which creates large bands in the 3400 and 1630 cm^{-1} regions, hampering the observation of signature bands for amines, epoxides, or diols.

Table III-1. Surface composition (atomic fractions and ratios) of the characterized membrane carriers obtained by XPS.

Membrane Carrier	Mole fraction (%)								
	Na[a]	**Ca[a]**	**Cl[a]**	**F[a]**	**O**	**N**	**C**	**N/C**	**O/C**
PAN	0.5	*bd* [b]	*bd* [b]	1.9	8.9	17.8	70.9	0.25	0.13
HPAN	1.3	*bd* [b]	*bd* [b]	2.1	13.8	14.9	67.9	0.22	0.20
HPAN_PEI	*bd* [b]	*bd* [b]	*bd* [b]	2.6	16.4	16.4	64.6	0.25	0.25
PP	*bd* [b]	*bd* [b]	*bd* [b]	*bd* [b]	1.8	*bd* [b]	98.2	/ [c]	0.02
PP_PDA	*bd* [b]	1.8	*bd* [b]	*bd* [b]	24.1	8.0	66.1	0.12	0.36
PP_PDA_GDE	*bd* [b]	*bd* [b]	2.8	1.1	28.0	6.0	62.1	0.10	0.45
PP_PDA_GDE_PEI	*bd* [b]	*bd* [b]	1.9	0.6	20.7	12.2	64.6	0.19	0.32

[a] : These elements were detected in significant amounts (in some samples), but their presence is exclusively due to contaminations (either present on the original commercial membranes, or generated during the experiments).

[b] : *below detection limit.*

[c] : The value of the obtained ratio was < 0.01.

In XPS, pristine PP membranes (Figure SIII-6) showed nearly exclusively aliphatic C-(C,H) signal (Figure SIII-7), no nitrogen, and only traces of oxygen. Upon addition of PDA (Figure SIII-8) signals for oxygen and nitrogen logically appeared. Notably, the N/C ratio of the PP_PDA reaches a similar value to that of the theoretical value of the polydopamine polymer ($N/C_{PDA} = 0.125$), suggesting the formation of a PDA coating of at least 10 nm thickness at the PP surface [397]. As expected, the grafting of GDE (Figure SIII-9) on the amine residues present at the PP_PDA surface increased the oxygen surface concentration at the expense of nitrogen (Table III-1, line 6), and the addition of PEI on PP_PDA_GDE (Figure SIII-10) resulted in a marked increase in the nitrogen content (and N/C ratio) (Table III-1, line 7).

Scanning electron microscopy (SEM) allowed to verify that the morphology of the PP membrane was preserved after functionalization: the surface of pristine PP and PP_PDA_GDE_PEI showed similar porosity (Figure III-7, top), which confirmed that the membrane remains porous after functionalization. No change was pictured on cross-sections images either (Figure III-7, bottom), which indicates that the membrane porosity was intact.

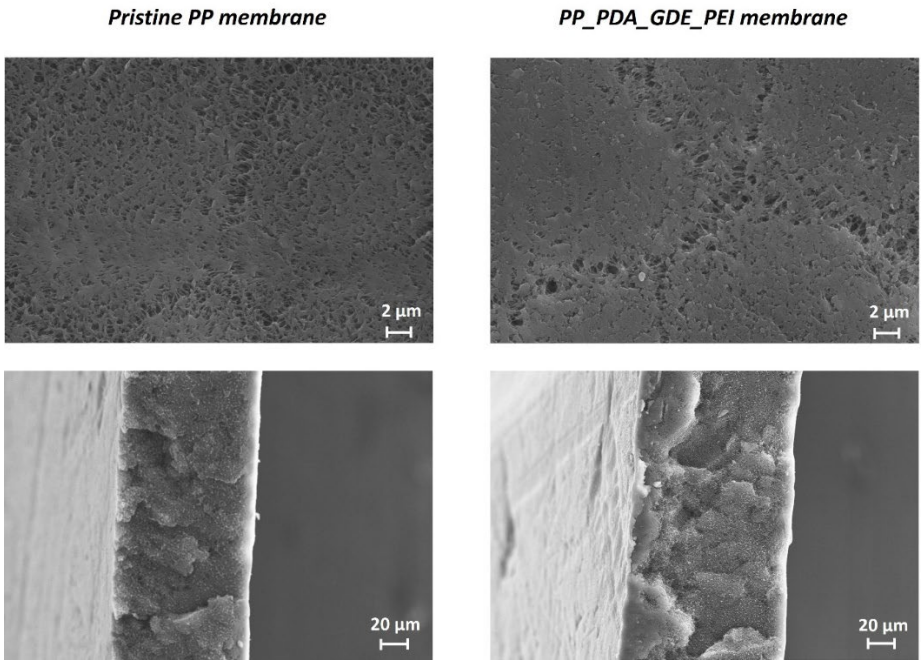

Figure III-7. SEM images showing the surface from a top view (left) and the cross-section (right) and of the pristine PP and PP_PDA_GDE_PEI membranes.

4.2 Transamination with membrane-immobilized TAs

TAs were immobilized on the membranes described above and tested in the kinetic resolution of BMBA. Figure III-8 shows the activity (in terms of BAP yield) displayed by the different heterogeneous biocatalysts obtained by

the immobilization of TsRTA on the different membrane supports. When using the pristine PP or PAN membranes as supports for the enzyme, the activity was virtually nil. However, upon functionalization – and depending on the parameters of functionalization and immobilization (*vide infra*) – significant biocatalytic activity was observed. In general, PP-immobilized TAs exhibited superior performance as compared to the PAN-immobilized TAs. Similar activity trends were obtained when employing HeWT as immobilized transaminase on these supports (Figure SIII-11).

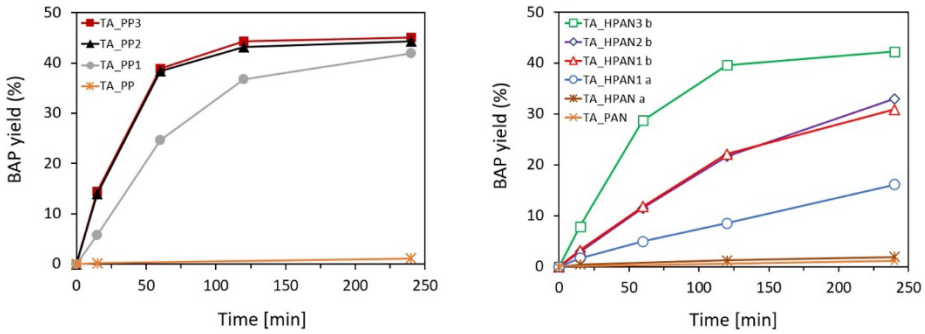

Figure III-8. Activity profiles displayed by the different PP-immobilized (left) and PAN-immobilized (right) TA biocatalysts in the kinetic resolution of BMBA. TA immobilization was always applied using a nominal enzyme concentration of C_0 = 0.25 mg/mL, and TsRTA was used as TA. Reaction conditions: 10 mM rac-BMBA, 10 mM pyruvate, 1 mM PLP in 0.1 M HEPES pH 8 buffer, 37 °C (5 mL reaction volume).

As matter of comparison, activity profiles and specific activities obtained with soluble TAs (HeWT and TsRTA) are shown in Figure III-9.

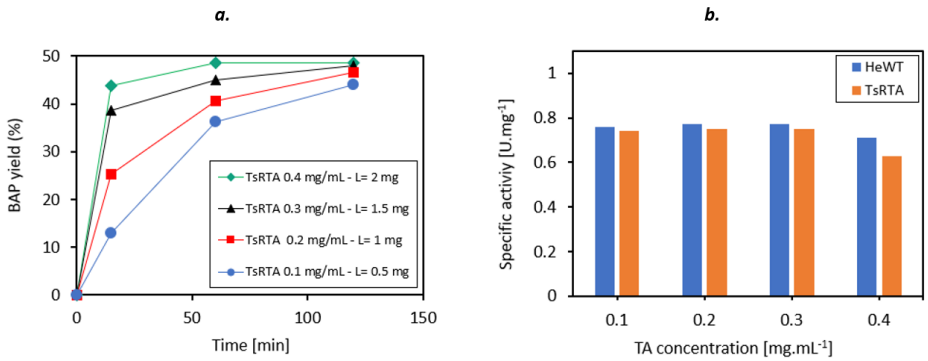

Figure III-9. Activity profiles displayed by soluble TsRTA at different concentrations (in mg/mL) and corresponding enzyme content L (in mg) (left) and specific activity of the soluble TAs (HeWT in blue and TsRTA in orange) at different enzyme concentrations (right).

To interpret the raw yields obtained with the different enzyme-loaded membranes, complementary indicators must be considered. Table III-2 gathers the immobilization yield, specific activity recovery, and leaching fraction displayed by the obtained membrane-immobilized TAs, for both immobilization strategies. Regarding the HPAN_PEI immobilized biocatalysts, it can be observed that the immobilization yield is boosted when the TA immobilization was performed at pH 5.5 (HeWT_HPAN1b (Entry 2) and TsRTA_HPAN1b (Entry 6)) rather than 8 (HeWT_HPAN1a (Entry 1) and TsRTA_HPAN1a (Entry 5)). This can be explained by the fact the PEI is more positively charged at low pH and favors the electrostatic adsorption of a larger amount of TA at the membrane surface. Accordingly, the observed activity is higher. Importantly, the specific activity (activity normalized by the amount of immobilized TA on the membrane) was the same, which indicates that, on average, the intrinsic activity of each additional immobilized transaminases was maintained. However, leaching after catalytic test was important, highlighting the need of post-treatment strategies to improve the anchoring of the immobilized TAs at the membrane surface.

Table III-2. Immobilization and catalytic performance (mean values) obtained by the different membrane-immobilized biocatalysts (upper part: HPAN_PEI membranes , lower part: PP_PDA membranes). TA immobilization was always applied using a nominal enzyme concentration of C_0 = 0.25 mg/mL. Reaction conditions: 10 mM rac-BMBA, 10 mM pyruvate, 1 mM PLP in 0.1 M HEPES pH 8 buffer, 37 °C (5 mL reaction volume).

Entry	Immobilized TA	Membrane carrier	Immob. pH	Post-treatment	TA immob. Yield (%) [a]	Sp. activity recovery (%) [b,d]	Leaching fraction (%) [c]
1	HeWT_HPAN1a	HPAN_PEI	8	/	24	12 ± 1.4	6
2	HeWT_HPAN1b	HPAN_PEI	5.5	/	58	12 ± 2.3	14
3	HeWT_HPAN2b	HPAN_PEI	5.5	SA	56	12	7
4	HeWT_HPAN3b	HPAN_PEI	5.5	GA	75	22 ± 1.6	1
5	TsRTA_HPAN1a	HPAN_PEI	8	/	23	19 ± 1.7	6
6	TsRTA_HPAN1b	HPAN_PEI	5.5	/	46	19 ± 2.7	14
7	TsRTA_HPAN2b	HPAN_PEI	5.5	SA	44	18	7
8	TsRTA_HPAN3b	HPAN_PEI	5.5	GA	64	36 ± 2.1	2

9	HeWT_PP1	PP_PDA	8	/	60	19 ± 2.6	19
10	HeWT_PP2	PP_PDA_GDE	8	/	84	27 ± 2.3	2
11	HeWT_PP3	PP_PDA_GDE_PEI	8	/	62	45 ± 2.1	2
12	TsRTA_PP1	PP_PDA	8	/	40	39 ± 2.9	15
13	TsRTA_PP2	PP_PDA_GDE	8	/	73	59 ± 3.8	3
14	TsRTA_PP3	PP_PDA_GDE_PEI	8	/	54	85 ± 3.3	2

*a: TA immobilization yield (%) = (TA loading / Total TA offered for immobilization)*100 =* $\left(\frac{L}{C_0 \, x \, V_0}\right)$**100*

b: Sp. activity recovery (%) = (Sp. activity $_{immTA}$ */ Sp. activity* $_{free\ TA}$*)*100.*

At the considered enzyme concentrations, the specific activities of free TsRTA and free HeWT were of 0.74 µmol.min^{-1}.mg^{-1} and 0.76 µmol.min^{-1}.mg^{-1}, respectively.

*c: TA leaching fraction (%) = (TA leaching after test / TA loading)*100.*

d: some experiments have been made in triplicate (n=3) and always showed relatively small standard deviations.

Inspired by Shi et al. [385], we attempted to entrap the immobilized TA into a polymeric matrix formed by sodium alginate (SA, see Figure III-10; bottom). This biopolymer is able to electrostatically interact with the PEI layer, bringing additional negative charges that can in principle help stabilizing the enzyme. This post-treatment was found to preserve the enzyme loading and the specific activity, and concomitantly to reduce enzyme leaching (Table III-2, compare HeWT_HPAN2b (Entry 3) and TsRTA_HPAN2b (Entry 7) to HeWT_HPAN1b (Entry 2) and TsRTA_HPAN1b (Entry 6), respectively).

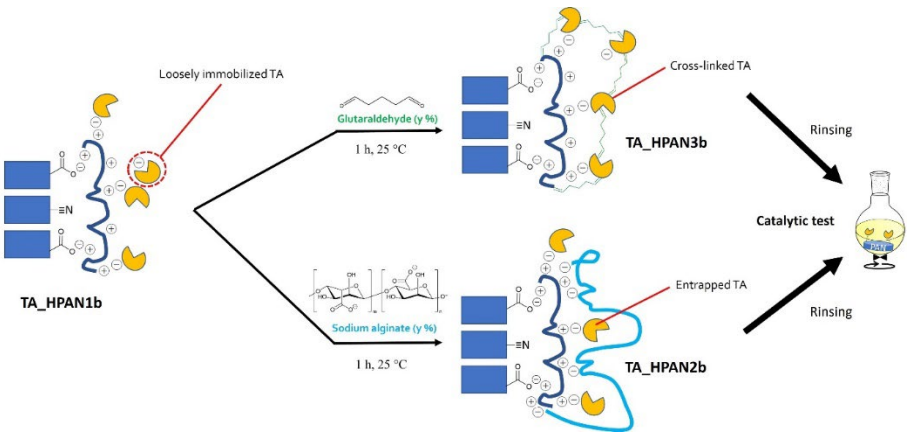

Figure III-10. Schematic representation of post-treatment strategies applied on TA_HPAN1 resulting in TA_HPAN2 and TA_HPAN3 biocatalysts.

Alternatively, inspired by Shi et al. [385] and Paradisi et al. [373], we attempted to covalently bind the enzymes to the PEI layer using glutaraldehyde (GA, see Figure III-10, top) as a coupling agent. Such post-treatment strategy was found to (i) boost the enzyme loading (by securing the fixation of otherwise loosely attached TAs to the membrane surface), (ii) enhance the specific activity, and (iii) drastically curb the extent of enzyme leaching (Table III-2, compare HeWT_HPAN3b (Entry 4) and TsRTA_HPAN3b (Entry 8) to HeWT_HPAN1b (Entry 2) and TsRTA_HPAN1b (Entry 6), respectively).

The surge in specific activity after treating with GA seems surprising, for cross-linking is known to rigidify the enzymes structure, and it is often argued to be the cause of partial deactivation (e.g. in cross-linked enzyme aggregates) [373]. Yet the measurements were repeated (immobilization, activity assays, and Bradford tests to determine the loading) and the improvement was verified to be statistically significant (see the standard deviations in Table III-2). Similar beneficial effect of such GA cross-linking of PEI-immobilized enzymes have been previously documented, with positive effects on specific activity (with lipases [398,399]), or on stability and reusability (with TAs [400]). In fact, here, TA enzymes are not only cross-linked together but also bound to PEI via GA. We surmise that bonding occurs preferentially with PEI (rather than cross-linking). Hence, one hypothesis is that the higher specific activity obtained for TAs_HPAN3b is linked to a more favorable (more hydrated, less constrained) chemical microenvironment conferred by the PEI layer to the immobilized TAs [190].

Simple adsorption of TA on PP_PDA membranes led to important leaching (Entry 9 and 12). However, using the covalent immobilization approach with GDE, TA leaching was significantly reduced (Table III-2, compare HeWT_PP2 (Entry 10) and TsRTA_PP2 (Entry 13) with HeWT_PP1 (Entry 9) and TsRTA_PP1 (Entry 12), respectively). This highlights the beneficial role of the epoxy functions, able to immobilize the TA *via* covalent coupling [131]. Interestingly, TA_PP2 also showed greater immobilization yield and specific activity with respect to TA_PP1 biocatalyst. Such enhanced specific activity obtained with GDE-immobilized TAs has already been observed in literature, and it was attributed to the hydrophilic and appropriate length of the epoxy linker-arm [226]. Further functionalization with PEI resulted in a lower immobilization yield, but a higher specific activity (Table III-2, compare HeWT_PP3 (Entry 11) and TsRTA_PP3 (Entry 14) with HeWT_PP2 (Entry 10) and TsRTA_PP2 (Entry 13) respectively). The enhanced specific activity recovery displayed by TA_PDA_GDE_PEI can be tentatively attributed to a

more favorable (hydrated) chemical microenvironment conferred by the PEI layer to the immobilized TAs [190].

In both immobilization methods, TsRTA displayed lower enzyme immobilization yields, but higher specific activity, as compared to HeWT (a more visual comparison is shown in Figure SIII-12 and Figure SIII-13).

The immobilization and catalytic performance obtained with TsRTA_HPAN3b and TsRTA_PP3 as shown in Table III-2 are the highest obtained in this study. In fact, various experimental parameters of the functionalization and immobilization steps have been studied systematically and optimized (see Supplementary, Figure SIII-14 to SIII-16) to lead to the results reported in Table III-2. Overall, the catalytic performance of these membrane-immobilized TAs compares well with other immobilized TAs described in literature. Indeed, typical transaminase immobilization *via* covalent grafting on metal-derivatized epoxy resins yields only 30–50 % recovered specific activity [131,222]. A more detailed comparison of the performance of the resulting biocatalytic membranes with other immobilized TAs is provided in section 4.4 of this Chapter.

4.3 Robustness, reusability and enantioselectivity of the biocatalytic membranes

In order to assess if the activity displayed by the developed immobilized TAs can only be attributed to heterogeneous catalysis, hot-filtration-tests were performed on both optimized TsRTA_HPAN3b and TsRTA_PP3 biocatalysts (Figure III-11). The TA-loaded membrane was removed from the reaction media after a short reaction time (15 minutes), and the activity was monitored and compared to a classical catalytic test (i.e. in which the membrane was not removed). Some residual activity could be detected after the removal of

TsRTA_HPAN3b (Figure III-11, left), which highlights the fact that a small fraction of leached TsRTA contributed to the observed activity. Such leaching fraction was either estimated to 5.1 % (in the form of immobilized TsRTA) or 1.8 % (in the form of soluble TsRTA), based on the slope between 15- and 60-minutes activity points. This can be explained by a slow hydrolysis of the imine bonds between GA and TsRTA or PEI. On the other hand, the hot-filtration test exhibited a completely flat profile after the removal of TsRTA_PP3 biocatalyst (Figure III-11, right), demonstrating that, in this case, only heterogeneous catalysis is involved in the observed activity.

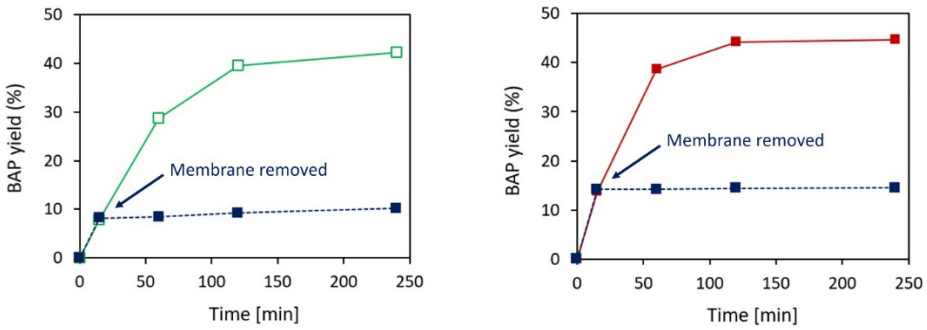

Figure III-11. Hot-filtration tests performed on TA_HPAN3b (left) and TA_PP3 (right), performed at equal immobilization concentration (C_0 = 0.25 mg/mL TA, using TsRTA as TA). Full curves represent the standard catalytic tests while dotted curves represent the hot-filtration tests (i.e. in which the membrane-immobilized TAs were removed after 15 minutes). Reaction conditions: 10 mM rac-BMBA, 10 mM pyruvate, 1 mM PLP in 0.1 M HEPES pH 8 buffer, 37 °C (5 mL reaction volume).

The two selected catalysts were also tested in 4 successive catalytic cycles to assess their recyclability. At the end of each cycle, the membrane-immobilized TAs were washed twice with 5 mL of buffer solution (i.e. HEPES 0.1 M pH 8 containing PLP 1 mM, pyruvate 10 mM), and then immersed into a fresh reaction medium. The obtained reaction profiles (Figure III-12) unambiguously show that the membrane discs were recyclable. In all cases, the same final conversion (close to thermodynamic equilibrium) could be

reached. More importantly, specific activity (approached by initial activity) was not affected throughout the successive catalytic cycles. This result paves the way toward a possible use of membrane-immobilized enzymes in continuous flow processes. Such robustness and recyclability was also confirmed with the S-selective HeWT enzyme (Figure SIII-17), as no significant decrease of specific activity could be observed throughout the cycles.

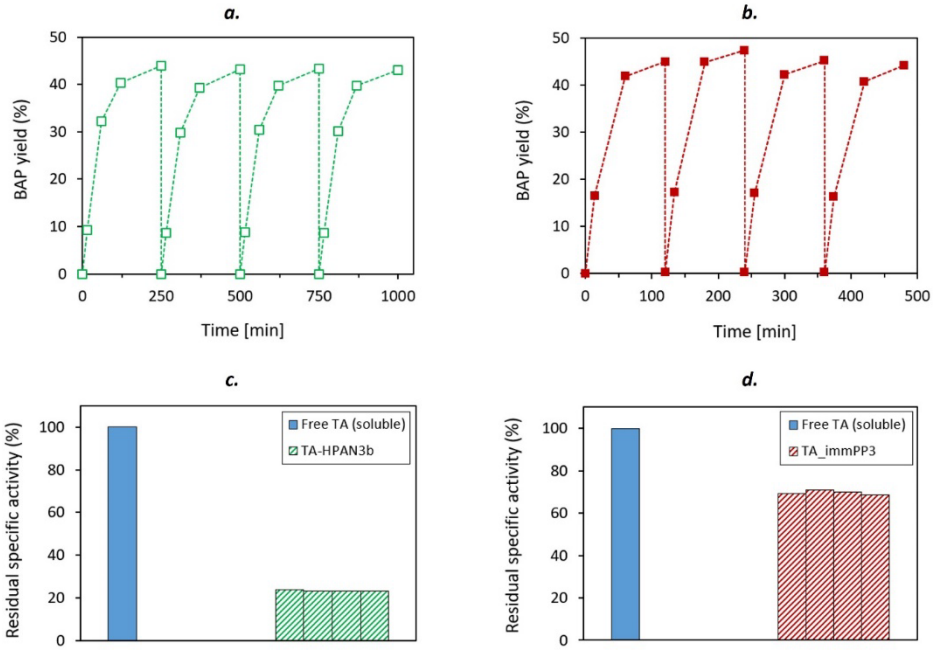

Figure III-12. Activity profiles **(a)** and **(b)** and residual specific activities **(c)** and **(d)** obtained from the recyclability tests performed with TA_HPAN3b (left) and TA_PP3 (right) at equal immobilization concentration (C_0 = 0.5 mg/mL TA, using TsRTA as TA). Each bar shown in **(c)** and **(d)** represent the residual specific activity (with respect to free TA), measured at each catalytic cycle (computed after 15 minutes, i.e. the first point of the activity profiles shown in **(a)** and **(b)**). Reaction conditions: 10 mM rac-BMBA, 10 mM pyruvate, 1 mM PLP in 0.1 M HEPES pH 8 buffer, 37 °C (5 mL reaction volume).

Another interesting aspect to investigate was the ability of the biocatalytic membrane to work in the absence of externally added co-factor (PLP). Such ability has already been reported on PEI-coated supports, onto which both PLP and TA could be co-immobilized [236,246,401]. This aspect would be particularly important in the perspective of a continuous flow membrane reactor, since it would allow to get rid of the costly PLP feed during the operation. Hence, TsRTA_PP3 (for which only the TA immobilization step is done in the presence of PLP) was tested in successive catalytic cycles without adding PLP to the reaction media (Figure III-13). In such case, the residual activity dropped after each reaction cycle (i.e. down from 78 % to 23 % after five cycles). This suggests a significant PLP leaching leading to immobilized TA deactivation.

In order to overcome this problem, we slightly adapted the immobilization process. Inspired from López-Gallego *et al.* [236] we implemented a two-step immobilization. Briefly, after performing classical enzyme immobilization (as always, in presence of PLP, i.e. 0.1 mM or 1 mM), a subsequent step of PLP immobilization was performed at lower ionic force in order to favor the co-factor grafting at the PEI-coated membrane surface. The resulting membrane was tested in 8 successive catalytic cycles without PLP addition, and exhibited much higher stability as compared to TA_PP3. In particular, TA_PP3_$SS_{0.1}$ did not show any activity drop. That remarkable stability displayed by TA_PP3_ $SS_{0.1}$ might be explained by the higher PLP loading achieved for this catalyst (0.97 µmol as compared to TA_PP3_ SS_1 (0.85 µmol) (Table III-3). These results suggest that upon this two-step immobilization strategy (and employing 0.1 mM PLP for TA immobilization step), PLP is suitably provided to the enzyme (i.e. available for the transamination catalytic act) in satisfying amounts. It is noteworthy that performing TA immobilization with 0.1 mM (instead of 1 mM) of PLP also enabled to boost the TA loading and increase the overall activity, but it lowered the specific activity of the catalyst (Table III-3, line 3).

Table III-3. Summary of the catalytic performance displayed by the membrane-immobilized self-sufficient catalysts obtained, using TsRTA as transaminase.

Heterogeneous biocatalyst	Imm. Steps	[PLP] for TA immob. [mM]	L_{PLP} [µmol]	TA imm. yield (%)	Activity [U]	Sp. activity [$U.mg_{TA}^{-1}$] **(recovery, in %)**
TA_PP3	1	1	0.46	42	0.55	0.54 **(74)**
TA_PP3_SS1	2	1	0.85	30	0.42	0.59 **(78)**
TA_PP3_SS0.1	2	0.1	0.97	79	0.63	0.28 **(41)**

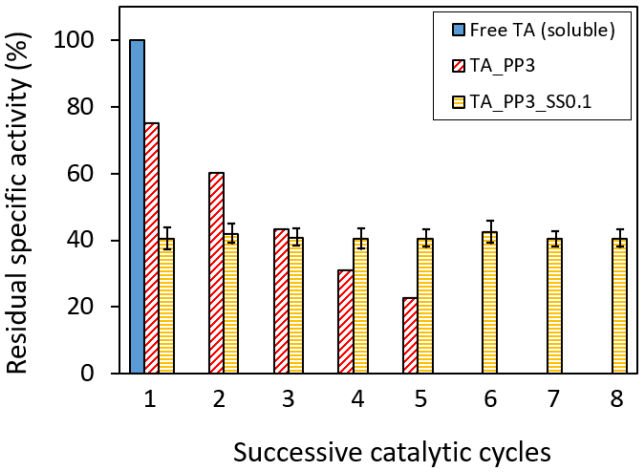

Figure III-13. Recyclability tests performed on TA_PP3 (red dashed bars) and TA_PP3_SS0.1 (yellow dashed bars) without PLP addition in the reaction media. For all three catalysts, TsRTA immobilization concentration was 0.5 mg/mL. Each catalytic cycle was separated by three buffer washings. Each bar represents the residual specific activity (with respect to free TsRTA), measured from the initial activity at each catalytic cycle (computed after 15 minutes). The error bars show the standard deviation measured on 3 different catalytic tests (n=3). Reaction conditions: 10 mM rac-BMBA, 10 mM pyruvate, 0 mM PLP (for TA_PP3 and TA_PP3_SS0.1) or 1 mM PLP (for free TA) in 0.1 M HEPES pH 8 buffer, 37 °C (5 mL reaction volume).

Finally, chiral HPLC analyses allowed us to confirm that the immobilization process did not affect the biocatalysts enantioselectivity (Table III-4). To this aim, the produced BMBA enantiomers obtained when employing the two best-performing immobilization strategies (namely TA_HPAN3b and TA_PP3) were analyzed and quantified. For all four membrane-immobilized TAs studied, only one BMBA enantiomer was detected, suggesting that the obtained biocatalytic membranes are enantioselective. Since the investigated reaction is a kinetic resolution (i.e. starting from a racemic mixture), the unconverted BMBA enantiomer (*e.g.* R-BMBA for HeWT, S-BMBA for TsRTA) was always detected by chiral HPLC (Figure SIII-18 to SIII-20).

Table III-4. Enantiomeric ratios obtained when employing TA_HPAN3b and TA_PP3 catalysts, using either HeWT or TsRTA as transaminase. S-and R-BMBA were detected when using TsRTA and HeWT enzymes, respectively.

	TA_HPAN3b	**TA_PP3**
HeWT	> 99 %	> 99 %
TsRTA	> 99 %	> 99 %

4.4 Comparison of the biocatalytic membranes performance with other immobilized TAs

In order to compare to compare the catalytic performance of different immobilized TAs, it is often useful to consider their specific activities (or specific activity recoveries, with respect to free enzymes) and immobilization yields (or immobilization efficiency). In this study, we employ small pieces of flat-sheet membranes (i.e. 5 cm^2, which corresponds to 25 mg and 40 mg

of functionalized PP and PAN membranes, respectively) as support, hence the enzyme loadings achieved on our heterogeneous catalysts are limited. This issue could be easily overcome by linear scaling-up of the membrane, and employing more ideal membrane configurations (i.e. reactors displaying higher interfacial area, e.g. industrial membrane modules) instead of simple flat-sheets.

As matter of comparison, our best-performing membrane-immobilized biocatalysts seem to perform better or similarly in terms of specific activity recovery and immobilization efficiency compared to a series of TAs immobilized on a variety of different supports (Table III-5), including polycarvone acrylate di-epoxide (PCADE)-functionalized membranes, 2D-zeolites, functionalized lignin, functionalized epoxy-resin). Among the best results that can be found in the literature, Heckmann and Paradisi managed to obtain 170 mg_{TA}/g_{resin} (corresponding to 70% immobilization yield) displaying 38% of specific activity recovery, and 400 mg_{TA}/g_{resin} with 62% specific activity recovery using *RTA-43 and HeWT_F48W, respectively [222].

Table III-5: Comparison of the immobilization and catalytic performance of the membrane-immobilized TAs reported in this work (using an enzyme concentration of C_0 = 0.5 mg/mL for the TA immobilization), with other immobilized TAs.

Ref.	Immob. biocatalyst	Immob. yield (%)	Immob. Efficiency [$mg_{TA}.g_{carrier}^{-1}$]	Sp. acti recovery (%)
This work	TSRTA_PP3	42	48	74
	TsRTA_PP3_SS	79	88	41
	TsRTA_HPAN3b	62	40	23
Howdle et al.[372]	HeWT_PCADE	62	6.2	44
Corma et al.[245]	TA_zeolites2D	80	50	62
Paradisi et al.[231]	HeWT_lignin	100	5	19
Paradisi et al.[131]	HeWT_resin	100	1	31
Paradisi and Heckmann[222]	HeWT_F48W_resin	100	400	62
	*RTA-43_resin	70	170	38

4.5 Process sustainability metrics evaluation

The "greenness" of the biocatalytic approach presented here can in theory be compared to common chemo-catalytic processes (A, B and C, represented in Figure SIII-21 to SIII-23) used for chiral amine synthesis, for example by comparing E-factors [14]. E-factors, defined as the mass of waste versus the mass of target product ratio, were calculated through the following formula (Eq. III-3), and results are reported in Table III-6.

$$E\ factor = \frac{\sum kg(unreact.reactants + by\ prod. + solv. + cat.)}{\sum kg\ target\ enantiopure\ (B)MBA} \quad Eq.III-3$$

Importantly, please note that in these calculations:

- Water was not considered as a waste in the processes, hence its contribution was not taken into account into E-factor calculation.
- The contribution of H_2 gas (i.e. reactant in excess in benchmark processes A and B) was also neglected, due to the lack of information in the reported studies (this omission drives the E-factor of chemo-catalytic reactions lower)
- The mass of catalyst in our process is considered as zero, considering the complete recyclability of the membrane-immobilized TA (as opposed to homogeneous chemo-catalysts which are lost in each batch)

Such metrics only cover the environmental performance **of the reactions**; the subsequent purification steps were not included in the E-factor calculation Rough estimations (Table III-6) show that the reaction itself (considering the reagents, solvent, and catalysts) is characterized by similar values of E-factors.

Table III-6: Comparison of environmental performance (E-factor) of our biocatalytic transamination (D) with different benchmark chemocatalytic processes (A, B, C) able to produce chiral amines.

Method (ref.)	**A** ([402])	**B** ([403])	**C** ([404])	**D (This work)**
Description	Imine red. amination	Ketone red. amination	Chiral resolution	Kinetic resolution
Precursors	Imine, H_2	Ketone, H_2, NH_4OAc	Racemic amine	Ketone, pyr
Catalyst	$[Rh(COD)Cl]_2$-(Ligand)	$Ru(OAc)_2$-(Ligand)	/ (resolv. agent) [a]	TA_PP3_SS
ee (%)	90	95	69	99.9
E-factor	58	18	19	31 (17 *)

[a] : A resolving agent, N-tosyl-(S)-phenylalanine (S-TPA), was used to resolve the racemic mixture.
* : if HEPES 0.05 M was used instead of HEPES 0.1 M

Yet, it is noteworthy that the biocatalytic strategy produces enantiopure products, which is not the case of the other methods. Further purifications (e.g. preferential crystallizations, catalyst removal, chiral chromatography) will be required in the chemo-catalytic processes, which will markedly increase the overall E-factor of such chemo-catalytic processes. Purification (not accounted for in these calculations due to lack of information) is known to be a major driver for the overall (environmental) cost of the process of chiral amine synthesis [18,284]. We therefore anticipate a significant advantage of the biocatalytic process when the whole process is considered.

5. Conclusion

To conclude, in this chapter, we report two efficient immobilization routes to obtain robust membrane-immobilized transaminases. These immobilization strategies consist in the TA electrostatic adsorption and covalent grafting, on polyethyleneimine (PEI)-coated polyacrylonitrile (PAN) and functionalized polypropylene (PP) membranes, respectively.

As important enzyme leaching was observed on the electrostatically immobilized TAs, post-treatment strategies of the electrostatically immobilized TAs were applied to improve TA anchoring at the functionalized PAN membrane surface. Among the developed strategies, the covalent binding of TAs and of the PEI layer using glutaraldehyde (GA) gave the most satisfying results (high specific activity, minor leaching). On the other hand, the TA covalent grafting on functionalized PP membranes yielded even more efficient biocatalysts (higher specific activity) displaying enhanced robustness (no leaching) and full recyclability. Importantly, these two strategies allowed to efficiently immobilize two different TAs (the S-selective HeWT, and the R-selective TsRTA), resulting in stereo-divergent biocatalytic membranes. Additionally, co-immobilization of TA and PLP was also achieved on functionalized PP membranes by adapting the immobilization protocol, which resulted in highly reusable membrane-immobilized biocatalysts capable of catalysing transaminations in absence of externally added PLP. Such self-sufficient ability should be attractive from an industrial point of view, since it should help increasing the cost-efficiency and reducing the E-factor of the transamination process. Thus, all in all, both studied routes to immobilize TAs on membranes led to functional biocatalytic materials exhibiting perfect enantioselectivity, high catalytic performance, minor leaching and excellent reusability. This paves the way to a future use in flow mode hybrid processes.

The transfer and implementation of such biocatalytic membranes in continuous flow (as a flat-sheet membrane reactor) has now to be carried out. Ultimately, more challenging transamination reactions (i.e. asymmetric synthesis) should be tackled with this immobilized TA, by taking benefit of the ability of the membrane carrier to act as a separation unit for (co)product removal.

6. Supplementary informations of Chapter III

6.1 Experimental details of Chapter III – Characterization of the membrane carriers and of the biocatalytic membranes

Soluble enzymes quantification : Bradford method

Soluble enzyme concentrations were assessed through the Bradford titration method [405]. Calibration was performed by mixing 250 µL of standard solutions of TA cell-free extracts in HEPES 0.1M buffer pH 8, sodium pyruvate 10 mM, PLP 1 mM (within 0–0.16 mg.mL^{-1} concentration range) with 750 µL of Bradford reagent. After 5 minutes incubation at room temperature, absorbances were read at 595 nm with a ThermoScientific Genesys 10S-Vis spectrophotometer, and values of A_{595} were plotted against TA concentration.

Immobilized PLP loading evaluation

When co-immobilization of TA and PLP was attempted, the amount of PLP loaded onto the membrane was determined by measuring the absorbance at 390 nm of 1 mL solutions using a ThermoScientific Genesys 10S-Vis spectrophotometer. Calibration curve was performed using standard solutions of HEPES 0.1M buffer pH 8, sodium pyruvate 10 mM containing different PLP concentrations (within 0–0.5 mM concentration range). The PLP immobilization yield (Y_{PLP}) was computed using Eq. S1, where $[PLP]_0$, $[PLP]_1$ and $[PLP]_{Ri}$ stand for the PLP concentration in the immobilization (i.e. 0.1 mM or 1 mM for TA immobilization, 1 mM for PLP immobilization), residual and rinsing solutions, respectively.

$$L_{PLP} = 5 \times ([PLP]_0 - [PLP]_1 - \Sigma[PLP]_{Ri}) \ [\mu mol] \qquad Eq.S1$$

Gas Chromatography (GC) analysis

After extraction of the analytes into dichloromethane, the analysis was performed on a Bruker Scion 456-GC with a WCOT fused silica BR-5 column (30 m x 0.32 mm ID x 1.0 µm) and helium as carrier gas (25 $mL.min^{-1}$), oven temperature at 150 °C, split ratio of 80, injector temperature at 250 °C, flame ionization detector temperature at 300 °C (air flow 300 $mL.min^{-1}$, H_2 flow 30 $mL.min^{-1}$).

Chiral High Performance Liquid Chromatography (cHPLC) analysis

R and S enantiomers of bromo-α-methylbenzylamine were detected by normal phase HPLC (Hitachi-koki, Chiyoda, Japan) at 252 nm using a Merck-Hitachi LaChrom L-7000 HPLC and a Chiralpak AD-H (250 mm × 4.6 mm) column with a flow rate of 1 mL/min (95% isohexane/5% 2-propanol/0.1% diethylamine) for 30 min. The retention times of the S- and R-enantiomers were 4.79 and 6.30 min, respectively.

6.2 Supplementary data of Chapter III – Figures, tables and remarks

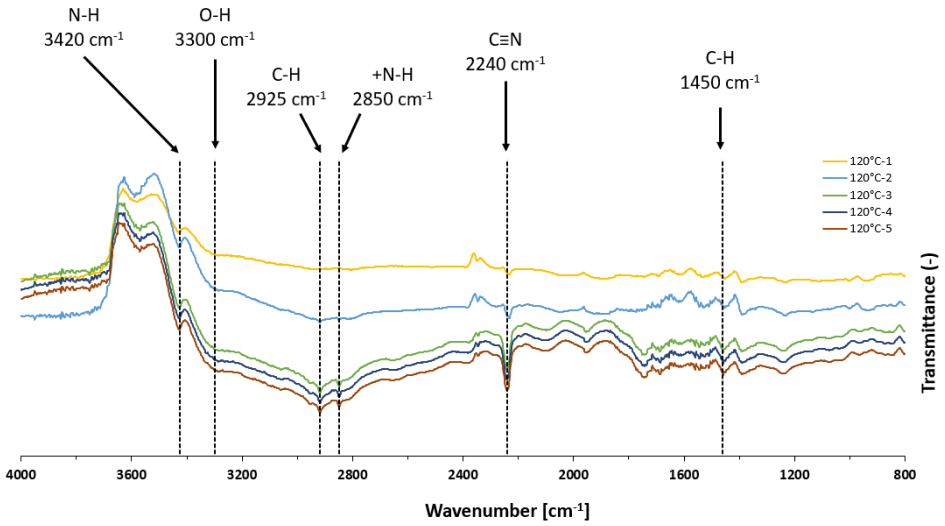

Figure SIII-1. Diffuse reflectance infrared Fourier transform spectroscopy (DRIFTS) spectra (in transmittance) obtained on the HPAN_PEI1 heated at 120 °C (under air). Each series on the graph (i.e. each line) represents a run of analysis. Each run was performed every two minutes.

Table SIII-1. Main bond vibrations wavenumbers (in cm^{-1}) of the different species of interest (i.e. amines, amides, carboxylic acids, alkanes, amides and nitriles)

Bond vibration mode	**Amines**		
	I	**II**	**III**
H-N-H scissors	1600-1650	/	/
$N-CH_3$ and $N-(CH_3)_2$ stretching	/	2780	2780 and 2850
N-H stretching	3300 and 3400	3300 (broad)	/
	Amine salts		
	I	**II**	**III**
+N-H bending	1560-1630	1500-1530 and 1560-1630	/
+N-H stretching	2800-3000	2800-3000	2300-2700
	Amides		
	I	**II**	
C-N stretching	1400	1250-1300	
C=O stretching	1650-1680	1650-1680	
N-H stretching	3150-3350	3150-3350	
	Carboxylic acids/carboxylates		
O-H stretching	2500-3300 (very broad and strong)		
C=O stretching	1730		
COO- stretching	1560		
O-H bending	1400		
	Alkanes		
C-H stretching	2925		
C-H bending	1450		
	Epoxides		
Ring stretching	1230-1280		
-C-O-C- stretching	810-950		
-C-O-C- stretching	750-880		
	Nitriles		
C≡N stretching	2240		

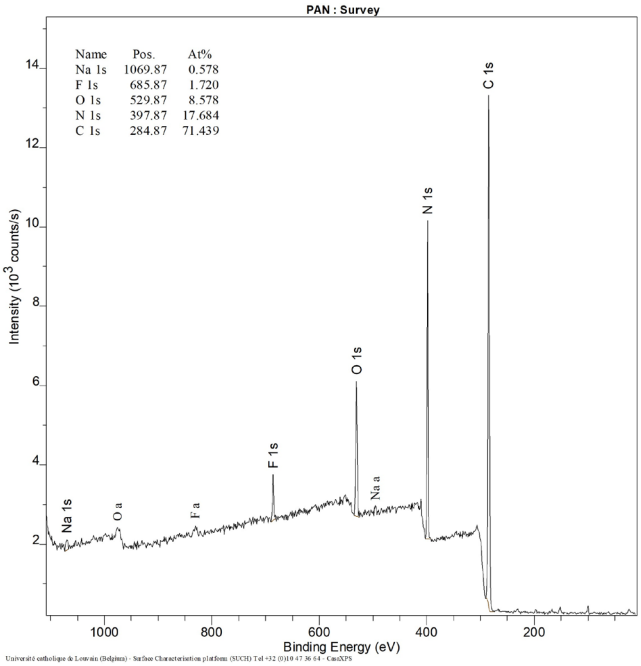

Figure SIII-2. XPS spectrum of the pristine PAN membrane

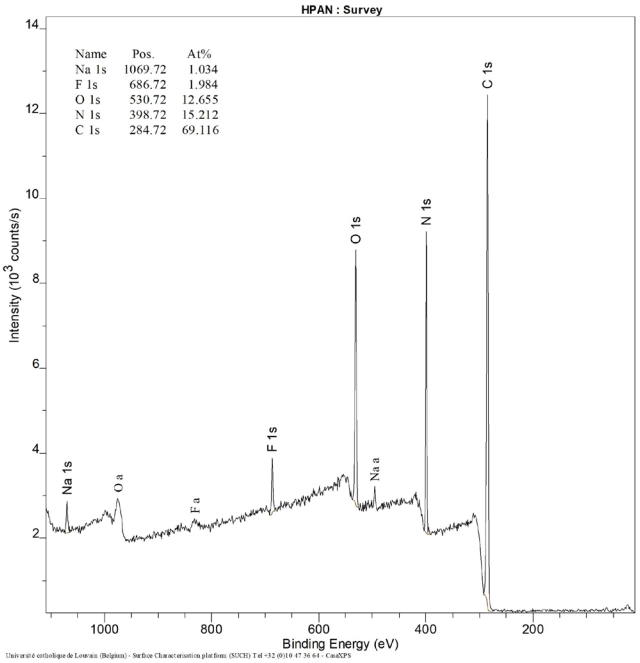

Figure SIII-3. XPS spectrum of the HPAN membrane

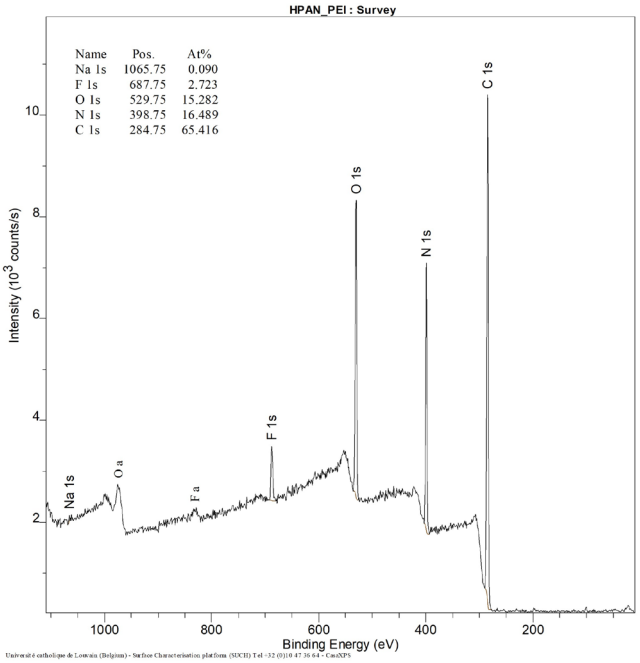

Figure SIII-4. XPS spectrum of the HPAN_PEI1 membrane

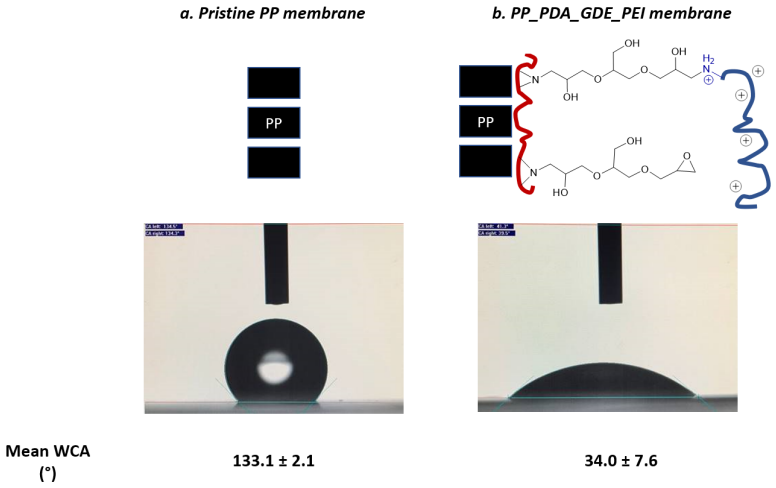

Figure SIII-5. Schematic representation (top) and water contact angle (WCA) measurements (bottom) of **a)** pristine PP and **b)** PP_PDA_GDE_PEI membranes. Mean WCA represent the average values of the measurements taken at 5 different spots of c.a. 3 cm^2 membranes sheets.

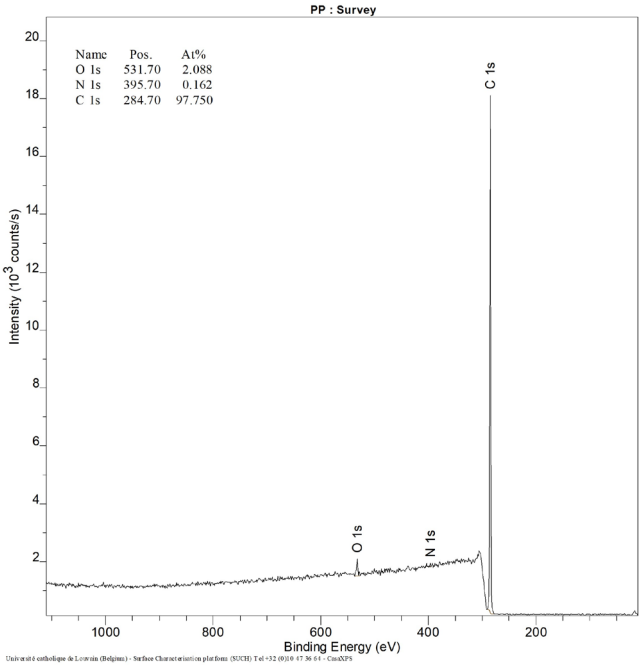

Figure SIII-6. XPS spectrum of the pristine PP membrane

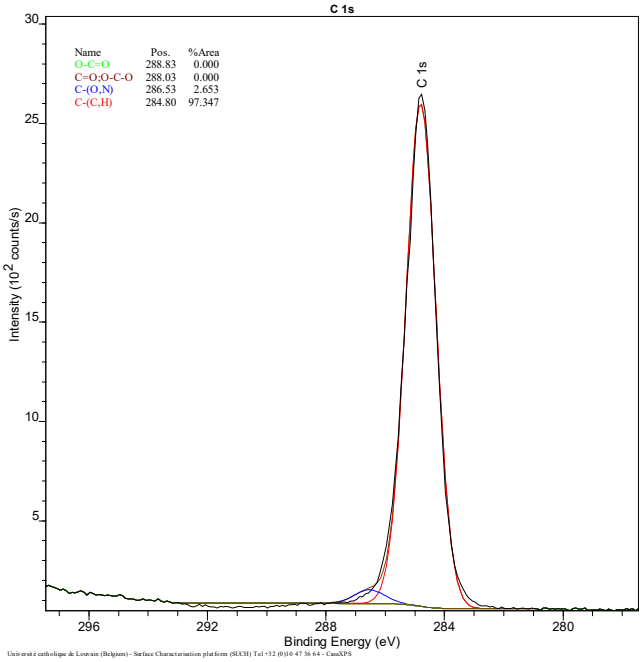

Figure SIII-7. C1s peak deconvolution (resulting from the pristine PP membrane analysis by XPS)

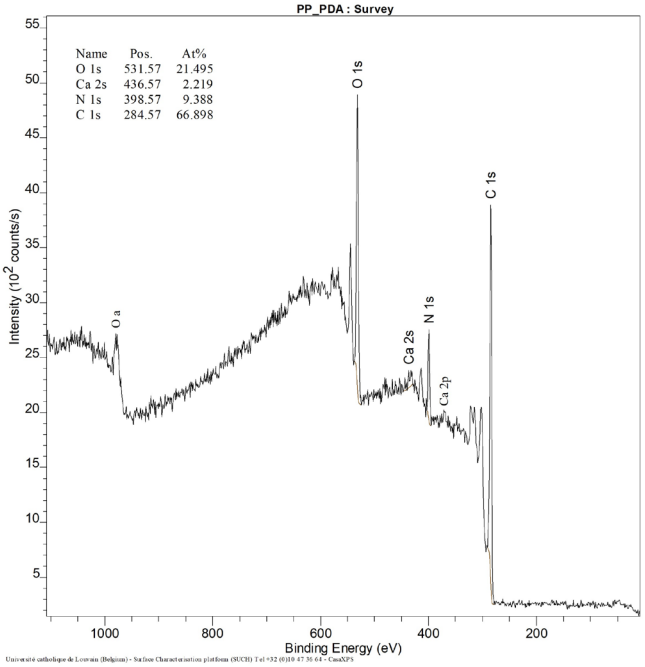

Figure SIII-8. XPS spectrum of the PP_PDA membrane

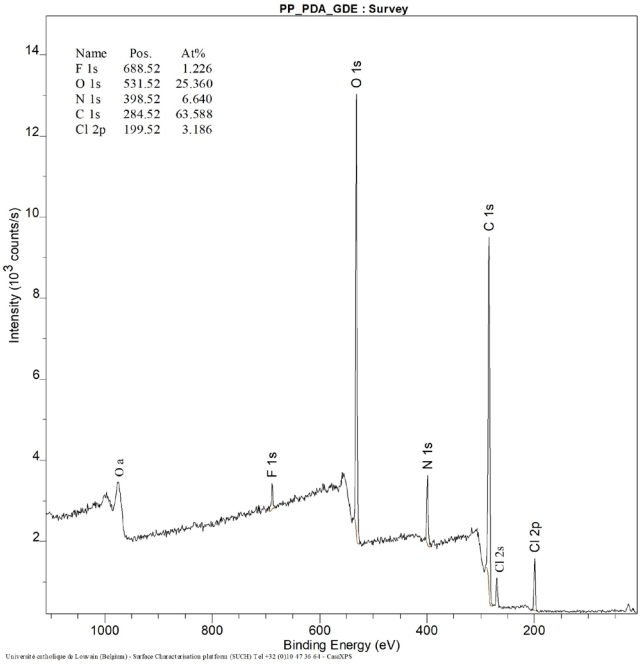

Figure SIII-9. XPS spectrum of the PP_PDA_GDE membrane

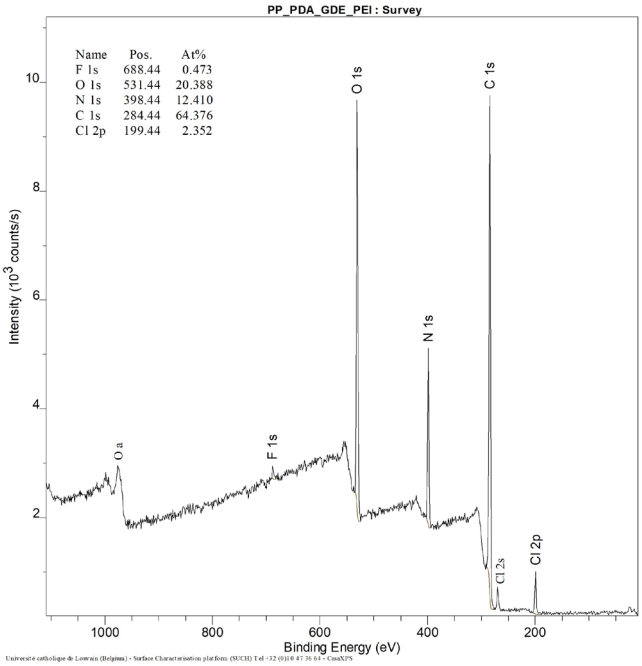

Figure SIII-10. XPS spectrum of the PP_PDA_GDE_PEI membrane

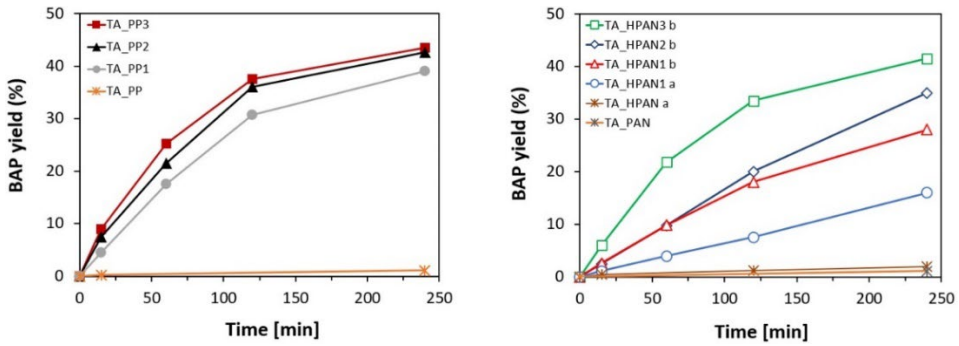

Figure SIII-11. Activity profiles displayed by the different PP-immobilized (left) and PAN-immobilized (right) HeWT biocatalysts in the kinetic resolution of BMBA (using C_0 = 0.25 mg/mL TsRTA as immobilization concentration).

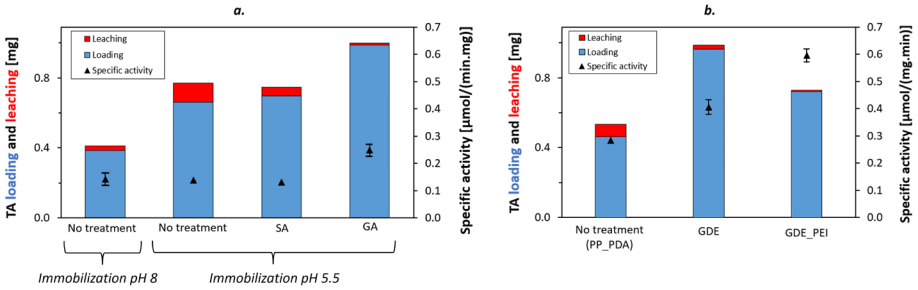

Figure SIII-12. Immobilized TsRTA loading (blue) and leaching (red) (left axis), and specific activity (black triangles) (right axis) observed on **a)** different HPANx supports (from left to right : HPAN1a, HPAN1b, HPAN2b, HPAN3b) and **b)** PPy carriers (from left to right : PP1, PP2, PP3) and **b)** PP_PDA carriers, at constant immobilization concentration (C_0 = 0.25 mg/mL TsRTA). Error bars represent the standard deviations obtained on triplicates.

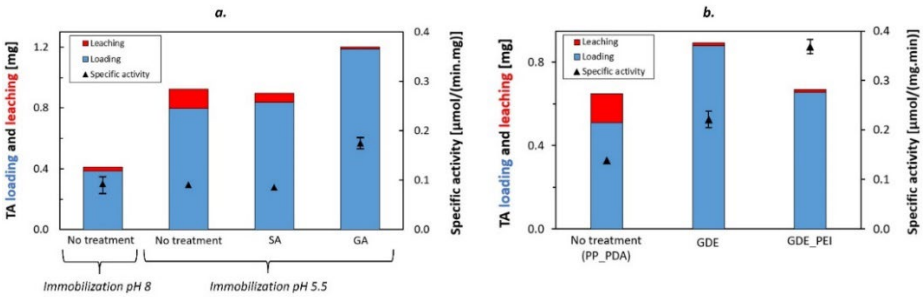

Figure SIII-13. Immobilized HeWT loading (blue) and leaching (red) (left axis), and specific activity (black triangles) (right axis) observed on **a)** different HPANx supports (from left to right : HPAN1a, HPAN1b, HPAN2b, HPAN3b) and **b)** PPy carriers (from left to right : PP1, PP2, PP3), at constant immobilization concentration (C_0 = 0.25 mg/mL HeWT). Error bars represent the standard deviations obtained on triplicates.

Optimization of TA immobilization

(a) TA on HPAN membranes

The best membrane functionalization and enzyme immobilization strategy (TsRTA_HPAN3b) was selected for further study, in an attempt to further boost catalytic performance of the resulting membranes. The effect of PEI

concentration and GA post-treatment duration were screened (Figure SIII-14). Functionalization with PEI did not affect markedly the enzyme loading, but a marked improvement of the specific activity of the immobilized TAs was observed from PEI concentrations of 0.5 wt.%. No further significant improvement could be achieved by further increasing the PEI concentration, which might indicate a saturation of this polyelectrolyte layer at the membrane surface. The TA leaching was always minor, whatever the PEI concentration, owing to the effective GA cross-linking. The effectiveness of this post-treatment with GA is similar whatever the duration (Figure SIII-14b).

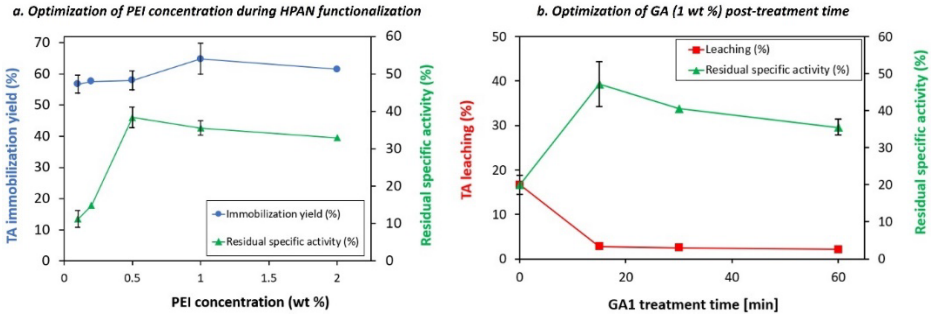

Figure SIII-14. Impact of **a)** PEI concentration (wt %) on TA_HPAN3b (post-treated with GA for 60 minutes) and of **b)** GA post-treatment time (minutes) on TA_HPAN3b (PEI 1 wt %) performance. Screenings were performed using C_0 = 0.25 mg/mL of TsRTA for immobilization. Error bars represent the standard deviations obtained on triplicates.

Note: the effect of PEI concentration (wt %) on TsRTA leaching fraction (%) was not presented on graph **a)** since no significant differences were observed (due to the immobilized enzymes post-treatment with glutaraldehyde).

(b) TA on PP membranes

Starting form the best system based on the PP membrane (TsRTA_PP3), the effects of PDA, GDE, and PEI functionalization times were studied. Increasing the dopamine polymerization time was found to have a significant impact on TA catalytic performance (Figure SIII-15a). Low PDA functionalization times (i.e. 6 and 10 hours) resulted in membrane displaying higher enzyme leaching and poorer specific activity than those functionalized for 20 hours. The higher TA leaching might either be explained either by a poor anchoring of the resulting polydopamine layer to the PP surface due to incomplete polymerization (i.e. leaching of the TA_PDA_GDE_PEI layers), or by a different TA immobilization mechanism. The latter hypothesis is based on the fact that different chemical moieties (primary and secondary amines, quinones, catechols, etc) might be present at the PDA coating surface, depending on the dopamine polymerization state (Figure SIII-16) [406]. Among all the reactive species generated, amines (I or II) will always be present in similar amounts, allowing the epoxy groups of GDE to be grafted onto the surface. However, there is a possibility that the TAs preferentially immobilize on other moieties (than epoxy) present at the carrier surface, such as quinones (covalent grafting) or catechols (electrostatic adsorption). Yet, this hypothesis is hard to prove due to the fact that the accurate structure and composition of PDA coatings is still questionable (despite being intensely characterized) [407]. On the contrary, the GDE grafting time (Figure SIII-15b) did not affect the immobilization and catalytic performance of the biocatalysts, which suggests that the epoxy coupling is already be completed in 2 hours. Finally, PEI derivatization times higher than 90 minutes seem to enhance the TA leaching. This can be explained by the fact that, when using longer PEI derivatization times, a higher fraction of epoxy groups of GDE will be consumed by reaction with the amine groups of PEI. Thus, in the subsequent step of TA immobilization, the enzyme will have a lower chance to form stable covalent

bonds by reactions with epoxy groups and instead mostly immobilize through (more labile) electrostatic adsorption. Thus, the TA electrostatic immobilization increases at the expense of the TA covalent grafting. Thus, the selected formulation of such catalyst seems to be achieved with 20 hours of PDA, 2 (or 18) hours of GDE, and 90 minutes of PEI.

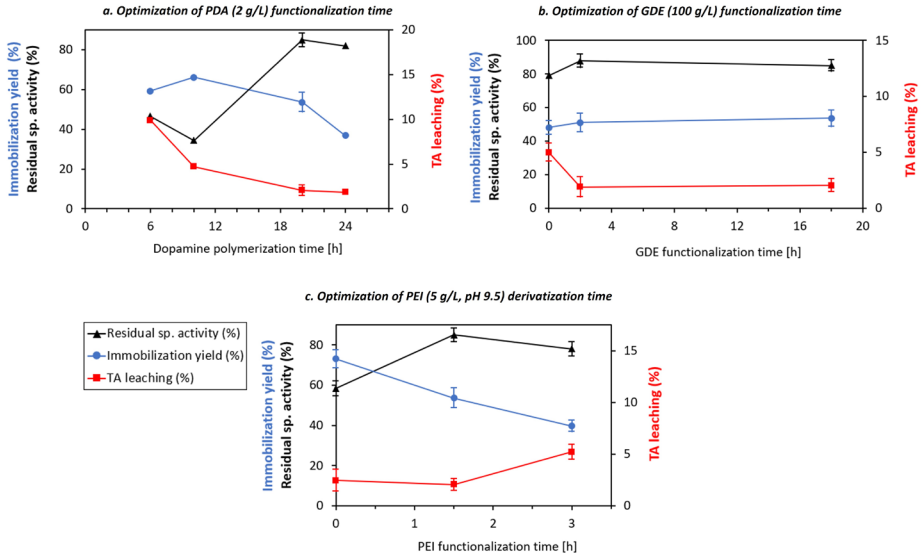

Figure SIII-15. Impact of **a)** the PDA functionalization time on TA_PP3 (functionalized with GDE (18 hours) and PEI (1.5 hours)) ; **b)** the GDE functionalization time on TA_PP3 (functionalized with PDA (20 hours) and PEI (1.5 hours)) and **c)** the PEI functionalization time on TA_PP3 (functionalized with PDA (20 hours) and GDE (18 hours))**)** performance. Screenings were performed using C_0 = 0.25 mg/mL of TsRTA for immobilization. Error bars represent the standard deviations obtained on triplicates.

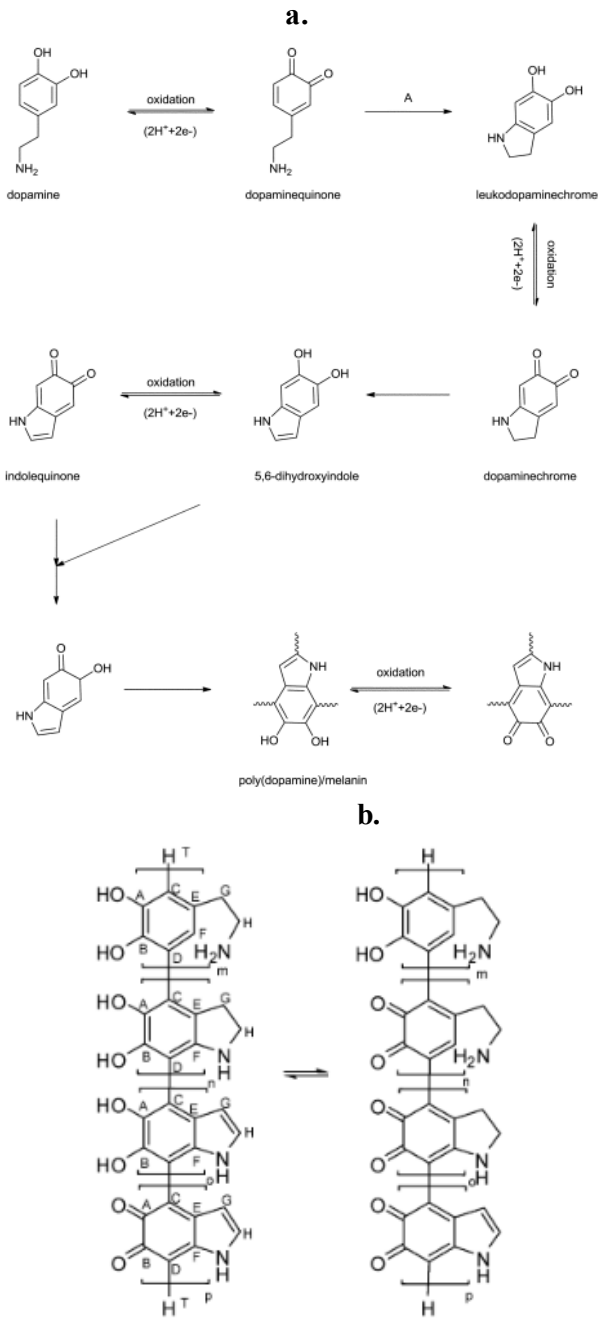

Figure SIII-16 a. Representation of one possible dopamine polymerization mechanism, reprinted from Kamperman et al. (2014) [388], **b.** Actual structure of PDA (obtained from 2 g/L dopamine hydrochloride in 10 mM Tris buffer pH 8.5, by air oxidation) proposed by Liebscher et al. (2013)[407].

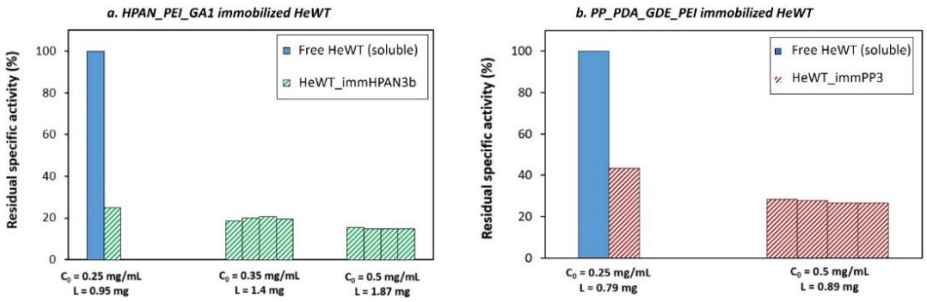

Figure SIII-17. Reusability tests performed with **a)** HeWT_HPAN3b and **b)** HeWT_PP3 at different enzyme loadings (L). Each bar shown in **a)** and **b)** represent the residual specific activity (with respect to free HeWT), measured at each catalytic cycle (computed after 15 minutes).

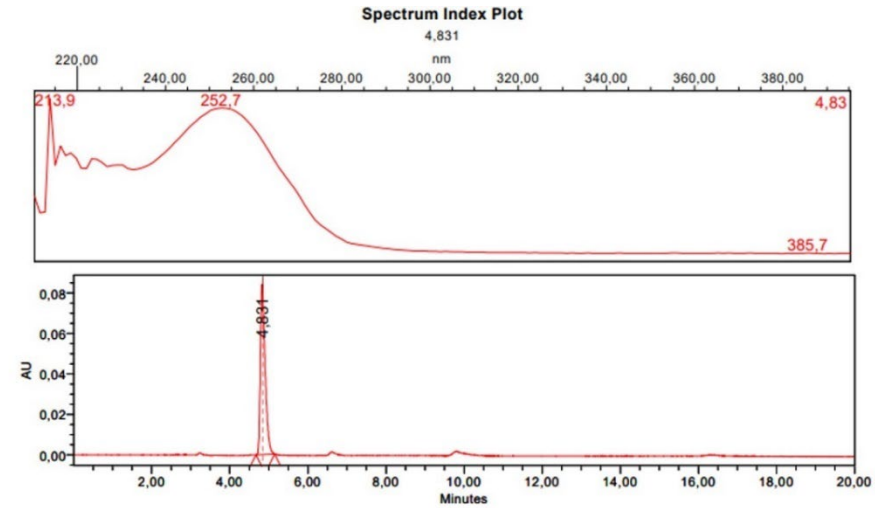

Peak Results

	Name	RT	Area	% Area
1		4,831	705943	100,00

Figure SIII-18. Chiral HPLC chromatogram obtained by analyzing the BMBA produced after kinetic resolution, using TsRTA_PP3.

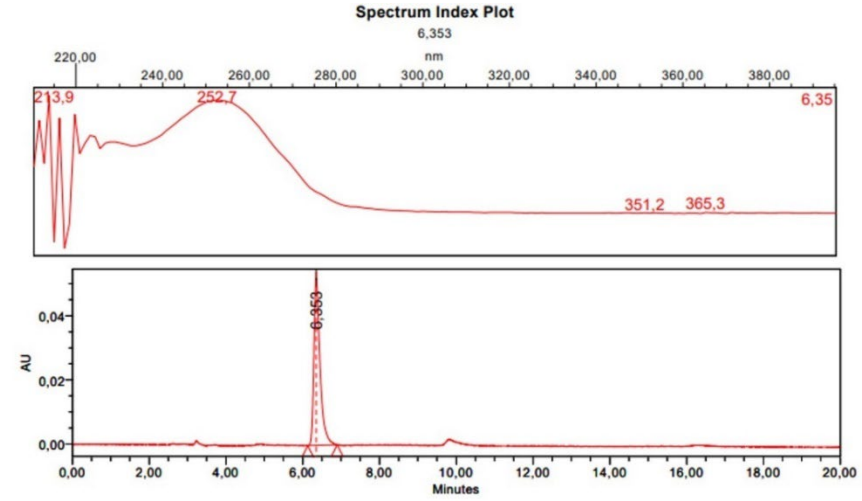

Peak Results

	Name	RT	Area	% Area
1		6,353	586111	100,00

Figure SIII-19. Chiral HPLC chromatogram obtained by analyzing the BMBA produced after kinetic resolution, using HeWT_PP_PDA_GDE_PEI.

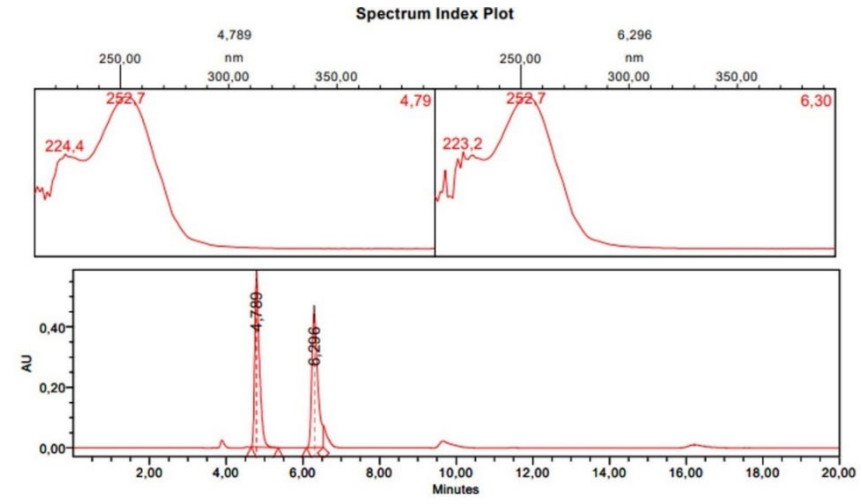

Peak Results

	Name	RT	Area	% Area
1		4,789	4788968	50,02
2		6,296	4785771	49,98

Figure SIII-20. Chiral HPLC chromatogram obtained by analyzing commercial racemic BMBA product

Sustainability metrics (E-factor) evaluation

In this work, a kinetic resolution was used as a model reaction to demonstrate the effectiveness of the biocatalytic reaction with immobilized TA. The reaction is limited to 50% of yield. Hence, its E-factor will be penalized as compared to classical asymmetric synthesis of chiral amines (theoretical yield of 100%). Additionally, the most important advantage brought by the use of TA is indeed the enantioselectivity, which facilitates subsequent purification. Thus, a fully informative comparison of E-factor should also include the crucial purification steps.

Nevertheless, rough E-factor estimations for our batch transamination processes can be compared to benchmark processes. Three common chemo-catalytic processes (methods A,B,C, see Figure SIII-21 to SIII-23) for the synthesis of such enantiopure amines (i.e. α-methylbenzylamine derivatives) [408] have been used as benchmark:

A. Imine asymmetric reductive amination (Figure SIII-21) [402]: MBA (2a)

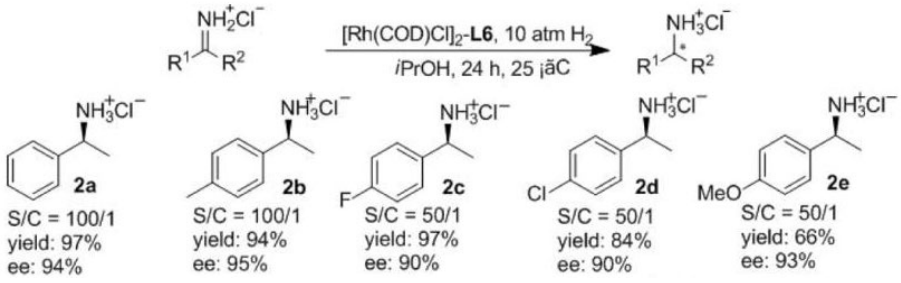

Figure SIII-21. Imine asymmetric hydrogenation reported by Zhang et al (2014) [402]

Protocol [402]: In nitrogen-filled glovebox, a solution of ligand L6 (1.1 eqv.) and $[Rh(COD)Cl]_2$ (3.0 mg, 0.006 mmol) in 6.0 mL anhydrous i-PrOH was stirred at room temperature for 30 min. A specified amount of the resulting solution (2 mL) was transferred to a vial charged with 1a (0.2 mmol) by syringe. The vials were transferred to an autoclave, which was then charged with 10 atm of H_2 and stirred at 25 °C for 24 h.

B. Asymmetric reductive amination of keto-substrates (Figure SIII-22) [403]**:** F-MBA (6j)

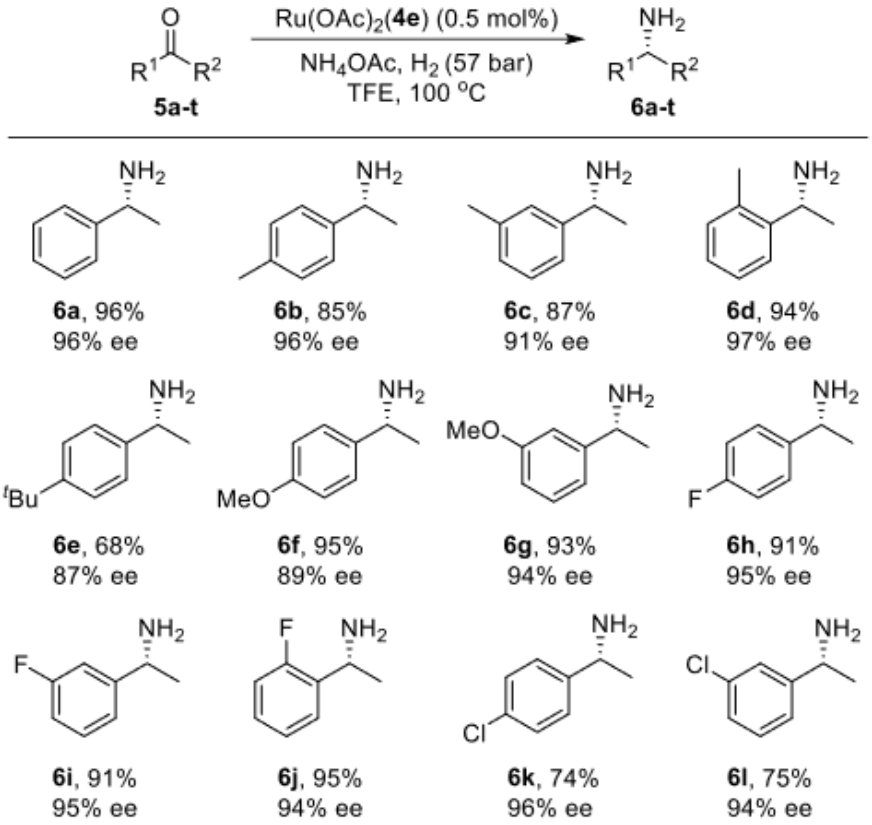

Figure SIII-22. Asymmetric reductive amination of keto-substrates reported by Zhang et al (2018) [403]

Protocol [403]: In a glovebox, required amount of the catalyst (0.5 mol %), substrate (0.2 mmol), ammonium salt (NH_4OAc, 0.4 mmol) and solvent (TFE = trifluoroethanol, 0.4 mL) were successively added to a vial equipped with a magnetic stirring bar. The mixture was then transferred to a stain-less autoclave and purged by three cycles of pressurization/venting with H_2. The required H_2 pressure was then installed and the autoclave was placed in an oil bath preheated to the indicated temperature. The autoclave was cooled down

in an ice bath after the indicated reaction time and the pressure was slowly released.

C. Solvent switch-assisted chiral resolution of racemates (Figure SIII-23) using a resolving agent [404]: MBA-TPA crystal salts.

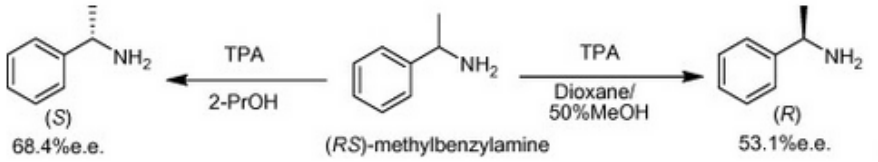

Figure SIII-23. Solvent switch-assisted chiral resolution of rac-MBA using N-tosyl-(S)-phenylalanine (S-TPA) as resolving agent, reported by Hirose et al (2008) [404]

Protocol [404]**:** A mixture of (RS)-MBA (121 mg, 1.0 mmol), N-tosyl-(S)-phenylalanine (S-TPA, 319 mg, 1.0 mmol), and the solvent (2-PrOH, using a 2-PrOH/(RS)-MBA ratio of 35 (v/w)) was heated to produce a clear solution. The solution was then cooled to room temperature to grow less-soluble salt crystals. The crystals were filtered off and washed with the respective solvent to afford the crude and less-soluble diastereomeric salt (S)-MBA:(S)-TPA. Yield (calculated based on half the amount of (RS)-MBA) and enantiomeric purity were of 69.8%.

NB: please note that here, the resulting enantiopure amine is in the form of a crystal salt of S-MBA:S-TPA. No purification steps are indicated by the authors to obtain the enantiopure S-MBA.

- .

Chapter IV – Crystallization-assisted asymmetric synthesis of amines using membrane-immobilized transaminases

ABSTRACT

In Chapter III, we reported the successful immobilization of transaminases (TAs) onto a functionalized polypropylene (PP) membrane. Here, in this chapter, we explore the ability of these biocatalytic membranes to efficiently catalyze an industrially relevant transamination, the asymmetric synthesis of R-2-fluoromethylbenzylamine (R-FMBA). Towards this reaction (in batch mode), the membrane-immobilized TAs exhibited superior activity and stability compared to soluble TAs, and outperformed conventional heterogeneous biocatalysts Two strategies were then implemented to further enhance the productivity of such process. First, the batch reaction is coupled with in-situ product separation to shift the equilibrium towards the product side. Here, we leverage on crystallization of R-FMBA with 3,3-diphenylpropionic acid (DPPA), which enables straightforward recovery of enantiopure amines in the form of crystals. This approach resulted in a 95% yield of pure R-FMBA crystals. The biocatalytic membrane was easily reusable, and was able to perform successive high-yield asymmetric syntheses with minor deactivation. In a second approach, the biocatalytic membranes were implemented in continuous flow mode. Here, both TA immobilization and subsequent transamination steps were performed in flow, in lab-scale enzyme-membrane-reactor. The improved hydrodynamics and mixing provided by the flow configuration allowed significantly increasing the immobilized TA loading and enhancing the productivity of the transamination. This study highlights the potential for scaling up this biocatalytic system, and paves the way to the set-up of hybrid flow processes.

1. Introduction

Enzyme immobilization has proven effective in creating heterogeneous biocatalysts that are more versatile and amenable to more productive flow processes [163,167,170,171,175,176]. Polymeric membranes can be seen as available and relatively cheap supports to immobilize biocatalysts (50 €/m^2 can be estimated for membrane contactors [284,409,410], which is comparable to other materials classically employed for enzyme immobilization purposes (e.g. epoxy-resins from ReliZyme) [381,411]), which typically offer high surface-to-volume ratios when implemented industrially (as membrane modules). Enzyme immobilization on polymeric membranes is now well-documented [166], and the TA membrane-immobilization has been demonstrated [372]. In Chapter III of this thesis, we reported two different transaminases membrane-immobilization protocols, leading to robust and reusable heterogeneous biocatalysts in batch mode. As discussed and exposed in Chapters II and III, immobilizing enzymes on membrane supports can be of particular interest, as it additionally offers the possibility to perform biocatalytic reactions along with membrane separation, in a one-pot fashion. For example, the removal of a product can favorably shift the biocatalytic reaction equilibrium toward product formation and hence increase the reaction yield. In the specific case of transaminations, this aspect is of great relevance since these reactions are highly limited by unfavourable thermodynamic equilibrium.

So far, different in-situ (co)product removal (ISPR) strategies have been applied in (recirculating) batch to drive transaminations towards the products, such as product extraction (using organic co-solvent or a membrane module), capture/absorption (using ion-exchange resins) and crystallization [94,103,139,214,249,284,412]. Among these product separations, crystallization of the target enantiopure amine product seems particularly suited for the pharmaceutical industry, owing to the high selectivity and high

(enantio)purity that can be generally obtained through such processes. Moreover, it enables the straightforward recovery of the API via simple filtration. Crystallization has notably been employed for the synthesis of (S,S)-Sertraline, as the last step of the chemo-catalytic process consisted in the chiral resolution of diastereoisomeric mixture (of (S,R) and (S,S) compounds) using R-mandelic acid: (S,S)-Sertraline forms an insoluble salt with R-mandelic acid, which crystallizes and is easy to recover, while the other (S,R)-Sertraline-mandelate salt remains soluble [46,47] Recently, von Langermann *et al.* [103] implemented a crystallization-assisted transamination for the gram-scale preparation of S-(3-methoxyphenyl)ethylamine, a precursor of Rivastigmine. The developed *in-situ* product crystallization strategy relied on the use of a crystallizing agent, 3,3-diphenylpropionic acid (DPPA), which is able to form low sloubility crystalline salts with amine compounds [139]. It enabled the production of a pure enantiopure amine product at high concentration (> 1 M) and its straightforward recovery via filtration, and was found applicable to a wide variety of amine targets [413].

One important aspect aiming at increasing the productivity of transaminations and the efficiency of crystallization processes, is the transfer from batch to continuous flow mode [165,167,172,173,209,255,256]. Continuous crystallization offers important advantages over batch crystallization including more consistent product quality, higher throughput per time and volume unit, and easier monitoring [414]. Indeed, in some cases, continuous crystallizers allow achieving more precise final size, particle size distributions, and desirable shape characteristics (due to more accurately controlled and homogeneous supersaturation) than in time-dependent processes, which can result in reduced downstream processing. When attempting to perform such reaction and/or crystallization processes in flow, leveraging on membrane technologies can be advantageous [175,259,260]. The porous surface of the membrane can act as suitable support to activate heterogeneous nucleation, hereby also impacting the mechanism of the

crystallization process [415]. Researchers have implemented membrane contactors at the outlet of the transamination flow reactor, as downstream processing, to separate their effluents [96,214,242]. Notably, pervaporation for acetone removal was recently demonstrated using PolyDiMethylSiloxane (PDMS) membranes [282], and it turned out that the higher the acetone concentration in the medium, the more pronounced the pervaporation effect. This study highlights the potential benefits a combination between membrane operations (e.g. co-product removal via pervaporation) and *in-situ* crystallization of the target amine.

Thus, it would be particularly relevant to develop bifunctional membranes allowing to simultaneously host the immobilized TAs and perform the product separation to intensify the transamination process. To our knowledge, no study has reported yet the use of a biocatalytic membrane reactor, in which the membrane would simultaneously act as the enzyme support and enhance the yield and/or kinetics of a transamination through membrane operations. Our final goal is to develop such combined reaction-separation process, using reusable membrane-immobilized transaminases as reactor and separation unit, coupled with product crystallization in continuous flow-mode.

Here, we demonstrate the proof of concept of a crystallization-assisted transamination using a membrane-immobilized TA at the lab scale, in batch mode. An industrially relevant transamination reaction was targeted, i.e. the asymmetric synthesis of R-2-fluoromethylbenzylamine (R-FMBA) from 2'-fluoroacetophenone (using isopropylamine as amino donor). R-FMBA is a precursor of valuable fluorinated chiral *N*-arylamines [416], and its separation is not straightforward (i.e. liquid at room temperature). To our best knowledge, such amine building block is not commercialized in an enantiopure form. We show that using a membrane-immobilized TA, in presence of DPPA, allowed reaching yields of pure FMBA:DPPA crystals markedly surpassing the equilibrium yield of the non-assisted reaction. The PP-immobilized TA was also stable, showing only minor deactivation, and being fully recyclable for 3

successive runs. The biocatalytic membrane was also shown the able to operate in continuous flow mode, highlighting the benefits of such flow regime (with respect to discontinuous batch processes). This paves the way to a future use in flow mode hybrid processes, concatenated with membrane-assisted purification strategies for co-product removal.

2. Materials

4'-bromoacetophenone (BAP; ≥ 98 %), R-4-bromo-α-methylbenzylamine (R-BMBA; 99 %), S-4-bromo-α-methylbenzylamine (S-BMBA; 99 %), hydrochloric acid (37 wt %, aqueous solution), pyridoxal 5'-phosphate hydrate (PLP; ≥ 98 %), glycerol diglycidyl ether (GDE; technical grade), carbonate-bicarbonate buffer capsules, Bradford reagent were purchased from Sigma-Aldrich. Sodium hydroxide (NaOH; ≥ 99 %), N-2-Hydroxyethylpiperazine-N'-2-ethane sulphonic acid (HEPES; ≥ 99.5 %), HEPES sodium salt (≥ 99 %) were purchased from Carl Roth. Branched polyethyleneimine (PEI; 50 wt %, aqueous solution, M.N. 60,000), isopropylamine (ISO; 99 %) were purchased from Acros Organics. Dichloromethane (DCM; HPLC grade), ethanol absolute (EtOH), dimethylformamide (DMF; ≥ 99.9 %) were purchased from VWR Chemicals. Tris(hydroxymethyl)aminomethane (Tris; > 99 %), 3-hydroxytyramine hydrochloride (dopamine hydrochloride; 98 %), tert-butyl methyl ether (MTBE; > 99 %), 3,3-diphenylpropionic acid (3-DPPA; 97 %), isopropyl alcohol (iPOH; 99.5 %), tert-butyl alcohol (tBuOH; > 99 %), 2'-fluoroacetophenone (FAP; 97 %), acetophenone (AP, 97 %), phenoxy-2-propanone (PhoxyP; 97 %), and phenylbutanone (PhB; 97 %) were purchased from Tokio Chemical Industry. Methanol (MeOH; 99.8 %) was purchased from Thermo scientific. 2-fluoro-α-methylbenzylamine (FMBA; 97%) was

purchased from BLD Pharm. Commercial polypropylene membranes (PP) were purchased from 3M (USA).

Whatman stainless steel membrane holder (employed in flow experiments) was purchased from Tisch scientific. Transaminases HeWT (from Halomonas elongata) and TsRTA (from Thermomyces stellatus) were expressed and lyophilized as previously described by Paradisi et al. [122,129], and then used as cell-free extracts. In some cases, the enzymes were also purified by immobilized metal affinity chromatography (IMAC) in order to be used as pure enzymes (pTA). Distilled water was applied for all synthesis and treatment processes.

3. Methods

3.1 Transaminase immobilization onto solid supports

In this work, only the transaminase from *Thermomyces stellatus* (TsRTA) was immobilized onto solid supports (functionalized polypropylene membranes and ReliZymes) to run the subsequent heterogeneous transaminations.

3.1.1 Polypropylene membrane (PP)

3.1.1.1 PP functionalization

Polypropylene (PP) membrane surface was functionalized prior to immobilization in order to enable the covalent grafting of TAs, following the method described in details in the section 3.2.1 of the Chapter III. In this work, only the fully functionalized PP (i.e. PP_PDA_GDE_PEI) were employed as membrane carriers for the TA immobilization.

3.1.1.2 TA immobilization

a. Batch mode

A disk of 7 cm^2 (c.a. 35 mg) functionalized PP membrane was immersed into 7.5 mL of buffered solution (HEPES 0.1 M buffer, PLP 1 mM) containing the desired TA concentration (C_0 = 1 $mg.mL^{-1}$) at pH 8, and incubated for 18 hours at 35 °C under gentle stirring. After immobilization, the resulting membrane-immobilized transaminase was rinsed with 7.5 mL of rinsing solution (containing PLP 1 mM in HEPES 0.1 M buffer pH 8) for 30 minutes (repeated two times) to eliminate the loosely attached TAs. The immobilization and washing steps were carried out in 10 mL round bottom glass flasks. The heterogeneous biocatalysts obtained upon immobilization of TA cell-free extract (cfe) and pure TA (pTA) were denoted TA_PP3 and pTA_PP3, respectively.

Importantly, when the TA immobilization in batch was compared to flow TA immobilizations (see section 3.1.1.2b), 1 cm^2 membrane discs and 5 mL immobilization solution were employed, respectively.

In a variation of this protocol, we also attempted to prepare self-sufficient biocatalysts. Inspired López-Gallego *et al.* [236], we immobilized the TA cfe (using 1 $mg.mL^{-1}$ into 0.1 mM PLP in HEPES 0.1 M buffer pH 8) onto a disk of 7 cm^2 functionalized PP, then rinsed the resulting membrane three time (with 7.5 mL HEPES 0.1 M buffer pH 8, 30 minutes), and directly incubated it with PLP (1 mM in HEPES 10 mM pH 8 for 90 minutes at room temperature under gentle stirring). Additional rinsing was applied again (four times 7.5 mL of HEPES 0.1 M buffer pH 8, 30 minutes). The obtained membrane was denoted TA_PP3_SS.

b. Flow mode

Flow TA cfe immobilizations and rinsings were carried out in 5 mL plastic syringes. A disk of 1 cm^2 functionalized PP membrane was placed at the junction between the head of the syringe and the metallic needle. The syringe was then filled with 5 mL of TA immobilization solution (HEPES 0.1 M buffer at pH 8, PLP 1 mM containing the desired TA cfe concentration (C_0 = 0.5 $mg.mL^{-1}$)), after which it was fixed on a NE-300 syringe pump in order to automatically push the contents of the syringe at a constant flow rate of 1 $mL.min^{-1}$. Once emptied, the syringe was refilled with 5 mL of rinsing solution (containing HEPES 0.1 M buffer, PLP 1 mM at pH 8), and the solution was pumped in order to wash-off the loosely attached TAs in the syringe. A desired flow rate of 2 $mL.h^{-1}$ was chosen for TA rinsing steps. The whole set-up was kept in an oven set at 35 °C.

The heterogeneous biocatalyst resulting from such flow membrane-immobilization of TA cfe was denoted TA_PP3F.

3.1.2 Benchmark carriers - ReliZymes

As matter of comparison, TA cfe immobilization was also performed in batch mode on epoxy-resins (ReliZymeEP and ReliZymeHFA), which are the ubiquitous support materials to immobilize transaminases. To this aim, 35 mg of epoxy-resin was immersed into 7.5 mL of buffered solution (HEPES 0.1 M buffer, PLP 1 mM) containing the desired TA cfe concentration (C_0 = 1 $mg.mL^{-1}$) at pH 8, and incubated for 18 hours at 35 °C under gentle shaking. After immobilization, the resulting immobilized transaminase was separated by centrifugation (5 minutes at 14,000 rpm in a Heraeus MultifugeX1R Centrifuge) and rinsed with 7.5 mL of rinsing solution (containing PLP 1 mM in HEPES 0.1 M buffer pH 8) for 30 minutes under gentle shaking (repeated two times) to eliminate the loosely attached TAs. The immobilization and

washing steps were carried out in 15 mL Falcon tubes. The resulting benchmark heterogeneous biocatalysts were labelled TA_ReliZymeEP and TA_ReliZymeHFA, depending on the employed epoxy-resin.

3.2 Immobilized enzymes loading evaluation

3.2.1 Batch mode

Enzyme loadings on the membranes were evaluated by mass balance. Typically, a functionalized membrane was incubated in a 7.5 mL (V_0) TA solution of known concentration, C_0 [mg.mL^{-1}]. After immobilization, the membrane was removed from the reactor and the TA concentration in the remaining solution (C_1) was measured by Bradford titration (see Supplementary informations of Chapter IV). The membrane was then washed with 7.5 mL (V_0) of rinsing solution, and the enzyme concentration in the resulting solution was measured (C_2). The same procedure was applied to the next rinsing solutions, leading to measure C_3 and C_4. The immobilized enzyme loading (L) was determined by Eq.IV-1. The immobilization yield (%) is defined as the ratio between immobilized TA (L) and the total TA mass introduced during the immobilization (7.5 x C_0).

$$L = V_0 \times (C_0 - C_1 - C_2 - C_3 - C_4) \ [mg] \qquad Eq.IV-1$$

The immobilization yield (%) is defined as the ratio between immobilized TA (L) and the total (offered) TA mass during the immobilization (7.5 x C_0).

3.2.2 Flow mode

Enzyme immobilization was also conducted in flow mode, and resulting immobilized enzyme loadings on heterogeneous biocatalyst were also evaluated by mass balance. The syringe was filled with 5 mL of TA immobilization solution of known concentration, C_0 [mg.mL^{-1}], and a flow rate of 1 mL.h^{-1} was fed in the reactor (flowing across the membrane). Samples of the outflow coming from the needle were collected every 30 minutes. In other words, as the immobilization is no longer dependent of time in flow mode, the enzyme concentration of every aliquots (of volume V_i) of residual solution (C_{1a}, C_{1b},…, C_{1n}) obtained after immobilization was quantified via Bradford titration. Once emptied, the syringe was refilled with 5 mL of rinsing solution in order to wash-off the loosely attached TAs in the syringe. The set flow rate was 2 mL.h^{-1} and samples (of volume V_j) were collected every 30 minutes, and their respective enzyme concentration (C_{2a}, C_{2b},…, C_{2n}) was quantified. To calculate the immobilized enzyme loadings, the quantities measured for each of the collected samples must be summed up (Eq. IV-2).

$$L = \sum(C_0 - C_{1i} - C_{2j}) \times V_{ij} \ [mg] \qquad Eq.IV-2$$

3.3 Asymmetric synthesis of R-2-fluoromethylbenzylamine

3.3.1 Crystallization-assisted transamination in batch

The asymmetric synthesis of R-2-fluoromethylbenzylamine (R-FMBA), was carried out in batch mode, using free or immobilized transaminases in batch mode (Figure IV-1). 2'-fluoroacetophenone (FAP) was employed as the amino-acceptor. In order to shift the transamination equilibrium, the reaction was run with an excess of isopropylamine (ISO). Typically, HEPES and PLP

were dissolved in distilled water to obtain HEPES 0.1 M, PLP 1 mM solution. ISO (125-500 mM range) was then added and the pH was adjusted to pH 8 (using HCl 37 %). TsRTA enzyme (free or immobilized (as (p)TA_PP3, TA_PP3, TA_ReliZymeEP or TA_ReliZymeHFA)) was then added in the solution. Then, FAP (10-50 mM range) and MeOH (0-10 % v/v range) were eventually added to start the biocatalytic reaction. Reactions were typically run at 35 °C in 7.5 mL total volume, in a batch reactor (10 mL round bottom glass flask) under moderate magnetic stirring (Figure IV-1).

Importantly, when aiming at comparing the catalytic performance obtained when running the transamination in batch *versus* in flow mode, 1 cm^2 TA_PP3 membrane and 5 mL reaction medium were employed, respectively.

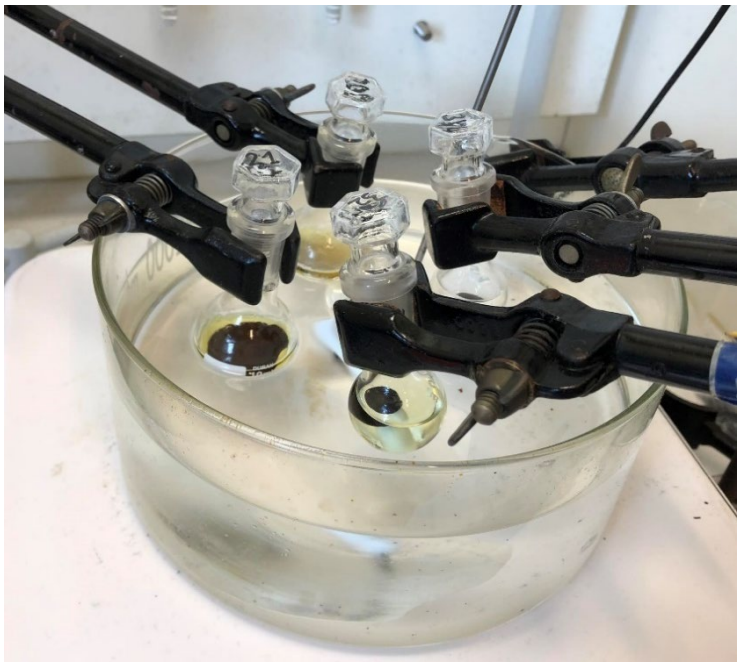

Figure IV-1 Experimental set-up for the transaminations carried out in batch mode. 10 mL round bottom flasks are embedded in oil sump fixed at 35 °C. Parameters of the wanted reaction (reagents concentrations, etc.) are different in each round bottom flask.

In some cases, 3,3-diphenylpropionic acid (DPPA) was added (concomitantly with the ISO addition) to crystallize the produced R-FMBA in the form of crystal salts to shift the transamination equilibrium (Figure IV-2). The crystals obtained at the end of reaction (when using DPPA as a crystallization agent) were recovered by filtration, rinsed two times with 7.5 mL of HEPES 0.1M buffer, then once with Methyl tert-butyl ether (MTBE). Crystals were then dried overnight before further analyses (NMR, chiral-HPLC, XRD, TGA, see section 3.6). They were labelled as FMBA:DPPA (x:y), where x and y correspond to the initial FAP concentration and to the total DPPA content (in mM) engaged to run the reaction-separation, respectively.

The FMBA:DPPA crystals recovery yield (Y_{cryst}) was defined as the ratio of the actual mass of FMBA:DPPA in the obtained crystals ($m_{FMBA:DPPA\ obt}$) compared to the maximum theoretical mass of FMBA:DPPA produced which is able to crystallize (Eq. IV-3).

$$Y_{cryst}\ (\%) = \left(\frac{m\ FMBA{:}\ DPPA_{obt}}{([FMBA]_{prod} - s_{FMBA}) * Mm_{FMBA:DPPA} * V} \right) * 100 \quad Eq.IV - 3$$

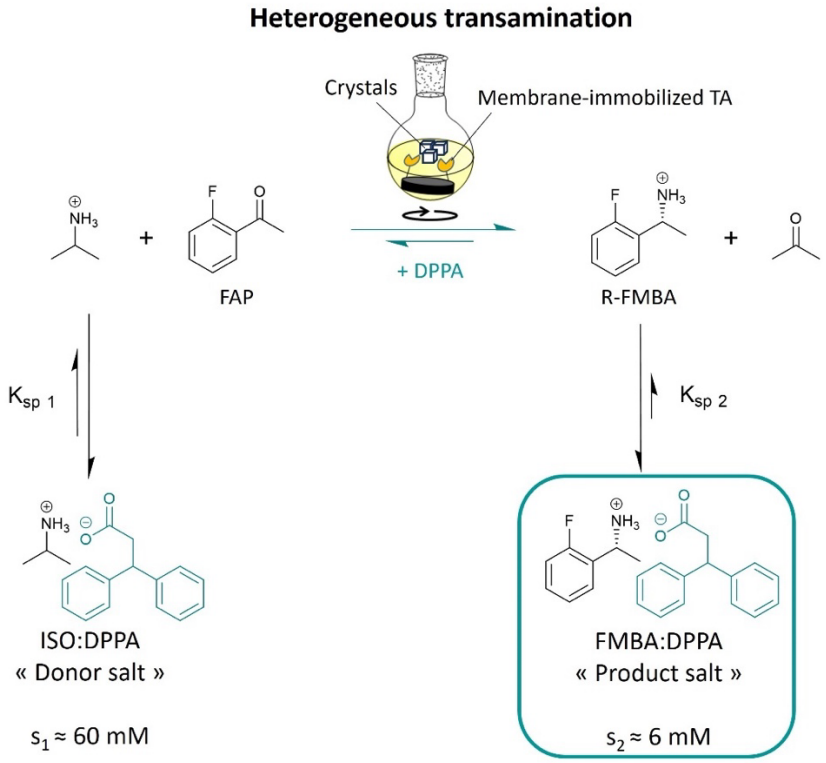

Figure IV-2. Schematic representation of the targeted heterogeneous asymmetric synthesis of R-2-fluoromethylbenzylamine (R-FMBA) assisted by product crystallization, using membrane-immobilized TsRTA in batch mode. Upon addition of 3,3-diphenylpropionic acid (DPPA) in the reaction medium, a donor crystal salt (of molar solubility and solubility product s1 and Ksp 1, respectively) is formed. As soon as transamination takes place, the produced R-FMBA is continuously removed from the medium through the formation of a product crystal salt (of molar solubility and solubility product s_2 and Ksp $_2$, respectively), thereby shifting the equilibrium towards the product side.

3.3.2 Continuous-flow transamination

Subsequently after the performing flow TA (cfe) immobilization and rinsings, TA_PP3F biocatalyst was tested in continuous-flow mode. Typically, HEPES and PLP were dissolved in distilled water to obtain HEPES 0.1 M, PLP 1 mM solution. ISO (125-500 mM range) was then added and the

pH was adjusted to pH 8 (using HCl 37 %), before FAP (10 mM) was added into the medium. The resulting solution was transferred into a 5 mL plastic syringe which it was fixed on a NE-300 syringe pump, and the TA_PP3F membrane (i.e. disk of 1 cm2) was placed at the junction between the head of the syringe and the metallic needle (Figure IV-3). The solution was then pumped at a desired flow rate (0.8 mL.h^{-1}, unless stated otherwise). The whole set-up was kept in an oven set at 35 °C. These flow transaminations were always run in absence of DPPA.

Figure IV-3 Experimental set-up for the transaminations carried out in flow-mode. The whole set-up is working in a drying oven set at 35 °C. The syringe is filled with reaction medium then pushed at a desired flow-rate via a syringe pump. TA immobilized-membrane lies at the junction between the head of the syringe and bottom of the needle. Samples of the outflow are collected in an Eppendorf each 30 minutes.

3.3.3 Reaction sampling and monitoring

Conversion was determined on 100 µL sample taken from the reaction medium (i.e. from the batch reactor, or collected from the outflows of the flow reactor). 30 µL of sodium hydroxide (2 M) was added to basify the sample, and the mixture was vortexed for 5 seconds. 400 µL of dichloromethane was

then added to the aqueous phase, vortexed for 15 seconds and rest for 5 minutes to allow extraction of reactants (ISO, FAP) and products (FMBA, acetone) into the organic phase. Extraction step was repeated twice and the organic phases were pooled and analyzed by gas chromatography (see Supplementary informations of Chapter IV) in order to determine FMBA production and FAP consumption.

The specific activity is defined as the number of µmol of 2'-fluoroacetophenone converted per minute per mg of immobilized enzymes. In the considered batch processes, it was evaluated by Eq. IV-4, where L is the immobilized enzyme loading (determined by mass balance via the Bradford method (in mg)) and, t is the reaction time (in min). In this study, the specific activity was determined after 20 hours of reaction (unless stated otherwise).

$$Sp.activity\ (Batch) = \frac{nFAP\ converted}{t \times L}\ [U.mg^{-1}_{imm.\ TA}] \qquad Eq.IV-4$$

The specific activity in flow mode is defined as the concentration of FMBA produced (in mM) at a certain set flow rate per mg of immobilized enzymes and per minute. It is evaluated by Eq. IV-5, where L is the immobilized enzyme loading (in mg) and F is the flow rate (in $mL.min^{-1}$) set in the syringe pump.

$$Sp.activity\ (Flow) = \frac{F \times [FMBA]_{prod}}{L}\ [U.mg^{-1}_{imm\ TA}] \qquad Eq.IV-5$$

3.4 Synthesis of other valuable enantiopure amines (expanding the substrate scope)

Aiming at producing new potential APIs with the same process, other asymmetric syntheses were targeted (in absence of product crystallization) by

changing only the keto substrate (the rest of the conditions remained unchanged). 4-bromoacetophenone (BAP), phenoxy-2-propanone (PhoxyP), and phenylbutanone (PhB) were tested as keto-substrates.

TA_PP3 catalyst (7 cm^2 membrane disc) was employed in these tests, and its specific activity (expressed in µmol of keto-substrate converted per minute per mg of immobilized enzymes) was assessed over increasing substrate concentration. Reaction conditions were: [0-35] mM keto-substrate, 250 mM ISO, 0 mM DPPA, 0 % v/v MeOH, 1 mM PLP in 0.1 M HEPES buffer pH 8, 35 °C. Reactions were typically run at 35 °C in 7.5 mL total volume, in a batch reactor (10 mL round bottom glass flask) under moderate magnetic stirring.

3.5 Keto-substrates and crystals solubility measurements

To measure the solubilities of the tested keto-substrates (FAP, BAP, PhoxyP, PhB) and of the crystals resulting from the crystallization-assisted asymmetric synthesis of R-FMBA in the considered reaction media (HEPES 0.1 M pH 8 buffer containing PLP 1 mM and [0-20] % v/v of co-solvent), it is necessary to first create an oversaturated medium. Hence, crystals or FAP were added to each medium at higher concentrations than their theoretical solubility limit, leading to the obtention of biphasic media (i.e. presence of emulsions or suspensions). Afterwards, 100 µL of the saturated aqueous phase of the resulting mixtures were sampled (i.e. by filtrating suspensions with 0.2 µm filter, or by exclusively pipetting the aqueous solution), basified with 25 µL NaOH 2 M and then extracted using DCM (as described in the previous section), and analyzed by gas chromatography (see Supplementary informations of Chapter IV).

3.6 Crystals characterization

After having been rinsed and filtered, the biocatalytically obtained crystals were analyzed and compared to reference crystals (namely, FMBA:DPPA ref and ISO:DPPA ref) which were chemically synthesized by 20 hours crystallization in Methyl Tert-Butyl Ether (MTBE), as methodically proposed by the von Langermann group [103].

3.6.1 Proton Nuclear Magnetic Resonance (^{1}H-NMR)

Crystals were analyzed in ^{1}H-NMR in order to qualitatively assess their chemical composition and compare their spectrum with that of chemically produced reference crystals, and quantitatively via the use of an internal standard, namely, N,N-Dimethylformamide (DMF), allowing to measure their purity (in %), thereby attesting the validity of the whole process in the aim of API crystals production.

More precisely, the FMBA:DPPA content of the crystals (x_{FMBA}) was determined by semi-quantitative ^{1}H-NMR analyses, by comparing the peak contributions of FMBA:DPPA (doublet 3H, at 1.57 ppm) and ISO:DPPA (doublet 6H, at 1.25 ppm) with each other (Eq. IV-6). DMF was used as standard for quantification during the ^{1}H-NMR analyses.

$$x_{FMBA}\,(\%) = \left(\frac{[FMBA{:}\,DPPA]}{[FMBA{:}\,DPPA] + [ISO{:}\,DPPA]}\right) * 100 \qquad Eq.\,IV-6$$

Experimental details about ^{1}H-NMR analyses are provided in the Supplementary informations of Chapter IV.

3.6.2 X-ray Diffraction (XRD)

The solid samples were analyzed via X-ray Diffraction (XRD) to assess their crystalline phases and characterize the solid composition of donor salt and/or product salt. Crystals were sprinkled on a sample holder coated with Nivea cream, which is then inserted in a Bruker-D8 Advance diffractometer with a Bragg-Brentano geometry. A copper anode under 40 kV and 30 mA produces the X-ray radiation with a Cu Kα wavelength (λ) of 1.54 Å. The Bruker detector was using a LynxEye XE-T technology and was recording values obtained with a 2θ value between 5° and 80° with 2θ increments of 0.015° and 0.15 seconds per step. The diffractograms obtained were analyzed with the DIFFRAC.EVA software (Bruker).

3.6.3 Enantiomeric excess (ee) determination

Enantiomeric excess (ee) of FMBA was determined using Chiral High Performance Liquid Chromatography (Chiral-HPLC) and through chiral Gas Chromatography (cGC) analysis, by dissolving the obtained product crystals (FMBA:DPPA) in the mobile phases. Details about the considered protocols and analytic methods are provided in the Supplementary informations of Chapter IV.

3.6.4 Thermogravimetric analysis (TGA)

Crystals were analyzed by Thermogravimetric Analyses (TGA) to assess their specific composition (e.g. water content) and thermal stability. TGA were performed on a Mettler Toledo TGA-STDA 851e, from 25 to 400 °C, at a scanning rate of 10 °C·min^{-1}. The solid samples (5 to 10 mg) were placed in aluminium oxide crucibles. The purge gas was nitrogen, with a continuous

flow rate of 50 mL·min^{-1}. The data were treated with the STARe 12.12 software.

4. Results and discussion

4.1 Asymmetric synthesis of R-2-fluoromethylbenzylamine

4.1.1 Catalytic performance of free and immobilized TAs in batch mode (without product crystallization)

Two membrane-immobilized biocatalysts, TA_PP3 and TA_PP3_SS, were employed to run the asymmetric synthesis of an enantiopure amine, R-2'-fluoromethylbenzylamine (R-FMBA). In both heterogeneous biocatalysts, the TsRTA enzyme was immobilized on the same functionalized polypropylene membrane support. Such TA immobilization strategy on such functionalized PP membranes was studied in Chapter III. However, while TA_PP3 is a "classical" immobilized transaminase, TA_PP3_SS results from a dual immobilization of TsRTA and PLP, which confers it the ability to catalyze transamination reactions without external addition of its PLP cofactor during reaction (i.e. self-sufficient catalyst) [401].

Importantly, owing to the configuration and dimensions of the batch reactors considered in this work, the amount of membrane employed per catalytic test was limited (i.e. 7 cm^2, which corresponds to c.a. 35 mg of flat-sheet membrane), resulting in very low TA loading in the reactor. Poor reaction rates were thus expected, given the low loading of biocatalysts (i.e. amount of immobilized enzymes on the carriers) obtained and employed in this study. The specific activities of both PP-immobilized TA were evaluated and compared to those of the soluble enzyme (free TsRTA) at identical enzyme loading/content (Figure IV-4, black triangles). We also compared

their specific activities to those of other immobilized TAs, i.e. TsRTA immobilized on commercially available epoxy resins (TA_RelizymeEP) and amino-epoxy resins (TA_RelizymeHFA), used as conventional "benchmark" catalysts. In order to compare the catalytic performance of the different heterogeneous biocatalysts, the TA immobilizations (and subsequent transaminations) were run with identical masses of supports (i.e. 35 mg of functionalized PP membrane (which corresponds to a 7 cm^2 membrane disc) or Relizyme™ beads).

It was observed that TA_RelizymeEP and TA_RelizymeHFA recovered 69 % and 84 % of specific activity (estimated using the first data point of the activity profiles shown in Figure SIV-1 (i.e. 20 hours)) respectively, with respect to free TA. Such specific activity recoveries observed for the TA_Relizyme benchmark catalysts are not surprising, since TAs immobilized on polymeric resins typically retain between 30 % and 60 % of their specific activity with respect to their soluble counterparts [131,222]. However, high TA loadings were observed on the Relizyme carriers (Figure IV-4, black triangles). These high TA immobilization yields recorded on the Relizyme carriers can easily be explained by the fact that resins display significantly higher surface area available to immobilize TAs, due to their smaller average pore diameters (i.e. 20 nm range) [381], with respect to the considered PP flat-sheet membranes (i.e. around 200 nm) [417]. However, the narrower pore diameter of the Relizymes may also bring additional restrictions (*e.g.* mass transport limitations, or highly constrained enzyme), which may partly explain the incomplete (< 100%) specific activity recoveries of those resin-immobilized biocatalysts. This aspect is even more pronounced at high enzyme loading since at some point, the increase of substrate consumption rate eventually surpasses the supply rate of substrate towards the immobilized enzyme [418].

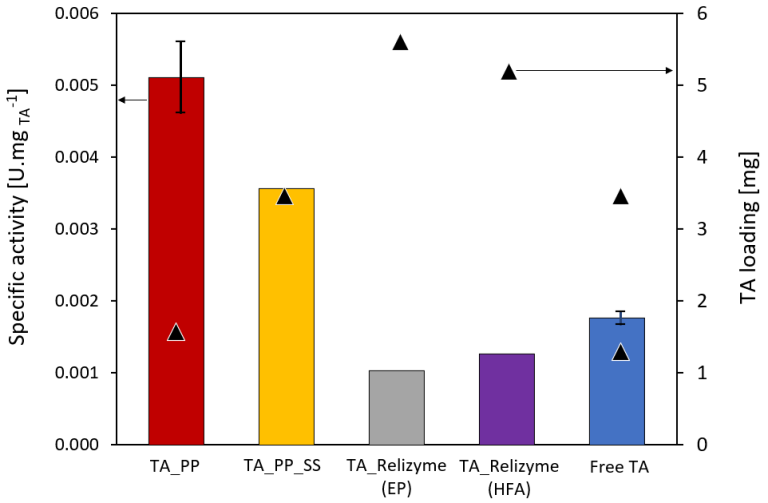

Figure IV-4. Immobilized TsRTA loading on solid biocatalysts (i.e. amount of enzymes immobilized on the carrier) or soluble enzyme concentration (triangles), and specific activity (histograms) displayed by the different biocatalysts. Reaction conditions were: 25 mM FAP, 250 mM ISO, 0 mM DPPA, 10 % v/v MeOH, 1 mM PLP (or 0 mM PLP for TA_PP3_SS) in 0.1 M HEPES buffer pH 8, 35 °C.

On the other side, the specific activities exhibited by both PP-immobilized TAs were by far superior to those of the other biocatalysts tested herein (Figure IV-4). Normalized activities ($U.g_{cat}^{-1}$) and specific activities ($U.mg_{TA}^{-1}$) observed in this study compared well with to the values obtained on other asymmetric syntheses (employing ISO as amine donor), as shown in Table IV-1 [222,225]. For example, the specific activities reported by Heckmann and Paradisi (towards the asymmetric synthesis of 2-aminobutane) [222] for two soluble cell-free extract TAs (*RTA-43 and HeWT_F84W) are similar to the values obtained in this work (see Table IV-1, lower part). Notably, the specific activities displayed by TA_PP3 and TA_PP3_SS catalysts correspond to specific activity recoveries of c.a. 340 % and 225 % with respect to free TA, respectively. These results notably highlight the robustness of the self-sufficient TA_PP3_SS biocatalyst, which was able to efficiently catalyze such asymmetric synthesis of R-FMBA in absence of externally added co-factor. Expectedly (as observed in Chapter III), its specific activity was lower than

that of the "classical" immobilized transaminase (TA_PP3), potentially due to the higher enzyme loading present on TA_PP3_SS, which is likely to cause molecular crowding effect [166,419].

Table IV-1. Catalytic performance obtained with different free and immobilized TsRTA cell-free extracts studied in this work (upper part), and comparison with immobilized TAs reported in the literature. Reaction conditions were: 25 mM FAP, 250 mM ISO, 0 mM DPPA, 10 % v/v MeOH, 1 mM PLP (or 0 mM PLP for TA_PP3_SS) in 0.1 M HEPES buffer pH 8, 35 °C.

Ref.	Biocatalyst	TA immob. yield (%)	Activity [U]	Norm. activity [$U.g_{cat}^{-1}$]	Sp. activity [$U.mg_{TA}^{-1}$] **(recovery, in %)**
This work	TA_PP3	22	0.0084	0.24	0.0051 **(340)**
	TA_PP3_SS	48	0.012	0.34	0.0034 **(225)**
	TA_RelizymeEP	81	0.0062	0.18	0.0010 **(69)**
	TA_RelizymeHFA	76	0.0070	0.2	0.0013 **(84)**
	TA free	/	/	/	0.0017 **(100)**
[222]	*RTA-43 free	/	/	/	0.0044 **(100)**
	HeWT_F84W free	/	/	/	0.0048 **(100)**
[225]	ATA_w12_EES	/	/	0.32	0.04 **(/)**

Specific activities of the PP immobilized TAs were also verified earlier during the catalytic test (i.e., after 6 hours of reaction, Figure IV-5) to confirm that the activity of the free enzyme was not underestimated due to early deactivation. Such high activity recoveries observed for TA_PP3 and TA_PP3_SS may be attributed to the hydrophilic coating layers (PDA, and predominantly PEI) on the PP membranes, which stabilize the immobilized TAs by providing a suitable hydrated microenvironment. [190,400] In terms of overall activity (i.e. reaction rate, in [U]), the transamination reaction was faster when employing the membrane immobilized TAs (Table IV-1, upper

part), despite the significantly higher TA loadings obtained on both TA_Relizymes.

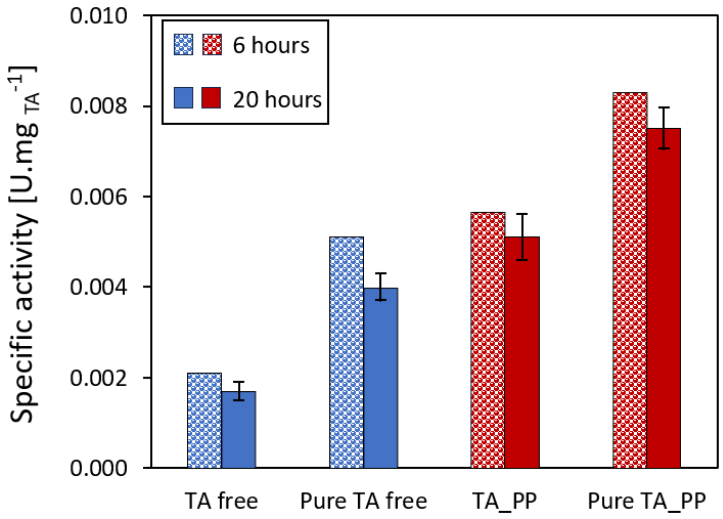

Figure IV-5. Specific activities displayed by different biocatalysts after 6 hours (dashed bars) or 20 hours (full bars) of reaction, when employing TsRTA cell-free extract (TA) or purified (pTA) enzyme, either free or immobilized. From left to right: TA_free, pTA free, TA_PP3 and pTA_PP3. Reaction conditions were: 25 mM FAP, 250 mM ISO, 0 mM DPPA, 10 % v/v MeOH, 1 mM PLP in 0.1 M HEPES buffer pH 8, 35 °C.

The activity dependence on FAP keto-substrate concentration was assessed for both soluble TA and TA_PP3 catalysts (Figure IV-6). 10 % v/v MeOH was used as co-solvent to ensure a proper dissolution of the substrate in the reaction medium. As expected, higher specific activities were observed when pure enzymes (pTAs ; immobilized or soluble; see empty points in Figure IV-6) were employed. Noteworthily, for both the free enzyme and TA_PP3, the optimum FAP concentration was found to be around 25 mM, while enzyme inhibition by this keto substrate seemed to occur at higher concentrations. Such inhibition was particularly marked around 50 mM FAP, at which both the free and immobilized TA specific activities dropped by c.a. 50 % (with respect to their maximal values). It should be noted that TsRTA has previously

been reported to run the asymmetric synthesis of the same R-FMBA up to 100 mM; yet this was measured at high enzyme concentration (i.e. 5 mg/mL) and with D-alanine as amino-donor [416].

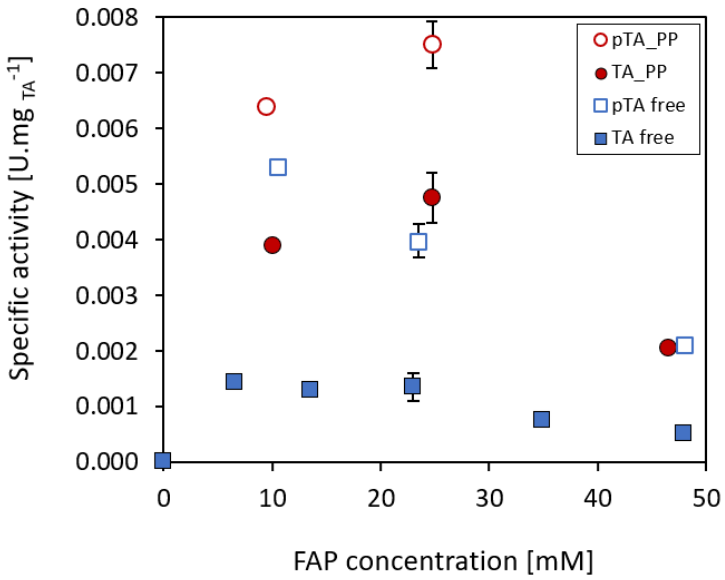

Figure IV-6. Specific activities obtained at different FAP initial concentrations, employing TA (TsRTA) cell-free extracts either soluble (blue squares) or immobilized as TA_PP3 (red dots), or purified TAs (pTAs) either soluble (empty squares) or immobilized as pTA_PP3 (red empty dots). Reaction conditions were: [6-48] mM FAP, 250 mM ISO, 0 mM DPPA, 10 % v/v MeOH, 1 mM PLP in 0.1 M HEPES buffer pH 8, 35 °C. All reactions were run at equal nominal enzyme concentration, i.e. 0.2 mg/mL TA. For (p)TA_PP3, this corresponds to an enzyme loading of c.a. L ~ 1.5 mg (p)TA on the membrane carrier.

The long-term stability of the pTA_PP3 was investigated and compared to the one of soluble TA (at identical enzyme concentration/loading), by running the reaction and monitoring the activity over time during extended durations. To this aim, 25 mM FAP with 10 molar equivalents (i.e. 250 mM) of ISO were standardly selected as reaction conditions (to avoid any undesirable substrate inhibition). It resulted that the pTA_PP3 displayed remarkable activity and stability over time, whereas the soluble TAs were rapidly deactivated (Figure

IV-7, full curves). Such result is not surprising as it is often observed that the TA immobilization enhances the operational stability of the resulting heterogeneous biocatalysts with respect to their free form [131]. When the FAP conversion began to stabilize (i.e. after 300 hours of reaction), the membrane (pTA_PP3) was separated from the liquid reaction mixture, washed with HEPES 0.1 M, PLP 1 mM pH 8 buffer (three times) and immersed into a new reaction medium (prepared in identical conditions, i.e. 250 mM ISO, 25 mM FAP). Very similar specific activity was observed in such recyclability experiments, which allowed to ensure that the "activity plateau" observed in Figure IV-7b for pTA_PP3 was exclusively due to thermodynamic limitations (and not to enzyme deactivation ; see Figure IV-8).

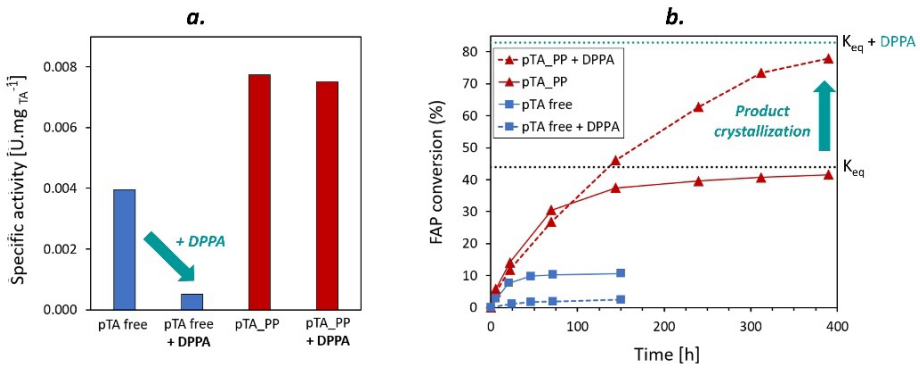

Figure IV-7. Catalytic performance (i.e. a) specific activity and b) reaction profiles) obtained with (50 mM) or without DPPA, employing pTAs either free (blue) or immobilized as pTA_PP3 (red). Reaction conditions were: 25 mM FAP, 250 mM ISO, 0 or 50 mM DPPA, 10 % v/v MeOH, 1 mM PLP in 0.1 M HEPES buffer pH 8, 35 °C. The reactions were run at equal nominal enzyme concentration, i.e. 0.2 mg/mL pTA. For pTA_PP3, this corresponds to an enzyme loading of c.a. L ~ 1.5 mg TA on the membrane carrier.

The observed plateauing of FAP conversion leads to estimate the equilibrium conversion ($x_{FAP\ eq}$) to be ≈ 44 %. From this value, the transamination equilibrium constant was estimated to be $K_{eq} \approx 3.9 \times 10^{-2}$ (Figure SIV-2), very close to the theoretical value computed using Gibbs free energies calculations ($K_{eq} = 4.7 \times 10^{-2}$, approximated by the MolCalc tool [420]),

and with other studies estimating the K_{eq} value of model asymmetric syntheses (using ISO as amino-donor) [421].

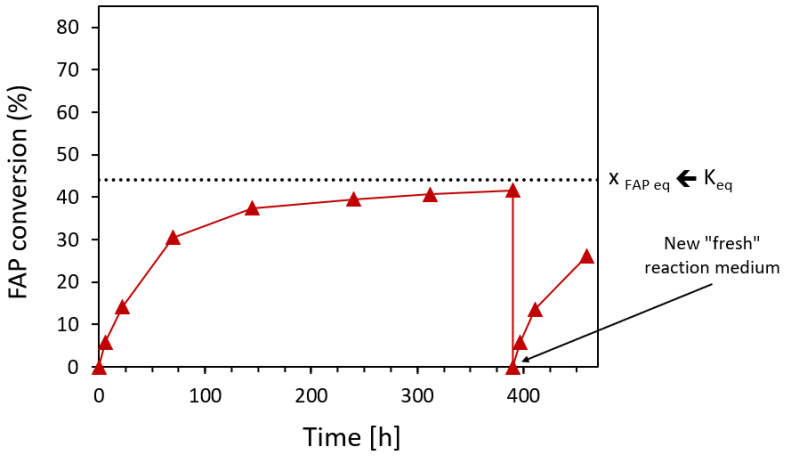

Figure IV-8. Reaction profile obtained for pTA_PP3 in absence of DPPA (see Figure IV-7b, full red curve). After some time (c.a. 150 hours), the FAP conversion started to stabilize and linearly tend towards an "activity plateau" ($x_{FAP\,eq} \approx 44$ %), suggesting that the reaction is nearing its thermodynamic limit (fixed by the equilibrium constant, K_{eq}). To support such hypothesis, the pTA_PP3 membrane was removed from the reaction medium (after 390 hours), washed with PLP 1 mM, HEPES 0.1 M buffer pH 8, and immersed into a new freshly prepared (identical) reaction medium. Similar activity was observed in such second catalytic cycle, suggesting that the "activity plateau" corresponds to the expected conversion at the equilibrium (determined by K_{eq}). Reaction conditions were: 25 mM FAP, 250 mM ISO, 0 mM DPPA, 10 % v/v MeOH, 1 mM PLP in 0.1 M HEPES buffer pH 8, 35 °C. The reaction was run at nominal enzyme concentration of 0.2 mg/mL pTA, which corresponds to an enzyme loading of c.a. L ~ 1.5 mg pTA on the membrane carrier.

All in all, these experiments confirmed that TA can be effectively immobilized on a PP membrane, and that the resulting biocatalyst is active, stable, and recyclable. The specific activity is higher than that of the free enzyme. And yields close to the theoretical thermodynamic equilibrium can be achieved. Experiments have been carried out on small membrane discs featuring a low absolute amount of enzyme, which explains that long reaction times are needed. Yet, it is known that membranes can be packed in dense modules, presumably solving the kinetic issue. Nevertheless, it appears

pertinent to develop strategies to push the reaction towards completion by displacing the position of the thermodynamic equilibrium.

4.1.2 Crystallization-assisted transamination using membrane-immobilized TAs in batch mode

pTA_PP3 was tested for asymmetric synthesis of R-FMBA in presence of crystallizing agent DPPA, with the idea to push the transamination towards completion. Also, crystallization is primed to facilitate product separation and recovery. In order to maximize the product crystallization driving force, we performed the reaction in presence of a DPPA suspension (i.e. above the solubility limit of the donor ISO:DPPA salt), in a *suspension-to-suspension* approach. This enables to keep the DPPA (and ISO) concentration constant over time (by progressive dissolution of the donor ISO:DPPA salt) [103].

In a first attempt, the transamination-crystallization was run in standard conditions (25 mM FAP, 250 mM ISO), in presence of 50 mM DPPA. In these precise conditions, the ISO and DPPA maximal soluble concentrations (i.e. dictated by the solubility product of the ISO:DPPA salt ($K sp_1 = 0.0036$)) were estimated to 215 mM and 15 mM, respectively. By taking into account the FMBA solubility limit in the present system (s_{FMBA}), and by considering the estimated value of K_{eq}, it was possible to compute a new expected FAP conversion at the equilibrium obtained in presence of DPPA (green dotted line in Figure IV-7b). This corresponds to an expected equilibrium conversion of ~83% (much higher than the 44% limit in the case of the non-assisted reaction). Here, the crystallization-assisted reaction indeed allow to overcome the initial equilibrium conversion, reaching as high as 77.4% conversion and thus (Figure IV-7b, dotted red curve). approaching the theoretical limit of the crystallization-assisted process. On the other hand, such DPPA addition

dramatically affected the activity of free TA (Figure IV-7b, dotted blue curve). Conversion was even lower than in the standard conditions.

We tentatively ascribe such free enzyme deactivation to an undesired precipitation or immobilization of the soluble TsRTA on the ISO:DPPA crystals. Indeed, when running the reaction in the presence of only 15 mM of DPPA (i.e. below the solubility limit, and thus in the absence of solid crystals), the enzyme was barely affected while dramatic enzyme deactivation occurred in a super-saturated reaction medium (i.e. with ISO:DPPA salt) (Figure IV-9).

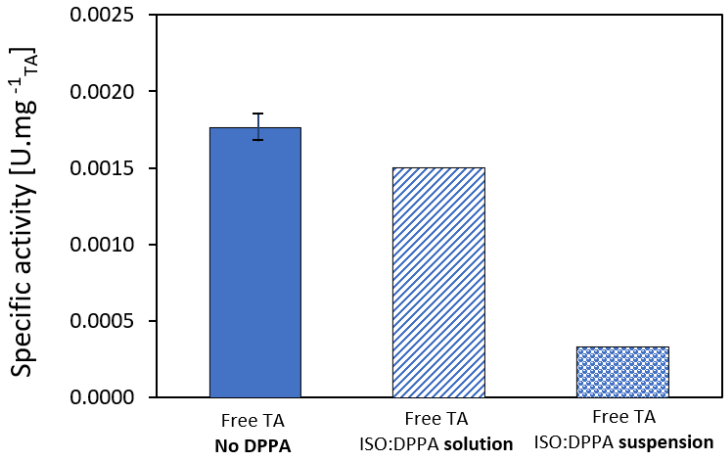

Figure IV-9. Specific activity of the free TsRTA cell-free extract (TAs) in absence or in presence of DPPA suspension in the transamination reaction medium**.** Left: 0 mM DPPA (solution), middle: 15 mM DPPA (ISO:DPPA saturated solution) and right: 50 mM DPPA (ISO:DPPA suspension). Reaction conditions were: 25 mM FAP, 250 mM ISO, [0-50] mM DPPA, 10 % v/v MeOH, 1 mM PLP in 0.1 M HEPES buffer pH 8, 35 °C. The reactions were run at nominal enzyme concentration of 0.2 mg/mL TA.

Further increasing the soluble enzyme concentration (from 0.2 mg/mL to 1 mg/mL pure TsRTA) did not change the activity profile obtained, as pronounced enzyme deactivation was also observed (Figure SIV-3). Interestingly, such free enzyme deactivation or precipitation induced by the presence of DPPA crystals was not observed when employing other TAs, such

as HeWT (employing acetophenone as substrate, see Figure SIV-3) or SpATA (used by the von Langermann group, employing 3-methoxy-acetophenone as substrate) [103], and appears thus to be an enzyme-dependent phenomenon.

The impact of such FMBA:DPPA crystallization on pTA_PP3 specific activity, on final transamination yield and on the obtained crystals purity was investigated. By comparing the ^{1}H-NMR spectra of crystals obtained *via* transamination-crystallization with those of chemically synthesized donor (i.e. ISO:DPPA ref., Figure IV-10) and product (i.e. rac-FMBA:DPPA ref., Figure IV-11) crystal salts, we estimate the relative amounts of FMBA:DPPA phase in the obtained crystals as well as the FMBA:DPPA crystals recovery yield (Table IV-2).

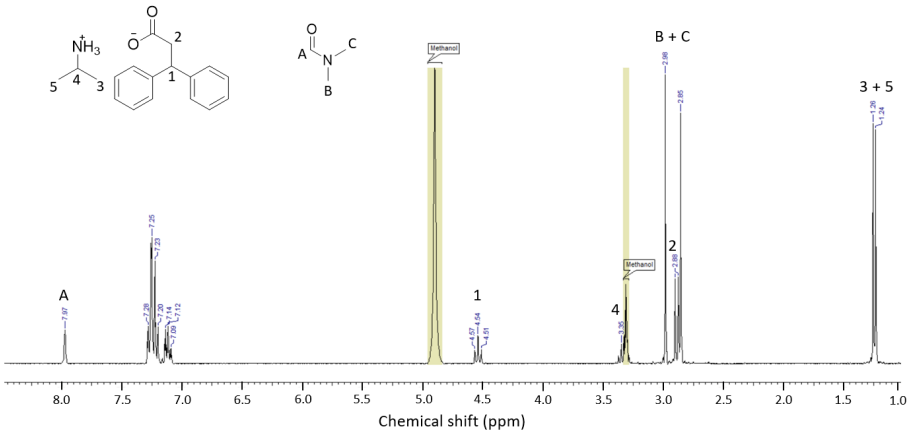

Figure IV-10. ^{1}H-NMR spectrum recorded in CD_3OD for the chemically synthesized donor crystals (ISO:DPPA ref.). DMF was used as standard for quantification during the analysis.
^{1}H NMR (600 MHz, CD_3OD): δ 7.97 (s, 1H, A), 7.25 (m, 8H, Ar), 7.12 (tt, 2H, J=7.0 Hz and J=2.0 Hz, Ar), 4.54 (t, 1H, J=8.0 Hz, 1), 3.35 (q, 1H, J=6.6 Hz, 4), 2.98 (s, 3H, B or C), 2.88 (d, 2H, J=8.0 Hz, 2), 2.85 (s, 3H, B or C), 1.25 (d, 6H, J=6.6 Hz, 3+5).

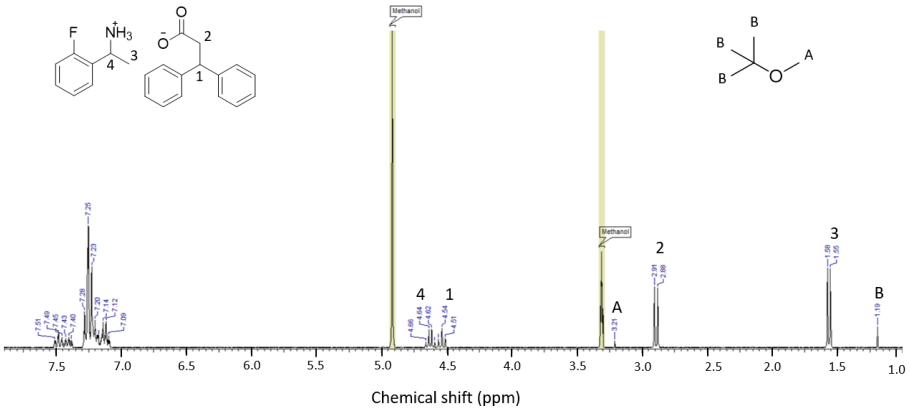

Figure IV-11. ^{1}H-NMR spectrum recorded in CD_3OD for the chemically synthesized donor crystals (rac-FMBA:DPPA ref.). DMF was used as standard for quantification during the analysis. Traces of organic solvent (MTBE) were detected. ^{1}H NMR (600 MHz, CD_3OD): 7.48 (m, 1H, Ar), 7.41 (m, 1H, Ar), 7.25 (m, 8H, Ar), 7.20 (m, 1H, Ar), 7.14 (m, 1H, Ar), 7.12 (tt, 2H, J=7.0 Hz and J=2.0 Hz, Ar), 4.64 (q, 1H, J=7.0 Hz, 4), 4.54 (t, 1H, J=8.0 Hz, 1), 3.21 (s, 3H, A), 2.90 (d, 2H, J=8.0 Hz, 2), 1.57 (d, 3H, J=7.0 Hz, 3), 1.19 (s, 9H, B)

As a reminder, in absence of product crystallization (i.e. without DPPA in the catalytic system), only moderated yields can be obtained as the transamination is limited by its unfavorable thermodynamic equilibrium (see Table IV-2, lines 1 and 4). Adding DPPA at the solubility limit (e.g. 15 mM) enabled the formation of the poorly soluble FMBA:DPPA crystal salt (Figure SIV-4), which drives the transamination reaction towards higher FAP conversion as compared to the non-assisted reaction (Table IV-2, compare line 2 to line 1). Further increasing the total DPPA content from 15 mM to 50 mM (suspension containing ISO:DPPA donor crystal salt) enabled to achieve an even higher final substrate conversion, owing to the higher crystallization driving force (i.e. constant DPPA concentration over time). Noteworthily, performing the heterogeneous transamination in such suspension-to-suspension approach did not alter the specific activity of the membrane biocatalyst (i.e. the initial activity was unchanged).

When employing low FAP substrate concentration (12.5 mM) with respect to the ISO:DPPA salt, the resulting crystals were not pure (i.e. contained only 62 % of FMBA:DPPA phase (and consequently, 38% of ISO:DPPA) see Figure SIV-5 and Table IV-2, line 3). Despite this aspect, high product crystal salt recovery was still obtained, resulting in 93 % overall FMBA:DPPA crystals recovery yield. Expectedly, doubling the FAP substrate concentration (to 25 mM) allowed to increase the proportion of FMBA:DPPA crystals in the collected solid (compare Table IV-2, line 5 to line 3), resulting in 99 % purity for the desired crystal phase (Figure IV-12) and 95 % crystals recovery yield. We argue that such excellent metrics are highly encouraging in the perspective of implementation for API production at the industrial scale [422]. In these conditions (25 mM FAP, 50 mM DPPA), a final FAP conversion of 77.5 % was reached, whereas only 44 % could be obtained without the product crystallization process (owing to the thermodynamic limit of the considered transamination).

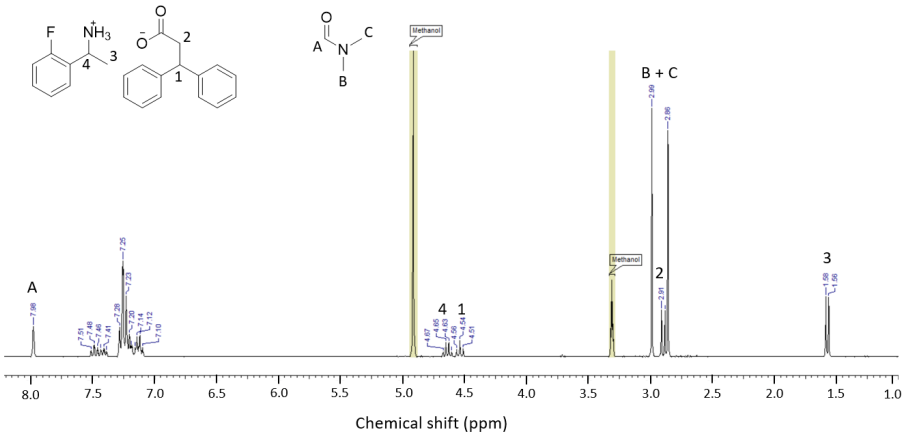

Figure IV-12. ^{1}H-NMR spectrum recorded in CD_3OD when analyzing the FMBA:DPPA (25:50) crystals produced via crystallization-assisted transamination. DMF was used as standard for quantification during the analysis.
^{1}H NMR (600 MHz, CD_3OD): δ 7.98 (s, 1H, A), 7.48 (m, 1H, Ar), 7.41 (m, 1H, Ar), 7.25 (m, 8H, Ar), 7.20 (m, 1H, Ar), 7.14 (m, 1H, Ar), 7.12 (tt, 2H, J=7.0 Hz and J=2.0 Hz, Ar), 4.64 (q, 1H, J=7.0 Hz, 4), 4.54 (t, 1H, J=8.0 Hz, 1), 2.99 (s, 3H, B or C), 2.91 (d, 2H, J=8.0 Hz, 2), 2.86 (s, 3H, B or C), 1.57 (d, 3H, J=7.0 Hz, 3).

It is noteworthy that the strategy can also be applied in the absence of externally added PLP, using the "self-sufficient" membrane biocatalyst (TA_PP3_SS) which reached 79.8 % FAP conversion and produced highly pure FMBA:DPPA crystals as the product (Table SIV-1).

Table IV-2. pTA_PP3 catalytic performance and crystallization metrics obtained when performing the transamination in presence of different DPPA and FAP contents). Reaction conditions were: [12.5-25] mM FAP, 250 mM ISO, [0-50] mM DPPA, 10 % v/v MeOH, 1 mM PLP in 0.1 M HEPES buffer pH 8, 35 °C. The enzyme loading was c.a. L ~ 1.5 mg pTA on the membrane carrier. The final FAP conversion was determined after 390 hours of reaction.

Crystal name	C_0 FAP [mM]	Initial reaction medium	C DPPA [mM]	Sp. activity [U.mg$_{TA}^{-1}$] ([U. m^{-2}])	$x_{FAP\ eq}$ (%) [a]	$x_{FAP\ obs}$ (%) [b]	$x_{FMBA:DPPA}$ crystals (mol %) [c]	Y_{cryst} FMBA:DPPA (%) [d]
/	12.5	Solution	0	0.0067 (16.9)	56.1	55.2	/	/
FMBA:DPPA (12.5:15)	12.5	Solution	15	0.0065 (16.5)	80.7	62.5	95	74 [d1]
FMBA:DPPA (12.5:50)	12.5	Suspension	50	0.0064 (16.3)	83.6	84.1	62	93 [d2]
/	25	Solution	0	0.0079 (21.7)	44.6	43.9	/	/
FMBA:DPPA (25:50)	25	Suspension	50	0.0075 (21.2)	81.9	77.5	97 ± 2 [e]	95 ± 3.2 [e]

[a]: Expected FAP conversion at the transamination equilibrium ($x_{FAP\ eq}$, see Eq. S4 and Eq. S5 in Supplementary informations of Chapter IV)

[b]: Observed FAP conversion after 390 hours of reaction

[c]: FMBA:DPPA content in the produced crystals ($x_{FMBA:DPPA}$, see Eq. IV-6)

[d]: FMBA:DPPA crystals recovery yield (Y_{cryst}, see Eq. IV-3)

[e] :Crystals have been produced three times (triplicate), hence mean values ± standard deviations are reported.

Additionally, ^{1}H-NMR confirmed that the mean relative amounts of FMBA and DPPA species (measured on triplicates on the obtained FMBA:DPPA (25:50) crystals) were 49:51 and 50:50 in FMBA:DPPA (25:50) and rac-FMBA:DPPA ref., respectively. This confirms the hypothesis that the crystal partners arrange iso-stoichiometrically (i.e. 1:1 equivalent) to form the target FMBA:DPPA crystal structure. Thermogravimetric analysis (TGA) (Figure IV-13) further revealed two distinct and clear weight losses corresponding to the FMBA (37.3 wt % (or 48.6 mol %), from c.a. 90 to 210 °C) and to the DPPA (59.7 wt % (or 48.4 mol %), from c.a. 210 to 325 °C), which highlights the fact that the crystals are not mono- or di-hydrates. Indeed, otherwise the weight residue would be at least of 4.7 wt % (monohydrate) or 8.9 wt % (dihydrate)).

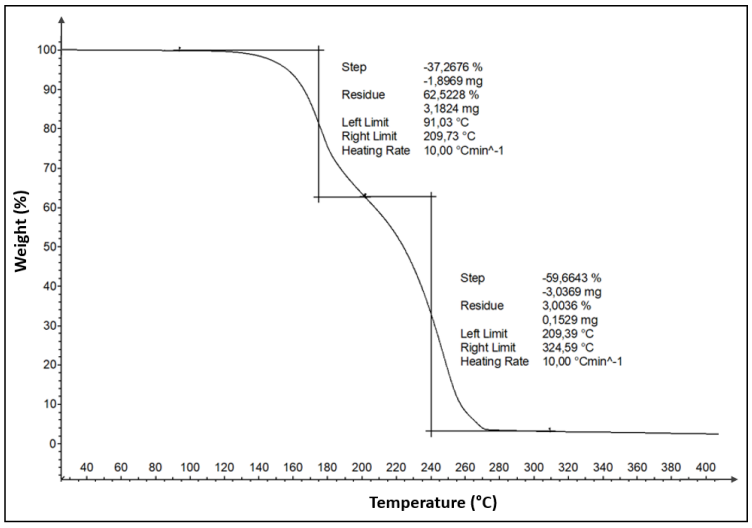

Figure IV-13. Thermogravimetric analysis (weight loss curve versus temperature) recorded on FMBA:DPPA (25:50) crystals produced via crystallization-assisted transamination.

XRD analyses revealed that crystals obtained *via* transamination-crystallization, FMBA:DPPA (25:50), displayed similar XRD patterns as the chemically synthesized rac-FMBA:DPPA ref. crystals (Figure IV-14, compare blue curve with red curve).

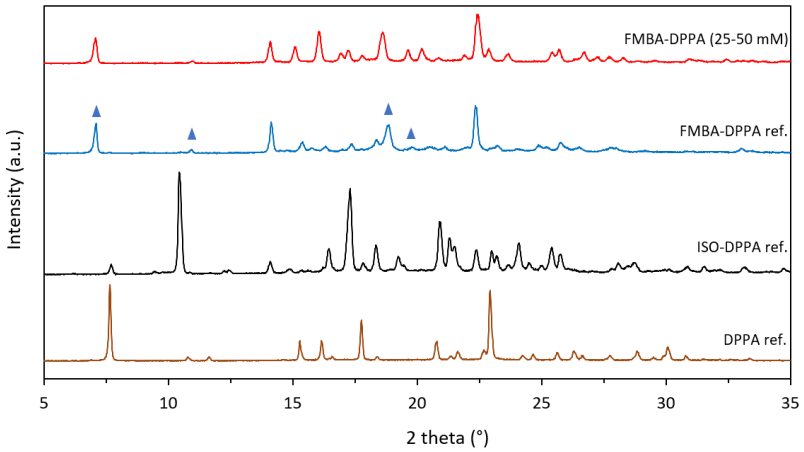

Figure IV-14. XRD diffractograms of the different crystals, respectively (from top to bottom): FMBA:DPPA 25:50 (resulting from transamination using pTA_PP3, in presence of FAP 25 mM, ISO 250 mM, DPPA 50 mM), rac-FMBA:DPPA ref. (synthesized by adding equimolar amounts of rac-FMBA and DPPA in MTBE), ISO:DPPA ref. (synthesized from ISO 250 mM and DPPA 50 mM suspension in HEPES 0.1 M, PLP 1 mM at pH 8), DPPA (commercially purchased).

However, when zooming in, it was observed that these XRD patterns did not perfectly match, as small shifts in their XRD peak positions were noticed (Figure IV-15).

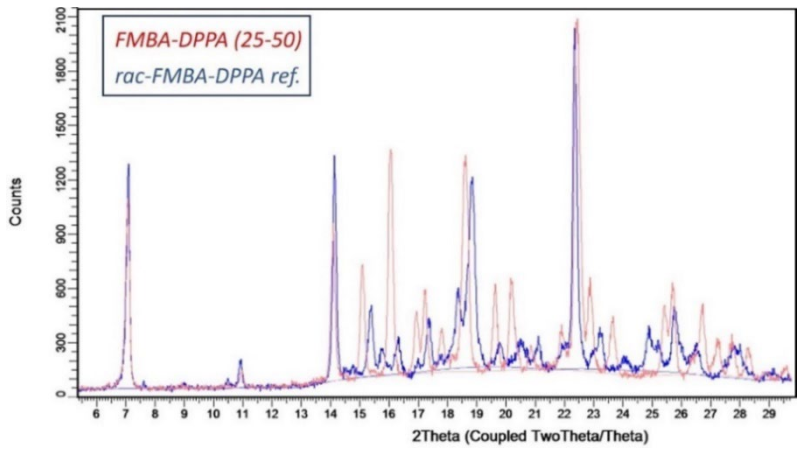

Figure IV-15. XRD patterns of the biocatalytically produced FMBA:DPPA (25:50) crystals (in red), and of the chemically synthesized rac-FMBA:DPPA ref. crystals (in blue).

Given the high purity of the produced FMBA:DPPA (25:50) crystals (i.e. 99 mol % according to ^{1}H-NMR), such dissimilarity is probably induced by the fact that the crystals formed during the crystallization-assisted reaction are enantiopure while those in rac-FMBA:DPPA ref. are racemic (as confirmed by chiral GC (Figure SIV-6) and chiral HPLC (Figure IV-16) analyses). This phenomenon was previously observed with other chiral organic crystals (e.g. 3-chloromandelic acid) [423,424]. We tentatively ascribe the differences in XRD patterns to the presence of a solid solution or a racemic compound crystal [425,426]. Additionally, significant XRD patterns differences were noticed with respect to other reference crystals (i.e. ISO:DPPA ref. and DPPA), which is not surprising given the high purity of the produced FMBA:DPPA (25:50) crystals (i.e. 99 mol % of FMBA:DPPA crystal phase, according to ^{1}H-NMR).)

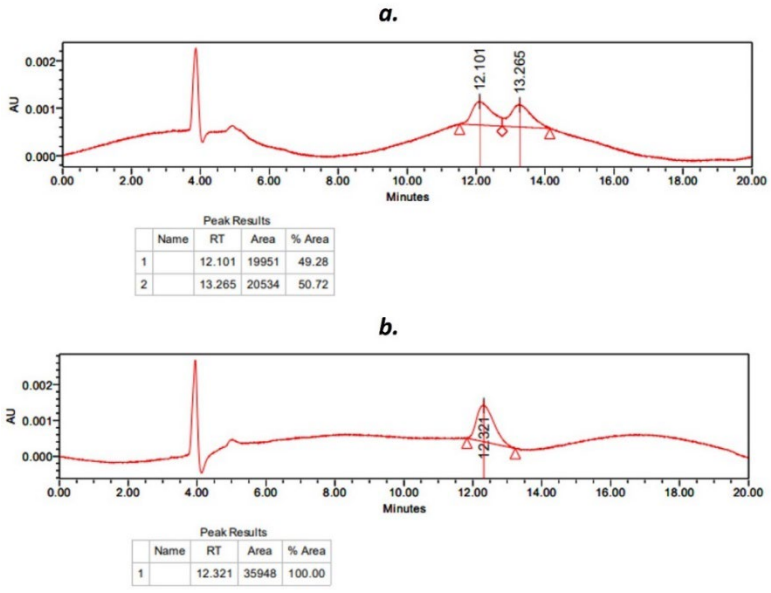

Figure IV-16. chiral-HPLC chromatograms resulting from the analysis of: **a.** the chemically synthesized rac-FMBA:DPPA ref. crystals (in red), and of: **b.** the biocatalytically produced FMBA:DPPA (25:50) crystals.

The reusability of the membrane-immobilized TA in this crystallization-assisted transamination process was investigated. To this aim, the pTA_PP3 catalyst was employed to run three successive catalytic cycles in presence of 50 mM DPPA. Each catalytic cycle was stopped when the FAP conversion approached the conversion plateau. After each cycle, the membrane was removed from the resulting reaction mixture, rinsed three times with HEPES 0.1 M buffer pH 8, and then re-immersed into a fresh reaction medium. As observed in Figure IV-17b, such pTA_PP3 was able to perform high-yield successive R-FMBA asymmetric syntheses: final FAP conversions tending towards the expected conversion dictated by the transamination equilibrium in presence of FMBA:DPPA crystallization (i.e. x $_{FAP\ eq}$' ≈ 87 % in these conditions) were always observed. Of course, possible deactivation should be quantitatively assessed far away from the thermodynamic equilibrium [427]. pTA_PP3 was shown to retain 77 % of its initial specific activity after two transaminations cycles (i.e. 1200 hours of operation). These results underline the robustness and the reusability of such membrane-immobilized TA.

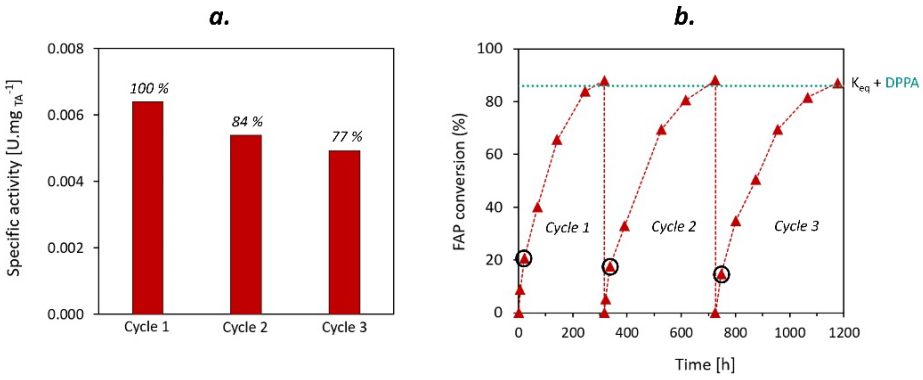

Figure IV-17. Recyclability tests (i.e. a) specific activity and b) reaction profiles) obtained when employing the pTA_PP3 catalyst. Reaction conditions were: 10 mM FAP, 250 mM ISO, 50 mM DPPA, 10 % v/v MeOH, 1 mM PLP in 0.1 M HEPES buffer pH 8, 35 °C. The enzyme loading was of c.a. L ~ 1.5 mg pTA on the membrane carrier.

4.1.3 Reaction engineering and process optimization

With a robust membrane biocatalyst and crystallization-assisted synthesis workflow in hands, we attempted to push the process further in terms of productivity. To this end, we explored the possibility to (i) optimize the solubility of the crystals in presence using co-solvents, (ii) accelerate the reaction by providing the substrates in excess, and (iii) transfer the process from batch mode to continuous flow mode.

4.1.3.1 Co-solvent addition

In order to thermodynamically enhance the targeted reaction (i.e. shift the equilibrium towards high chiral amines yields), we need an efficient crystallization process, hence $K_{sp\ 1} >> K_{sp\ 2}$ (Figure IV-2). The system described above already corresponds to this case (i.e. $K_{sp\ 1} \sim 3.6 \times 10^{-3}$ and $K_{sp\ 2} \sim 3.6 \times 10^{-5}$); however it would be ideal to further decrease the solubility of the targeted product crystal salt ("s_2") in the reaction medium. However, the soluble concentration of the crystallization agent (C_{DPPA}) is intrinsically related to that of the amino-donor (C_{ISO}) via $K_{sp\ 1}$; it is not possible to increase the concentration of DPPA while keeping high ISO concentrations. Higher C_{ISO} concentrations would result in lower C_{DPPA} (since they are fixed by $K_{sp\ 1}$) and hence in a higher s_{FMBA}, which is not suitable for the targeted FMBA crystallization. Such issue is represented in Figure SIV-7, which shows the impact of the ISO substrate concentration on the TA_PP3 specific activity and on the s_{FMBA} value (i.e. the estimated minimal FMBA concentration required to trigger a FMBA-DPPA crystallization). One idea to get around this issue is to run the transamination reaction in presence of a co-solvent that would increase the solubility gap between the donor and product crystal salts (s_1 vs. s_2) (*e.g.* by selectively decreasing the solubility of the product salt (s_2) without dramatically affecting the one of the donor salt (s_1)). The choice of the co-

solvents employed in this study (i.e. short-chain alcohols, DMF and ACN) was based on their compatibility with the enzyme used, TsRTA (Figure SIV-8 & SIV-9) [129]. Thus, the solubility of FMBA-DPPA crystals (Figure IV-18b) were estimated in the different reaction media containing the compatible solvents in 10 or 20 % v/v proportions.

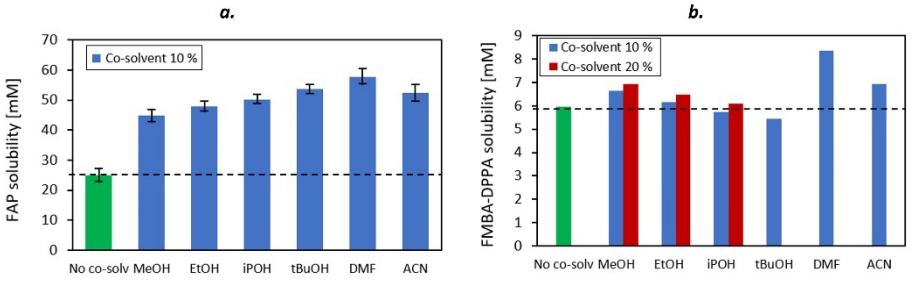

Figure IV-18. FAP and **b.** FMBA:DPPA (crystals) solubility limit in different reaction media (HEPES 0.1 M, PLP 1 mM, pH 8) without or with a given co-solvent (10 to 20 % v/v). The histograms represent the mean solubilities measured by GC-FID, while the error bars represent the standard deviation obtained on triplicates.

However, it was observed that the addition of such co-solvent to the transamination reaction medium was not beneficial, as it did not seem to significantly lower the FMBA-DPPA solubility in the considered reaction media. The co-solvent route aiming at lower the product crystals solubility was therefore abandoned.

4.1.3.2 External substrate reservoir (multiphasic reaction medium)

All the catalytic results presented so far were standardly performed in presence of MeOH in order to ensure the complete solubility of the FAP substrate in the reaction medium. However, the ketone substrate is known to provoke enzyme inhibition. A possible strategy to keep acceptable productivity levels in batch mode is to rely on the use of multiphasic media by taking advantage of the low FAP solubility limit in aqueous media, as proposed by von Langermann et al [103]. FAP solubility in the aqueous medium without co-solvent (with HEPES 0.1M buffer containing PLP 1 mM at pH 8)

was estimated to $s_{FAP} \sim 25$ mM (Figure IV-18a). Thus, running the reaction in the absence of co-solvent allows operating with an external substrate reservoir (FAP emulsions) but at a constant soluble FAP concentration (s_{FAP}).

In absence of MeOH in the system, if we introduce 50 mM of FAP, the actual concentration in the aqueous phase is ~25 mM (and the excess is present as a separate liquid phase (i.e. FAP emulsions, acting as external substrate reservoir)). This concentration, at which the enzyme is not inhibited is maintained constant as the FAP consumed by the reaction is continuously compensated by the dissolution of the FAP emulsion. The TA_PP3 specific activity was maintained (i.e. similar to that observed in presence of 25 mM of FAP) in this case, hence no enzyme inhibition was observed (Figure IV-19a, compare full black and dashed black bar). The presence of an FAP emulsion in the medium did not trigger any TA deactivation over time, and the obtained FMBA production profile showed a more pronounced linear regime/tendency (Figure IV-19b). The latter probably highlights a degenerescence of the kinetics ("zero-order" reaction), in which the reaction rate is constant over time due to the steady FAP substrate concentration present in the aqueous phase (i.e. its solubility limit, s_{FAP}). Once the biocatalytic consumption overcomes the s_{FAP}, the biocatalytic reaction bounces back to its "standard" kinetic regime.

Significantly improved productivity was achieved when the transamination was performed with such FAP substrate reservoir (i.e. without co-solvent) rather than with solubilized 50 mM FAP substrate (i.e. in presence of 10 % v/v MeOH). Thus, this strategy allowed to enhance the reaction kinetics, precisely by overcoming the enzyme inhibition by the FAP substrate, and afford to feed the process with higher substrate concentration.

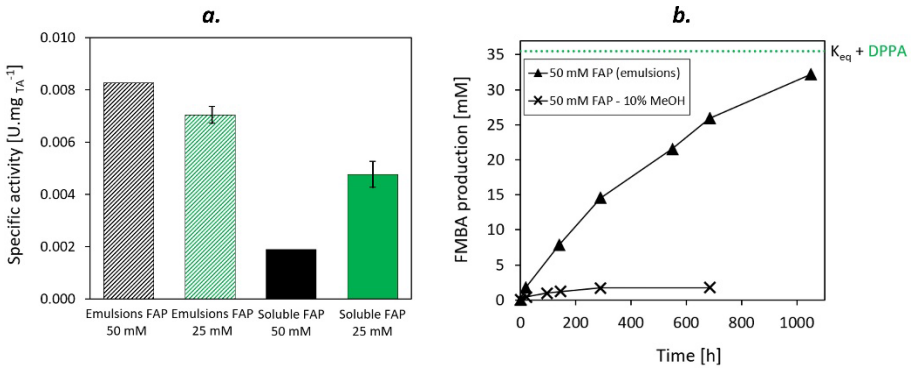

Figure IV-19. Catalytic performance (i.e. a) specific activity and b) reaction profiles) obtained when employing PP-immobilized TsRTA cell-free extract as TA_PP3 catalyst, using 25 mM (green) or 50 mM (black) FAP substrate, in presence (full bars) or in absence (dashed bars) of co-solvent in the reaction medium. Reaction conditions were: [25-50] mM FAP, 250 mM ISO, 50 mM DPPA, [0-10] % v/v MeOH, 1 mM PLP in 0.1 M HEPES buffer pH 8, 35 °C. The enzyme loading was of c.a. L ~ 1.5 mg TA on the membrane carrier.

To further assess the sustainability (environmental impact) of the studied batch crystallization-assisted transamination process, rough E-factor estimations were performed (Table IV-3) and compared them to three main chemocatalytic benchmark processes (methods A,B,C in Table IV-3), which are described in details in the Supplementary data of Chapter III (see Figure SIII-21 to SIII-23) for the synthesis of such enantiopure α-methylbenzylamine derivatives [408].

Table IV-3. Comparison of environmental performance (E-factor) of our optimized batch crystallization-assisted asymmetric synthesis processes (D) with different benchmark chemocatalytic processes (A,B,C) able to produce chiral amines**.** S-methylbenzylamine (S-MBA) was the target amine in A and C, while R-FMBA was targeted in B and D.

Method	**A**	**B**	**C**	**D**
(ref.)	([402])	([403])	([404])	**(This work)**
Description	Imine asymmetric hydrogenation	Ketone reductive amination	Chiral resolution + crystallization	Transamination + crystallization
Precursors	Imine, H_2	Ketone, H_2, NH_4OAc	Racemic amine + resolv. agent [a]	Ketone, ISO + DPPA
Catalyst	$[Rh(COD)Cl]_2$-(Ligand)	$Ru(OAc)_2$-(Ligand)	/	TA_PP3, PLP
ee (%)	90	95	69	99.9
E-factor	58	18	19	5 (or 2.6 *) [b]

[a] : N-tosyl-(S)-phenylalanine (S-TPA) was used as resolving agent.
[b] : Reaction conditions were: 50 mM FAP, 250 mM ISO, 50 mM DPPA, 1 mM PLP in 0.1 M (or 0.05 M *) HEPES buffer pH 8, 35 °C.

We observe that the targeted transamination process studied in this work displays significantly enhanced environmental metrics (E-factor) with respect to the benchmark chemocatalytic processes. Additionally, it is noteworthy that our biocatalytic strategy produces enantiopure (F)MBA product (99.9 % ee), which is not the case of the other methods (i.e. presence of significant fractions of the other enantiomer). Hence, further purifications (e.g. preferential crystallizations) of the target amines will be required in the chemo-catalytic processes, which will further markedly increase the overall E-factor of such processes and underline the superior performance of the crystallization-assisted biocatalytic route proposed herein.

4.1.3.3 Process intensification: transfer from batch to continuous flow reactor

Another appealing approach to enhance the productivity of the present heterogeneous transamination, is the transition from batch to continuous flow mode. Here, we will envisage two distinct aspects related to the transition to flow mode processing: (a) performing the TA immobilization in flow (we surmise that it might benefit from more favorable mixing conditions and result in higher immobilization yield) and (b) performing the transamination reaction in flow mode. For these experiments, disks of 1 cm^2 functionalized membrane were employed. As matter of comparison, these TA immobilization and transamination reactions were also performed in batch mode, but using the same 1 cm^2 membrane disks (in total volumes of 5 mL) to enable a rigorous comparison of the results obtained in batch and flow modes.

(a) Flow immobilization

To the best of our knowledge, only a handful in-flow TA immobilizations have been reported so far [172,218,228,428], while the vast majority of the studies report such immobilization step in batch mode prior to implement the heterogenized TAs in a packed-bed reactor. Here, 1 cm^2 membrane disks were loaded with the enzyme by either immerging it in a 5 mL TA solution (HEPES 0.1 M buffer at pH 8, PLP 1 mM containing 0.5 $mg.mL^{-1}$ of TA cfe) under stirring for 18 hours (i.e. batch immobilization, resulting in TA_PP3) or by flowing the same solution through the membrane disc at a 1 $mL.h^{-1}$ flow rate (i.e. flow immobilization, resulting in TA_PP3F). While the immobilization yield was only 20 % when performed in a batch reactor, it surged to 72 % when performed in flow mode (using identical volumes of solutions, and equal TA immobilization concentration, see left part of Table IV-4). This can be related to the better contact between the enzymes and the membrane carriers

offered by the flow operation (i.e. flow-through configuration), which improves (and forces) the accessibility of the TAs to the porous surface of the membrane. Moreover, the immobilization process occurred significantly faster in flow mode, which allowed to drastically reduce the immobilization duration required to achieve such this higher TA loadings (Figure IV-20a). Indeed, while 18 hours of immobilization were required to achieve a loading of c.a. 0.45 mg in batch, 6 hours of continuous immobilization enabled to immobilize c.a. 1.7 mg TA on the membrane.

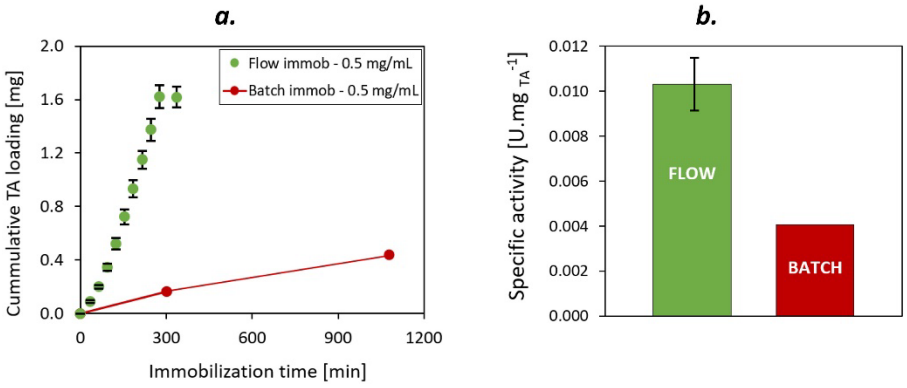

Figure IV-20. a) Cumulative TA loading profile obtained when TA immobilization was performed on 1 cm^2 disk of functionalized PP membranes in batch (red ; TA_PP3) and in flow (green ; TA_PP3F) mode. TA immobilization concentration was 0.5 $mg.mL^{-1}$. **b)** Specific activity of the catalysts when transamination was conducted in batch (with TA_PP3) and flow reactors at 0.8 $mL.h^{-1}$ (with TA_PP3F catalyst). Reaction conditions were: 10 mM FAP, 250 mM ISO, 0 mM DPPA, 0 % v/v MeOH, 1 mM PLP in 0.1 M HEPES buffer pH 8, 35 °C.

(b) Flow transamination

After immobilization, the resulting heterogeneous biocatalysts were rinsed with buffer, either continuously (when using TA_PP3F) or via successive washings (when employing TA_PP3) until no TA was detected in the residual solutions. The activity of the biocatalytic membranes was then assessed in

flow (when using TA_PP3F) and in batch (when employing TA_PP3), in absence of product crystallization (i.e. without DPPA). Prior to flow catalytic tests, blank experiments (i.e. simulation of a catalytic test, but without putting the membrane in the flow reactor) were run. These consisted in feeding the reaction mixture (i.e. 20 mM FAP, 250 mM ISO in HEPES 0.1 M, PLP 1 mM at pH 8) through the empty reactor set-up. Expectedly, no product (i.e. FMBA nor acetone) peaks were detected by GC in the outflows in this case. Yet the concentration of FAP was lower than in the feed solution, resulting in an incomplete carbon balance profile (see Figure IV-21a). Such result highlighted an undesired FAP adsorption on the plastic syringe and tubing, which limits the FAP aqueous concentration of the reaction medium to c.a. 10 mM instead of 20 mM. But this was temporary during the blank test; once the system is saturated, $[FAP]_{out} = [FAP]_{in}$. Hence, we saturated our set-up with the FAP substrate, and kept the same saturated set-up for the next steps so that no adsorption issues occurred during the experiments. Noteworthily, additional blank experiments revealed that no FMBA nor TA adsorption was observed in the flow reactor (Figure IV-21b). The FMBA production (instead of the FAP substrate consumption) was now used as main indicator to compute the specific activity of our biocatalysts.

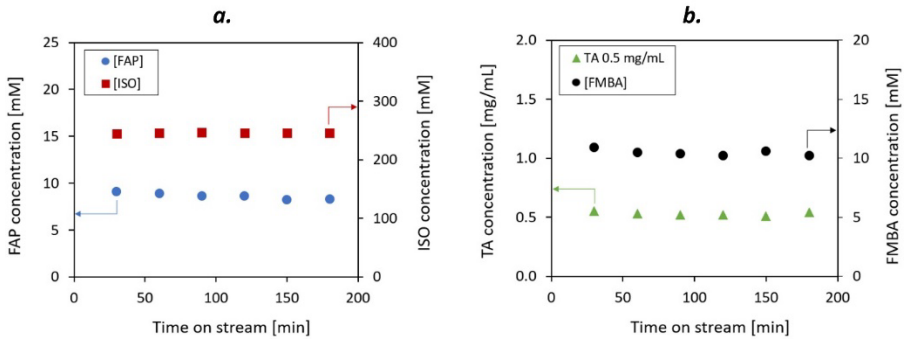

Figure IV-21. Carbon balance profiles over time obtained in the blank tests. **a)** Every 30 minutes, FAP (blue dots; left y axis) and ISO (red squares; right y axis) concentrations in outflows of syringe were assessed. No enzymes (free nor immobilized) were used when flowing the medium in the syringe. Reaction conditions were: HEPES 0.1 M, pH 8, 35°C, 20 mM FAP, 250 mM ISO, no DPPA, no co-solvent**. b)** TsRTA (green triangles, left y axis) and FMBA (black dots, right y axis) solutions in HEPES 0.1 M, pH 8, 35°C were separately fed in the flow reactor, and their concentrations were monitored in outflows of syringe.

Performing the transamination in continuous flow-mode was shown to boost the specific activity of TA_PP3F biocatalyst (with respect to the batch operation, see Figure IV-20b). This can putatively be explained by the improved mixing efficiency achievable in flow reactors, which translates into improved mass transfer [170]. In flow reactors, the boundary layer is typically much thinner compared to batch reactors hence facilitating a higher mass transfer rate as the resistance to diffusion across the layer is decreased [429]. The lower specific activity in batch mode might be attributed to limitations such as accumulation of products which may inhibit the catalyst, less effective mixing, or periodic rather than constant exposure to substrate.

Given the tiny surface of membrane discs considered in the reactor, the flow transaminations were run using very low flow rates (i.e. typically 0.8 $mL.h^{-1}$). By taking into account the volume of the heterogeneous biocatalyst which is flowed-through, V_{mbr} (i.e. the volume of the membrane disc to 0.012 mL (i.e. cross-section of c.a. 1 cm^2, and a thickness of c.a. 120 µm (see SEM images in Figure IV-22)), we were able to estimate the residence time and

space time yield (STY) of the continuous operation to 1 min and 93 µmol.h^{-1}.mL$_{mbr}^{-1}$, respectively (Table IV-4).

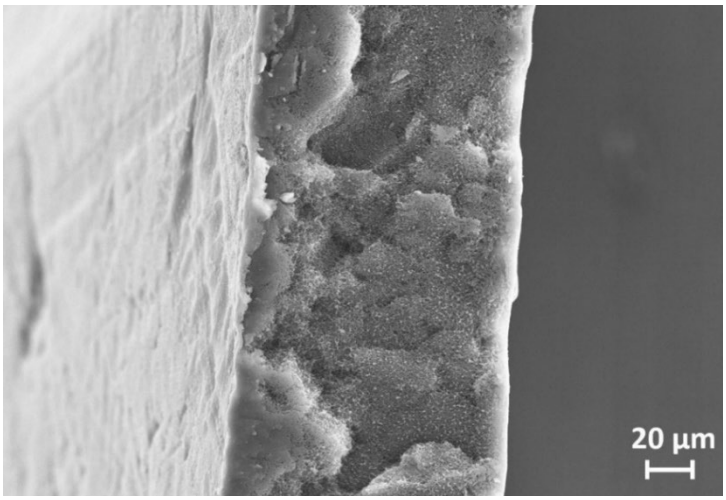

Figure IV-22. SEM image (cross-section) of the functionalized PP carrier employed in this work.

Such STY is 3-4 orders of magnitude higher than in batch (taking the whole volume of solution into account), unambiguously showing the intensification of the process. Such flow mode STY value is similar to or higher than that of other asymmetric syntheses using immobilized TsRTA (and employing ISO as amino donor) in continuous flow. For instance, Heckmann et al. performed the continuous-flow synthesis of 2-aminobutane using covalently immobilized HEwT_F84W and RTA-43 transaminases and resulting STY was around 45 µmol.mL^{-1}.h^{-1} [222].

Table IV-4. TA loading, specific activity and space time yield of the TA_PP3 (up) and TA_PP3F (down) catalysts when immobilization and transamination were conducted in batch and flow reactors**.** In all cases, 1 cm^2 of membrane were employed. conditions were: 10 mM FAP, 250 mM ISO, 0 mM DPPA, 0 % v/v MeOH, 1 mM PLP in 0.1 M HEPES buffer pH 8, 35 °C.

Immobilization	TA loading [a] [$mg_{TA}{}^{-1}$]	Reaction	Sp. activity [U.mg $_{TA}{}^{-1}$] ([U. $m^{-2}{}_{ext}$]) [c]	STY [b] [µmol.h^{-1}.mL^{-1}]
Batch	0.45	Batch	0.0039 (17.5)	0.015
Flow	1.69	Flow	0.011 (180)	93.3

[a] : obtained after 18 hours in batch, and after 6 hours in flow.

[b] : $STY_{batch} = \frac{C_{FMBA}}{t_{batch}}$ and $STY_{flow} = \left(\frac{F}{V_{mbr}}\right) \text{x } C_{FMBA}$. STY were estimated at similar FMBA product concentration levels (C_{FMBA}), i.e. obtained after 100 hours of batch operation (t_{batch}), or at a 0.8 $mL.h^{-1}$ flow rate (F). For the batch operation, the total reaction volume is considered, while only the catalyst volume (V_{mbr}) is taken into account.

[c] : refers to the productivity of the biocatalysts, expressed in activity units per square meter of external membrane surface.

TA_PP3F catalyst also exhibited good stability in continuous flow transamination, as no visible enzyme deactivation occurred over 200 minutes of time on stream (Figure SIV-10). Importantly, the activity was monitored using two different flow rates (1.2 $mL.h^{-1}$ or 0.8 $mL.h^{-1}$) to qualitatively compare the impact of such parameter on the enzymatic activity. An increase in R-FMBA yield was detected when increasing the contact time (i.e. decreasing the flow rate), as expected.

It is also interesting to compare the flow rate that would pass in our lab-scale membrane reactors (TA_PP3F) if it was operating at equal residence time with respect to other studies using microreactors or packed-bed reactors (PBR). In this work, the operating conditions set for the flow transaminations were the following: flow rate: F = 0.8 $mL.h^{-1}$, catalyst volume: V_{mbr} = 0.012 mL (hence, residence time was: τ = 0.9 min). Table IV-5 gathers some

examples of flow transaminations taking place in microreactor or PBR, and reports the consequent the flow rate that would pass in our lab-scale membrane reactors (TA_PP3F) if it was performed at equal residence time. Overall, it appears that we operated at a shorter residence time compared to other studies performing flow transaminations. Consequently, if we had used similar residence times, we would have observed higher flow rates in our EMR.

Table IV-5. Example of flow transaminations (left columns) and consequent flow rates that would pass in our lab-scale membrane reactors (TA_PP3F, V_{mbr} = 0.012 mL), if it was performed at equal residence times (right column).

Ref.	Parameters of the study	Resulting **flow rate** in our EMR
Paradisi et al. [131]	τ = 2 min , V = 0.78 mL, F = 23.4 mL.h^{-1}	At τ = 2 min: **F = 1.8 mL.h^{-1}**
Turner et al. [371]	τ = 4 min , V = 35 µL, F = 0.5 mL.h^{-1}	At τ = 4 min: **F = 3.6 mL.h^{-1}**
Paradisi and Heckmann [222]	τ = 15.5 min , V = 7.7 mL, F = 30 mL.h^{-1}	At τ = 15.5 min: **F = 13.7 mL.h^{-1}**
López-Gallego et al. [236]	τ = 1 min , V = 1.4 mL, F = 84 mL.h^{-1}	At τ = 1 min: **F = 0.9 mL.h^{-1}**

Eventually, when taking into account the productivity (i.e. activity normalized by the external membrane surface, 180 µmol.min^{-1}.m$^{-2}_{ext}$ or 94.6 mol.year^{-1}.m$^{-2}_{ext}$) achieved by our lab-scale EMR (see Table IV-4), we can roughly estimate the surface of membrane reactor that would be required to meet the industrial demand. Typically, an annual amine production of 62 500 mol/year was set as target by Yang et al. [284] in their techno-economical analysis (as "5000 L reactors and 1 week for one process step, are common in the pharmaceutical industry" [430]). However, 250 000 mol/year can be envisaged for the production of widely used building blocks in pharmaceutical and agrochemical industry [284].

Taking this upper annual production limit (250 000 mol/year), it would require 2643 m^2 of EMR surface. On the other hand, a total membrane surface area of only 661 m^2 would be needed to produce 62 500 mol/year, which seems feasible for industrial membrane reactor plants. For example, in large municipal wastewater treatment plants, membrane modules with high packing density and surface areas in the range of 500 to 1000 m^2 (up to 8000 m^2 [431]) are common to handle daily flow rates of tens of thousands of cubic meters [432].

4.2 Expanding the substrate scope (preliminary screening)

In the previous sections of results, we have focused exclusively on the catalytic conversion of FAP into R-FMBA, using our PP-immobilized transaminases under a variety of conditions. We have thoroughly examined strategies for optimization of the process, such as the multiphasic system, the optimal use of crystallization to enhance conversions and finally, we implemented the works in continuous flow mode to prove the robustness of the process. However, to further explore the versatility and scope of such biocatalytic transamination process, it was interesting to test a broader range of keto substrates. We first relied on substrates that were structurally similar to FAP and that were already screened for this transaminase (TsRTA): 4-bromoacetophenone (BAP), phenoxy-2-propanone (PhoxyP), and phenylbutanone (PhB). The goal of this preliminary screening (only performed in batch mode, in absence of DPPA) was to expand the scope of the different APIs we could possibly produce with the same process, thus testifying, once again, its robustness and versatility. Notably, R-phenoxypropan-2-amine (i.e. the transamination product when using PhoxyP as keto-substrate) is an analogue and intermediate of R-mexiletine, a well-known efficient antiarrhythmic drug [433].

It is crucial to note that the specific strategies and optimizations developed for FAP could not be directly applied to these new keto substrates without first evaluating their compatibility and effectiveness for our transaminase. Ideally, for kinetic reasons, one should work at high reagent concentrations, hence, at the keto-substrate's solubility limit. Thus, the first step was to test each substrate's solubility in HEPES 0.1 M pH 8 buffer. For the FAP substrate, we have seen that it was optimal to work at its solubility limit, i.e. 25 mM (since no inhibition was observed at smaller concentrations). However, this is not automatically true for other substrates, as inhibition can happen before their solubility limit. Consequently, an inhibition test was routinely conducted for each substrate screened: the specific activity of our immobilized transaminase (TA_PP3) was measured with increasing concentration of each of these substrates.

To measure their solubility limit, each keto-substrate (PhoxyP, PhB, BAP) were put in excess in the HEPES 0.1 M PLP 1 mM pH 8 medium, so that the aqueous phase (that is analyzed by GC) is at the substrate's solubility limit. We intentionally engage very high excesses in order to generate emulsions; they allow to sample the aqueous phase more accurately and with less variability. Mean values for PhoxyP and PhB solubilities were respectively 35 and 25 mM, while BAP solubility limit was only at roughly 4.5 mM. Aiming at working at acceptable rates, we consequently increased BAP solubility by adding 10 % v/v of MeOH, which allowed to increase the solubility until 12 mM (Figure IV-23a). Inhibition tests were run on PhoxyP and PhB to check if any inhibition would happen before reaching their solubility limit (now known), to measure the optimal concentration for highest activity. There was, fortunately, no enzyme inhibition by phenylbutanone; the activity only increasing until reaching the solubility limit, which augurs well for the production of the chiral amines corresponding to this substrate (Figure IV-23b). For phenoxy-2-propanone however, a peak of activity was seen at around 16 mM, after which the activity declined when increasing substrate

concentration, suggesting inhibition. Because of BAP's very low solubility and due to the low enzyme activity detected for this substrate, we did not conduct any inhibition test on it.

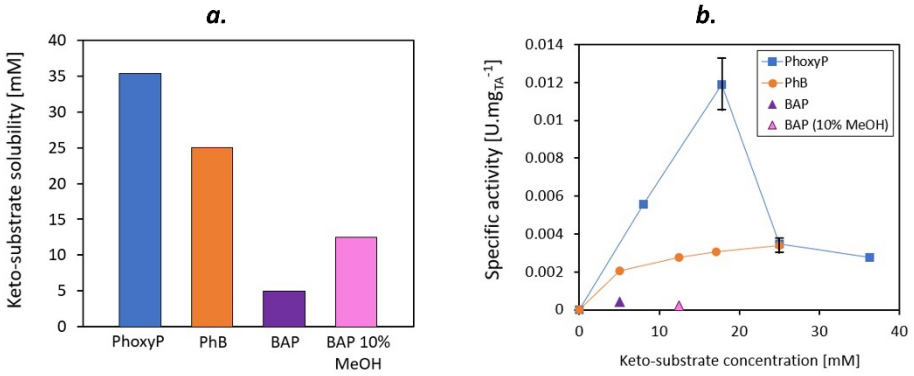

Figure IV-23 a) Solubilities of keto-substrates in the considered medium (1 mM PLP in 0.1 M HEPES buffer pH 8, 35 °C) and **b)** Inhibition test for PhoxyP and PhB keto-substrates. Specific activity of TA_PP3 catalyst was assessed over increasing substrate concentration. Reaction conditions were: [0-35] mM keto-substrate, 250 mM ISO, 0 mM DPPA, 0 % v/v MeOH, 1 mM PLP in 0.1 M HEPES buffer pH 8, 35 °C.

Now that TA_PP3 biocatalyst inhibition studies have been performed with these different keto-substrates, crystallization-assisted asymmetric syntheses and long-term stability tests should now be performed in batch mode to close the loop. For the upcoming crystallization-assisted transamination process, we will therefore set the PhoxyP and PhB substrate concentrations at, respectively, 16 and ≥ 25 mM.

5 Conclusion

In this work, we present the immobilization of a R-selective TA (TsRTA) onto polypropylene membrane (PP) and its application to catalyze an industrially relevant transamination, the asymmetric synthesis of R-2-fluoromethylbenzylamine (R-FMBA), aided by two distinct strategies.

Firstly, the reaction was carried out in batch mode and coupled with an *in-situ* product separation. Here, crystallization of the R-FMBA with 3,3-diphenylpropionic acid (DPPA) was used in order to push the transamination reaction towards the products, and to recover the enantiopure targeted amine by simple filtration (in the form of a salt). For the TA membrane-immobilization, PP was coated with polydopamine to provide amine functions at its surface, which were further functionalized with epoxy groups to covalently graft the TA. The immobilized TA showed enhanced specific activity and stability towards the studied transamination compared to their soluble counterparts. It also exhibited superior catalytic performance than widely employed heterogeneous TAs (i.e. Relizyme™-immobilized TAs), which highlights the interest of the immobilization strategy reported herein. Importantly, the presence of DPPA in the reaction medium enabled to overcome the equilibrium concentration, and to produce pure FMBA:DPPA crystals with excellent yields (95 %). Such PP-immobilized TA was also shown to be easily recoverable and reusable, being able to perform successive high-yield asymmetric syntheses with minor deactivation. In an attempt to further optimize the process, the addition of various co-solvents was envisaged. This, however, was found inconclusive, since no co-solvent addition enabled to significantly lower the product crystal solubility. On the contrary, working in the absence of co-solvent (in water only) resulted in the formation of an FAP emulsion, and a low (c.a. 25 mM) but constant concentration of soluble FAP (the emulsion playing the role of an FAP

reservoir). In this configuration, enzyme inhibition was minimized, and the resulting productivity was boosted.

Secondly, the biocatalytic membranes were implemented in continuous flow mode. Both the immobilization of TA on the membrane and the transamination reaction (asymmetric synthesis) were demonstrated in a flow-through configuration. These conditions allowed to boost the immobilization yield (i.e. a four-fold increase of TA loading was obtained, with respect to the batch immobilization). Correspondingly, R-FMBA productivity and space-time-yields were markedly boosted in flow mode. Probably owing to better hydrodynamic conditions (mixing), the TA specific activity in flow was more than 2 time higher in flow as compared to the batch process. While these promising results represent, to our best knowledge, the first example of flow asymmetric synthesis of chiral amines using membrane-immobilized TAs, it is clear that the biocatalytic system is not yet optimized.

Eventually, a preliminary screening of other keto substrates was also performed to expand the scope of enantiopure amine production via crystallization-assisted transamination in batch mode, paving the way for new API synthesis using this biocatalytic process.

6 Supplementary information of Chapter IV

6.1 Experimental details of Chapter IV

6.1.1 Soluble enzymes quantification: Bradford method

Soluble enzyme concentrations were assessed through the Bradford titration method [405]. Calibration was performed by mixing 250 µL of standard solutions of TA cell-free extracts in HEPES 0.1M buffer pH 8, PLP 1 mM (within 0–0.25 $mg.mL^{-1}$ concentration range) with 750 µL of Bradford reagent. After 5 minutes incubation at room temperature, absorbances were read at 595 nm with a ThermoScientific Genesys 10S-Vis spectrophotometer, and values of A_{595} were plotted against TA concentration.

6.1.2 Gas Chromatography (GC) analysis

After extraction of the analytes into dichloromethane, the GC analyses were performed on a Bruker SCION 456-GC with a WCOT fused silica BR-5 column (30 m x 0.32 mm ID x 1.0 µm) and helium as carrier gas (25 $mL.min^{-1}$), oven temperature initially at 50 °C for 5 min, then heated to 150 °C with a heating rate of 20 $°C.min^{-1}$, then maintained at 150 °C for 10 min. Split ratio of 80, injector temperature at 250 °C, flame ionization detector (FID Bruker MicroCT) temperature at 300 °C (air flow 300 $mL.min^{-1}$, H_2 flow 30 $mL.min^{-1}$).

To quantify the concentration of FAP and FMBA in DCM, two calibrations curves were produced. First, two stock solutions of FAP in DCM and FMBA in DCM were prepared with a targeted concentration of respectively 15 mM and 5 mM. To this end, the volumes in µL of FAP or FMBA corresponding to this concentration were added to a chosen volume of DCM.

In order to assess the efficiency of the extraction process, we checked whether the FAP and FMBA concentrations classically extracted from aqueous medium containing HEPES 0.1 M fitted with their expected concentrations in DCM. For instance, by sampling 100 µL of a 10 mM FAP solubilized in HEPES 0.1 M solution and extracting it in DCM for analysis in GC, one should get a response value close to that of the calibration point corresponding to 1 mM FAP in DCM (concentrations in reaction medium being roughly 10 times that of the vials 40 analyzed in GC). This would suggest that after those 3 extractions, all of the FAP has effectively passed into the organic phase. Calibration curves for acetone and ISO were also made in order to verify the mass balance when working in multiphasic medium (FAP emulsions) because, in that case, neither FAP nor FMBA are completely homogeneous in the medium (contrary to acetone, which is solubilized in the medium). In that sense, these calibration curves test the reliability of responses obtained via GC for FAP or FMBA quantification when working in multiphasic systems.

6.1.3 Chiral High-Performance Liquid Chromatography (cHPLC) and chiral Gas Chromatography (cGC) analyses

In order to be analyzed via Chiral High Performance Liquid Chromatography (cHPLC), FMBA:DPPA crystals (i.e. chemically synthesized in MTBE or obtained through crystallization-assisted transamination) were dissolved in the mobile phases (99.4 % isohexane/0.5 % isopropanol/0.1 % diethylamine). FMBA enantiomers were detected and analyzed by normal phase HPLC (Hitachi-koki) at 262 nm in a Merck-Hitachi LaChrom L-700 and a chiral column Daicel OD-H (250 mm x 4.6 mm) at a flow rate of 1 mL/min (99.4 % isohexane/0.5 % isopropanol/0,1 % diethylamine) for 30 minutes. Retention time of R- and S-enantiomers are respectively 12.3 and 13.4 minutes.

When chiral Gas Chromatography (cGC) analysis was performed, FMBA:DPPA crystals were suspended in HEPES 0.1 M pH 8 buffer, then 100 µL of mixture was sampled and basified by adding 30 µL of sodium hydroxide (2 M). 400 µL of dichloromethane was then added to the aqueous phase, vortexed for 15 seconds and rest for 5 minutes to allow extraction of FMBA into the organic phase. Extraction step was repeated twice and the organic phases were pooled and analyzed by gas chromatography on a Bruker SCION 456-GC with a CP Cyclodextrin B-2,3,6-M-19 column (50 m x 0.25 mm ID x 0.25 µm) and helium as carrier gas (25 $mL.min^{-1}$), oven temperature initially at 50 °C for 5 min, then heated to 90 °C with a heating rate of 3 $°C.min^{-1}$, then maintained at 90 °C for 10 min, then heated to 130 °C with a heating rate of 1 $°C.min^{-1}$. Split ratio of 20, injector temperature at 230 °C, flame ionization detector (FID Bruker MicroCT) temperature at 230 °C (air flow 300 $mL.min^{-1}$, H_2 flow 30 $mL.min^{-1}$).

6.1.4 Proton Nuclear Magnetic Resonance (^{1}H-NMR)

Crystals were first weighted (dry) then dissolved in solvent (deuterated methanol (CD_3OD), deuterated chloroform ($CDCl_3$) or dimethyl sulfoxide-d6 (DMSO d6)) in an Eppendorf. 500 µL of this solution was then filled in NMR tubes for analysis. Quantification was made possible via the simultaneous analysis of an internal standard, namely DMF, of known concentration (5 mM).

NMR spectra were recorded at room temperature on a Jeol JNM-ECZL G series spectrometer operating at a field strength of 14.1 T (Larmor frequency was 600.09 MHz for ^{1}H). Experiments were run under Delta 6.2 program (Jeol) using a 5 mm HFX probe equipped with a z-gradient coil. Spectral multiplicities are noted as follows: singlet = s, doublet = d, triplet = t, quartet = q and multiplet = m.

6.2 Supplementary data of Chapter IV

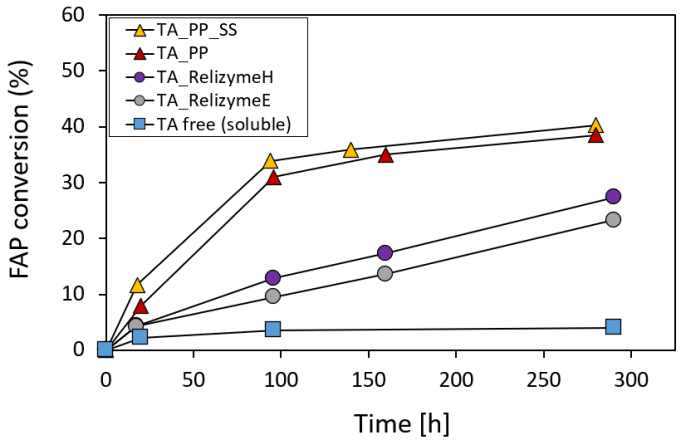

Figure SIV-1. Reaction profiles obtained with different free and immobilized TsRTA cell-free extracts (TAs) studied in this work**.** Reaction conditions were: 25 mM FAP, 250 mM ISO, 0 mM DPPA, 10 % v/v MeOH, 1 mM PLP (or 0 mM PLP for TA_PP3_SS) in 0.1 M HEPES buffer pH 8, 35 °C. The reactions were run at equal nominal enzyme concentration, i.e. 0.2 mg/mL TA. For TA_PP3, this corresponds to an enzyme loading of c.a. L ~ 1.5 mg TA on the membrane carrier. TsRTA cell-free extract was used as (free or immobilized) TA in these tests.

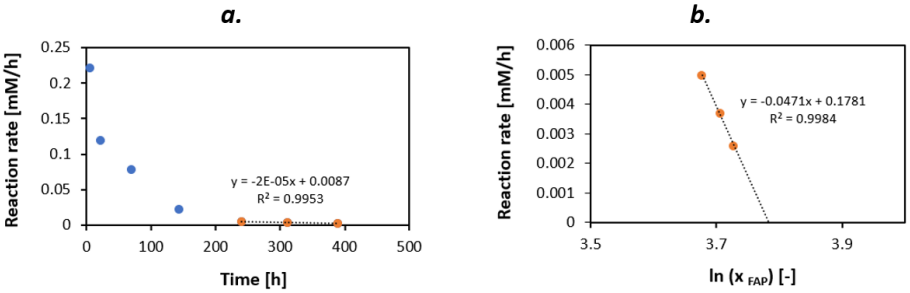

Figure SIV-2. a) Reaction rate evolution over time obtained for pTA_PP3 in absence of DPPA (see Figure IV-7, full curves)**.** The last three activity points (in orange) showed linear evolution (tending towards reaction rates of zero), suggesting that the reaction is nearing its thermodynamic limit.
When these three last points were plotted as in **b)** Reaction rate versus the logarithm of FAP conversion (ln (x_{FAP})), a linear relationship was also observed, allowing to estimate the FAP conversion at the equilibrium ($x_{FAP\,eq}$) by a simple regression. In this case, the following value was estimated to : $x_{FAP\,eq} = 44$ %. Hence, the equilibrium constant value of such transamination was to estimated to $K_{eq} = 0.039$.

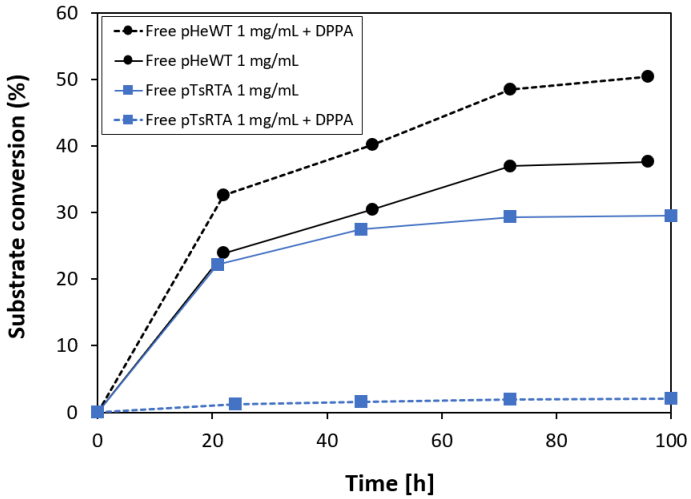

Figure SIV-3. Reaction profiles obtained with different free purified TAs (pTAs) in solution, namely TsRTA (blue curves) and HeWT (black curves), in absence (full curves) or in presence (dotted curves) of DPPA suspension. Reaction conditions were: 25 mM keto-substrate (FAP for TsRTA, AP for HeWT), 250 mM ISO, [0-50] mM DPPA, 10 % v/v MeOH, 1 mM PLP in 0.1 M HEPES buffer pH 8, 35 °C. The reactions were run at nominal enzyme concentration of 1 mg/mL TA.

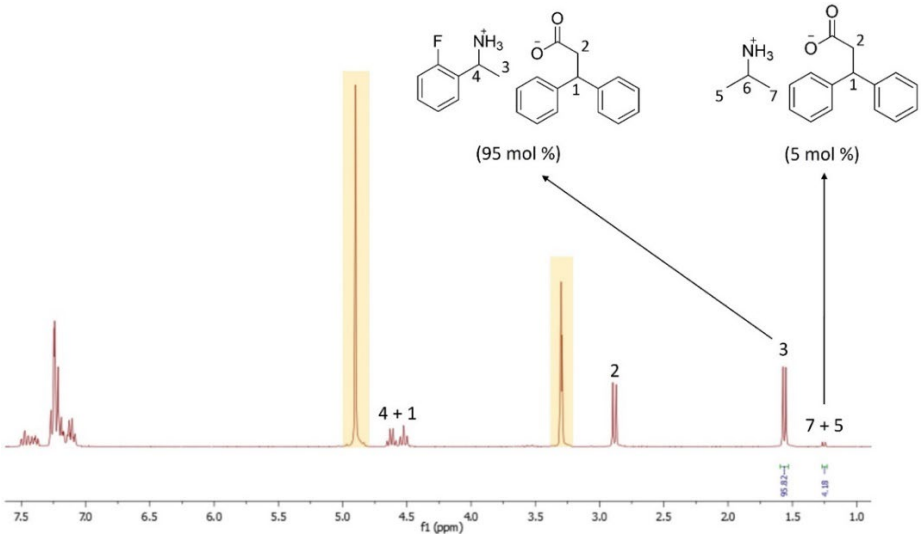

Figure SIV-4. ^{1}H-NMR spectrum recorded in CD_3OD when analyzing the FMBA:DPPA (12.5:15) crystals produced via crystallization-assisted transamination.

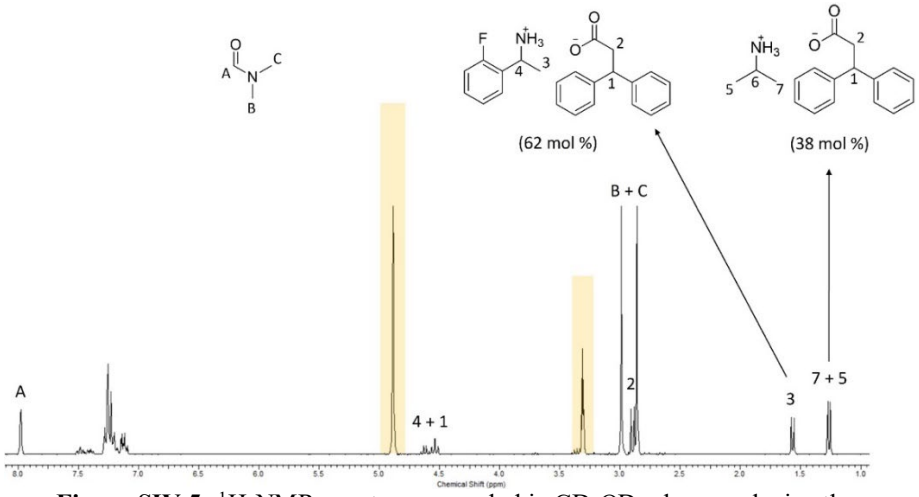

Figure SIV-5. ^{1}H-NMR spectrum recorded in CD_3OD when analyzing the FMBA:DPPA (12.5:50) crystals produced via crystallization-assisted transamination. DMF was used as standard for quantification during the analysis.

Table SIV-1. TA_PP3_SS catalytic performance and crystallization metrics obtained when performing the transamination (in presence of different DPPA concentrations). Reaction conditions were: 25 mM FAP, 250 mM ISO, [0-50] mM DPPA, 0 % v/v MeOH, 0 mM PLP in 0.1 M HEPES buffer pH 8, 35 °C. The final FAP conversion was determined after 390 hours of reaction. "MR at t_0" stands for initial reaction mixture (either in the form of solution (sol.) or suspension (susp.)).

C_0 FAP [mM]	MR at t_0	C_0 DPPA [mM]	Sp. activity [$U.mg_{TA}^{-1}$]	$x_{FAP\ eq}$ (%) [a]	$x_{FAP\ obs}$ (%) [b]	$x_{FMBA:DPPA}$ crystals (mol %) [c]	Y_{cryst} FMBA:DPPA (%) [d]
25	Sol.	0	0.0049	44.6	43.9	/	/
25	Susp	50	0.0046	81.9	79.8	99	97

Theoretical calculations: crystals recovery yield and conversion at the equilibrium

[a]: The expected FAP conversion at the transamination equilibrium ($x_{FAP\ eq}$) was approached by considering the estimated value of the transamination

equilibrium constant ($K_{eq} \approx 3.9*10^{-2}$) and the initial concentrations of FAP and ISO substrates (A and B, respectively). In absence of DPPA, at the equilibrium, we have Eq. S1 :

$$K_{eq} = \frac{[FMBA] * [Acetone]}{[FAP] * [ISO]} = \frac{\alpha^2}{(A - \alpha) * (B - \alpha)} \qquad Eq.S1$$

with α being the substrate concentration converted at the equilibrium.
However, when DPPA is present in the reaction mixture, formation of highly insoluble FMBA:DPPA product salt ($K_{sp\,2} \approx 3.5*10^{-5}$) occurs, meaning that the FMBA concentration will be fixed at its solubility limit, s_{FMBA} (as soon as its production reaches this concentration). Hence, a new substrate concentration converted at the equilibrium (α') will be observed owing to the product crystallization phenomenon, as we will have Eq. S2 :

$$K_{eq} = \frac{[FMBA] * [Acetone]}{[FAP] * [ISO]} = \frac{s_{FMBA} * \alpha'}{(A - \alpha') * (B - \alpha')} \qquad Eq.S2$$

and

$$s_{FMBA}\ [mM] = \frac{K_{sp\,2}}{[DPPA]} = \frac{K_{sp\,2} * [ISO]}{K_{sp\,1}} \qquad Eq.S3$$

with $K_{sp\,1}$ and $K_{sp\,2}$ being the solubility product of the donor (ISO:DPPA) and of the product crystal salts, respectively. Thus, the larger the solubility gap between these salts, the lower the solubility of FMBA in the aqueous reaction medium.
By solving the Eq. S1 and Eq. S2, we access to the values of α and α' and hence, to the expected FAP conversions at the transamination equilibrium in absence ($x_{FAP\,eq}$) or in presence ($x_{FAP\,eq}$') of DPPA :

$$x_{FAP\,eq}\,(\%) = \left(\frac{\alpha}{A}\right) * 100 \qquad Eq.S4$$

and

$$x'_{FAP\ eq}(\%) = \left(\frac{\alpha'}{A}\right) * 100 \qquad Eq.S5$$

[c]: The FMBA:DPPA content of the crystals (x_{FMBA}) was determined by semi-quantitative ^{1}H-NMR analyses, by comparing the peak contributions of FMBA:DPPA (doublet 3H, at 1.57 ppm) and ISO:DPPA (doublet 6H, at 1.25 ppm) with each other (see Eq. IV-6). DMF was used as standard for quantification during the ^{1}H-NMR analyses.

[d]: The FMBA:DPPA crystal recovery yield (Y_{cryst}) was defined as the ratio of the actual mass of FMBA:DPPA in the obtained crystals ($m_{FMBA:DPPA\ obt}$) compared to the maximum theoretical mass of FMBA:DPPA produced which is able to crystallize (see Eq. IV-3).

The actual mass of FMBA:DPPA in the obtained crystals were estimated (by ^{1}H-NMR) to 10.2, 19.3 and 36.9 mg for d1, d2 and d3, respectively. The maximal mass of crystallizable FMBA:DPPA were of :

$m_{FMBA:DPPA\ max} = (C_{FAP\ converted} - s_{FMBA:DPPA}) * M_{m\ FMBA\text{-}DPPA} * V_{residual} = (7.9 - 2.24) * 365 * 6.7*10^{-3} = 13.8$ mg for d1.

$m_{FMBA:DPPA\ max} = (C_{FAP\ converted} - s_{FMBA:DPPA}) * M_{m\ FMBA\text{-}DPPA} * V_{residual} = (10.5 - 1.98) * 365 * 6.7*10^{-3} = 20.8$ mg for d2.

$m_{FMBA:DPPA\ max} = (C_{FAP\ converted} - s_{FMBA:DPPA}) * M_{m\ FMBA\text{-}DPPA} * V_{residual} = (19.3 - 1.98) * 365 * 6.7*10^{-3} = 38.1$ mg for d3.

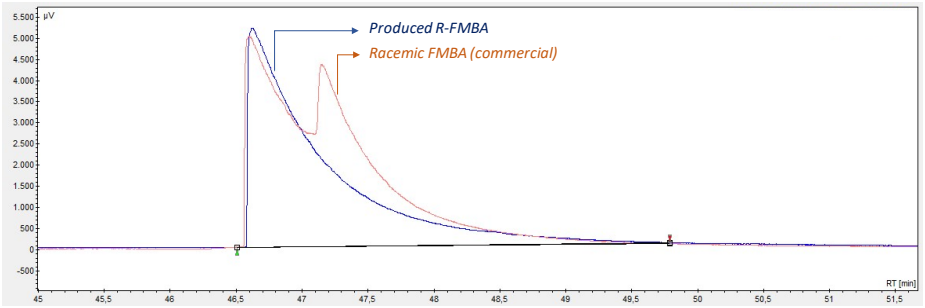

Figure SIV-6. Caption of superimposed chiral-GC chromatograms resulting from the analysis of biocatalytically produced FMBA:DPPA (25:50) crystals (in blue), and of the chemically synthesized rac-FMBA:DPPA ref. crystals (in red).

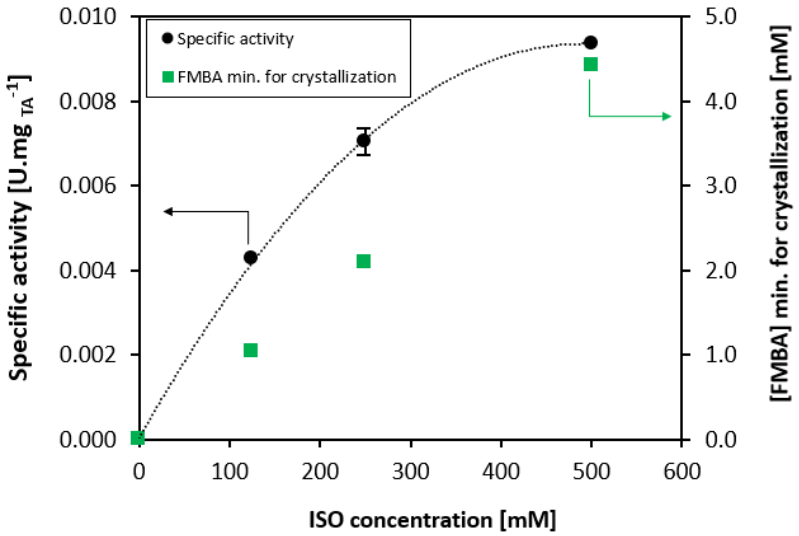

Figure SIV-7. Impact of the ISO substrate concentration on pTA_PP3 specific activity (left axis) and on the resulting FMBA solubility limit, s_{FMBA}, in the system (right axis). Reaction conditions were: 25 mM FAP, [0-500] mM ISO, 50 mM DPPA, 10 % v/v MeOH, 1 mM PLP in 0.1 M HEPES buffer pH 8, 35 °C. The reaction were run at nominal enzyme concentration of 0.2 mg/mL TA, which corresponds to an enzyme loading of c.a. L ~ 1.5 mg pTA on the membrane carrier. The error bar represents the standard deviation obtained on triplicates.

Co-solvents addition into the crystallization-transamination system

The choice of the anti-solvent employed in this study was entirely based on its compatibility with the enzyme used (TsRTA). Figures SIV-8 and SIV-9 show the residual activity and the stability over storage time displayed by free TsRTA in different reaction media containing co-solvents. As it can be observed, TsRTA show good to excellent tolerance and stability in reaction media containing 10 % v/v of co-solvent like short-chain alcohols, DMSO, DMF or ACN. However, its catalytic performance significantly drop in presence of 20 % v/v co-solvent, except when employing MeOH, EtOH and DMSO. DMSO is not a suitable candidate for anti-solvent crystallization, as it is known to dissolve a large variety of dissolves both polar and nonpolar compounds. Thus, the solubility of FAP (see Figure IV-18a.) and FMBA-DPPA crystals (see Figure IV-18b.) were estimated in the different reaction media containing the compatible solvents in appropriate amount (from 10 and 20 % v/v). It resulted that all an addition of all the screened anti-solvents tend to significantly increase the FAP solubility with respect to the original reaction medium (i.e. aqueous, with HEPES 0.1M buffer containing PLP 1 mM at pH 8). A similar situation was observed with FMBA-DPPA, since no anti-solvent addition enabled to significantly lower the crystal solubility (at the exception of tBuOH 10 % v/v). Hence, we can conclude that the addition of such anti-solvent to the transamination reaction medium was not beneficial, as it did not seem to significantly lower the FMBA-DPPA nor the FAP solubility in the reaction media.

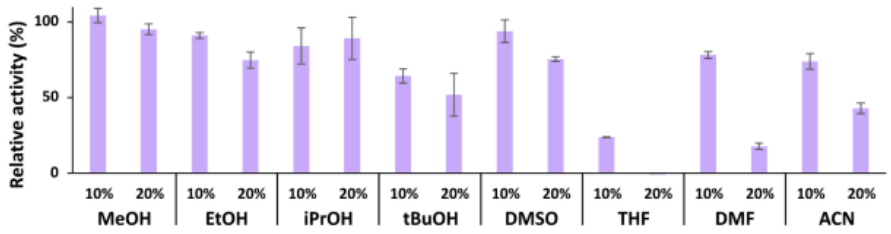

Figure SIV-8. TsRTA activity recovery in presence of co-solvent (v/v %), from Paradisi *et al.,* 2020 [129].

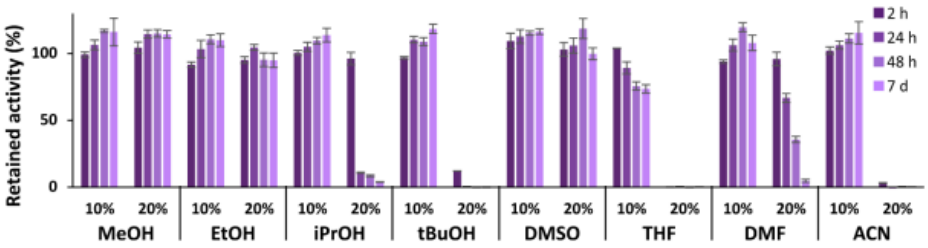

Figure SIV-9. TsRTA stability (activity recovery after incubation) in presence of co-solvent (v/v %), from Paradisi *et al.,* 2020 [129].

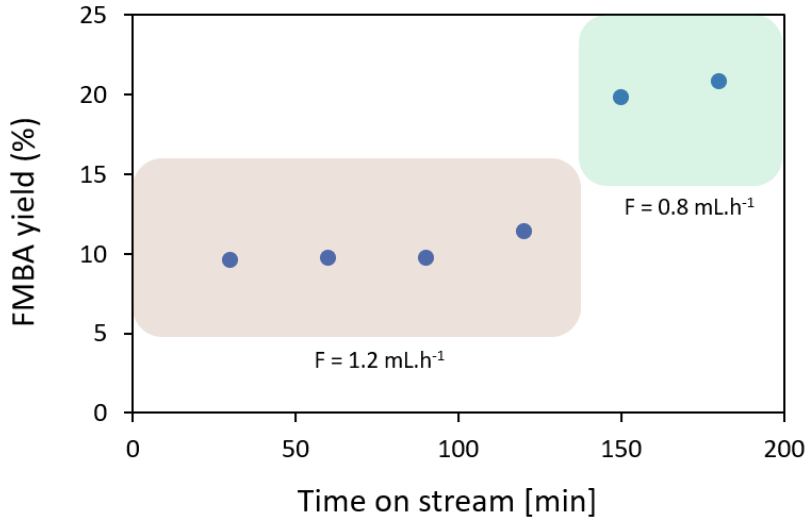

Figure SIV-10. Time on stream stability of the TA_PP3F catalysts when transamination was conducted in flow reactor (at 1.2 mL.h^{-1}, then at 0.8 mL.h^{-1}. Reaction conditions were: 10 mM FAP, 250 mM ISO, 0 mM DPPA, 0 % v/v MeOH, 1 mM PLP in 0.1 M HEPES buffer pH 8, 35 °C.

Conclusion and future work

1. General conclusion

Enantiopure amines are essential building blocks to manufacture a plethora of valuable compounds, including active pharmaceutical ingredients (API). However, their current production often involves multi-step synthesis requiring expensive homogeneous catalysts and high energy consumption for subsequent purification. Biocatalytic routes have gained considerable attention in the last decades, as effective and potentially more sustainable alternatives. Indeed, transaminases (TAs) can catalyze the chiral amines production through transamination reactions with excellent enantioselectivity and in mild conditions. Industrial applications of biocatalytic transamination, however, remain scarce as the enzymes often operate in restricted operational conditions and display limited stability. Batch reactors utilizing the free enzyme in solution also face issues regarding catalyst separation, recovery, and reuse. Moreover, the synthesis of most compounds of interest is thermodynamically unfavoured.

Taking a side step, catalysis scientists design heterogenized biocatalysts that are more versatile, more stable, and amenable to continuous flow processes. A number of improvement strategies have been deployed to address the main issues and limitations of transaminations: modifications of the transaminase itself (via genetic engineering), optimization of immobilization strategies, design of structured supports, development of integrated equilibrium shifting strategies, concatenation with purification, etc. Here, through the first chapter of this thesis, we critically summarize and exemplify these advances leading to more efficient heterogeneous biocatalytic systems based on transaminases operating in continuous flow mode.

In the second chapter of this work, the interests of coupling enzymes with membrane reactors in so called “enzyme-membrane-reactors” (EMR) for development of hybrid flow processes, were presented and exposed. The

recent applications and trends of such EMR for the synthesis of pharmaceutical building blocks and fine chemicals were extensively reviewed.

The experimental chapters (Chapters III and IV) of the thesis propose steps forward in the direction of transamination reactions, by relying on the use of membrane-immobilized transaminase reactor and hybrid processes. We aimed at designing an innovative biocatalytic process in which membrane operations enhance the productivity of a crystallization-assisted transamination. To achieve this ambitious goal, the membrane-immobilization of transaminases first needs to be mastered and optimized.

In Chapter III, we reported two efficient immobilization routes to obtain robust membrane-immobilized transaminases. These methods involve electrostatic adsorption and covalent grafting of transaminases onto polyethyleneimine (PEI)-coated polyacrylonitrile (PAN) and polydopamine (PDA)-functionalized polypropylene (PP) membranes, respectively. Significant enzyme leaching was observed with electrostatically immobilized TAs, prompting post-treatment strategies to enhance enzyme attachment on the PAN membrane. Of these, the covalent bonding of TAs and the PEI layer using glutaraldehyde (GA) yielded the best results, with high specific activity and minimal leaching. Meanwhile, covalent grafting on functionalized PP membranes enabled to produce even more efficient biocatalysts, demonstrating higher specific activity, greater robustness (no leaching), and recyclability. Both strategies successfully immobilized two different TAs (S-selective HeWT and R-selective TsRTA), resulting in stereo-divergent biocatalytic membranes. Additionally, by modifying the immobilization protocol, co-immobilization of TA and PLP on PP membranes was achieved, enabling the creation of reusable membrane-immobilized biocatalysts capable of catalyzing transamination reactions without externally added PLP. In summary, both immobilization approaches led to biocatalytic materials with

excellent enantioselectivity, high catalytic performance, minimal leaching, and optimal reusability.

In Chapter IV, we demonstrated the application of these PP-immobilized TAs to catalyze an industrially relevant transamination reaction: the asymmetric synthesis of R-2-fluoromethylbenzylamine (R-FMBA), coupled with *in-situ* product separation. Crystallization of R-FMBA (using 3,3-diphenylpropionic acid (DPPA) as a crystallizing agent) was attempted to shift the transamination equilibrium towards the product side, and recover the pure amine target through simple filtration. The membrane-immobilized TAs exhibited enhanced specific activity and stability in this transamination compared to the soluble transaminases. They also outperformed widely used Relizyme™-immobilized TAs (used as benchmark catalysts in this work), emphasizing the efficiency of our immobilization strategy. This further highlights the benefit of our immobilization strategy (elaborated in Chapter III), which seems provide an appropriate balance of covalent anchoring points (resulting in a optimal level of rigidification of the enzyme structure) and a sufficiently hydrated microenvironment for the immobilized TAs.

The addition of DPPA, in presence of the PP-immobilized TAs, enabled to overcome the transamination thermodynamic limit and resulted in the production of pure FMBA crystals with excellent yields (95%). Additionally, the PP-immobilized TAs achieved successive high-yield asymmetric syntheses with minimal deactivation. This successful proof of concept demonstrated the feasibility of crystallization-assisted asymmetric amine synthesis using membrane-immobilized TAs in batch mode, with R-FMBA as the enantiopure target molecule.

To further optimize of the batch reaction-crystallization process, we leveraged on the use of a multiphasic medium using supersaturated FAP substrate. This strategy allowed to maintain a constant FAP concentration at its solubility limit in the aqueous phase (due to the presence of FAP emulsions

acting as external substrate reservoirs), hence counteracting enzyme inhibition and affording enhanced enzymatic activity.

Eventually, the obtained membrane-immobilized transaminase technology was then transferred to continuous flow mode. Not only the biocatalytic asymmetric synthesis (in absence of product separation) was performed in a continuous flow reactor (in flow-through configuration), but also TA membrane-immobilization, which represents an innovative advance in this field. This EMR configuration tripled the TA loading on the membrane compared to batch immobilization, and the specific activity of the heterogeneous biocatalyst doubled when performing the asymmetric synthesis of R-FMBA in flow mode. While these promising results represent, to our best knowledge, the first example of flow asymmetric synthesis of chiral amines using membrane-immobilized TAs, it is clear that the biocatalytic system is not yet optimized.

2. Future work

In the end, this study has addressed some of the challenging issues that persist in the development of intensified biocatalytic transaminations for enantiopure amines production.

First, additional modifications and optimizations of the transaminase immobilization step on membranes could be implemented to make the biocatalytic membranes even more robust. Verifying the enzyme loading on the membrane using an alternative method (in addition to the mass-balance method coupled with Bradford assay) would allow us to obtain a more reliable measure of the specific activity of our immobilized enzymes. Additionally, expanding the range of membrane supports (by demonstrating our transaminase immobilization strategy on other industrially relevant polymers (such as PVDF, PES) or on ceramics), could prove useful for targeting various

membrane operations. The use of composite membranes as supports is also of interest, as they may exhibit innovative properties (e.g., improved tolerance to organic solvents) and thus be applicable in a variety of operational settings. Given the high versatility of the polydopamine deposition method onto various materials [388,397], we anticipate that demonstrating our transaminase immobilization strategy on different membrane carriers should be achievable. However, to make these membrane-immobilized biocatalysts industrially viable, we should also optimize their cost efficiency. Indeed, two different kinds of carriers were employed to immobilize TA in this: polymeric membranes (PP flat sheets), and Relizyme (used as benchmark carriers). Table F-1 provides insights about the cost of the supports (€/m^2_{ext} or €/g) and of the resulting immobilized biocatalysts (€/$mg_{TA\ imm}$) obtained in our work. The latter indicator takes into account the observed TA loading obtained after batch immobilization (see IV-4, black triangles). Overall, the cost of the membrane-immobilized TAs used in our study is approximately 10 times higher than that of the benchmark TA_Relizyme. However, it is important to note that the price of polymeric membranes varies significantly depending on the supplier.

Table F-1. Cost estimation of the enzyme supports (normalized by external surface (€/m^2_{ext}) or weight (€/g) of carrier) and of the resulting immobilized biocatalysts (€/$mg_{TA\ imm}$) used in our work.

Biocatalyst	**Cost of support [€/g] (or €/m^2_{ext})**	**Cost of biocatalyst [€/mg $_{TA\ imm}$]**
TA_PP3	4 (200)	0.082
TA_PP3_SS	4 (200)	0.039
TA_RelizymeHFA	1.2 (/)	0.007
TA_RelizymeEP	0.5 (/)	0.003

Second, the integration of the membrane-immobilized TAs (currently implemented in a dead-end configuration) into a flat-sheet membrane reactor

(operating in cross-flow), will be of prime interest for upcoming membrane operations. It is noteworthy that the scalability of our lab-scale EMR (into large-scale membrane modules) must also be demonstrated to transfer this technology at the industrial scale. To be industrially viable, the implemented (recirculating) flow process must operate at high FAP substrate concentration to enable sufficient productivity.

Mastering the coupling of flow transamination, continuous crystallization, and membrane processes (such as acetone pervaporation or controlled FAP addition) will be crucial for the set-up of hybrid flow (recirculating) processes. As an initial approach, we can consider implementing a membrane-assisted separation process (e.g. the acetone co-product removal via pervaporation, as demonstrated by Dejonghe et al. [282] in batch mode), with the aim to further enhance the productivity of the biocatalytic membrane process. In such process (Figure F-1), the EMR also acts as a pervaporation unit. The FMBA:DPPA crystallization would afford to primary shift the transamination equilibrium. The produced API (in the form of crystals) can be recovered by filtration upon recirculation of the retentate. However, since low DPPA concentrations should be engaged in the feed (i.e. under ISO:DPPA solubility limit) to avoid the feeding of crystals in the reactor, the crystallization driving force is limited. Hence, the equilibrium will only be mildly shifted towards the product side. This problem may be solved by the simultaneous progressive removal of the acetone through pervaporation, which would enable to push the reaction towards completion. It would, in principle, also help minimizing the TA inhibition by the keto by-product (acetone) when working at high FAP concentration (i.e. when the FAP substrate is fed in the form of emulsions).

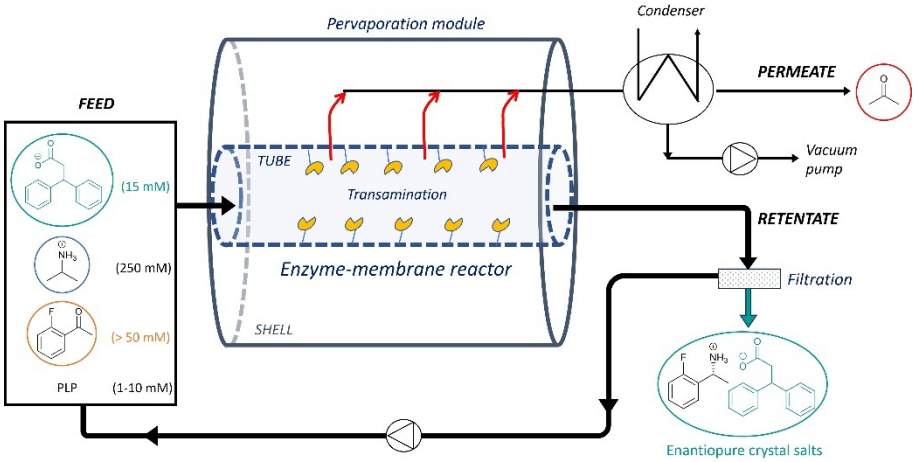

Figure F-1. Schematical representation of the pervaporation-aided crystallization-assisted transamination process, taking place in an EMR in recirculating mode. Red arrows represent the acetone flux passing through the membrane and reaching the condenser in the permeate side. The feed (consisting in an aqueous mixture of soluble ISO:DPPA salt, FAP and PLP in an HEPES 0.1M pH 8 buffer) is filtrated and continuously recirculated in the retentate side.

If the continuous feeding of FAP emulsions is problematic (e.g. causes TA deactivation), another strategy must be implemented to operate at high substrate concentration. An alternative method to enhance the transamination process involves the membrane-assisted continuous addition of the FAP keto-substrate to the feed (Figure F-2). In this approach, the EMR would act as a membrane contactor implemented in a pressure-driven membrane process. In principle, the continuous recirculation of two reservoirs at each compartment of the membrane should result in the controlled addition of FAP and DPPA (saturated aqueous solutions) from reservoir II to the feed. If the transamination kinetics matches with the mass transport across the membrane, this process may allow maintaining a constant FAP substrate concentration (around 25 mM) while preventing enzyme inhibition during recirculation (Figure F-2). It is analogous to the use of batch multiphasic systems (i.e., with FAP emulsions acting as an external substrate reservoir), but in continuous recirculating mode. Constant crystallization driving force should be also

afforded by the continuous addition of the DPPA in the system. The FMBA:DPPA crystallization would enable to shift the transamination equilibrium and achieved high product yield. The produced API (in the form of crystals) can be recovered by filtration upon recirculation of the retentate.

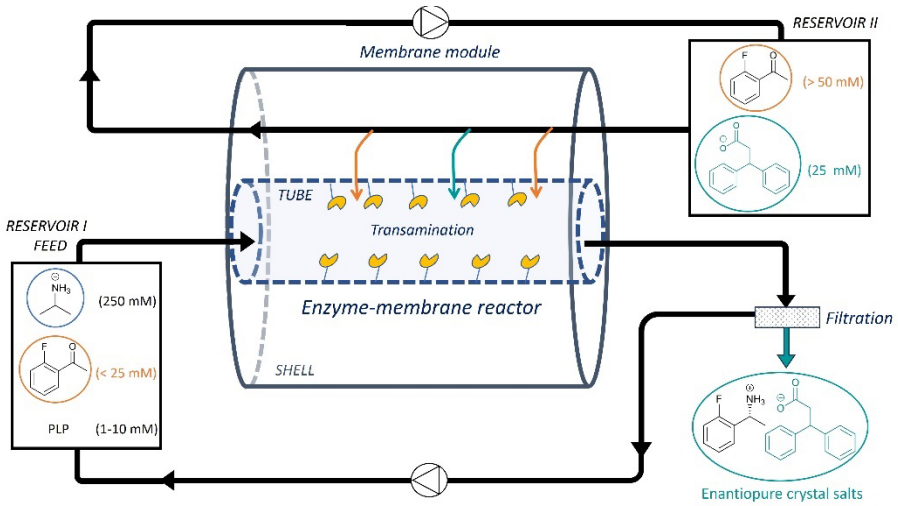

Figure F-2. Schematical representation of the membrane-assisted transamination - crystallization process, taking place in an EMR in recirculating mode. In this case, Reservoir II (containing an aqueous mixture of FAP and saturated DPPA) and the feed (consisting in a aqueous solution of ISO, FAP and PLP in an HEPES 0.1M pH 8 buffer) are continuously recirculated on each side of the membrane. Green and orange arrows represent the DPPA and FAP flux passing from Reservoir II to the feed through the membrane, respectively.

Eventually, to further ensure the robustness of the presented process, targeting the production via crystallization-assisted transamination of other high-value chiral amines is of particular interest. Based on the substrate affinity of the TsRTA enzyme (which accepts various α keto-substrates), the production of R-bromomethylbenzylamine, R-phenylbutanamine, R-phenylpropanamine (i.e. R-amphetamine [434]) and R-phenoxypropan-2-amine (i.e. R-mexiletine precursor [433]) using TA_PP3 catalyst should be conducted.

References

1 S. M. Carl, D. J. Lindley, G. T. Knipp, K. R. Morris, E. Oliver, G. W. Becker and R. D. Arnold, in *Pharmaceutical Manufacturing Handbook*, John Wiley & Sons, Ltd, 2008, pp. 1–32.

2 M. D. Truppo, *ACS Med. Chem. Lett.*, 2017, **8**, 476–480.

3 R. A. Sheldon and J. M. Woodley, *Chem. Rev.*, 2018, **118**, 801–838.

4 D. J. C. Constable, P. J. Dunn, J. D. Hayler, G. R. Humphrey, J. Johnnie L. Leazer, R. J. Linderman, K. Lorenz, J. Manley, B. A. Pearlman, A. Wells, A. Zaks and T. Y. Zhang, *Green Chem.*, 2007, **9**, 411–420.

5 T. C. Nugent, *Chiral Amine Synthesis. Methods, Developments and Applications. Edited by Thomas C. Nugent.*, 2010, vol. 49.

6 L. J. Diorazio, P. Richardson, H. F. Sneddon, A. Moores, C. Briddell and I. Martinez, *ACS Sustain. Chem. Eng.*, 2021, **9**, 16862–16864.

7 M. D. Patil, G. Grogan, A. Bommarius and H. Yun, *Catalysts*, 2018, **8**, 254.

8 D. Ghislieri and N. J. Turner, *Top. Catal.*, 2014, **57**, 284–300.

9 Iwao Ojima, *Catalytic Asymmetric Synthesis*, John Wiley & Sons, Hoboken, 2010.

10 J. Ward and R. Wohlgemuth, *Curr. Org. Chem.*, 2010, **14**, 1914–1927.

11 T. C. Nugent and M. El-Shazly, *Adv. Synth. Catal.*, 2011, **353**, 804–804.

12 P. Kelefiotis-Stratidakis, T. Tyrikos-Ergas and I. V. Pavlidis, *Org. Biomol. Chem.*, 2019, **17**, 1634–1642.

13 P. T. Anastas and J. C. Warner, *Green Chemistry: Theory and Practice*, Oxford University Press, New York, 1998, vol. 2.

14 D. P. Debecker, K. Kuok (Mimi) Hii, A. Moores, L. M. Rossi, B. Sels, D. T. Allen and B. Subramaniam, *ACS Sustain. Chem. Eng.*, 2021, **9**, 4936–4940.

15 C. Jimenez-Gonzalez, C. S. Ponder, Q. B. Broxterman and J. B. Manley, *Org. Process Res. Dev.*, 2011, **15**, 912–917.

16 P. J. Dunn, A. S. Wells and M. T. Williams, *Green Chemistry in the Pharmaceutical Industry*, Wiley-VCH, Mörlenbach, 2010.

17 F. Hollmann, D. J. Opperman and C. E. Paul, *Angew. Chem. Int. Ed.*, 2021, **60**, 5644–5665.

18 C. K. Savile, J. M. Janey, E. C. Mundorff, J. C. Moore, S. Tam, W. R. Jarvis, J. C. Colbeck, A. Krebber, F. J. Fleitz, J. Brands, P. N. Devine, G. W. Huisman and G. J. Hughes, *Science*, 2010, **329**, 305–309.

19 I. Slabu, J. L. Galman, R. C. Lloyd and N. J. Turner, *ACS Catal.*, 2017, **7**, 8263–8284.

20 T. Sehl, H. C. Hailes, J. M. Ward, R. Wardenga, E. Von Lieres, H. Offermann, R. Westphal, M. Pohl and D. Rother, *Angew. Chem. - Int. Ed.*, 2013, **52**, 6772–6775.

21 F. Guo and P. Berglund, *Green Chem.*, 2017, **19**, 333–360.

22 L. A. Nguyen, H. He and C. Pham-Huy, *Int. J. Biomed. Sci.*, 2006, **2**, 85–100.

23 I. Slabu, J. L. Galman, C. Iglesias, N. J. Weise, R. C. Lloyd and N. J. Turner, *Catal. Today*, 2018, **306**, 96–101.

24 D. L. Nelson and M. M. Cox, *Lehninger Principles of Biochemistry*, Macmillan Learning, New-York, 2013, vol. 1.

25 Roger Crossley, 1992, **48**, 8155–8178.

26 J. S. Lee, W. K. Yang, E. Y. Han, S. Y. Lee, Y. H. Park, M. A. Lim, H. S. Chung and J. H. Park, *Forensic Sci. Int.*, 2007, **173**, 68–72.

27 W. F. Kean, H. E. Howard-Lock and C. J. L. Lock, *The Lancet*, 1991, **338**, 1565–1568.

28 W. H. De Camp, *J. Pharm. Biomed. Anal.*, 1993, **11**, 1167–1172.

29 U.S. Food and Drug Administration, *Chirality*, 1992, **4**, 338–340.

30 B. Yuan, D. P. Debecker, X. Wu, J. Xiao, Q. Fei and N. J. Turner, *ChemCatChem*, 2020, **12**, 6191–6195.

31 Sanofi-Aventis, sanofi, http://en.sanofi.com/Images/13723_20100326_Clopidogrel_en.pdf, (accessed 30 August 2015).

32 J. M. Grohol, psychcentral, http://psychcentral.com/lib/top-25-psychiatric-medication-prescriptions-for-2011, (accessed 30 August 2015).

33 A. Petri, V. Colonna and O. Piccolo, *Beilstein J. Org. Chem.*, 2019, **15**, 60–66.

34 H. U. Blaser, F. Spindler and M. Studer, *Appl. Catal. Gen.*, 2001, **221**, 119–143.

35 H. U. Blaser, A. Indolese and A. Schnyder, *Curr. Sci.*, 2000, **78**, 1336–1344.

36 D. J. Cole-Hamilton, *Science*, 2003, **299**, 1702–1706.

37 D. Ager, *Handbook of Chiral Chemicals*, Taylor & Francis, Boca Raton, 2005.

38 L. Yin, W. Shan, X. Jia, X. Li and A. S. C. Chan, *J. Organomet. Chem.*, 2009, **694**, 2092–2095.

39 World Intellectual Property Organization, WO2009080469A1, 2009.

40 K. B. Hansen, Y. Hsiao, F. Xu, N. Rivera, A. Clausen, M. Kubryk, S. Krska, T. Rosner, B. Simmons, J. Balsells, N. Ikemoto, Y. Sun, F. Spindler, C. Malan, E. J. J. Grabowski and J. D. Armstrong, *J. Am. Chem. Soc.*, 2009, **131**, 8798–8804.

41 D. J. Ager, *Platin. Met. Rev.*, 2009, **53**, 203–208.

42 P.-C. Yan, G.-L. Zhu, J.-H. Xie, X.-D. Zhang, Q.-L. Zhou, Y.-Q. Li, W.-H. Shen and D.-Q. Che, *Org. Process Res. Dev.*, 2013, **17**, 307–312.

43 M. Breuer, K. Ditrich, T. Habicher, B. Hauer, M. Keßeler, R. Stürmer and T. Zelinski, *Angew. Chem. - Int. Ed.*, 2004, **43**, 788–824.

44 R. W. Stringham and Y. K. Ye, *J. Chromatogr. A*, 2006, **1101**, 86–93.

45 Q. He, S. Rohani, J. Zhuh and A. Gomaa, *Chirality*, 2012, **24**, 119–128.

46 K. Vukics, T. Fodor, J. Fischer, I. Fellegvari and S. Levai, *Org. Process Res. Dev.*, 2002, **6**, 82–85.

47 World Intellectual Property Organization, WO2006027658A2, 2006.

48 K. E. Jaeger, *Curr. Opin. Biotechnol.*, 2004, **15**, 269–271.

49 F. H. Arnold, *Angew. Chem. Int. Ed.*, 2019, **58**, 14420–14426.

50 R. C. Simon, N. Richter, E. Busto and W. Kroutil, *ACS Catal.*, 2014, **4**, 129–143.

51 F. Rudroff, M. D. Mihovilovic, H. Gröger, R. Snajdrova, H. Iding and U. T. Bornscheuer, *Nat. Catal.*, 2018, **1**, 12–22.

52 A. Schmid, F. Hollmann, J. B. Park and B. Bühler, *Curr. Opin. Biotechnol.*, 2002, **13**, 359–366.

53 S. C. Cosgrove, A. Brzezniak, S. P. France, J. I. Ramsden, J. Mangas-Sanchez, S. L. Montgomery, R. S. Heath and N. J. Turner, in *Methods in Enzymology*, ed. N. Scrutton, Academic Press, 2018, vol. 608, pp. 131–149.

54 A. Schmid, J. S. Dordick, B. Hauer, A. Kiener, M. Wubbolt and B. Witholt, *Nature*, 2001, **409**, 258–268.

55 N. J. Weise, F. Parmeggiani, S. T. Ahmed and N. J. Turner, *J. Am. Chem. Soc.*, 2015, **137**, 12977–12983.

56 T. Knaus, W. Böhmer and F. G. Mutti, *Green Chem.*, 2017, **19**, 453–463.

57 A. K. Gilio, T. W. Thorpe, N. Turner and G. Grogan, *Chem. Sci.*, 2022, **13**, 4697–4713.

58 G. A. Aleku, S. P. France, H. Man, J. Mangas-Sanchez, S. L. Montgomery, M. Sharma, F. Leipold, S. Hussain, G. Grogan and N. J. Turner, *Nat. Chem.*, 2017, **9**, 961–969.

59 R. Kumar, M. J. Karmilowicz, D. Burke, M. P. Burns, L. A. Clark, C. G. Connor, E. Cordi, N. M. Do, K. M. Doyle, S. Hoagland, C. A. Lewis, D. Mangan, C. A. Martinez, E. L. McInturff, K. Meldrum, R. Pearson, J. Steflik, A. Rane and J. Weaver, *Nat. Catal.*, 2021, **4**, 775–782.

60 J. A. McIntosh, P. S. Coelho, C. C. Farwell, Z. J. Wang, J. C. Lewis, T. R. Brown and F. H. Arnold, *Angew. Chem. - Int. Ed.*, 2013, **52**, 9309–9312.

61 E. O'Reilly and N. J. Turner, *Perspect. Sci.*, 2015, **4**, 55–61.

62 I. Rowles, K. J. Malone, L. L. Etchells, S. C. Willies and N. J. Turner, *ChemCatChem*, 2012, **4**, 1259–1261.

63 F. Hollmann, I. W. C. E. Arends and D. Holtmann, *Green Chem.*, 2011, **13**, 2285–2314.

64 L. J. Hepworth, S. P. France, S. Hussain, P. Both, N. J. Turner and S. L. Flitsch, *ACS Catal.*, 2017, **7**, 2920–2925.

65 S. A. Kelly, S. Pohle, S. Wharry, S. Mix, C. C. R. Allen, T. S. Moody and B. F. Gilmore, *Chem. Rev.*, 2018, **118**, 349–367.

66 A. Gomm and E. O'Reilly, *Curr. Opin. Chem. Biol.*, 2018, **43**, 106–112.

67 R. A. John, *Biochim. Biophys. Acta*, 1995, **1248**, 81–96.

68 T. Lütke-Eversloh and G. Stephanopoulos, *Metab. Eng.*, 2008, **10**, 69–77.

69 W. D. Fessner, *New Biotechnol.*, 2015, **32**, 658–664.

70 P. K. Mehta, T. I. Hale and P. Christen, *Eur. J. Biochem.*, 1993, **561**, 549–561.

71 S. Mathew and H. Yun, *ACS Catal.*, 2012, **2**, 993–1001.

72 A. Iwasaki, Y. Yamada, N. Kizaki, Y. Ikenaka and J. Hasegawa, *Appl. Microbiol. Biotechnol.*, 2006, **69**, 499–505.

73 A. Iwasaki, K. Matsumoto, J. Hasegawa and Y. Yasohara, *Appl. Microbiol. Biotechnol.*, 2012, **93**, 1563–1573.

74 L.-J. Guan, J. Ohtsuka, M. Okai, T. Miyakawa, T. Mase, Y. Zhi, F. Hou, N. Ito, A. Iwasaki, Y. Yasohara and M. Tanokura, *Sci. Rep.*, 2015, **5**, 10753.

75 M. Girardin, S. G. Ouellet, D. Gauvreau, J. C. Moore, G. Hughes, P. N. Devine, P. D. O'Shea and L. C. Campeau, *Org. Process Res. Dev.*, 2013, **17**, 61–68.

76 C. Molinaro, P. G. Bulger, E. E. Lee, B. Kosjek, S. Lau, D. Gauvreau, M. E. Howard, D. J. Wallace and P. D. O'Shea, *J. Org. Chem.*, 2012, **77**, 2299–2309.

77 Sebastian Schätzle, Ernst-Moritz-Arndt-Universität Greifswald, 2011.

78 A. Mozzarelli and S. Bettati, *Chem. Rec.*, 2006, **6**, 275–287.

79 L. Rios-Solis, N. Bayir, M. Halim, C. Du, J. M. Ward, F. Baganz and G. J. Lye, *Biochem. Eng. J.*, 2013, **73**, 38–48.

80 D. Koszelewski, K. Tauber, K. Faber and W. Kroutil, *Trends Biotechnol.*, 2010, **28**, 324–332.

81 K. E. Cassimjee, B. Manta and F. Himo, *Org Biomol Chem*, 2015, **13**, 8453–8464.

82 K. E. Cassimjee, M. S. Humble, V. Miceli, C. G. Colomina and P. Berglund, *ACS Catal.*, 2011, **1**, 1051–1055.

83 J. S. Shin and B. G. Kim, *Biotechnol. Bioeng.*, 1999, **65**, 206–11.

84 M. D. Truppo, J. D. Rozzell and N. J. Turner, *Org. Process Res. Dev.*, 2010, **14**, 234–237.

85 M. M. Musa, F. Hollmann and F. G. Mutti, *Catal. Sci. Technol.*, 2019, **9**, 5487–5503.

86 D. Koszelewski, D. Clay, D. Rozzell and W. Kroutil, *Eur. J. Org. Chem.*, 2009, 2289–2292.

87 M. Fuchs, J. E. Farnberger and W. Kroutil, *Eur. J. Org. Chem.*, 2015, **2015**, 6965–6982.

88 O. US EPA, Presidential Green Chemistry Challenge, https://www.epa.gov/greenchemistry/presidential-green-chemistry-challenge-2010-greener-reaction-conditions-award, (accessed 17 May 2022).

89 A. A. Desai, *Angew. Chem. Int. Ed.*, 2011, **50**, 1974–1976.

90 I. K. Mangion, B. D. Sherry, J. Yin and F. J. Fleitz, *Org. Lett.*, 2012, **14**, 3458–3461.

91 D. J. Wallace, I. Mangion and P. Coleman, in *Comprehensive Accounts of Pharmaceutical Research and Development: From Discovery to Late-Stage Process Development Volume 1*, American Chemical Society, 2016, vol. 1239, pp. 1–36.

92 J. Y. L. Chung, Y.-L. Zhong, K. M. Maloney, R. A. Reamer, J. C. Moore, H. Strotman, A. Kalinin, R. Feng, N. A. Strotman, B. Xiang and N. Yasuda, *Org. Lett.*, 2014, **16**, 5890–5893.

93 J. Y. L. Chung, B. Marcune, H. R. Strotman, R. I. Petrova, J. C. Moore and P. G. Dormer, *Org. Process Res. Dev.*, 2015, **19**, 1418–1423.

94 L. Frodsham, M. Golden, S. Hard, M. N. Kenworthy, D. J. Klauber, K. Leslie, C. Macleod, R. E. Meadows, K. R. Mulholland, J. Reilly, C. Squire, S. Tomasi, D. Watt and A. S. Wells, *Org. Process Res. Dev.*, 2013, **17**, 1123–1130.

95 E. E. Ferrandi and D. Monti, *World J. Microbiol. Biotechnol.*, 2017, **34**, 13.

96 J.-S. Shin and B.-G. Kim, *Biotechnol. Bioeng.*, 1997, **55**, 348–358.

97 M. Burns, C. A. Martinez, B. Vanderplas, R. Wisdom, S. Yu and R. A. Singer, *Org. Process Res. Dev.*, 2017, **21**, 871–877.

98 S. J. Novick, N. Dellas, R. Garcia, C. Ching, A. Bautista, D. Homan, O. Alvizo, D. Entwistle, F. Kleinbeck, T. Schlama and T. Ruch, *ACS Catal.*, 2021, **11**, 3762–3770.

99 C. K. Chung, P. G. Bulger, B. Kosjek, K. M. Belyk, N. Rivera, M. E. Scott, G. R. Humphrey, J. Limanto, D. C. Bachert and K. M. Emerson, *Org. Process Res. Dev.*, 2014, **18**, 215–227.

100 K. S. Midelfort, R. Kumar, S. Han, M. J. Karmilowicz, K. McConnell, D. K. Gehlhaar, A. Mistry, J. S. Chang, M. Anderson, A. Villalobos, J. Minshull, S. Govindarajan and J. W. Wong, *Protein Eng. Des. Sel. PEDS*, 2013, **26**, 25–33.

101 S. Pedragosa-Moreau, A. Le Flohic, V. Thienpondt, F. Lefoulon, A. M. Petit, N. Rïos-Lombarda, F. Moras and J. Gonzalez-Saban, *Adv. Synth. Catal.*, 2017, **359**, 485–493.

102 E. Busto, R. C. Simon, B. Grischek, V. Gotor-Fernández and W. Kroutil, *Adv. Synth. Catal.*, 2014, **356**, 1937–1942.

103 J. Neuburger, F. Helmholz, S. Tiedemann, P. Lehmann, P. Süss, U. Menyes and J. von Langermann, *Chem. Eng. Process. - Process Intensif.*, 2021, **168**, 108578.

104 J. T. Kohrt, P. H. Dorff, M. Burns, C. Lee, S. V. O'Neil, R. J. Maguire, R. Kumar, M. Wagenaar, L. Price and M. S. Lall, *Org. Process Res. Dev.*

105 P. Grunwald, in *Biocatalysis: Biochemical Fundamentals and Applications*, Imperial College Press, Hamburg, Germany, 2009, pp. 727–729.

106 P. Tufvesson, J. Lima-Ramos, J. S. Jensen, N. Al-Haque, W. Neto and J. M. Woodley, *Biotechnol. Bioeng.*, 2011, **108**, 1479–1493.

107 U. T. Bornscheuer, G. W. Huisman, R. J. Kazlauskas, S. Lutz, J. C. Moore and K. Robins, *Nature*, 2012, **485**, 185–194.

108 S. Gargiulo and P. Soumillion, *Curr. Opin. Chem. Biol.*, 2021, **61**, 107–113.

109 H. Yun, B. Y. Hwang, J. H. Lee and B. G. Kim, *Appl. Environ. Microbiol.*, 2005, **71**, 4220–4224.

110 N. J. Turner and R. Kumar, *Curr. Opin. Chem. Biol.*, 2018, **43**, A1–A3.

111 S. A. Kelly, D. J. Magill, J. Megaw, T. Skvortsov, T. Allers, J. W. McGrath, C. C. R. Allen, T. S. Moody and B. F. Gilmore, *Appl. Microbiol. Biotechnol.*, 2019, **103**, 5727–5737.

112 J. A. Littlechild, *Front. Bioeng. Biotechnol.*

113 T. Börner, S. Rämisch, E. Reddem, S. Bartsch, A. Vogel, A.-M. Thunnissen, P. Adlercreutz and C. Grey, *ACS Catal.*, , DOI:10.1021/acscatal.6b02100.

114 G. Antranikian, C. E. Vorgias and C. Bertoldo, *Adv. Biochem. Eng. Biotechnol.*, 2005, **96**, 219–262.

115 J. A. Littlechild, J. Guy, S. Connelly, L. Mallett, S. Waddell, C. A. Rye, K. Line and M. Isupov, *Biochem. Soc. Trans.*, 2007, **35**, 1558–1563.

116 S. DasSarma and P. DasSarma, *Curr. Opin. Microbiol.*, 2015, **25**, 120–126.

117 T. Fukushima, T. Mizuki, A. Echigo, A. Inoue and R. Usami, *Extrem. Life Extreme Cond.*, 2005, **9**, 85–89.

118 D. Alsafadi and F. Paradisi, *Extrem. Life Extreme Cond.*, 2013, **17**, 115–122.

119 G. A. Sellek and J. B. Chaudhuri, *Enzyme Microb. Technol.*, 1999, **25**, 471–482.

120 T. N. Stekhanova, A. L. Rakitin, A. V. Mardanov, E. Y. Bezsudnova and V. O. Popov, *Enzyme Microb. Technol.*, 2017, **96**, 127–134.

121 K. M. Boyko, T. N. Stekhanova, A. Yu. Nikolaeva, A. V. Mardanov, A. L. Rakitin, N. V. Ravin, E. Yu. Bezsudnova and V. O. Popov, *Extremophiles*, 2016, **20**, 215–225.

122 L. Cerioli, M. Planchestainer, J. Cassidy, D. Tessaro and F. Paradisi, *J. Mol. Catal. B Enzym.*, 2015, **120**, 141–150.

123 S. A. Kelly, S. Mix, T. S. Moody and B. F. Gilmore, *Appl. Microbiol. Biotechnol.*, 2020, **104**, 4781–4794.

124 S. L. Márquez, J. Atalah and J. M. Blamey, *Enzyme Microb. Technol.*, 2019, **131**, 109423.

125 E. E. Ferrandi, A. Previdi, I. Bassanini, S. Riva, X. Peng and D. Monti, *Appl. Microbiol. Biotechnol.*, 2017, **101**, 4963–4979.

126 Y. Chen, D. Yi, S. Jiang and D. Wei, *Appl. Microbiol. Biotechnol.*, 2016, **100**, 3101–3111.

127 S. Mathew, K. Deepankumar, G. Shin, E. Y. Hong, B.-G. Kim, T. Chung and H. Yun, *RSC Adv.*, 2016, **6**, 69257–69260.

128 B. Guidi, M. Planchestainer, M. L. Contente, T. Laurenzi, I. Eberini, L. J. Gourlay, D. Romano, F. Paradisi and F. Molinari, *Sci. Rep.*, 2018, **8**, 16441.

129 C. M. Heckmann, L. J. Gourlay, B. Dominguez and F. Paradisi, *Front. Bioeng. Biotechnol.*, 2020, **8**, 707.

130 D. Koszelewski, M. Göritzer, D. Clay, B. Seisser and W. Kroutil, *ChemCatChem*, 2010, **2**, 73–77.

131 M. Planchestainer, M. L. Contente, J. Cassidy, F. Molinari, L. Tamborini and F. Paradisi, *Green Chem.*, 2017, **19**, 372–375.

132 M. D. Truppo, J. D. Rozzell, J. C. Moore and N. J. Turner, *Org Biomol Chem*, 2009, **7**, 395–398.

133 L. Rios-Solis, P. Morris, C. Grant, A. O. O. Odeleye, H. C. Hailes, J. M. Ward, P. A. Dalby, F. Baganz and G. J. Lye, *Chem. Eng. Sci.*, 2015, **122**, 360–372.

134 E. S. Park, J. Y. Dong and J. S. Shin, *Org. Biomol. Chem.*, 2013, **11**, 6929–6933.

135 R. E. Meadows, K. R. Mulholland, M. Schürmann, M. Golden, H. Kierkels, E. Meulenbroeks, D. Mink, O. May, C. Squire, H. Straatman and A. S. Wells, *Org. Process Res. Dev.*, 2013, **17**, 1117–1122.

136 J.-S. Shin, B.-G. Kim and D.-H. Shin, *Enzyme Microb. Technol.*, 2001, **29**, 232–239.

137 J. S. Shin and B. G. Kim, *Biotechnol. Bioeng.*, 2002, **77**, 832–837.

138 B. K. Cho, H. J. Cho, H. Yun and B. G. Kim, *J. Mol. Catal. B Enzym.*, 2003, **26**, 273–285.

139 D. Hülsewede, M. Tänzler, P. Süss, A. Mildner, U. Menyes and J. von Langermann, *Eur. J. Org. Chem.*, 2018, **2018**, 2130–2133.

140 A. P. Green, N. J. Turner and E. O'Reilly, *Angew. Chem. - Int. Ed.*, 2014, **53**, 10714–10717.

141 H. H. Lo, S. K. Hsu, W. De Lin, N. L. Chan and W. H. Hsu, *Biotechnol. Prog.*, 2005, **21**, 411–415.

142 D. Koszelewski, I. Lavandera, D. Clay, D. Rozzell and W. Kroutil, *Adv. Synth. Catal.*, 2008, **350**, 2761–2766.

143 F. G. Mutti, C. S. Fuchs, D. Pressnitz, J. H. Sattler and W. Kroutil, *Adv. Synth. Catal.*, 2011, **353**, 3227–3233.

144 M. Höhne, S. Kühl, K. Robins and U. T. Bornscheuer, *ChemBioChem*, 2008, **9**, 363–365.

145 D. Koszelewski, I. Lavandera, D. Clay, G. M. Guebitz, D. Rozzell and W. Kroutil, *Angew. Chem. - Int. Ed.*, 2008, **47**, 9337–9340.

146 K. E. Cassimjee, C. Branneby, V. Abedi, A. Wells and P. Berglund, *Chem. Commun.*, 2010, **46**, 5569.

147 S. Schätzle, F. Steffen-Munsberg, A. Thontowi, M. Höhne, K. Robins and U. T. Bornscheuer, *Adv. Synth. Catal.*, 2011, **353**, 2439–2445.

148 Y. Li, S. Jing, C. Cuijie, W. Shaoming, Z. Liande, X. Wenlin and G. Liping, *Electrophoresis*, 2009, **30**, 3527–3533.

149 R. Ye, J. Zhao, B. B. Wickemeyer, F. D. Toste and G. A. Somorjai, *Nat. Catal.*, 2018, **1**, 318–325.

150 D. P. Debecker, V. Smeets, M. Van der Verren, H. Meersseman Arango, M. Kinnaer and F. Devred, *Curr. Opin. Green Sustain. Chem.*, 2021, **28**, 100437.

151 U. T. Bornscheuer, *Angew. Chem. Int. Ed.*, 2003, **42**, 3336–3337.

152 J. M. Bolivar and F. López-Gallego, *Curr. Opin. Green Sustain. Chem.*, 2020, **25**, 100349.

153 D. Grajales, J. C. Mateos, D. Padro, P. Ramos-Cabrer and F. López-Gallego, *New Biotechnol.*, 2018, **47**, 25–30.

154 R. A. Sheldon and S. van Pelt, *Chem Soc Rev*, 2013, **42**, 6223–6235.

155 A. Basso and S. Serban, *Mol. Catal.*, 2019, **479**, 110607.

156 N. Khalaf, C. P. Govardhan, J. J. Lalonde, R. A. Persichetti, Y. F. Wang and A. L. Margolin, *J. Am. Chem. Soc.*, 1996, **118**, 5494–5495.

157 C. Mateo, J. M. Palomo, G. Fernandez-Lorente, J. M. Guisan and R. Fernandez-Lafuente, *Enzyme Microb. Technol.*, 2007, **40**, 1451–1463.

158 L. Cao, F. van Rantwijk and R. A. Sheldon, *Org. Lett.*, 2000, **2**, 1361–1364.

159 R. A. Sheldon, *Adv. Synth. Catal.*, 2007, **349**, 1289–1307.

160 D. Brady and J. Jordaan, *Biotechnol. Lett.*, 2009, **31**, 1639–1650.

161 R. DiCosimo, J. McAuliffe, A. J. Poulose and G. Bohlmann, *Chem. Soc. Rev.*, 2013, **42**, 6437–6474.

162 N. S. Mosier and M. R. Ladisch, *Modern Biotechnology: Connecting Innovations in Microbiology and Biochemistry to Engineering Fundamentals*, John Wiley & Sons, 2011.

163 A. I. Benítez-Mateos, M. L. Contente, D. R. Padrosa and F. Paradisi, *React. Chem. Eng.*, 2021, **6**, 599–611.

164 L. Cao, *Carrier-bound Immobilized Enzymes: Principles, Application and Design*, Wiley, Hoboken, USA, 2005.

165 W. Khanam and N. C. Dubey, *Mater. Today Chem.*, 2022, **24**, 100922.

166 P. Jochems, Y. Satyawali, L. Diels and W. Dejonghe, *Green Chem.*, 2011, **13**, 1609–1623.

167 H. M. Arango, L. van den Biggelaar, P. Soumillion, P. Luis, T. Leyssens, F. Paradisi and D. P. Debecker, *React. Chem. Eng.*, 2023, **8**, 1505–1544.

168 F. Guo and P. Berglund, *Green Chem.*, 2017, **19**, 333–360.

169 M. Girardin, S. G. Ouellet, D. Gauvreau, J. C. Moore, G. Hughes, P. N. Devine, P. D. O'Shea and L.-C. Campeau, *Org. Process Res. Dev.*, 2013, **17**, 61–68.

170 L. Tamborini, P. Fernandes, F. Paradisi and F. Molinari, *Trends Biotechnol.*, 2018, **36**, 73–88.

171 M. Romero-Fernández and F. Paradisi, *Curr. Opin. Chem. Biol.*, 2020, **55**, 1–8.

172 L. van den Biggelaar, P. Soumillion and D. P. Debecker, *RSC Adv.*, 2019, **9**, 18538–18546.

173 L. Van den Biggelaar, P. Soumillion and D. P. Debecker, *Catalysts*, 2017, **7**, 54.

174 M. P. Thompson, I. Peñafiel, S. C. Cosgrove and N. J. Turner, *Org. Process Res. Dev.*, 2019, **23**, 9–18.

175 R. Gérardy, D. P. Debecker, J. Estager, P. Luis and J.-C. M. Monbaliu, *Chem. Rev.*, 2020, **120**, 7219–7347.

176 S. G. Newman and K. F. Jensen, *Green Chem.*, 2013, **15**, 1456–1472.

177 R. A. Sheldon, A. Basso and D. Brady, *Chem. Soc. Rev.*, 2021, **50**, 5850–5862.

178 S. G. Koenig, D. K. Leahy and A. S. Wells, *Org. Process Res. Dev.*, 2018, **22**, 1344–1359.

179 A. I. Benítez-Mateos and F. Paradisi, *J. Flow Chem.*, 2024, **14**, 211–218.

180 U. Hanefeld, L. Gardossi and E. Magner, *Chem. Soc. Rev.*, 2009, **38**, 453–468.

181 D. N. Tran and K. J. Balkus, *ACS Catal.*, 2011, **1**, 956–968.

182 V. Smeets, W. Baaziz, O. Ersen, E. M. Gaigneaux, C. Boissière, C. Sanchez and D. P. Debecker, *Chem. Sci.*, 2020, **11**, 954–961.

183 M. Van der Verren, V. Smeets, A. vander Straeten, C. Dupont-Gillain and D. P. Debecker, *Nanoscale Adv.*, 2021, **3**, 1646–1655.

184 R. A. Sheldon, R. Schoevaart and L. M. Van Langen, *Biocatal. Biotransformation*, 2005, **23**, 141–147.

185 J. Zdarta, A. Meyer, T. Jesionowski and M. Pinelo, *Catalysts*, 2018, **8**, 92.

186 D. Koszelewski, N. Müller, J. H. Schrittwieser, K. Faber and W. Kroutil, *J. Mol. Catal. B Enzym.*, 2010, **63**, 39–44.

187 T. Menegatti and P. Žnidaršič-Plazl, *Front. Bioeng. Biotechnol.*, 2021, **9**, 752064.

188 S. Zhang, P. Xin, S. Demoustier-Champagne and A. M. Jonas, *Colloids Surf. Physicochem. Eng. Asp.*, 2021, **631**, 127698.

189 C. Bernal, A. Illanes and L. Wilson, *Langmuir*, 2014, **30**, 3557–3566.

190 A. Vander Straeten, D. Lefèvre, S. Demoustier-Champagne and C. Dupont-Gillain, *Adv. Colloid Interface Sci.*, 2020, **280**, 102161.

191 C. Vranckx, L. Lambricht, V. Préat, O. Cornu, C. Dupont-Gillain and A. vander Straeten, *Langmuir*, 2022, **38**, 5579–5589.

192 K. E. Cassimjee, R. Kourist, D. Lindberg, M. Wittrup Larsen, N. H. Thanh, M. Widersten, U. T. Bornscheuer and P. Berglund, *Biotechnol. J.*, 2011, **6**, 463–469.

193 K. E. Cassimjee, M. Trummer, C. Branneby and P. Berglund, *Biotechnol. Bioeng.*, 2008, **99**, 712–716.

194 L. van den Biggelaar, P. Soumillion and D. P. Debecker, *Catalysts*, 2017, **7**, 54.

195 F. López-Gallego, L. Betancor, A. Hidalgo, N. Alonso, R. Fernández-Lafuente and J. M. Guisán, *Biomacromolecules*, 2005, **6**, 1839–1842.

196 F. López-Gallego, L. Betancor, C. Mateo, A. Hidalgo, N. Alonso-Morales, G. Dellamora-Ortiz, J. M. Guisán and R. Fernández-Lafuente, *J. Biotechnol.*, 2005, **119**, 70–75.

197 S. Velasco-Lozano, F. López-Gallego, J. C. Mateos-Díaz and E. Favela-Torres, *Biocatalysis*, 2016, **1**, 166–177.

198 K. E. Cassimjee, M. Kadow, Y. Wikmark, M. S. Humble, M. L. Rothstein, D. M. Rothstein and J.-E. Bäckvall, *Chem. Commun.*, 2014, **50**, 9134–9137.

199 M. D. Truppo, H. Strotman and G. Hughes, *ChemCatChem*, 2012, **4**, 1071–1074.

200 S. S. Yi, C. won Lee, J. Kim, D. Kyung, B. G. Kim and Y. S. Lee, *Process Biochem.*, 2007, **42**, 895–898.

201 H. Mallin, U. Menyes, T. Vorhaben, M. Höhne and U. T. Bornscheuer, *ChemCatChem*, 2013, **5**, 588–593.

202 H. Mallin, M. Höhne and U. T. Bornscheuer, *J. Biotechnol.*, 2014, **191**, 32–37.

203 M. Päiviö and L. T. Kanerva, *Process Biochem.*, 2013, **48**, 1488–1494.

204 I. Patramani, *Eur. J. Biochem.*, 1969, **11**, 28–36.

205 S. Mascia, P. L. Heider, H. Zhang, R. Lakerveld, B. Benyahia, P. I. Barton, R. D. Braatz, C. L. Cooney, J. M. B. Evans, T. F. Jamison, K. F. Jensen, A. S. Myerson and B. L. Trout, *Angew. Chem.*, 2013, **125**, 12585–12589.

206 D. Andrés-Sanz, E. Diamanti, D. Di Silvo, J. Gurauskis and F. López-Gallego, *ACS Appl. Mater. Interfaces*, 2022, **14**, 4285–4296.

207 G. Jas and A. Kirschning, *Chem. - Eur. J.*, 2003, **9**, 5708–5723.

208 A. Kirschning, W. Solodenko and K. Mennecke, *Chem. - Eur. J.*, 2006, **12**, 5972–5990.

209 P. D. Santis, L.-E. Meyer and S. Kara, *React. Chem. Eng.*, 2020, **5**, 2155–2184.

210 J. Britton, S. Majumdar and G. A. Weiss, *Chem. Soc. Rev.*, 2018, **47**, 5891–5918.

211 M. Santi, L. Sancineto, V. Nascimento, J. Braun Azeredo, E. V. M. Orozco, L. H. Andrade, H. Gröger and C. Santi, *Int. J. Mol. Sci.*, 2021, **22**, 990.

212 R. Gérardy, R. Morodo, J. Estager, P. Luis, D. P. Debecker and J.-C. M. Monbaliu, in *Accounts on Sustainable Flow Chemistry*, eds. T. Noël and R. Luque, Springer International Publishing, Cham, 2020, pp. 111–145.

213 L. Rogers and K. F. Jensen, *Green Chem.*, 2019, **21**, 3481–3498.

214 G. Rehn, P. Adlercreutz and C. Grey, *J. Biotechnol.*, 2014, **179**, 50–55.

215 Z. Molnár, E. Farkas, Á. Lakó, B. Erdélyi, W. Kroutil, B. G. Vértessy, C. Paizs and L. Poppe, *Catalysts*, 2019, **9**, 438.

216 L. H. Andrade, W. Kroutil and T. F. Jamison, *Org. Lett.*, 2014, **16**, 6092–6095.

217 N. Miložič, G. Stojkovič, A. Vogel, D. Bouwes and P. Žnidaršič-Plazl, *New Biotechnol.*, 2018, **47**, 18–24.

218 W. Böhmer, T. Knaus, A. Volkov, T. K. Slot, N. R. Shiju, K. Engelmark Cassimjee and F. G. Mutti, *J. Biotechnol.*, 2019, **291**, 52–60.

219 A. W. H. Dawood, J. Bassut, R. O. M. A. de Souza and U. T. Bornscheuer, *Chem. – Eur. J.*, 2018, **24**, 16009–16013.

220 A. P. Mattey, G. J. Ford, J. Citoler, C. Baldwin, J. R. Marshall, R. B. Palmer, M. Thompson, N. J. Turner, S. C. Cosgrove and S. L. Flitsch, *Angew. Chem. Int. Ed.*, 2021, **60**, 18660–18665.

221 E. Hegarty and F. Paradisi, *Chimia*, 2020, **74**, 890–894.

222 C. M. Heckmann, B. Dominguez and F. Paradisi, *ACS Sustain. Chem. Eng.*, 2021, **9**, 4122–4129.

223 M. L. Contente, F. Dall'Oglio, L. Tamborini, F. Molinari and F. Paradisi, *ChemCatChem*, 2017, **9**, 3843–3848.

224 M. L. Contente and F. Paradisi, *Nat. Catal.*, 2018, **1**, 452–459.

225 X. Wang, Y. Xie, Z. Wang, K. Zhang, H. Wang and D. Wei, *Org. Process Res. Dev.*, 2022, **26**, 1351–1359.

226 E. Abaházi, P. Sátorhelyi, B. Erdélyi, B. G. Vértessy, H. Land, C. Paizs, P. Berglund and L. Poppe, *Biochem. Eng. J.*, 2018, **132**, 270–278.

227 R. Semproli, G. Vaccaro, E. E. Ferrandi, M. Vanoni, T. Bavaro, G. Marrubini, F. Annunziata, P. Conti, G. Speranza, D. Monti, L. Tamborini and D. Ubiali, *ChemCatChem*, 2020, **12**, 1359–1367.

228 World Intellectual Property Organization, WO2014133928A1, 2014.

229 T. Heinks, L. M. Merz, J. Liedtke, M. Höhne, L. M. van Langen, U. T. Bornscheuer, G. Fischer von Mollard and P. Berglund, *Catalysts*, 2023, **13**, 875.

230 S. P. de Souza, I. I. Junior, G. M. A. Silva, L. S. M. Miranda, M. F. Santiago, F. L.-Y. Lam, A. Dawood, U. T. Bornscheuer and R. O. M. A. de Souza, *RSC Adv.*, 2016, **6**, 6665–6671.

231 A. I. Benítez-Mateos, S. Bertella, J. Behaghel de Bueren, J. S. Luterbacher and F. Paradisi, *ChemSusChem*, 2021, **14**, 3198–3207.

232 S. Matosevic, G. J. Lye and F. Baganz, *J. Biotechnol.*, 2011, **155**, 320–329.

233 A. Abdul Halim, N. Szita and F. Baganz, *J. Biotechnol.*, 2013, **168**, 567–575.

234 E. Peris, O. Okafor, E. Kulcinskaja, R. Goodridge, S. V. Luis, E. Garcia-Verdugo, E. O'Reilly and V. Sans, *Green Chem.*, 2017, **19**, 5345–5349.

235 M. Bajić, I. Plazl, R. Stloukal and P. Žnidaršič-Plazl, *Process Biochem.*, 2017, **52**, 63–72.

236 A. I. Benítez-Mateos, M. L. Contente, S. Velasco-Lozano, F. Paradisi and F. López-Gallego, *ACS Sustain. Chem. Eng.*, 2018, **6**, 13151–13159.

237 M. L. Contente and F. Paradisi, *ChemBioChem*, 2019, **20**, 2830–2833.

238 X.-J. Zhang, H.-H. Fan, N. Liu, X.-X. Wang, F. Cheng, Z.-Q. Liu and Y.-G. Zheng, *Enzyme Microb. Technol.*, 2019, **130**, 109362.

239 M. Romero-Fernandez and F. Paradisi, *Green Chem.*, 2021, **23**, 4594–4603.

240 M. Romero-Fernandez, C. M. Heckmann and F. Paradisi, *ChemSusChem*, 2022, **15**, e202200811.

241 L. Nagy-Győr, E. Abaházi, V. Bódai, P. Sátorhelyi, B. Erdélyi, D. Balogh-Weiser, C. Paizs, G. Hornyánszky and L. Poppe, *ChemBioChem*, 2018, **19**, 1845–1848.

242 J. S. Shin, B. G. Kim, A. Liese and C. Wandrey, *Biotechnol. Bioeng.*, 2001, **73**, 179–187.

243 C. Mateo, V. Grazú, B. C. C. Pessela, T. Montes, J. M. Palomo, R. Torres, F. López-Gallego, R. Fernández-Lafuente and J. M. Guisán, *Biochem. Soc. Trans.*, 2007, **35**, 1593–1601.

244 A. Azimi, S. Caramuta, B. Seashore-Ludlow, J. Boström, J. L. Robinson, F. Edfors, R. Tuominen, K. Kemper, O. Krijgsman, D. S. Peeper, J. Nielsen, J. Hansson, S. Egyhazi Brage, M. Altun, M. Uhlen and G. Maddalo, *Mol. Syst. Biol.*, 2018, **14**, e7858.

245 J. M. Carceller, K. S. Arias, M. J. Climent, S. Iborra and A. Corma, *Natl. Sci. Rev.*, 2022, **9**, nwac135.

246 S. Velasco-Lozano, A. I. Benítez-Mateos and F. López-Gallego, *Angew. Chem. Int. Ed.*, 2017, **56**, 771–775.

247 R. A. Sheldon, *ACS Sustain. Chem. Eng.*, 2018, **6**, 4464–4480.

248 J. H. Schrittwieser, S. Velikogne, M. Hall and W. Kroutil, *Chem. Rev.*, 2018, **118**, 270–348.

249 D. Hülsewede, E. Temmel, P. Kumm and J. von Langermann, *Crystals*, 2020, **10**, 345.

250 A. Adamo, R. L. Beingessner, M. Behnam, J. Chen, T. F. Jamison, K. F. Jensen, J.-C. M. Monbaliu, A. S. Myerson, E. M. Revalor, D. R. Snead, T. Stelzer, N. Weeranoppanant, S. Y. Wong and P. Zhang, *Science*, 2016, **352**, 61–67.

251 S. Chakraborty, H. Rusli, A. Nath, J. Sikder, C. Bhattacharjee, S. Curcio and E. Drioli, *Crit. Rev. Biotechnol.*, 2016, **36**, 43–58.

252 I. Slabu, J. L. Galman, R. C. Lloyd and N. J. Turner, *ACS Catal.*, 2017, **7**, 8263–8284.

253 R. A. Sheldon and S. van Pelt, *Chem. Soc. Rev.*, 2013, **42**, 6223–6235.

254 D. Remonatto, R. H. Miotti Jr., R. Monti, J. C. Bassan and A. V. de Paula, *Process Biochem.*, 2022, **114**, 1–20.

255 A. S. Dunn, V. Svoboda, J. Sefcik and J. H. ter Horst, *Org. Process Res. Dev.*, 2019, **23**, 2031–2041.

256 A. Hyer, D. Gregory, K. Kay, Q. Le, J. Turnage, F. Gupton and J. K. Ferri, *Adv. Synth. Catal.*, 2024, **366**, 357–389.

257 R. M. Lindeque and J. M. Woodley, *Catalysts*, 2019, **9**, 262.

258 L.-E. Meyer, M. Hobisch and S. Kara, *Curr. Opin. Biotechnol.*, 2022, **78**, 102835.

259 P. Luis, *Fundamental Modeling of Membrane Systems*, Elsevier, 1st Edition., 2018.

260 W. Li, J. Estager, J.-C. M. Monbaliu, D. P. Debecker and P. Luis, *J. Chem. Technol. Biotechnol.*, 2020, **95**, 2311–2334.

261 J. G. Crespo and K. W. Böddeker, *Membrane Processes in Separation and Purification*, Springer Science & Business Media, 2013.

262 S. B. Ameur, C. Luminiţa Gîjiu, M.-P. Belleville, J. Sanchez and D. Paolucci-Jeanjean, *J. Membr. Sci.*, 2014, **455**, 330–340.

263 M. Pinelo, G. Jonsson and A. S. Meyer, *Sep. Purif. Technol.*, 2009, **70**, 1–11.

264 J. E. L. Mijares, *J. Membr. Sci.*

265 Y. Satyawali, K. Vanbroekhoven and W. Dejonghe, *Biochem. Eng. J.*, 2017, **121**, 196–223.

266 W. Qing, X. Li, S. Shao, X. Shi, J. Wang, Y. Feng, W. Zhang and W. Zhang, *J. Membr. Sci.*, 2019, **583**, 118–138.

267 Y.-K. Cen, Y.-X. Liu, Y.-P. Xue and Y.-G. Zheng, *Adv. Synth. Catal.*, 2019, **361**, 5500–5515.

268 J. Kujawa, M. Głodek, G. Li, S. Al-Gharabli, K. Knozowska and W. Kujawski, *Sci. Total Environ.*, 2021, **801**, 149647.

269 J. Luo, S. Song, H. Zhang, H. Zhang, J. Zhang and Y. Wan, *Eng. Life Sci.*, 2020, **20**, 441–450.

270 J. Agustian, A. H. Kamaruddin and S. Bhatia, *J. Chem. Technol. Biotechnol.*, 2011, **86**, 1032–1048.

271 L. Giorno, R. Mazzei and E. Drioli, in *Membrane Operations*, John Wiley & Sons, Ltd, 2009, pp. 397–409.

272 A. B. Sitanggang, A. Drews and M. Kraume, *Chem. Eng. Process. - Process Intensif.*, 2022, **180**, 108729.

273 G. Ranieri, R. Mazzei, T. Poerio, F. Bazzarelli, Z. Wu, K. Li and L. Giorno, *Chem. Eng. Sci.*, 2018, **185**, 149–156.

274 A. Kayvani Fard, G. McKay, A. Buekenhoudt, H. Al Sulaiti, F. Motmans, M. Khraisheh and M. Atieh, *Materials*, 2018, **11**, 74.

275 R. N. Patel, *Enzyme Microb. Technol.*, 2002, **31**, 804–826.

276 K. Goldberg, K. Schroer, S. Lütz and A. Liese, *Appl. Microbiol. Biotechnol.*, 2007, **76**, 237–248.

277 *Chirality*, 1992, **4**, 338–340.

278 W. H. De Camp, *J. Pharm. Biomed. Anal.*, 1993, **11**, 1167–1172.

279 A. Liese, T. Zelinski, M.-R. Kula, H. Kierkels, M. Karutz, U. Kragl and C. Wandrey, *J. Mol. Catal. B Enzym.*, 1998, **4**, 91–99.

280 J. Haberland, W. Hummel, T. Daussmann and A. Liese, *Org. Process Res. Dev.*, 2002, **6**, 458–462.

281 T. Börner, G. Rehn, C. Grey and P. Adlercreutz, *Org. Process Res. Dev.*, 2015, **19**, 793–799.

282 Y. Satyawali, D. F. Del Pozo, P. Vandezande, I. Nopens and W. Dejonghe, *Biotechnol. Prog.*, 2019, **35**, e2731.

283 Y. Satyawali, E. Ehimen, L. Cauwenberghs, M. Maesen, P. Vandezande and W. Dejonghe, *Biochem. Eng. J.*, 2017, **117**, 97–104.

284 J. Yang, A. Buekenhoudt, M. V. Dael, P. Luis, Y. Satyawali, R. Malina and S. Lizin, *Org. Process Res. Dev.*, 2022, **26**, 2052–2066.

285 R. Ciriminna and M. Pagliaro, *Org. Process Res. Dev.*, 2013, **17**, 1479–1484.

286 K. Sakaki, L. Giorno and E. Drioli, *J. Membr. Sci.*, 2001, **184**, 27–38.

287 E. Battistel, D. Bianchi, P. Cesti and C. Pina, *Biotechnol. Bioeng.*, 1991, **38**, 659–664.

288 M. B. Ansorge-Schumacher and O. Thum, *Chem. Soc. Rev.*, 2013, **42**, 6475–6490.

289 C.-S. Chen and C. J. Sih, *Angew. Chem. Int. Ed. Engl.*, 1989, **28**, 695–707.

290 K. Sakaki, A. Aoyama, T. Nakane, T. Ikegami, H. Negishi, K. Watanabe and H. Yanagishita, *Desalination*, 2006, **193**, 260–266.

291 Z. Findrik, Z. Németh, G. Rački, K. Bélafi-Bakó, K. Csanádi, Z. Gubicza and L. Gubicza, *Process Biochem.*, 2012, **47**, 1715–1722.

292 W. Zhang, W. Qing, Z. Ren, W. Li and J. Chen, *Bioresour. Technol.*, 2014, **172**, 16–21.

293 L. Gubicza, N. Nemestóthy, T. Fráter and K. Bélafi-Bakó, *Green Chem.*, 2003, **5**, 236–239.

294 A. Van der Padt, J. J. W. Sewalt and K. Van't Riet, *J. Membr. Sci.*, 1993, **80**, 199–208.

295 Y. Satyawali, L. Cauwenberghs, M. Maesen and W. Dejonghe, *Chem. Eng. Process. - Process Intensif.*, 2021, **166**, 108475.

296 V. Narisetty, P. Parhi, B. Mohan, S. Hakkim Hazeena, A. Naresh Kumar, B. Gullón, A. Srivastava, L. M. Nair, M. Paul Alphy, R. Sindhu, V. Kumar, E. Castro, M. Kumar Awasthi and P. Binod, *Bioresour. Technol.*, 2022, **346**, 126590.

297 T. Loftsson and D. Duchêne, *Int. J. Pharm.*, 2007, **329**, 1–11.

298 D. Kim and D. F. Day, *Enzyme Microb. Technol.*, 1994, **16**, 844–848.

299 Z. Su, J. Luo, M. Pinelo and Y. Wan, *J. Membr. Sci.*, 2018, **555**, 268–279.

300 O. Ibrahim, *J. Food Chem. Nanotechnol.*, , DOI:10.17756/jfcn.2018-060.

301 E. Zokaityte, D. Cernauskas, D. Klupsaite, V. Lele, V. Starkute, P. Zavistanaviciute, M. Ruzauskas, R. Gruzauskas, G. Juodeikiene, J. M. Rocha, S. Bliznikas, P. Viskelis, R. Ruibys and E. Bartkiene, *Microorganisms*, 2020, **8**, 1182.

302 T. Sar, S. Harirchi, M. Ramezani, G. Bulkan, M. Y. Akbas, A. Pandey and M. J. Taherzadeh, *Sci. Total Environ.*, 2022, **810**, 152253.

303 M. G. Gänzle, in *Encyclopedia of Dairy Sciences (Third Edition)*, eds. P. L. H. McSweeney and J. P. McNamara, Academic Press, Oxford, 2022, pp. 96–102.

304 S. Chockchaisawasdee, V. I. Athanasopoulos, K. Niranjan and R. A. Rastall, *Biotechnol. Bioeng.*, 2005, **89**, 434–443.

305 M. Akbarian, A. Khani, S. Eghbalpour and V. N. Uversky, *Int. J. Mol. Sci.*, 2022, **23**, 1445.

306 W. a. m. Mutilangi, D. Panyam and A. Kilara, *J. Food Sci.*, 1995, **60**, 1104–1109.

307 W. Qu, H. Ma, W. Li, Z. Pan, J. Owusu and C. Venkitasamy, *Process Biochem.*, 2015, **50**, 245–252.

308 M. Sajid and J. H. McKerrow, *Mol. Biochem. Parasitol.*, 2002, **120**, 1–21.

309 B. Nidetzky, W. Neuhauser, D. Haltrich and K. D. Kulbe, *Biotechnol. Bioeng.*, 1996, **52**, 387–396.

310 MWCO, https://www.lenntech.com/services/mwco.htm, (accessed 5 September 2024).

311 J. Luo, R. T. Nordvang, S. T. Morthensen, B. Zeuner, A. S. Meyer, J. D. Mikkelsen and M. Pinelo, *Bioresour. Technol.*, 2014, **166**, 9–16.

312 D. Valinger, A. Vrsalović Presečki, Ž. Kurtanjek, M. Pohl, Z. Findrik Blažević and Đ. Vasić-Rački, *J. Mol. Catal. B Enzym.*, 2014, **102**, 132–137.

313 C. Kohlmann, S. Leuchs, L. Greiner and W. Leitner, *Green Chem.*, 2011, **13**, 1430–1436.

314 A. Heyse, C. Plikat, M. Ansorge-Schumacher and A. Drews, *Catal. Today*, 2019, **331**, 60–67.

315 Y. Satyawali, W. Van Hecke, M. N. Khan, P. Vandezande, P. Van der Weeën and W. Dejonghe, *J. Clean. Prod.*, 2023, **426**, 139050.

316 I. Ioannou, E. Barboza, G. Willig, T. Marié, A. Texeira, P. Darme, J.-H. Renault and F. Allais, *Pharmaceuticals*, 2021, **14**, 319.

317 H. Ren, J. Fei, X. Shi, T. Zhao, H. Cheng, N. Zhao, Y. Chen and H. Ying, *Sep. Purif. Technol.*, 2015, **144**, 70–79.

318 K. Hofmann and C. Hamel, *Chem. Ing. Tech.*, 2023, **95**, 767–772.

319 M. Ebrahimi, L. Placido, L. Engel, K. S. Ashaghi and P. Czermak, *Desalination*, 2010, **250**, 1105–1108.

320 A. Córdova, C. Astudillo, C. Vera, C. Guerrero and A. Illanes, *J. Biotechnol.*, 2016, **223**, 26–35.

321 V. A. Botelho, M. Mateus, J. C. C. Petrus and M. N. de Pinho, *Membranes*, 2022, **12**, 171.

322 T. Cao, M. Pázmándi, I. Galambos and Z. Kovács, *Membranes*, 2020, **10**, 203.

323 A. B. Sitanggang, A. Drews and M. Kraume, *Bioresour. Technol.*, 2014, **167**, 108–115.

324 A. B. Sitanggang, A. Drews and M. Kraume, *Biochem. Eng. J.*, 2016, **109**, 65–80.

325 A. B. Sitanggang, A. Drews and M. Kraume, *J. Biotechnol.*, 2015, **203**, 89–96.

326 J. A. Rodríguez Gastón, H. Costa and S. A. Ferrarotti, *Biotechnol. Prog.*, 2015, **31**, 695–699.

327 V. C. Fenelon, J. H. Miyoshi, C. S. Mangolim, A. S. Noce, L. N. Koga and G. Matioli, *Carbohydr. Polym.*, 2018, **192**, 19–27.

328 A. Trusek-Holownia, M. Lech and A. Noworyta, *Chem. Eng. J.*, 2016, **305**, 61–68.

329 S. Jakovetić, N. Ognjanovic Lukovic, B. Jugović, G. Milica, S. Grbavčić, J. Jovanović and Z. Knežević-Jugović, *Food Bioprocess Technol.*, 2014, **8**, 287–300.

330 T. Eisele, T. Stressler, B. Kranz and L. Fischer, *Eur. Food Res. Technol.*, , DOI:10.1007/s00217-012-1894-5.

331 W.-H. Huang, J. Sun, H. He, H.-W. Dong and J.-T. Li, *Food Chem.*, 2011, **128**, 968–973.

332 J. Ewert, W. Claaßen, T. Stressler and L. Fischer, *Biochem. Eng. J.*, 2019, **150**, 107261.

333 M. Merz, T. Eisele, W. Claaßen, D. Appel, S. Rabe, T. Stressler and L. Fischer, *Biochem. Eng. J.*, 2015, **99**, 114–123.

334 R. Das, S. Ghosh and C. Bhattacharjee, *LWT*, 2012, **47**, 238–245.

335 S. Huang, Y. Gong, Y. Li, S. Ruan, S. M. Roknul Azam, Y. Duan, X. Ye and H. Ma, *Process Biochem.*, 2020, **92**, 130–137.

336 J. O'Halloran, M. O'Sullivan and E. Casey, *Food Bioprocess Technol.*, 2019, **12**, 799–808.

337 C. R. Thomas and D. Geer, *Biotechnol. Lett.*, 2011, **33**, 443–456.

338 Z.-G. Wang, L.-S. Wan, Z.-M. Liu, X.-J. Huang and Z.-K. Xu, *J. Mol. Catal. B Enzym.*, 2009, **56**, 189–195.

339 S. B. Sigurdardóttir, J. Lehmann, S. Ovtar, J.-C. Grivel, M. D. Negra, A. Kaiser and M. Pinelo, *Adv. Synth. Catal.*, 2018, **360**, 2578–2607.

340 H. Zhang, J. Luo, S. Li, Y. Wei and Y. Wan, *Langmuir*, 2018, **34**, 2585–2594.

341 J. Luo, A. S. Meyer, R. V. Mateiu, D. Kalyani and M. Pinelo, *ACS Appl. Mater. Interfaces*, 2014, **6**, 22894–22904.

342 Z.-Y. Xi, Y.-Y. Xu, L.-P. Zhu, Y. Wang and B.-K. Zhu, *J. Membr. Sci.*, 2009, **327**, 244–253.

343 F. Marpani, J. Luo, R. V. Mateiu, A. S. Meyer and M. Pinelo, *ACS Appl. Mater. Interfaces*, 2015, **7**, 17682–17691.

344 L. Sie Yon, F. N. Gonawan, A. H. Kamaruddin and M. H. Uzir, *Ind. Eng. Chem. Res.*, 2013, **52**, 9441–9453.

345 S. Y. Lau, F. N. Gonawan, S. Bhatia, A. H. Kamaruddin and M. H. Uzir, *Chem. Eng. J.*, 2011, **166**, 726–737.

346 S. Ming, S. Li, Z. Chen, X. Chen, F. Wang, S. Deng, K. Marszałek, Z. Zhu, W. Zhang and F. J. Barba, *Antioxidants*, 2022, **11**, 1906.

347 F. Ugur Nigiz and N. Durmaz Hilmioglu, *Int. J. Energy Res.*, 2016, **40**, 71–80.

348 G. Bayramoğlu, B. Hazer, B. Altıntaş and M. Y. Arıca, *Process Biochem.*, 2011, **46**, 372–378.

349 J. Kujawa, M. Głodek, I. Koter, B. Ośmiałowski, K. Knozowska, S. Al-Gharabli, L. F. Dumée and W. Kujawski, *Materials*, 2021, **14**, 201.

350 T. Palai, A. K. Singh and P. K. Bhattacharya, *Biochem. Eng. J.*, 2014, **88**, 68–76.

351 T. Palai and P. K. Bhattacharya, *J. Biosci. Bioeng.*, 2013, **115**, 668–673.

352 D. Sen, A. Sarkar, A. Gosling, S. L. Gras, G. W. Stevens, S. E. Kentish, P. K. Bhattacharya, A. R. Barber and C. Bhattacharjee, *J. Membr. Sci.*, 2011, **378**, 471–478.

353 D. Sen, A. Sarkar, S. Das, R. Chowdhury and C. Bhattacharjee, *Ind. Eng. Chem. Res.*, 2012, **51**, 10671–10681.

354 A. Chenafa, A. A. A. Abdo, A. A. Mahdi, Q. Zhang, C. Chen, Y. Zhu, J. Li, G. Fan and J. Liu, *Int. J. Biol. Macromol.*, 2024, **270**, 132312.

355 P. Jochems, Y. Satyawali, S. Van Roy, W. Doyen, L. Diels and W. Dejonghe, *Enzyme Microb. Technol.*, 2011, **49**, 580–588.

356 A. Córdova, C. Aburto, V. Carrasco, C. Guerrero, P. Henriquez, C. Astudillo-Castro, S. Catalán, T. Poerio and R. Mazzei, *Process Saf. Environ. Prot.*, 2024, **188**, 1081–1092.

357 F. N. Gonawan, M. Z. A. Bakar, K. A. Karim and A. H. Kamaruddin, *RSC Adv.*, 2016, **6**, 59865–59874.

358 C. Conidi, R. Mazzei, A. Cassano and L. Giorno, *J. Membr. Sci.*, 2014, **454**, 322–329.

359 R. Mazzei, E. Drioli and L. Giorno, *J. Membr. Sci.*, 2012, **390–391**, 121–129.

360 R. Mazzei, E. Drioli and L. Giorno, *J. Membr. Sci.*, 2010, **352**, 166–172.

361 E. Piacentini, R. Mazzei, F. Bazzarelli, G. Ranieri, T. Poerio and L. Giorno, *Ind. Eng. Chem. Res.*, 2019, **58**, 16813–16822.

362 Z. Su, K. Jankowska, S. Björk Sigurdardóttir, W. A. Zhang, A. Kaiser, J. Luo and M. Pinelo, *Chem. Eng. Sci.*, 2024, **283**, 119367.

363 P. Berends, D. Appel, T. Eisele, S. Rabe and L. Fischer, *LWT - Food Sci. Technol.*, 2014, **58**, 534–540.

364 Z. Chen, Z. Sun, S. Ming, S. Li, Z. Zhu and W. Zhang, *Sep. Purif. Technol.*, 2021, **259**, 118214.

365 A. Vanangamudi, D. Saeki, L. F. Dumée, M. Duke, T. Vasiljevic, H. Matsuyama and X. Yang, *ACS Appl. Mater. Interfaces*, 2018, **10**, 27477–27487.

366 Z. Chen, S. Zhu, H. Zhang, F. Wang, K. Marszałek and Z. Zhu, *Chem. Eng. J.*, 2023, **453**, 139792.

367 A. Muñiz-Mouro, B. Gullón, T. A. Lu-Chau and G. Eibes, *Food Bioprod. Process.*, 2020, **124**, 434–444.

368 C. Algieri, L. Donato, P. Bonacci and L. Giorno, *Biochem. Eng. J.*, 2012, **66**, 14–19.

369 L. Donato, C. Algieri, V. Miriello, R. Mazzei, G. Clarizia and L. Giorno, *J. Membr. Sci.*, 2012, **407–408**, 86–92.

370 C. Algieri, L. Donato and L. Giorno, *Biotechnol. Appl. Biochem.*, 2017, **64**, 92–99.

371 B. Šketa, J. L. Galman, N. J. Turner and P. Žnidaršič-Plazl, *New Biotechnol.*, 2024, **83**, 46–55.

372 U. Montanari, D. Cocchi, T. M. Brugo, A. Pollicino, V. Taresco, M. Romero Fernandez, J. C. Moore, D. Sagnelli, F. Paradisi, A. Zucchelli, S. M. Howdle and C. Gualandi, *Polymers*, 2021, **13**, 1804.

373 D. Roura Padrosa, Z. Nisar and F. Paradisi, *Catalysts*, 2021, **11**, 520.

374 L. K. Thalén, D. Zhao, J.-B. Sortais, J. Paetzold, C. Hoben and J.-E. Bäckvall, *Chem. – Eur. J.*, 2009, **15**, 3403–3410.

375 D. Nakmode, V. Bhavana, P. Thakor, J. Madan, P. K. Singh, S. B. Singh, J. M. Rosenholm, K. K. Bansal and N. K. Mehra, *Pharmaceutics*, 2022, **14**, 831.

376 J. T. McConville, T. C. Carvalho, S. A. Kucera and E. Garza, *Pharm. Technol.*, 2009, **33**, 74–80.

377 R. E. Meadows, K. R. Mulholland, M. Schürmann, M. Golden, H. Kierkels, E. Meulenbroeks, D. Mink, O. May, C. Squire, H. Straatman and A. S. Wells, *Org. Process Res. Dev.*, 2013, **17**, 1117–1122.

378 M. D. Truppo, J. D. Rozzell, J. C. Moore and N. J. Turner, *Org. Biomol. Chem.*, 2008, **7**, 395–398.

379 K. E. Cassimjee, C. Branneby, V. Abedi, A. Wells and P. Berglund, *Chem. Commun.*, 2010, **46**, 5569–5571.

380 A. P. Green, N. J. Turner and E. O'Reilly, *Angew. Chem. Int. Ed.*, 2014, **53**, 10714–10717.

381 Resindion srl, https://www.resindion.com/relizyme.php?content=technical-information, (accessed 3 January 2024).

382 S. Chergaoui, D. P. Debecker, T. Leyssens and P. Luis, *Cryst. Growth Des.*, 2023, **23**, 6418–6430.

383 A. Tejeda-Mansir, R. M. Montesinos and R. Guzmán, *J. Biochem. Biophys. Methods*, 2001, **49**, 1–28.

384 E. Lalli, J. S. Silva, C. Boi and G. C. Sarti, *Membranes*, 2019, **10**, 1.

385 Y. Li, H. Wang, J. Lu, A. Chu, L. Zhang, Z. Ding, S. Xu, Z. Gu and G. Shi, *Bioresour. Technol.*, 2019, **274**, 9–17.

386 L. Pérez-Álvarez, L. Ruiz-Rubio, I. Moreno and J. L. Vilas-Vilela, *Polymers*, 2019, **11**, E1843.

387 Z. Niu, Y. Zhao, W. Sun, S. Shi and Y. Gong, *Appl. Surf. Sci.*, 2016, **386**, 41–50.

388 J. Yang, M. A. C. Stuart and M. Kamperman, *Chem. Soc. Rev.*, 2014, **43**, 8271–8298.

389 S. Gámez, E. de la Torre and E. M. Gaigneaux, *Chem. Eng. J.*, 2022, **427**, 131820.

390 IR Spectrum Table, https://www.sigmaaldrich.com/BE/en/technical-documents/technical-article/analytical-chemistry/photometry-and-reflectometry/ir-spectrum-table, (accessed 8 August 2022).

391 G. Zhang, H. Meng and S. Ji, *Desalination*, 2009, **242**, 313–324.

392 B. Smith, *Infrared Spectral Interpretation: A Systematic Approach*, CRC Press, 1998.

393 J. Cai, T. Chen, L. Cui, Q. Jia, M. Liu, R. Zheng, G. Yan, D. Wei and J. Liu, *Int. J. Hydrog. Energy*, 2020, **45**, 6592–6603.

394 H. Lee, N. F. Scherer and P. B. Messersmith, *Proc. Natl. Acad. Sci. U. S. A.*, 2006, **103**, 12999–13003.

395 J. Jiang, L. Zhu, L. Zhu, B. Zhu and Y. Xu, *Langmuir*, 2011, **27**, 14180–14187.

396 B. Smith, *Spectroscopy*, 2017, **32**, 19–23.

397 H. Lee, S. M. Dellatore, W. M. Miller and P. B. Messersmith, *Science*, 2007, **318**, 426–430.

398 S. Arana-Peña, N. S. Rios, C. Mendez-Sanchez, Y. Lokha, D. Carballares, L. R. B. Gonçalves and R. Fernandez-Lafuente, *Int. J. Biol. Macromol.*, 2020, **145**, 856–864.

399 J. M. Palomo, R. L. Segura, G. Fernandez-Lorente, R. Fernandez-Lafuente and J. M. Guisán, *Enzyme Microb. Technol.*, 2007, **40**, 704–707.

400 S. Velasco-Lozano, E. Jackson, M. Ripoll, F. López-Gallego and L. Betancor, *Int. J. Biol. Macromol.*, 2020, **164**, 4318–4328.

401 B. Reus, M. Damian and F. G. Mutti, *J. Flow Chem.*, , DOI:10.1007/s41981-024-00315-2.

402 Q. Zhao, J. Wen, R. Tan, K. Huang, P. Metola, R. Wang, E. V. Anslyn and X. Zhang, *Angew. Chem. Int. Ed Engl.*, 2014, **53**, 8467–8470.

403 X. Tan, S. Gao, W. Zeng, S. Xin, Q. Yin and X. Zhang, *J. Am. Chem. Soc.*, 2018, **140**, 2024–2027.

404 T. Hirose, M. Begum, Md. Sadequl Islam, K. Taniguchi and M. Yasutake, *Tetrahedron Asymmetry*, 2008, **19**, 1641–1646.

405 M. M. Bradford, *Anal. Biochem.*, 1976, **72**, 248–254.

406 Y. Liu, K. Ai and L. Lu, *Chem. Rev.*, 2014, **114**, 5057–5115.

407 J. Liebscher, R. Mrówczyński, H. A. Scheidt, C. Filip, N. D. Hădade, R. Turcu, A. Bende and S. Beck, *Langmuir*, 2013, **29**, 10539–10548.

408 Q. Yin, Y. Shi, J. Wang and X. Zhang, *Chem. Soc. Rev.*, 2020, **49**, 6141–6153.

409 G. Noriega-Hevia, J. Serralta, A. Seco and J. Ferrer, *Sep. Purif. Technol.*, 2021, **275**, 119128.

410 B. Verrecht, T. Maere, I. Nopens, C. Brepols and S. Judd, *Water Res.*, 2010, **44**, 5274–5283.

411 U. M. Kahar, M. H. Sani, K.-G. Chan and K. M. Goh, *Molecules*, 2016, **21**, 1196.

412 M. Doeker, L. Grabowski, D. Rother and A. Jupke, *Green Chem.*, 2022, **24**, 295–304.

413 S. Tiedemann, J. E. Neuburger, A. Gazizova and J. von Langermann, *Eur. J. Org. Chem.*, 2024, **27**, e202400068.

414 T. Wang, H. Lu, J. Wang, Y. Xiao, Y. Zhou, Y. Bao and H. Hao, *J. Ind. Eng. Chem.*, 2017, **54**, 14–29.

415 G. Di Profio, E. Curcio, S. Ferraro, C. Stabile and E. Drioli, *Cryst. Growth Des.*, 2009, **9**, 2179–2186.

416 C. M. Heckmann and F. Paradisi, *Chem. – Eur. J.*, 2021, **27**, 16616–16620.

417 S. Chergaoui, J. Lauzer, D. P. Debecker, T. Leyssens and P. Luis, *J. Membr. Sci.*, 2024, **694**, 122415.

418 A. Liese and L. Hilterhaus, *Chem. Soc. Rev.*, 2013, **42**, 6236–6249.

419 D. Bhattacharyya, *Biotechnol. Prog.*

420 MolCalc, http://molcalc.org/, (accessed 29 March 2024).

421 P. Tufvesson, J. S. Jensen, W. Kroutil and J. M. Woodley, *Biotechnol. Bioeng.*, 2012, **109**, 2159–2162.

422 C. Brown, T. McGlone and A. Florence, in *Continuous Manufacturing of Pharmaceuticals*, John Wiley & Sons, Ltd, 2017, pp. 169–226.

423 T. L. Minh, J. V. Langermann, H. Lorenz and A. Seidel-Morgenstern, *J. Pharm. Sci.*, 2010, **99**, 4084–4095.

424 R. K. Hylton, G. J. Tizzard, T. L. Threlfall, A. L. Ellis, S. J. Coles, C. C. Seaton, E. Schulze, H. Lorenz, A. Seidel-Morgenstern, M. Stein and S. L. Price, *J. Am. Chem. Soc.*, 2015, **137**, 11095–11104.

425 S. Datta and D. J. W. Grant, *Nat. Rev. Drug Discov.*, 2004, **3**, 42–57.

426 L. F. Diniz, P. S. Jr. Carvalho, W. da Nova Mussel, M. I. Yoshida, R. Diniz and C. Fernandes, *Cryst. Growth Des.*, 2019, **19**, 4498–4509.

427 F. Schüth, M. D. Ward and J. M. Buriak, *Chem. Mater.*, 2018, **30**, 3599–3600.

428 L. van den Biggelaar, UCL - Université Catholique de Louvain, 2018.

429 G. F. Froment, K. B. Bischoff and J. D. Wilde, *Chemical Reactor Analysis and Design*, Wiley, 2010.

430 B. Bennett and G. Cole, *Pharmaceutical Production: An Engineering Guide*, IChemE, 2003.

431 I. Bodík, D. Vilím, A. Dorňáková, P. Németh and M. Buday, *Desalination Water Treat.*, 2011, **35**, 247–254.

432 S. Judd, *The MBR Book: Principles and Applications of Membrane Bioreactors for Water and Wastewater Treatment*, Elsevier, 2010.

433 C. Franchini, A. Carocci, A. Catalano, M. M. Cavalluzzi, F. Corbo, G. Lentini, A. Scilimati, P. Tortorella, D. C. Camerino and A. De Luca, *J. Med. Chem.*, 2005, **48**, 3094–3094.

434 D. J. Heal, S. L. Smith, J. Gosden and D. J. Nutt, *J. Psychopharmacol. Oxf. Engl.*, 2013, **27**, 479–496.